NAVAL POSTGRADUATE SCHOOL

Monterey, California

THESIS

CONTROL OF EMBEDDED VORTICES
USING WALL JETS

by

Geoffrey E. Schwartz

September 1988

Thesis Advisor: P. M. Ligrani

UNCLASSIFIED

SECURITY CLASSIFICATION OF THIS PAGE

REPORT DOCUMENTATION PAGE

1a. REPORT SECURITY CLASSIFICATION

1b. RESTRICTIVE MARKINGS

2a. SECURITY CLASSIFICATION AUTHORITY

2b. DECLASSIFICATION / DOWNGRADING SCHEDULE

3. DISTRIBUTION / AVAILABILITY OF REPORT
Approved for public release; distribution is unlimited

4. PERFORMING ORGANIZATION REPORT NUMBER(S)

5. MONITORING ORGANIZATION REPORT NUMBER(S)

6a. NAME OF PERFORMING ORGANIZATION
Naval Postgraduate School

6b. OFFICE SYMBOL (If applicable)
Code 69

7a. NAME OF MONITORING ORGANIZATION
Naval Postgraduate School

6c. ADDRESS (City, State, and ZIP Code)
Monterey, California, 93943-5000

7b. ADDRESS (City, State, and ZIP Code)
Monterey, CA 93943-5000

8a. NAME OF FUNDING / SPONSORING ORGANIZATION

8b. OFFICE SYMBOL (If applicable)

9. PROCUREMENT INSTRUMENT IDENTIFICATION NUMBER

8c. ADDRESS (City, State, and ZIP Code)

10. SOURCE OF FUNDING NUMBERS

PROGRAM ELEMENT NO.	PROJECT NO.	TASK NO.	WORK UNIT ACCESSION NO.

11. TITLE (Include Security Classification)
CONTROL OF EMBEDDED VORTICES USING WALL JETS

12. PERSONAL AUTHOR(S) Geoffrey E. Schwartz

13a. TYPE OF REPORT	13b. TIME COVERED	14. DATE OF REPORT (Year, Month, Day)	15. PAGE COUNT
Master's Thesis	FROM ____ TO ____	1988 September	292

16. SUPPLEMENTARY NOTATION The views expressed in this thesis are those of the author and do not reflect the official policy or position of the Department of Defense or the U.S. Government.

17. COSATI CODES

FIELD	GROUP	SUB-GROUP

18. SUBJECT TERMS (Continue on reverse if necessary and identify by block number)
Embedded vortex, vortex control, (mgm) theses. (proc.)

19. ABSTRACT (Continue on reverse if necessary and identify by block number)

A wall jet inclined at 30° to horizontal was used to alter the structural characteristics of streamwise vortices embedded in a turbulent boundary layer developing in a zero pressure gradient. The vortices were created using a half-delta wing attached to the floor of a wind tunnel. With the jet opposing the vortex downwash and blowing ratio increasing from 0 to 4.8, streamwise vorticity decreased from ~750 to ~150/s^{-1}, while circulation decreased from ~0.15 to ~0.05 m^2/s. The average vortex core radius increased from ~0.9 to ~2.4 cm, while the vortex moved ~3 cm spanwise toward the jet. With the jet at the vortex upwash and blowing ratio increasing from 0 to 6.7, streamwise vorticity decreased from ~860 to ~570/s^{-1} while circulation decreased from ~0.17 to ~0.15 m^2/s. With a vortex having greater circulation (produced by a larger vortex generator), the jet opposing the vortex downwash, and blowing ratio

20. DISTRIBUTION / AVAILABILITY OF ABSTRACT
☒ UNCLASSIFIED/UNLIMITED ☐ SAME AS RPT ☐ DTIC USERS

21. ABSTRACT SECURITY CLASSIFICATION
UNCLASSIFIED

22a. NAME OF RESPONSIBLE INDIVIDUAL	22b. TELEPHONE (Include Area Code)	22c. OFFICE SYMBOL
Phillip M. Ligrani	(408) 646-3382	69Li

DD FORM 1473, 84 MAR — 83 APR edition may be used until exhausted. All other editions are obsolete

SECURITY CLASSIFICATION OF THIS PAGE

UNCLASSIFIED

Block 19 (continued)

increasing from 0 to 3.0, streamwise vorticity decreased from ~1000 to ~700 s^{-1} while circulation decreased from ~0.34 to ~0.27 m^2/s. At high blowing ratios (>2.0) wall heat tramsfer rates were not altered significantly compared to a boundary layer with an embedded vortex and no injection on a heated wall. It is thus apparent that a wall jet with high momentum lifts off the wall, causing little alteration of the near-wall region of the boundary layer already disturbed by an embedded vortex.

Control of Embedded Vortices Using Wall Jets

by

Geoffrey E. Schwartz
Lieutenant Commander, United States Navy
A.B., University of California at Berkeley, 1975
M.S., Crummer Graduate School of Business,
Rollins College, Winter Park, Florida, 1982

Submitted in partial fulfillment of the
requirements for the degree of

MASTER OF SCIENCE IN MECHANICAL ENGINEERING

from the

NAVAL POSTGRADUATE SCHOOL
September 1988

Author: Geoffrey E. Schwartz

Approved by: Phillip M. Ligrani, Thesis Advisor

A.J. Healey, Chairman
Department of Mechanical Engineering

G.E. Schacher,
Dean of Science and Engineering

ABSTRACT

A wall jet inclined at 30° to horizontal was used to alter the structural characteristics of streamwise vortices embedded in a turbulent boundary layer developing in a zero pressure gradient. The vortices were created using a half-delta wing attached to the floor of a wind tunnel. With the jet opposing the vortex downwash and blowing ratio increasing from 0 to 4.8, streamwise vorticity decreased from ~750 to ~150 s^{-1}, while circulation decreased from ~0.15 to ~0.05 m^2/s. The average vortex core radius increased from ~0.9 to ~2.4 cm, while the vortex moved ~3 cm spanwise toward the jet. With the jet at the vortex upwash and blowing ratio increasing from 0 to 6.7, streamwise vorticity decreased from ~860 to ~570 s^{-1} while circulation decreased from ~0.17 to ~0.15 m^2/s. With a vortex having greater circulation (produced by a larger vortex generator), the jet opposing the vortex downwash, and blowing ratio increasing from 0 to 3.0, streamwise vorticity decreased from ~1000 to ~700 s^{-1} while circulation decreased from ~0.34 to ~0.27 m^2/s. At high blowing ratios (>2.0) wall heat transfer rates were not altered significantly compared to a boundary layer with an embedded vortex and no injection on a heated wall. It is thus apparent that a wall jet with high momentum lifts off the wall, causing little alteration of the near-wall region

of the boundary layer already disturbed by an embedded vortex.

TABLE OF CONTENTS

NOMENCLATURE

Symbol	Name	Units
A	Area	m^2
d	Injection Hole Diameter	m
x, X	Freestream Length	m
y	Vertical Length	m
z	Spanwise Length	m
y_{core}, z_{core}	Average Vortex Core Radii	m
U_∞	Freestream Mean Velocity	m/s
U_c	Injectant Mean Velocity	m/s
U_x	Streamwise Mean Velocity Component	m/s
U_y, U_z	y,z Mean Velocity Components	m/s
V	Secondary Flow Velocity Magnitude	m/s
R	Gas Constant (Air)	J/Kg·K
C_p	Constant Pressure Specific Heat (Air)	J/Kg·K
α_F, α_{BL}	Freestream and Boundary Layer Recovery Factors	
P_∞, P_{stat}	Freestream Static Pressure	Pa or mm Hg or H_2O
Po_∞	Freestream Stagnation Pressure	Pa
P_{amb}	Ambient Pressure	Pa
P_{tot}	Total Pressure	Pa
T_∞	Freestream Temperature	^oC

Symbol	Name	Units
Tr_{∞}	Boundary Layer Recovery Temperature	^{o}C
$Tr_{\infty}F$	Freestream Recovery Temperature	^{o}C
T_{amb}	Ambient Temperature	^{o}C
ρ_{∞}	Freestream Density	Kg/m^3
ρ_{amb}	Ambient Density	Kg/m^3
$\dot{q}w$	Convective Heat Transfer Rate from Wall to Freestream	W
St	Stanton Number	(Dimensionless)
ω_x	Streamwise Vorticity	s^{-1}
Γ or Cr	Circulation in yz Plane	m^2/s
$ND\Gamma_1, ND\Gamma_2$	Dimensionless Circulation Parameters	(Dimensionless)
m	Blowing Ratio	
I	Momentum Flux Ratio	
α	Pitch Angle of 5-hole Probe	degrees
β	Yaw angle of 5-hole Probe	degrees
K_p, K_y	5-hole Probe Calibration Curve Slope for Pitch and Yaw Angles	
V_T	Total Velocity	m/s
$P_1, P_2, P_3, P_4, P_5, \bar{P}$	5-hole Probe Pressures	In H_2O
$C_{py}, C_{pp}, C_{pt}, C_{pts}$	5-hole Probe Calibration Coefficients	

FORMULAE

$$U_\infty = \left[\frac{2(Pc_\infty - P_\infty)}{\rho_{amb}}\right]^{1/2}$$

$$\rho = \frac{P}{RT}$$

$$T_\infty = Tr_{\infty F} - \frac{\alpha_F U_\infty^{\ 2}}{2C_p}$$

$$Tr_\infty = T_\infty + \frac{\alpha_{BL} U_\infty^{\ 2}}{2C_p}$$

$$St = \frac{\dot{q}w}{A(T_w - Tr_\infty)\rho_\infty U_\infty C_p}$$

$$\omega_x = \frac{\partial w}{\partial y} - \frac{\partial v}{\partial z}$$

$$\Gamma = \oint_A \omega_x dA$$

$$ND\Gamma_1 = \frac{\Gamma}{U_\infty\left[\frac{y_{core} + z_{core}}{2}\right]}$$

$$ND\Gamma_2 = \frac{\Gamma}{U_c \cdot d}$$

$$m = \frac{\rho_c U_c}{\rho_\infty U_\infty}$$

$$I = m^2$$

$$V_T = [U_x^{\ 2} + U_y^{\ 2} + U_z^{\ 2}]^{1/2} = [2C_{pts}(P_1 - \bar{P})/\rho]^{1/2}$$

$$U_x = V_T \cos(\alpha) \cos(\beta)$$

$$U_y = V_T \sin(\alpha)$$

$$U_z = V_T \cos(\alpha) \sin(\beta)$$

$$C_{py} = (P_2 - P_3)/(P_1 - \overline{P})$$

$$C_{pp} = (P_4 - P_5)/(P_1 - \overline{P})$$

$$C_{pt} = (P_1 - P_{tot})/(P_1 - \overline{P})$$

$$C_{pts} = (\overline{P} - P_{stat})/(P_1 - \overline{P})$$

$$\overline{P} = (P_2 + P_3 + P_4 + P_5)/4$$

I. INTRODUCTION

Numerous mechanical devices exist which contain secondary flows including streamwise vortices. The effects of these vortices are important in regard to the efficiencies and operations of many types of machinery involving fluid flow. Vortices may cause significant changes in wall heat transfer rates, wall shear stress, and film coolant distributions, as well as in the development of transition from laminar to turbulent flow.

A. APPLICATIONS OF VORTEX CONTROL

One device which contains streamwise vortices is the gas turbine. Fluid motions in a gas turbine passage are depicted in Figure 1 (adapted from Reference 1). As the inlet boundary layer approaches the leading edge of a blade, flow splits into several streams. One stream, labelled "crossflow A" in Figure 1, flows from the pressure (concave) side of a blade to the suction (convex) side of the adjacent blade. A second flow impinges on the leading edge of the blade, where, at the "saddlepoint" a horseshoe vortex forms. One leg of this vortex flows to the suction side and one leg to the pressure side. These legs are the "counter vortex" and "passage vortex" in Figure 1. The passage vortex moves in "crossflow B" toward the suction side of the adjacent blade. These vortices may be embedded in the blade

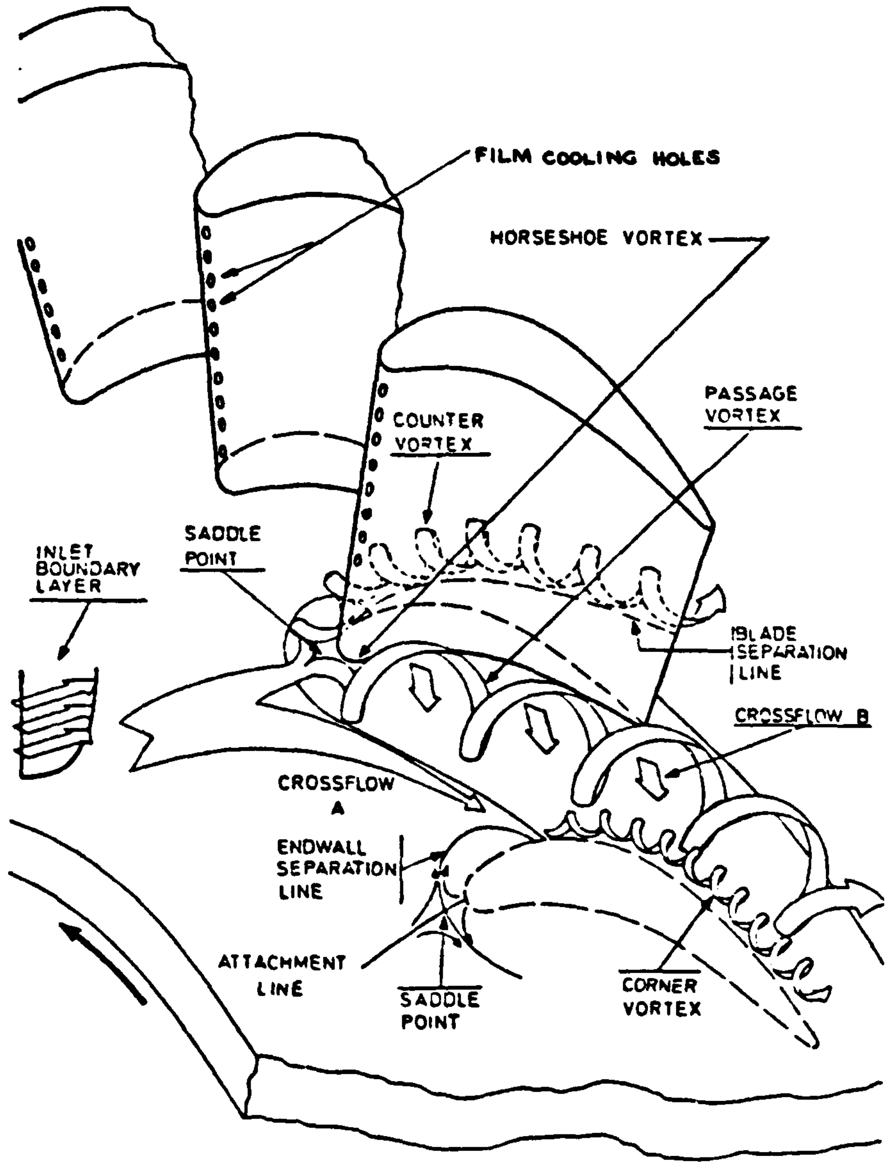

Figure 1. Flow Between Gas Turbine Blades

wall boundary layer, causing significant changes in local wall heat transfer rates [Refs. 2-7]. If film cooling is present, local "hot spots" may form at the vortex downwash. Many other examples, such as aircraft wings, missiles, and reentry vehicles, exist in which streamwise vortices affect operation.

B. LITERATURE SURVEY

Numerous studies have been performed on heat transfer effects of streamwise vortices. The present study is part of the ongoing studies of References 2-6. Reference 8 discussed heat transfer measurements on a film-cooled turbine endwall, indicating significant variations in heat transfer and film cooling effectiveness due to vortex formation. References 9-11 discuss the influence of a turbine endwall on film cooling of gas turbine blades with various injection configurations. One of the most important influences is that injectant is swept away from a blade surface by the passage vortex. Reference 12 discusses secondary flows in general within gas turbine blade passages. Reference 13 discusses structural characteristics of embedded vortices in a turbulent boundary layer with a streamwise pressure gradient.

Attempts to influence and control vortices by injection seem to be confined almost entirely to aeronautical engineering. Reference 14 presents an empirical three-dimensional stud of vortex-lift control for an airfoil using spanwise

blowing. It was found that spanwise blowing just downstream of the region of vortex shedding results in adverse pressure gradients which often reduce periodic and steady shedding of vortices. Wall jets were found to increase spanwise vortex circulation over a wing upper surface, augmenting vortex lift. Reference 15 provides a survey and critical assessment of the known devices for aircraft wing trailing vortex attenuation. Devices such as wing tip sails affect vortex roll-up in the vicinity of aircraft. This report recommends that further analysis is needed prior to actual incorporation of attenuation devices into aircraft. Reference 16 discusses two methods for removing vortices which are intentionally generated in a boundary layer to suppress turbulence. The methods are unwinding (introduction of vortex generators of opposite sign) and self-annihilation (spanwise spacing for co-rotating generated vortices is too small to allow continued vortex development). Such methods would be difficult to apply to turbomachinery. Reference 17 discusses the use of energy concentrated in strong aircraft forebody vortices by controlling lateral orientation of the vortices. It proposes that this be done to provide directional control for fighter aircraft at high angles of attack. Reference 18 discusses the use of wall suction to stabilize an incompressible laminar boundary layer along a slightly concave wall, preventing onset of Taylor-Görtler (streamwise) vortices.

Many other studies, too numerous to list here, exist in regard to airfoils. No papers are known to the present author which describe means to control vortices in turbomachines.

C. OBJECTIVES OF THE PRESENT STUDY

The present study focuses on the use of wall jets to induce structural changes in streamwise vortices. The embedded vortices are generated using a half-delta wing attached to the floor of a wind tunnel with a zero pressure gradient maintained along the test section. Fluid mechanics and heat transfer observations were made in order to understand how to control streamwise vortices by appropriate placement of and adjustment of the flow rate through wall jets.

D. ORGANIZATION OF THE STUDY AND THE THESIS

The study consisted of the following four experiments.

1. Experiment 1

Fluid mechanics measurements (pressures, velocities, streamwise vorticity, circulation of streamwise vorticity, and various vortex dimensions) at $x/d = 41.9$ (x = streamwise distance from origin of jet, d = wall jet hole diameter) with a wall jet at a vortex downwash, and blowing ratio increasing from 0 to 4.8.

2. <u>Experiment 2</u>

Heat transfer measurements (Stanton numbers and Stanton number ratios) at 21 spanwise locations for X = 1.15, 1.25, 1.4, 1.6, 1.8, 2.0 m (X = streamwise distance from origin of velocity boundary layer), and fluid mechanics measurements at x/d = 5.2, 41.9, 82.9, 109.2, with a wall jet at a vortex downwash, and blowing ratio increasing from 0 to 3.5.

3. <u>Experiment 3</u>

Heat transfer measurements at 21 spanwise locations for X = 1.15, 1.25, 1.4, 1.6, 1.8, 2.0 m, and fluid mechanics measurements at x/d = 41.9, with a wall jet at a vortex upwash, and blowing ratio increasing from 0 to 6.7.

4. <u>Experiment 4</u>

Fluid mechanics measurements at x/d = 41.9 with a wall jet at the downwash of a vortex having greater circulation of streamwise vorticity (created with a larger vortex generator) than in Experiment 1, and blowing ratio increasing from 0 to 3.0.

In the remainder of the thesis, Chapter II discusses the experimental apparatus and procedures used in the study, Chapter III gives results of the experiments, and Chapter IV gives a summary and conclusions. Appendix A contains additional experimental results, Appendix B describes software used in the study, Appendix C gives uncertainty levels for the parameters measured and calculated in the

experiments, and Appendices D and E give brief descriptions of the author's contributions to several related projects.

II. EXPERIMENTAL APPARATUS AND PROCEDURES

A. WIND TUNNEL AND TEST SECTION

The wind tunnel used in this study is located in the laboratories of the Department of Mechanical Engineering of the Naval Postgraduate School. It is described in full detail, including qualification, in Reference 2. The wind tunnel contains a variable speed centrifugal blower, diffuser, header box with a honeycomb and three screens, a nozzle, and a test section. A portion of the test section bottom wall has a uniformly heated surface instrumented with thermocouples. The test section is a rectangular duct 3.05 m in length and 0.61 m wide, with an adjustable top wall which allows pressure gradient control. For the present study, a zero pressure gradient was maintained without a vortex or injection to within 0.007 inches of water differential pressure along the test plate. Air speed through the test section is adjustable from 5 to 40 m/s. The freestream turbulence intensity is about 0.1% at a free-stream velocity of 30 m/s. The test section also contains a single row of 13 injection (wall jet) holes to provide film cooling by means of an injection system described in Reference 2. Figure 2 (from Reference 2) shows the test section coordinate system, including the location of the vortex generator, unheated starting length, injection holes,

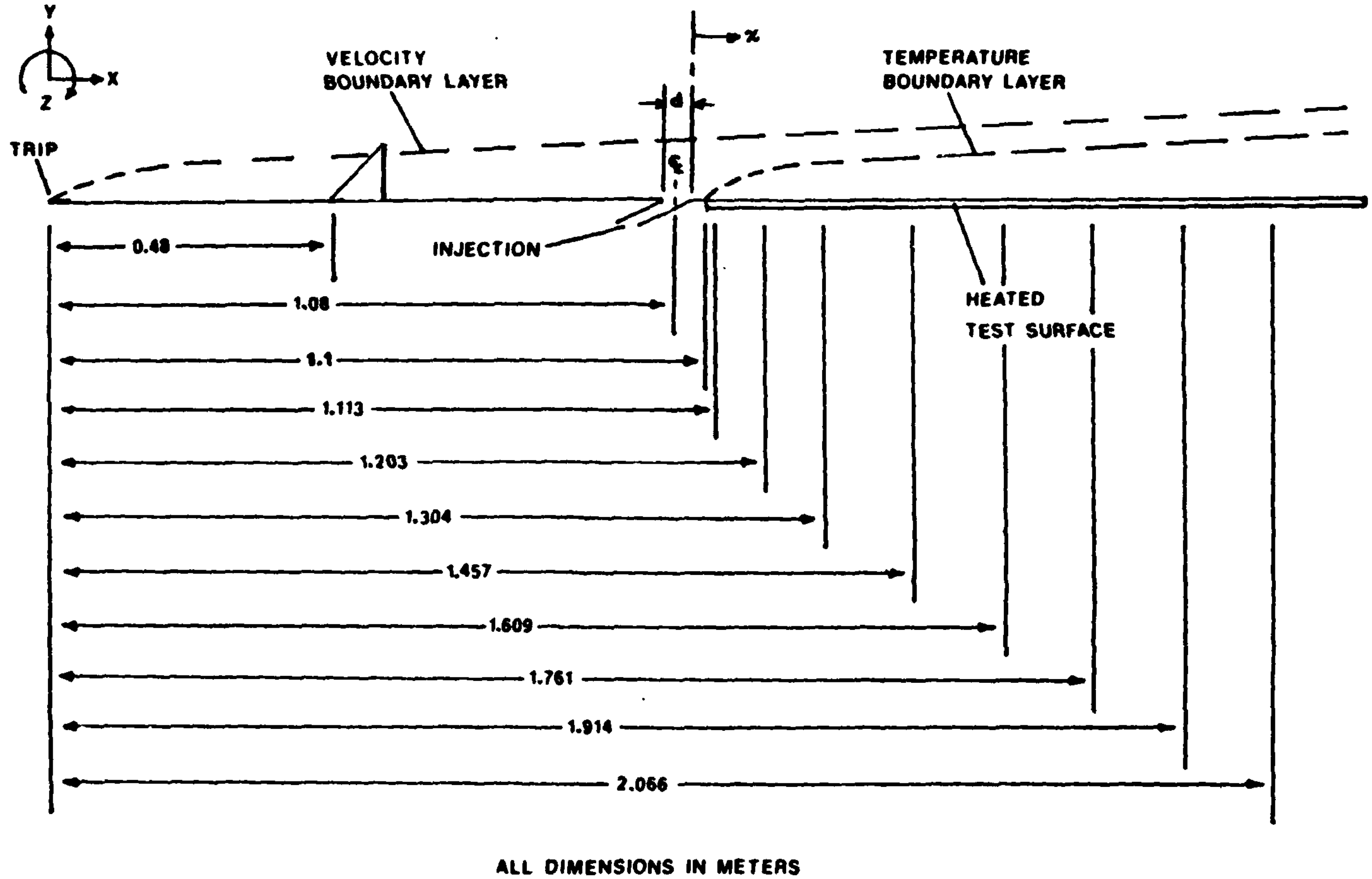

Figure 2. Wind Tunnel Test Section and Coordinate System

and thermocouple rows. The wind tunnel has removable side wall ports for access to the test section. The top wall is fitted with sealable openings to allow insertion of thermocouples and pressure probes. The injection system provides injectant at temperatures above ambient. Injection tubing is inclined at 30° to horizontal, and injection holes have a diameter of 0.95 cm with three diameter spacing between adjacent holes.

B. DATA ACQUISITION SYSTEM

Voltages used to measure pressures and temperatures are taken by a Hewlett-Packard 3497A Data Acquisition/Control Unit, with a 3498A extender. These units were controlled by a Hewlett Packard series 300 Model 9000-236 computer.

C. VORTEX GENERATORS

Of the four vortex generators constructed for the study of Reference 2, numbers 2 and 3 were used in the present study. Dimensions are indicated in Figure 3. Generators are constructed of thin stainless steel, and oriented with respect to flow as indicated. In each of the experiments described in Chapter III, vortex generator position is determined by the location of the upper right corner of the generator base with respect to the tunnel floor centerline.

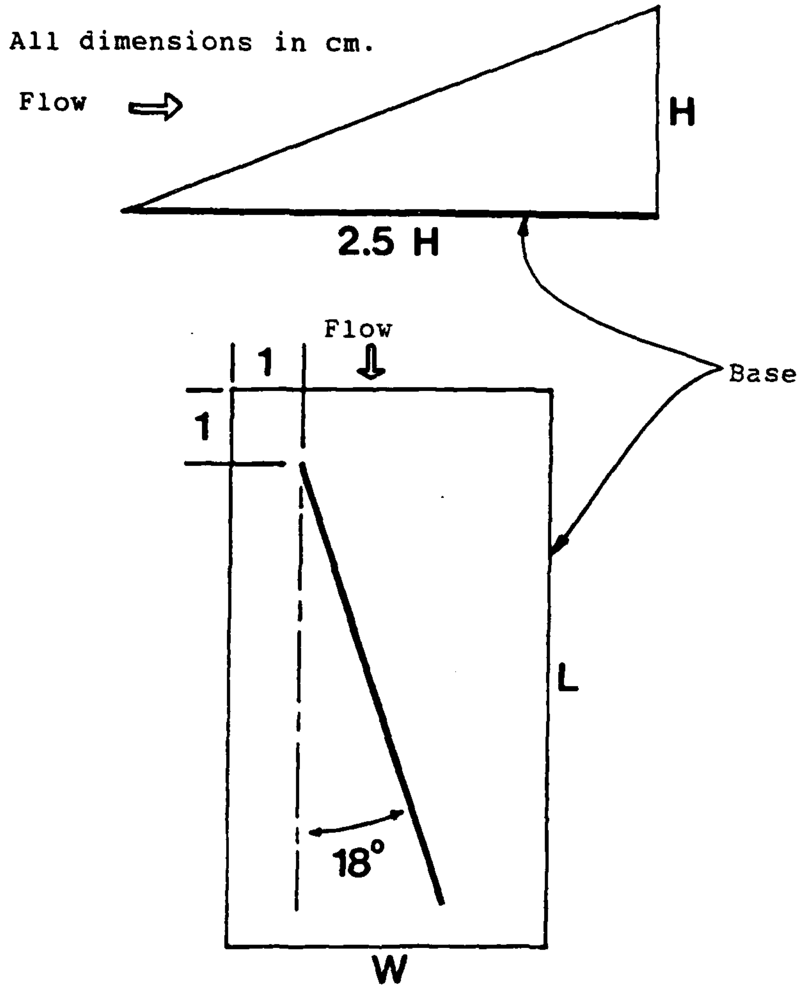

	H	2.5 H	L	W
#2	3.0	7.50	9.50	4.50
#3	5.0	12.50	14.00	6.00

Figure 3. Vortex Generator Geometry

D. MEAN VELOCITY MEASUREMENTS

Mean velocity data were taken at four streamwise locations using a United Sensor five-hole pressure probe. The four streamwise probe positions are:

probe position A: x/d = 5.2 (x = 0.0494 m, X = 1.129 m)

probe position B: x/d = 41.9 (x = 0.398 m, X = 1.478 m)

probe position C: x/d = 82.9 (x = 0.788 m, X = 1.808 m)

probe position D: x/d = 109.2 (x = 1.037 m, X = 2.117 m)

Here, x is length from the downstream edge of the injection holes and d is injection hole diameter, while X is streamwise length from the velocity boundary layer origin. Probe calibration and measurement procedures are described in detail in References 3 and 22. The five-hole probe is connected to five Calesco LCVR pressure transducers, each with a 2 cm of water differential pressure full scale range. Each transducer is connected to a Calesco Carrier Demodulator, used to convert transducer output to DC voltage. Pressures were sampled over an 800 point matrix covering a 12 cm x 22 cm area in the y-z plane (Figure 2) at each Streamwise location. This was accomplished by mounting the probe on a two-component automated traversing device constructed in the Naval Postgraduate School engineering shop. The device is driven by two Superior Electric Company electric motors. The three mean velocity components and total pressures were computed from transducer voltages using software developed

specifically for this purpose. This software is described in Appendix B. A full 800 point sample required ~3.5 hours.

E. HEAT TRANSFER MEASUREMENTS

Copper-constantan thermocouples manufactured by Omega Engineering Company were used to measure heated plate and air temperatures. Twenty-one spanwise thermocouples at six streamwise positions were used in Stanton number determination, using the data acquisition system described above. Thermocouple installation in the wind tunnel test section is described in detail in Reference 4. Stanton numbers and Stanton number ratios were computed using software developed especially for this purpose, which is also described in Appendix B.

III. RESULTS

A. INTRODUCTION

The results presented in this chapter describe the influence of a wall jet on a streamwise vortex embedded in a turbulent boundary layer with zero pressure gradient. The wall jet was placed either at the vortex downwash or upwash. All experiments were performed with a freestream velocity (U_∞) of 9.9 m/s. Individual experimental runs are listed in Tables 1 and 2. Using the apparatuses described in Chapter II, and the software listed in Appendix B, pressure and surface heat transfer measurements were made. From these measurements, various parameters characterizing the vortex/jet interactions were determined. These included: (1) injection parameters such as blowing ratio and momentum flux ratio, (2) distributions in the y-z plane of total pressure and mean velocity components, from which streamwise vorticity, circulation, and vortex dimensions were calculated, and (3) wall heat transfer parameters such as Stanton numbers and Stanton number ratios.

1. Calculation of Streamwise Vorticity (ω_x) and Circulation (Γ)

The traversing mechanism described in Chapter II was used to move the five-hole pressure probe over a matrix of 800 evenly spaced points in the y-z plane, at a given streamwise location (x/d). The matrix was dimensioned with

TABLE 1

WIND TUNNEL FLUID MECHANICS EXPERIMENTS(1)

Run # (Date/ Time)	(2) Probe Posit.	Vortex Gen. #	(3) Vortex Gen. Posit.	m	Data Disk File Name
51288.0855	B	2	0	0	VEL4
52788.1615	B	2	0	1.5	VEL10
50588.1115	B	2	0	2.1	VEL0
60388.1735	B	2	0	2.6	VEL15
60888.0715	B	2	0	3.0	VEL21
52988.1145	B	2	0	3.5	VEL12
53188.1705	B	2	0	4.375	VEL13
60188.0735	B	2	0	4.8	VEL14
71488.0625	A	2	0	0	VEL31
71488.1355	A	2	0	2.1	VEL32
71488.1725	A	2	0	3.5	VEL33
72188.0755	B	2	0	0	VEL40
72188.1145	B	2	0	2.1	VEL41
72288.0825	B	2	0	3.5	VEL42
71588.0625	C	2	0	0	VEL34
71588.1055	C	2	0	2.1	VEL35
71588.1705	C	2	0	3.5	VEL36
71688.0825	D	2	0	0	VEL37
71688.1205	D	2	0	2.1	VEL38
71788.0915	D	2	9	3.5	VEL39
70588.1645	B	2	+5.08	0	VEL24
70688.1625	B	2	+5.08	1.0	VEL26
70688.2025	B	2	+5.08	2.0	VEL27
70788.0625	B	2	+5.08	3.0	VEL28
71288.1405	B	2	+5.08	5.0	VEL29
71388.0635	B	2	+5.08	6.7	VEL30
60488.1035	B	2	0	0	VEL16
60688.1735	B	2	0	1.5	VEL17
60788.0625	B	2	0	2.1	VEL18
60788.1255	B	2	0	2.6	VEL19
60788.1715	B	2	0	3.0	VEL20

(1) $U_\infty = 9.9$ m/s

(2) A: x/d = 5.2
B: x/d = 41.9
C: x/d = 82.9
D: x/d = 109.2

(3) z dimension in cm; tunnel centerline is z = 0.

TABLE 2

WIND TUNNEL WALL HEAT TRANSFER EXPERIMENTS[1]

Run # (Date/Time)	[2]Vortex Gen Posit.	m	Data Disk File Names
72988.2030	None	0	TEMP01,INP01,STAN01
72988.1915	0	0	TEMP0,INP0,STAN0
72988.1215	0	2.1	TEMP21,INP21,FCD21, STAN21,STR21
72988.1135	0	3.5	TEMP35,INP35,FCD35, STAN35,STR35
72988.1630	+2	0	TEMP02,INP02,STAN02
72988.1430	+2	3.0	TEMP30,INP31,FCD31, STAN30,STR30

[1]Vortex generator number 2, U_∞ = 9.9 m/s

[2]z dimension in cm; tunnel centerline is z = 0.

20 vertical (y) points and 40 horizontal (z) points. The distance between matrix points was $\Delta y = \Delta z$ = 0.508 cm (0.2 in). Coordinate ranges were z = -12.7 cm (-5.0 in) to 7.112 cm (2.8 in), and y = 0.4445 cm (0.175 in) to 10.0965 cm (3.975 in). Voltages acquired with the probe and data acquisition system were used with the software to calculate total pressure (P_{tot}) and mean velocity components (U_x,U_y,U_z) at each matrix point as described in References 3 and 22.

a. Streamwise Vorticity

Streamwise vorticity (ω_x) is given by

$$\omega_x = \frac{\partial U_z}{\partial y} - \frac{\partial U_y}{\partial z} \tag{1}$$

Streamwise vorticity was estimated using a finite difference equation for each matrix point (y,z) given by

$$\omega_x(y,z) = \frac{U_z(y+\Delta y,z)-U_z(y,z)}{2\cdot\Delta y} - \frac{U_y(y,z+\Delta z)-U_y(y,z)}{2\cdot\Delta z} \tag{2}$$

Matrix points were close enough together that no spline fit was needed to calculate derivatives.

b. Circulation

Circulation (Γ) over a region A in the y-z plane is given by

$$\Gamma = \oint_A \omega_x \, dA \; . \tag{3}$$

The region of matrix points over which this integration was estimated was defined using a threshold vorticity of 20% of the maximum vorticity of an undisturbed (m = 0) vortex. This was determined in experimental run #51288.0855 (vortex generator #2 at z = 0, m = 0) to be approximately 100 s^{-1}. This value for threshold vorticity was used in all experimental runs. Circulation was calculated by summing

vorticity at each matrix point above the threshold and then multiplying the result by $\Delta y \times \Delta z = 0.258\ cm^2$ ($0.04\ in^2$).

2. Dimensionless Circulation Parameters

Two dimensionless circulation parameters were defined for this study. The first is given by

$$ND\Gamma_1 = \Gamma/[U_\infty(y_{core} + z_{core})/2] \tag{4}$$

where y_{core} and z_{core} are vortex core dimensions, defined below. This parameter relates vortex circulation (or strength) to vortex core size. Thus if $ND\Gamma_1$ remains constant at different blowing ratios and/or streamwise locations, it indicates that circulation and core size are changing (increasing, decreasing) proportionately. The second dimensionless circulation parameter is given by

$$ND\Gamma_2 = \Gamma/(U_c \cdot d) \ , \tag{5}$$

where U_c is wall jet (injection) velocity. This parameter relates the strength of the vortex to the strength of the jet. Thus if increasing jet momentum results in decreased circulation, then $ND\Gamma_2$ will decrease as m increases. With no injection ($m = 0$), $ND\Gamma_2$ is not used.

3. Vortex Structural Parameters

In this study, vortices behave similar to the "combined vortices" described in Reference 19. In this model,

the vortex center is the point in the y-z plane where streamwise vorticity is maximum. The vortex "core" extends radially in the y-z plane from the center to the point of maximum tangential velocity ($\sqrt{U_y^2 + U_z^2}$). The core contains most of the total streamwise vorticity. Average vortex core radii in the horizontal and vertical directions (z_{core}, y_{core}) are then calculated using

$$z_{core} = (A + B)/2 , \tag{6}$$

and

$$y_{core} = (C + D)/2 . \tag{7}$$

In equations (6) and (7), A and B are the distances in the -z and +z directions from the vortex center to the point of maximum secondary flow velocity ($\sqrt{U_y^2 + U_z^2}$), while C and D are the same quantities in the -y and +y directions.

4. <u>Wall Heat Transfer Parameters</u>

The method of acquiring raw data for and calculating Stanton numbers is discussed in detail in References 2 and 4. Stanton numbers for different situations are denoted with different symbols: (1) St: Stanton number with vortex and injection; (2) Stv: Stanton number with vortex and no injection; (3) Sto: Stanton number with no vortex and no injection (baseline).

5. <u>Method of Presentation of Results</u>

For each experimental run, software listed in Appendix B was used to generate six plots: (1) secondary flow vectors, physically depicting secondary flow motion from the vortex in the y-z plane; (2) streamwise vorticity (ω_x) contours in the y-z plane; (3) total pressure contours (P_{tot}) in the y-z plane; (4) streamwise velocity component (U_x) in the y-z plane; (5) secondary flow velocity magnitude ($\sqrt{U_y^2 + U_z^2}$) distribution, horizontally (z direction) from the vortex center in the y-z plane; and (6) Stanton number ratios: St/Sto, Stv/Sto, St/Stv.

6. <u>Description of the Experiments</u>

The study consisted of four experiments, each focusing on a different aspect of vortex/jet interactions. The individual experimental runs are listed in Tables 1 and 2.

The first experiment consisted of observing fluid mechanics parameters at x/d = 41.9 (x = streamwise length from edge of wall jet, d = wall jet (injection) hold diameter, 0.95 cm), with the jet opposing the vortex downwash. The objective of the experiment was to determine the effect of jet momentum on the vortex in general and the downwash region in particular. Individual experimental runs were performed at m = 0, 1.5, 2.1, 2.6, 3.0, 3.5, 4.375, and 4.8. Without blowing, the vortex downwash generally causes thinning of the boundary layer and the formation of a local "hot spot" on a heated wall [Refs. 5,6].

Prior to conducting the first experiment, the optimal position of the jet relative to the downwash was determined. It was chosen to be the position at which circulation of streamwise vorticity was lowest with $m = 2.1$. This occurred when the vortex generator was placed on the tunnel centerline ($z = 0$) with injection through the center wall jet. Fluid mechanics data were taken at $x/d = 41.9$.

The second experiment consisted of observing fluid mechanics and wall heat transfer parameters at various streamwise locations, with the jet again opposing the vortex downwash. The objective of the experiment was to determine the streamwise development of the flow with vortex/jet interaction, and how that development is influenced by blowing ratio. Fluid mechanics parameters were determined at $x/d = 5.2$, 41.9, 82.9, and 109.2, for $m = 0$, 2.1, and 3.5. Spanwise Stanton number ratios were determined at $X = 1.15$, 1.25, 1.6, 1.8, and 2.0 meters ($x/d = 7.37$, 17.89, 33.68, 54.74, 75.79, and 96.84), for $m = 2.1$ and 3.5. These blowing ratios were chosen because the first experiment indicated $m = 3.0$ to be significant in regard to the influence of the jet on the vortex.

The third experiment consisted of observing fluid mechanics and wall heat transfer parameters with the jet at the vortex upwash. The vortex generator was placed at $z = +5.08$ cm (+2.0 in), and injection was from the center hole. It was expected that opposite trends from those of

the first experiment would be observed. Fluid mechanics measurements were made at $x/d = 41.9$ with $m = 0$, 1.0, 2.0, 3.0, 5.0, and 6.7. Stanton number ratios were determined at $X = 1.15$, 1.25, 1.4, 1.6, 1.8, and 2.0 meters ($x/d = 7.37$, 17.89, 33.68, 54.74, 75.79, and 96.84), with $m = 3.0$.

The fourth experiment consisted of observing fluid mechanics parameters at $x/d = 41.9$ and $m = 0$, 1.5, 2.1, 2.6, and 3.0, with the jet again opposing the vortex downwash. This experiment was similar to the first experiment (up to $m = 3.0$), except that a vortex having greater undisturbed circulation was used. The objective of the experiment was to compare results with the first experiment in order to determine the effect of vortex strength (characterized by circulation) on vortex/jet interaction.

The results of the experiments are now discussed.

B. EXPERIMENTAL RESULTS FOR INJECTION AT VORTEX DOWNWASH: x/d = 41.9 (PROBE POSITION B); UNDISTURBED VORTEX CIRCULATION = 1.48×10^{-1} m^2/s.

For this experiment, vortex generator #2 was placed at the tunnel centerline and injection was through the center wall jet, so that the jet opposed the vortex downwash. The five-hole pressure probe was placed at $x/d = 41.9$ (position B). Blowing ratio was increased from 0 to 4.8. Results are summarized in Table 3 and Figures 4-27 in this chapter, and Figures 89-113 in Appendix A.

Figures 4-12 indicate that the wall jet significantly influences the vortex fluid mechanics parameters (ω_x, Γ, V,

TABLE 3

FLUID MECHANICS MEASUREMENTS FOR VORTEX GENERATOR #2 AT TUNNEL CENTERLINE, PROBE POSITION B*

m	V_{max} (m/s)	U_{xmax} (m/s)	ω_{xmax} (1/s)	$\left(\frac{Y_{core}+Z_{core}}{2}\right)$ (cm)	Y_{cen} (cm)	Z_{cen} (cm)	Γ (m^2/s)	$ND\Gamma_1$	$ND\Gamma_2$	P_{max} (Pa)
0	2.63	10.0	725.9	0.89	2.98	-4.57	0.148	0.0168	-	60.4
1.5	2.46	10.3	665.3	0.89	3.49	-3.56	0.135	0.0153	0.955	63.8
2.1	1.77	10.0	459.5	1.02	3.49	-3.05	0.108	0.0107	0.546	59.8
2.6	1.64	10.4	304.4	1.27	3.49	-3.05	0.099	0.0079	0.405	64.4
3.0	1.68	10.9	187.1	1.91	2.48	-3.05	0.077	0.0041	0.273	69.4
3.5	1.62	11.5	146.6	2.03	2.98	-2.03	0.058	0.0029	0.175	78.0
4.375	1.46	12.7	136.5	2.41	2.98	-1.52	0.048	0.002	0.117	94.1
4.8	1.52	12.6	128.3	1.65	2.98	-1.52	0.047	0.0029	0.103	93.7

*$x/d = 41.9$

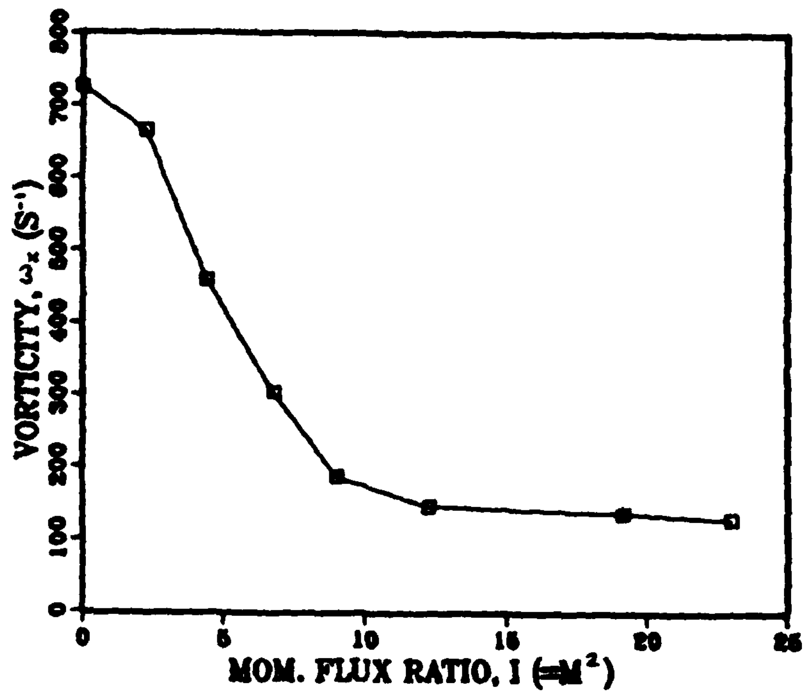

Figure 4. Maximum Streamwise Vorticity (ω_{xmax}) vs. Momentum Flux Ratio

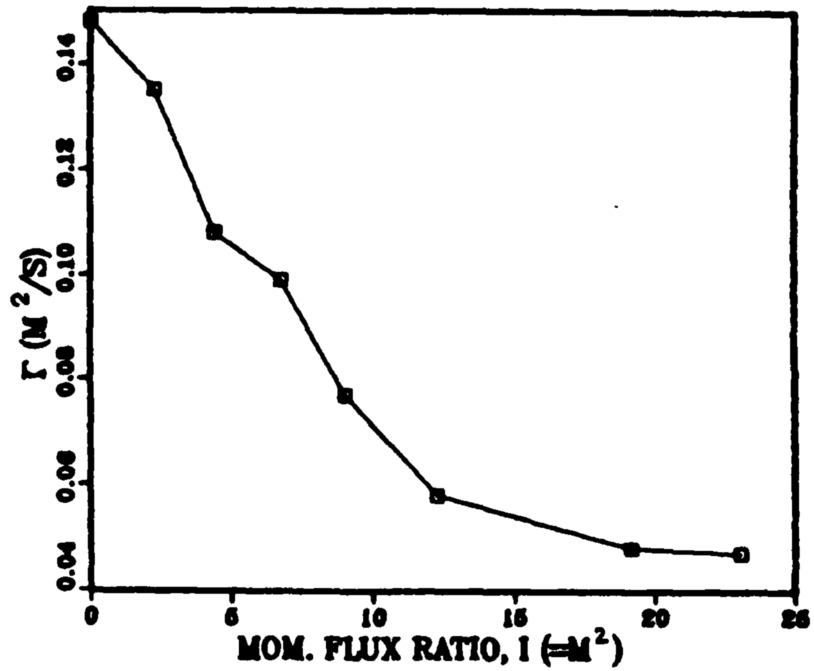

Figure 5. Circulation (Γ) vs. Momentum Flux Ratio

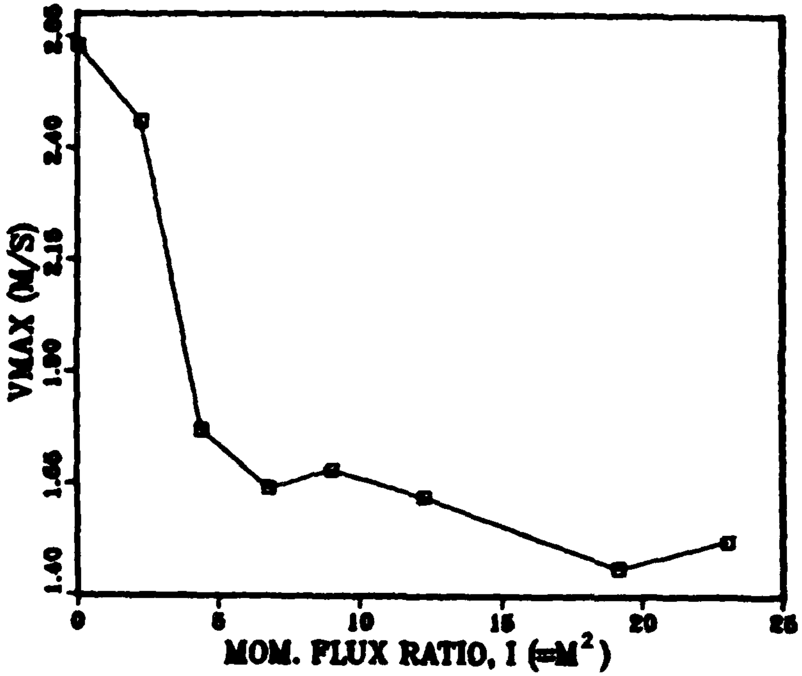

Figure 6. Maximum Secondary Flow Vector Magnitude (V_{max}) vs. Momentum Flux Ratio

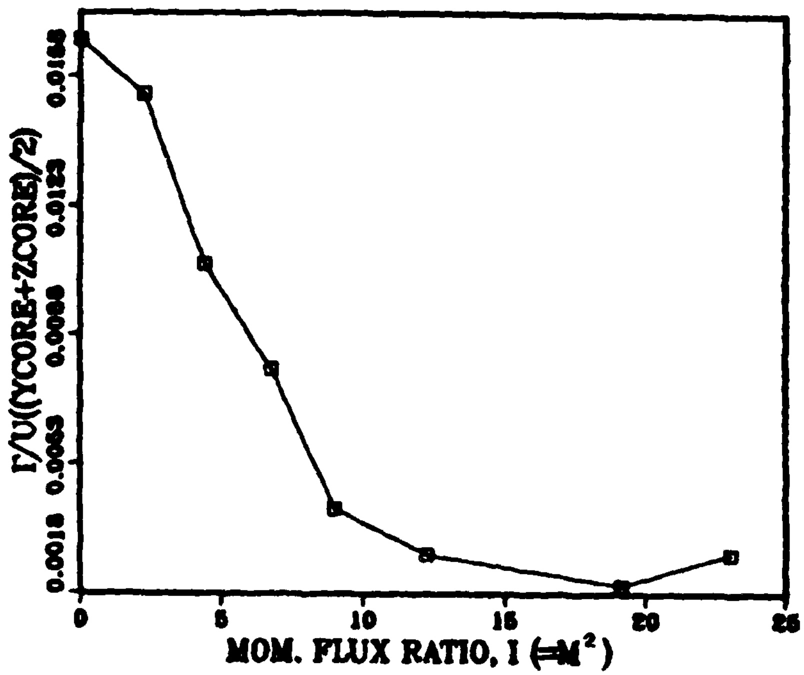

Figure 7. $ND\Gamma_1$ vs. Momentum Flux Ratio

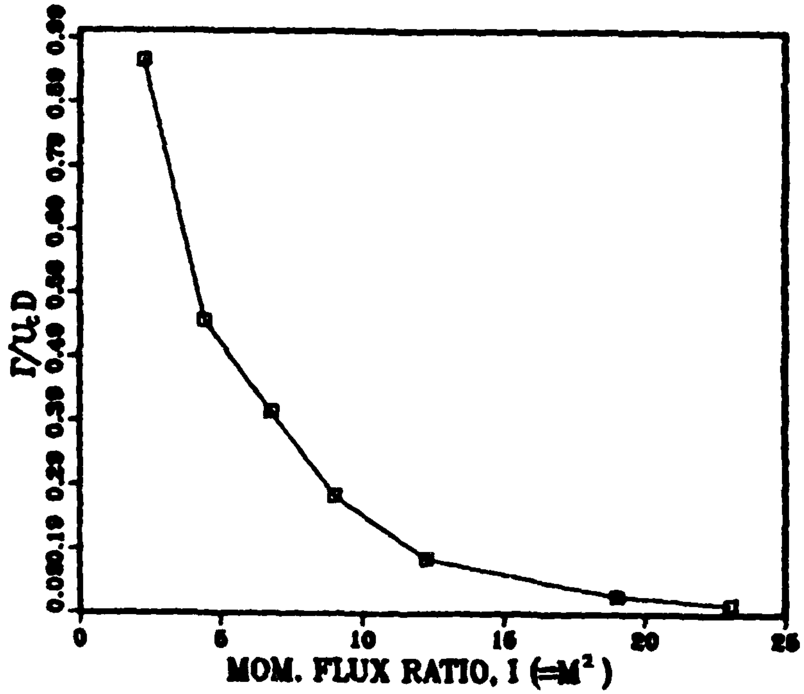

Figure 8. $ND\Gamma_2$ vs. Momentum Flux Ratio

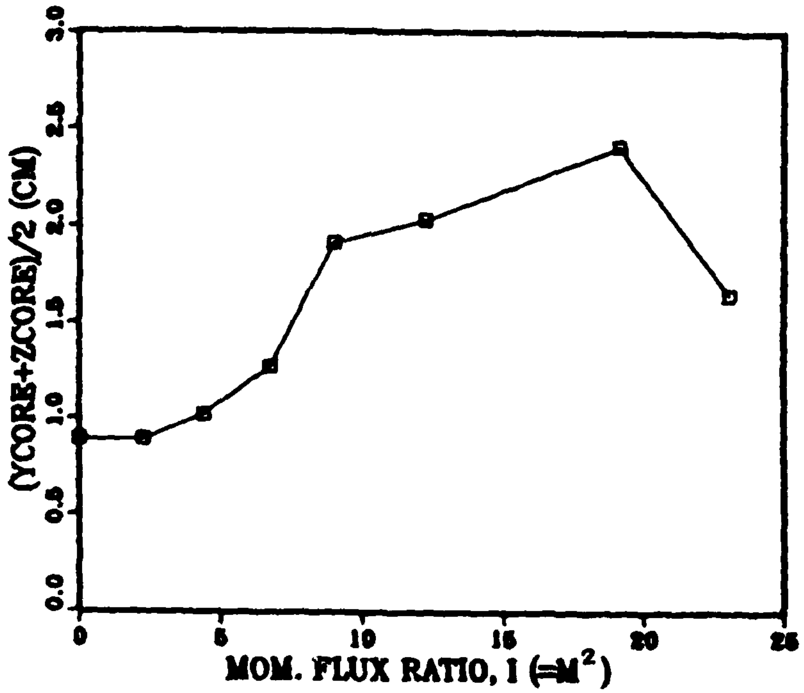

Figure 9. Average Vortex Core Radius vs. Momentum Flux Ratio

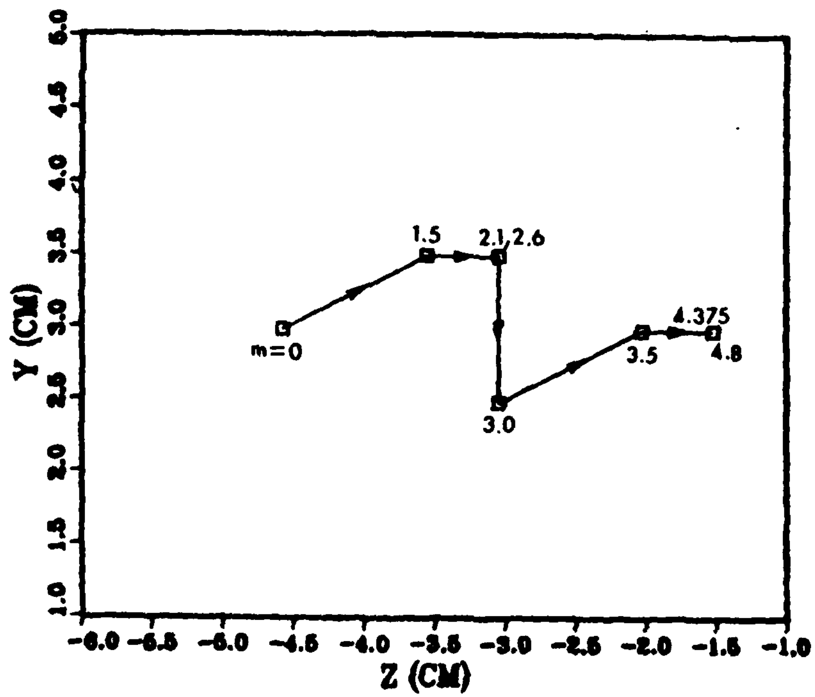

Figure 10. Vortex Center (Y_{cen},Z_{cen}) Position

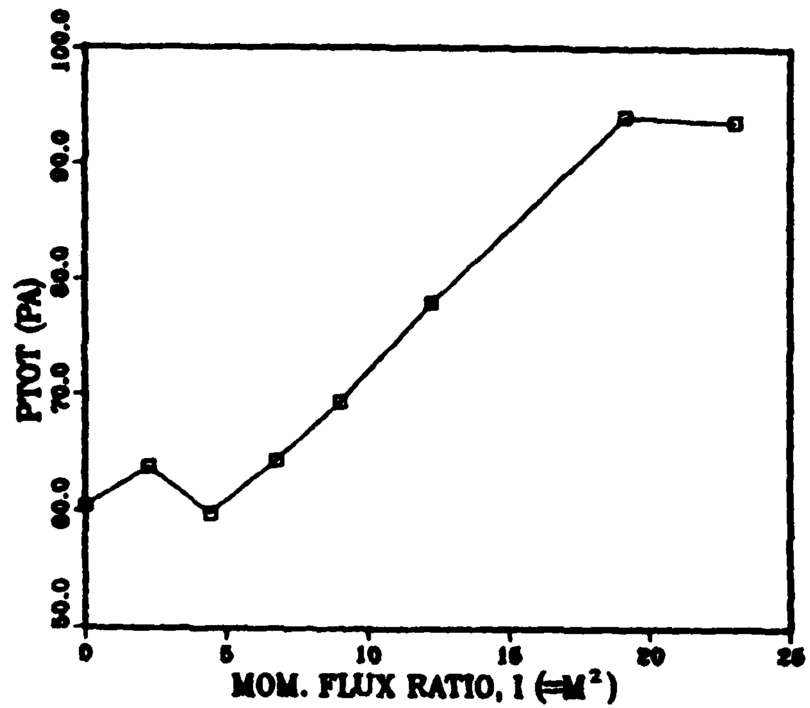

Figure 11. Maximum Streamwise Velocity Component (U_{xmax}) vs. Momentum Flux Ratio

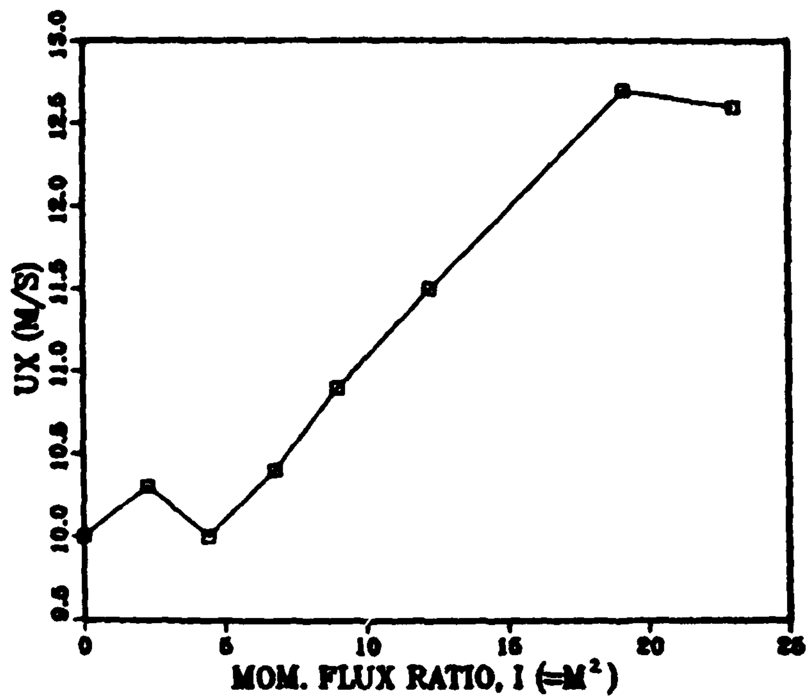

Figure 12. Maximum Total Pressure (P_{tot}) vs. Momentum Flux Ratio

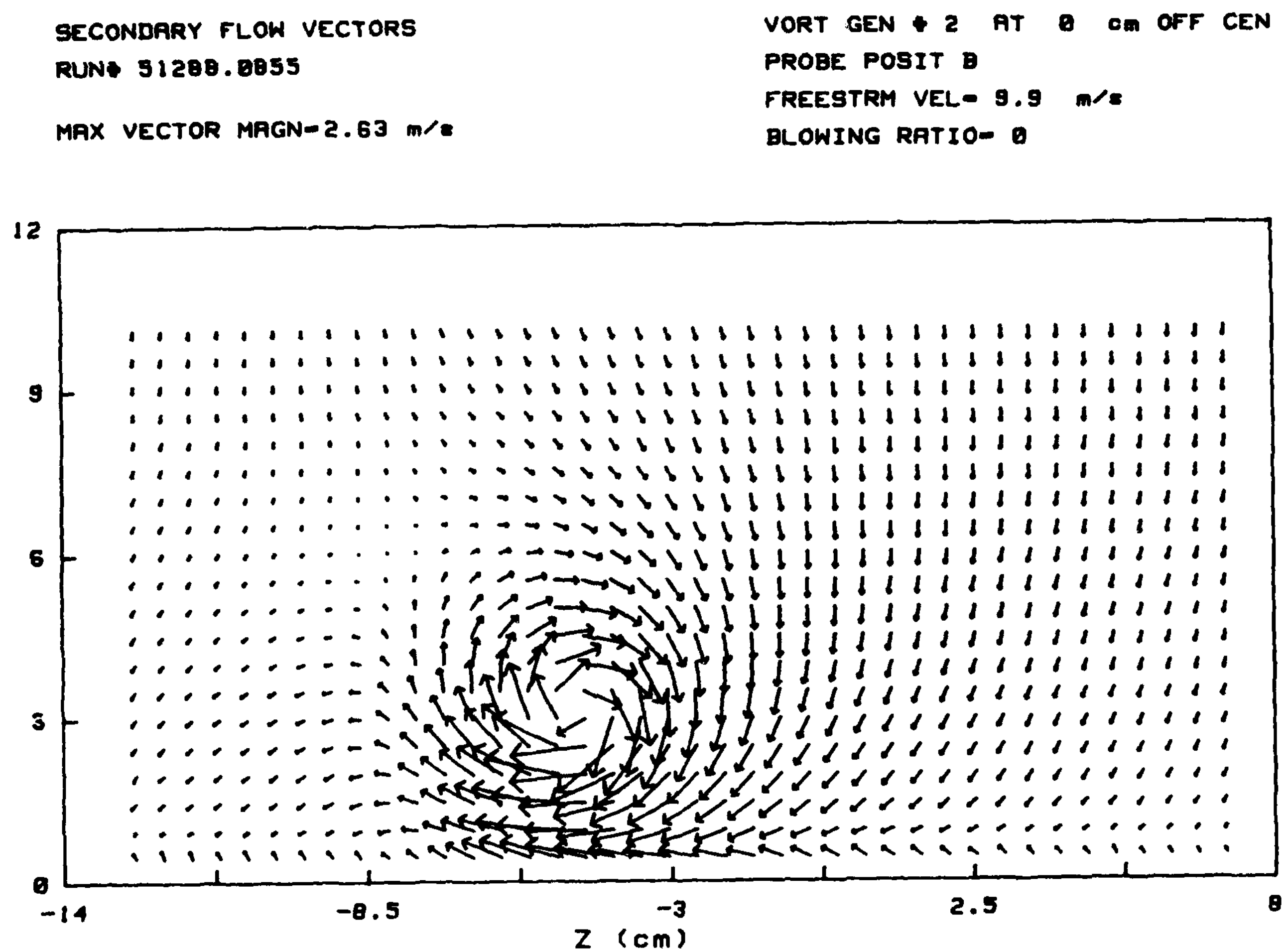

Figure 13. Secondary Flow Vectors

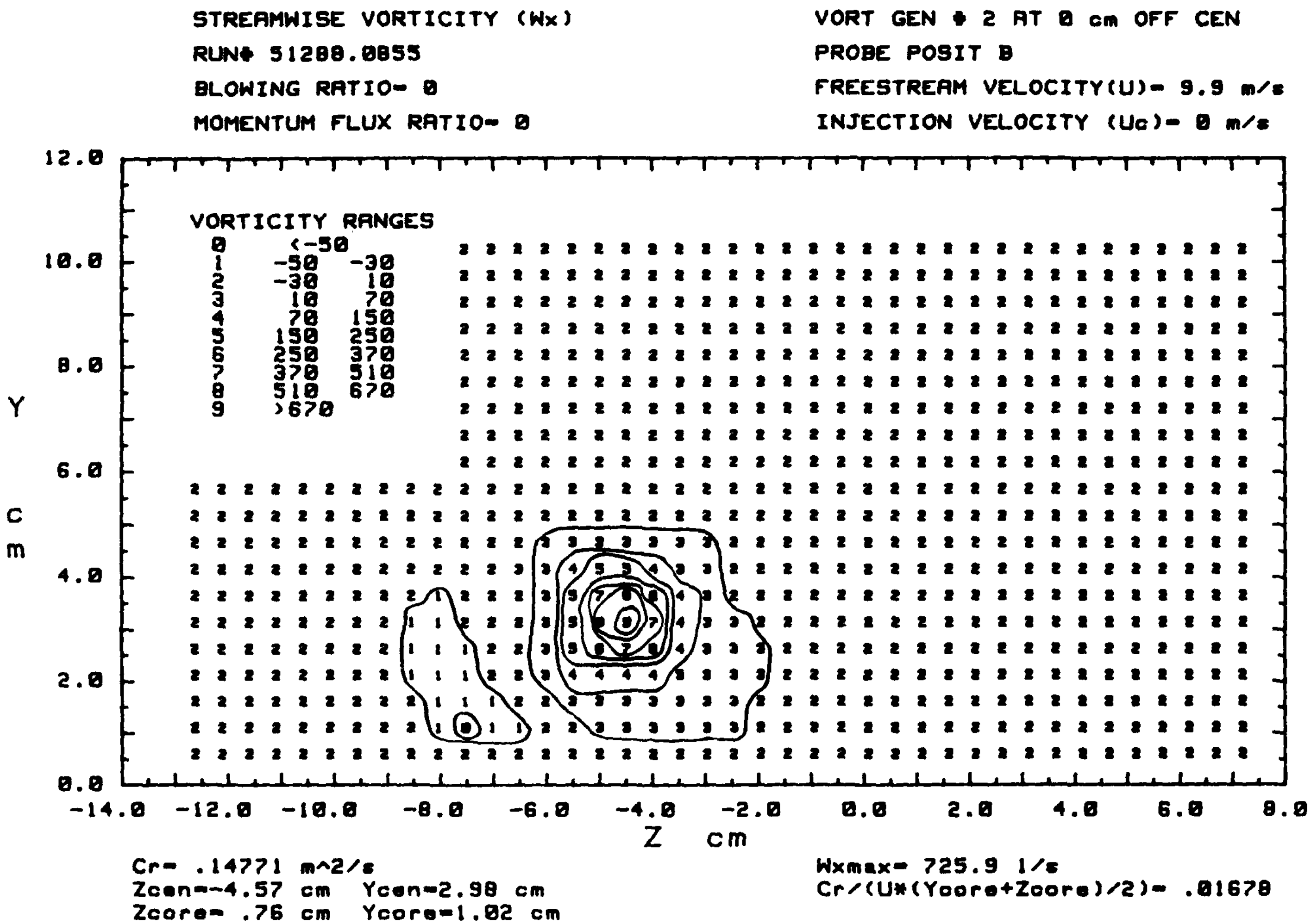

Figure 14. Streamwise Vorticity Contours

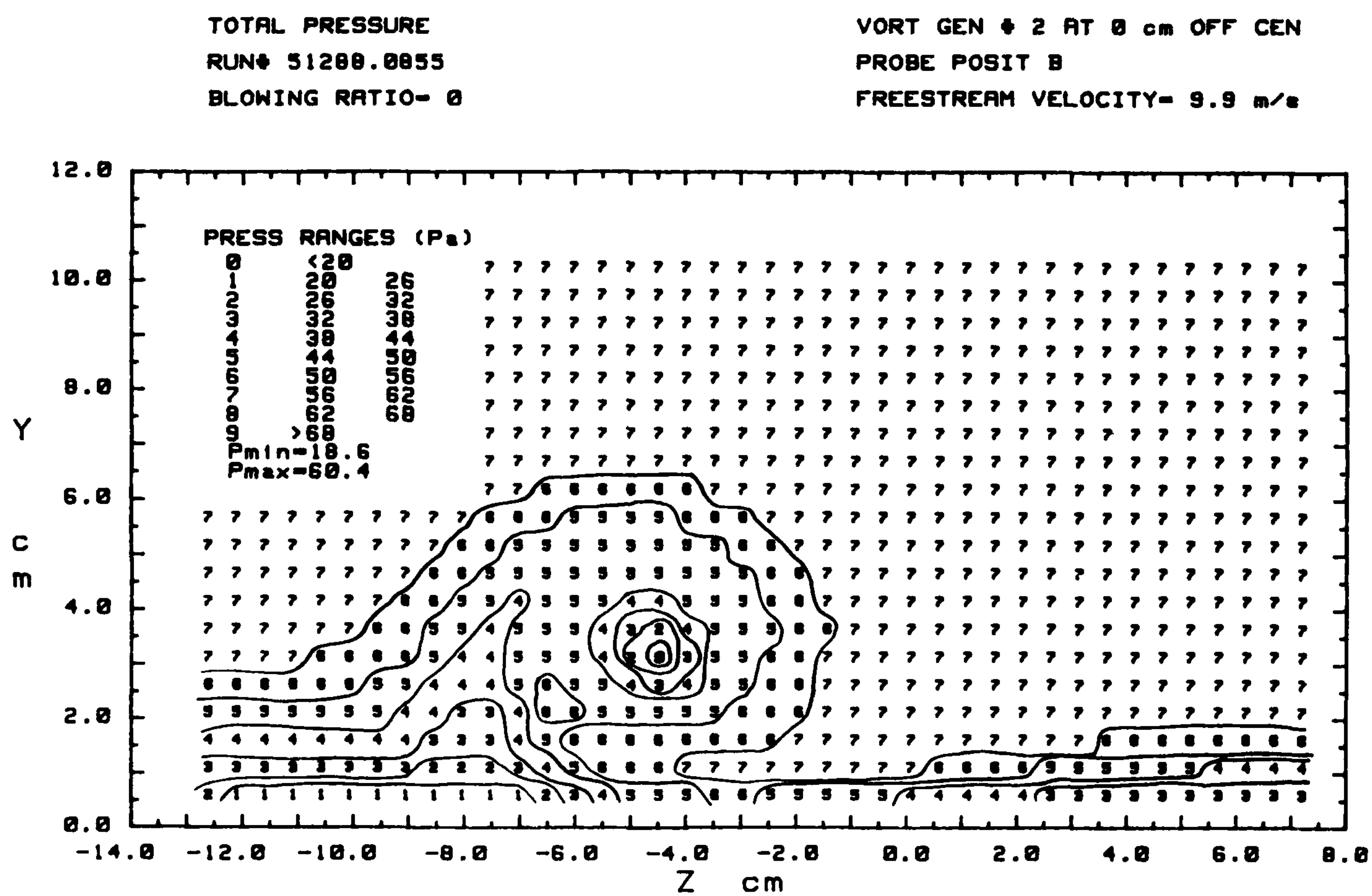

Figure 15. Total Pressure Contours

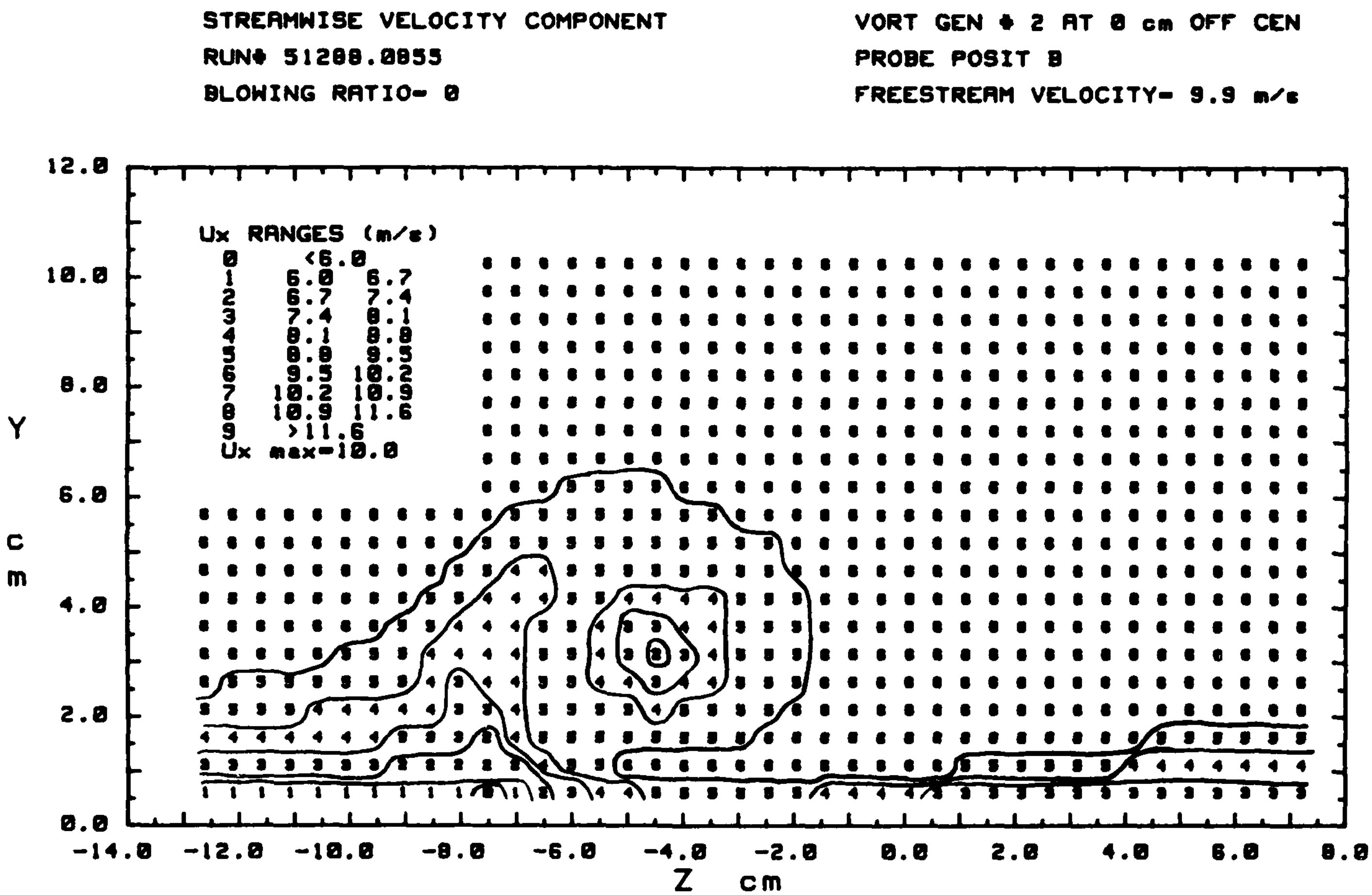

Figure 16. Streamwise Velocity Component Contours

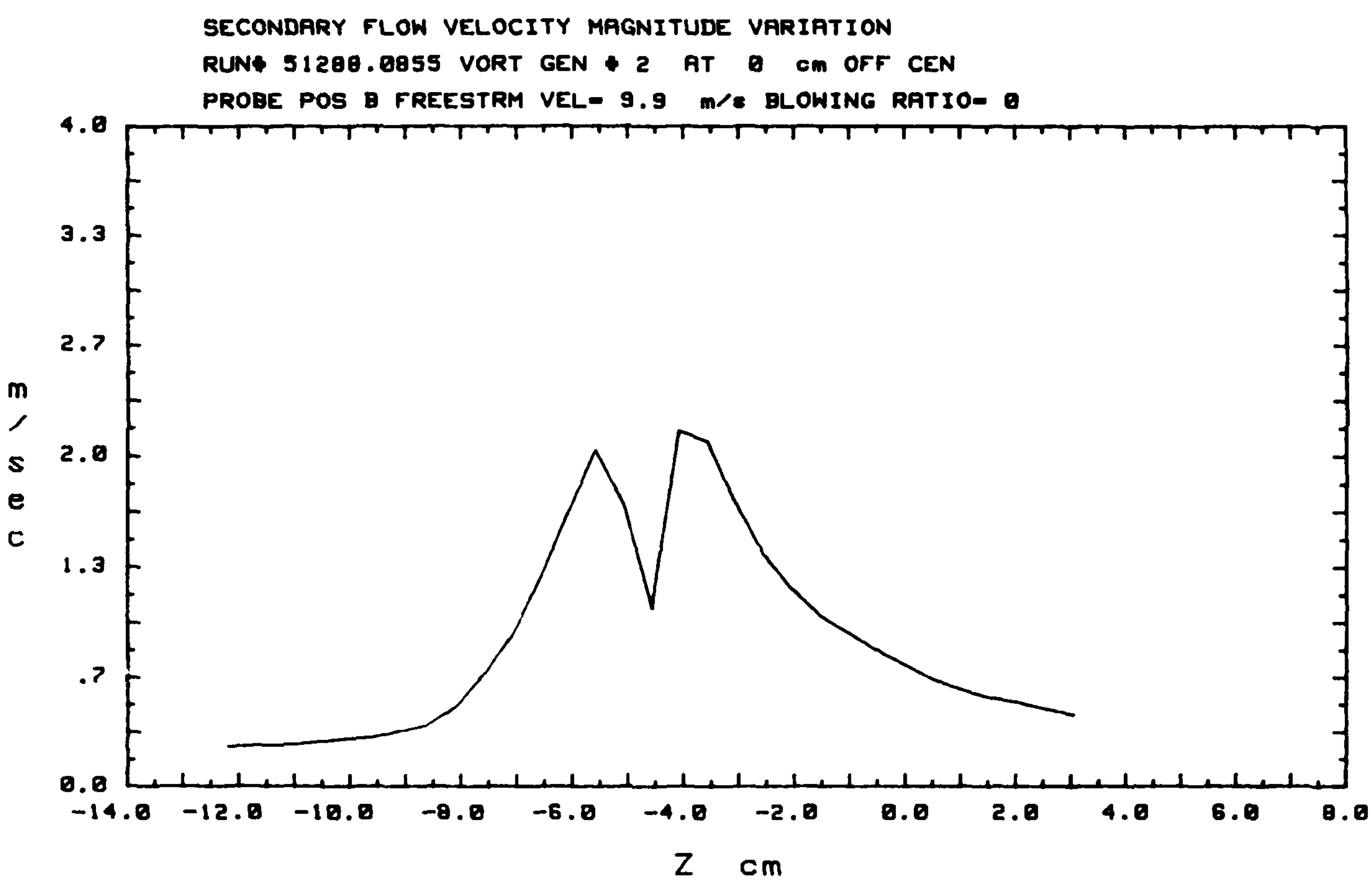

Figure 17. Secondary Flow Velocity (Radially)

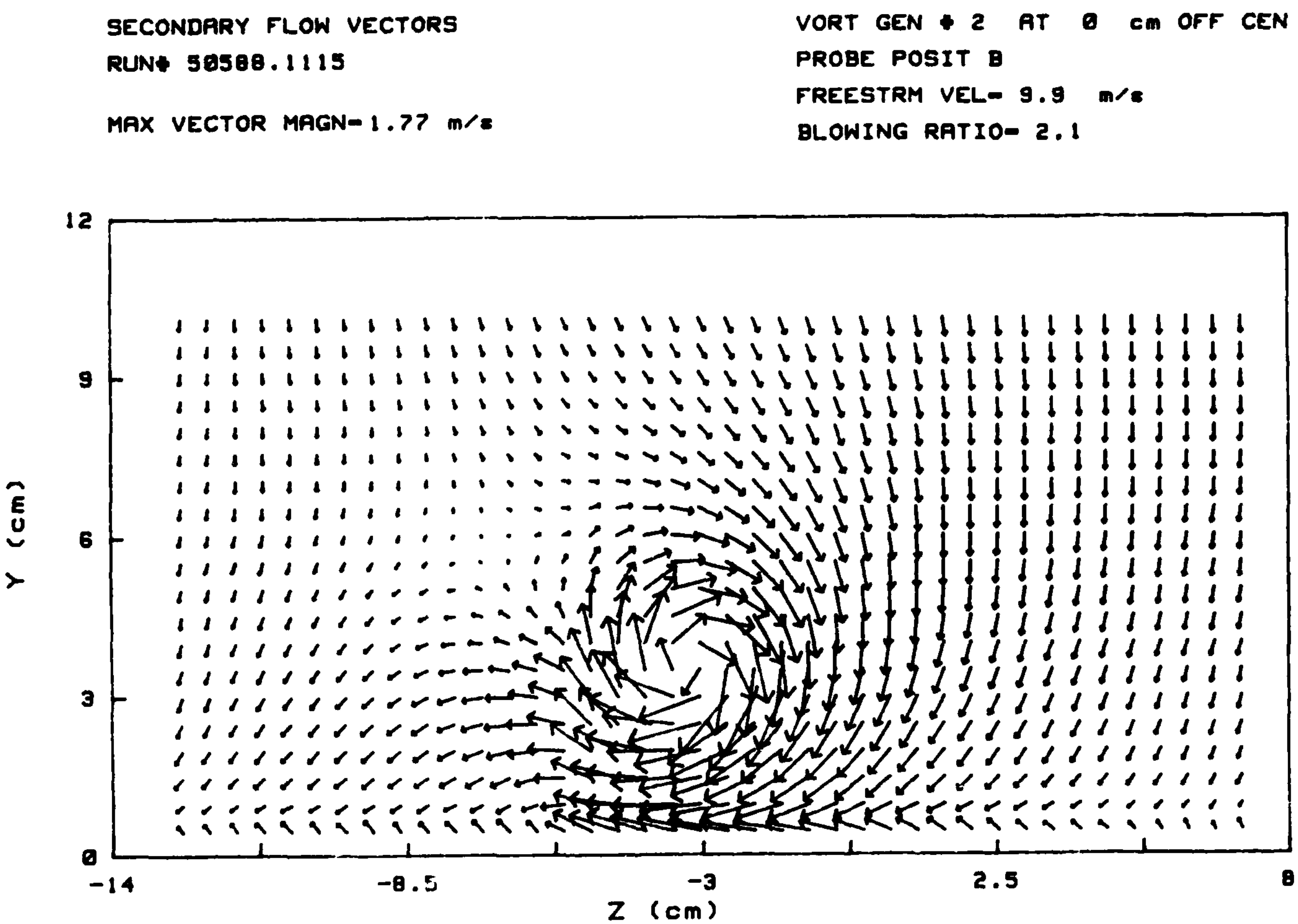

Figure 18. Secondary Flow Vectors

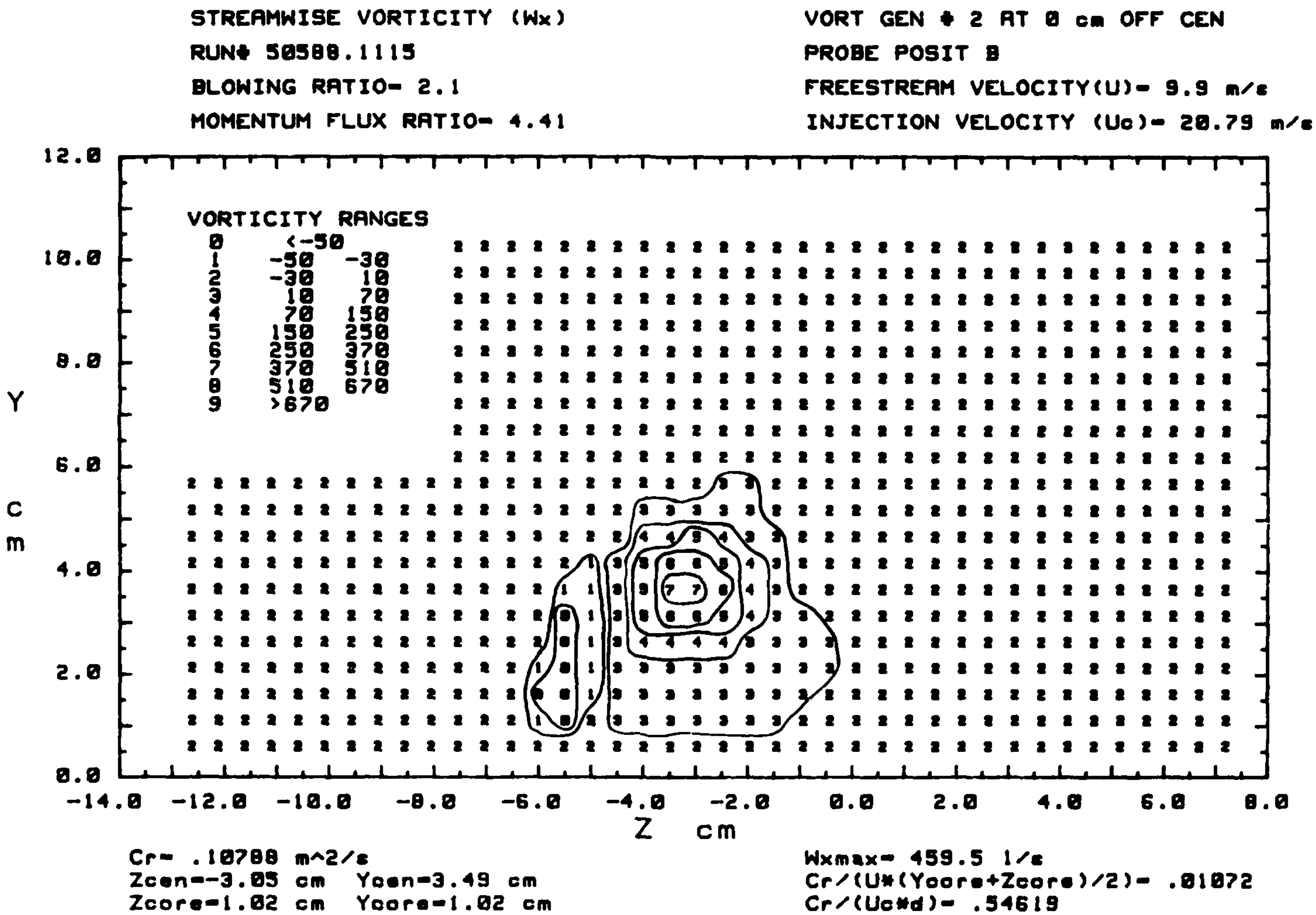

Figure 19. Streamwise Vorticity Contours

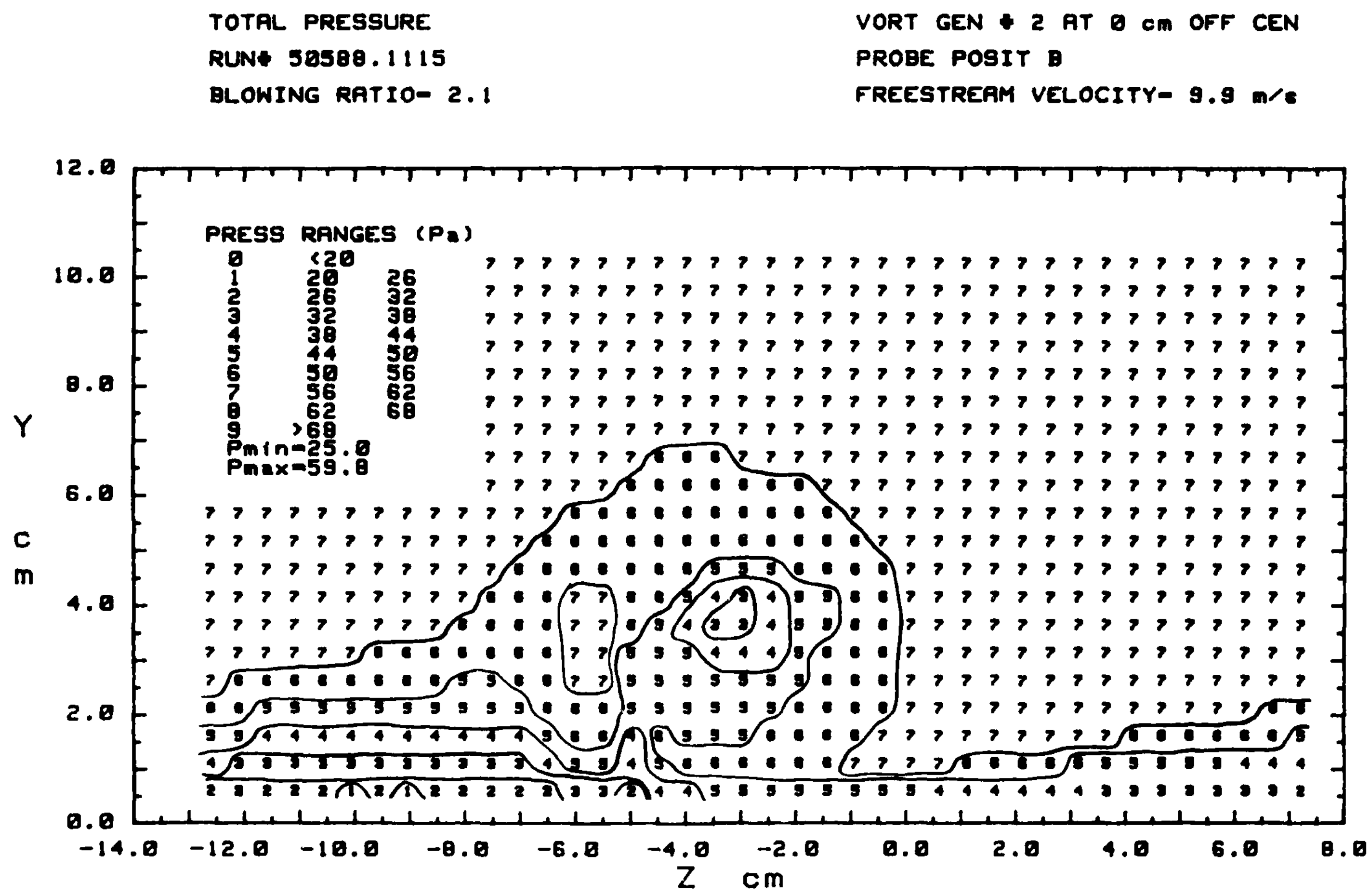

Figure 20. Total Pressure Contours

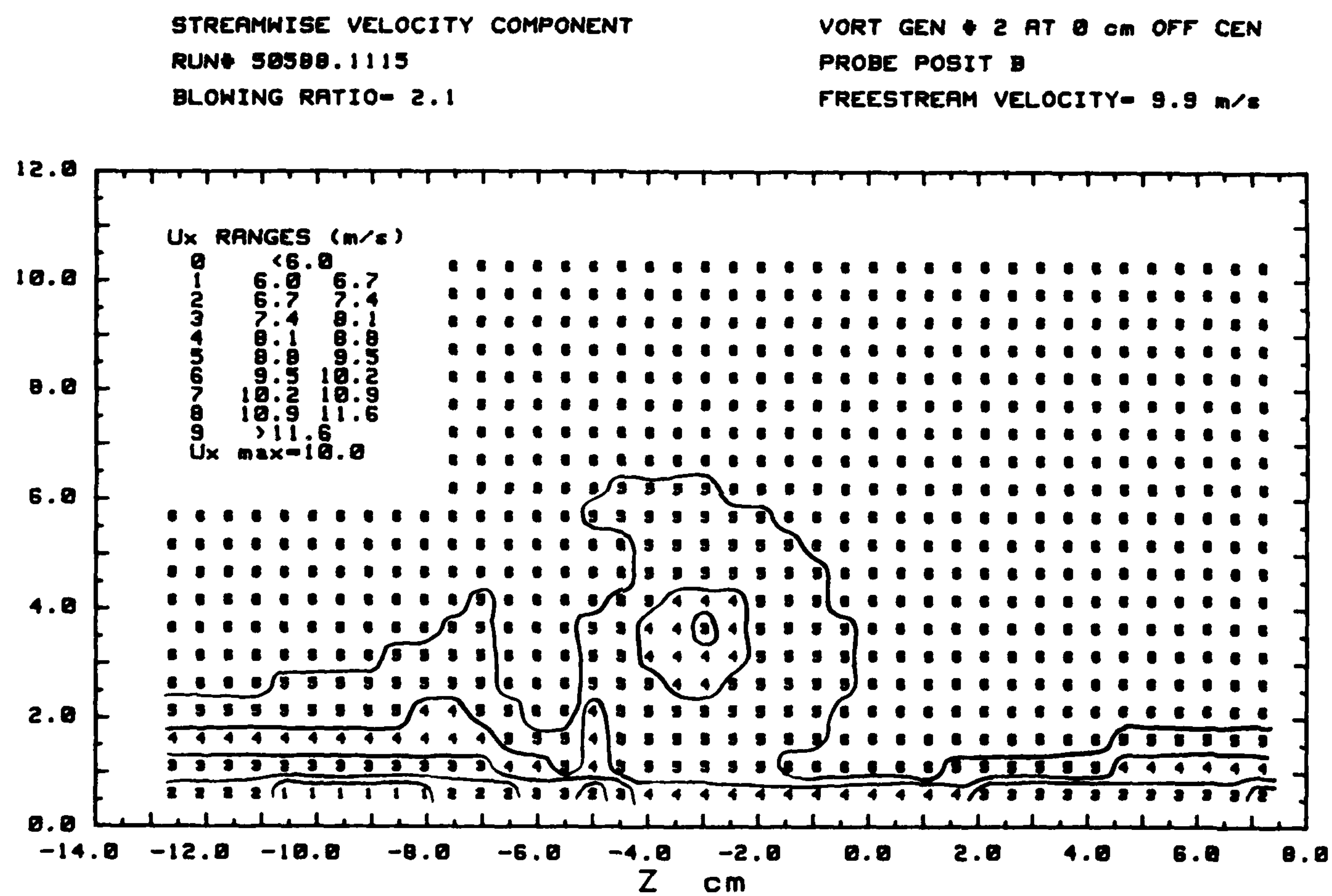

Figure 21. Streamwise Velocity Component Contours

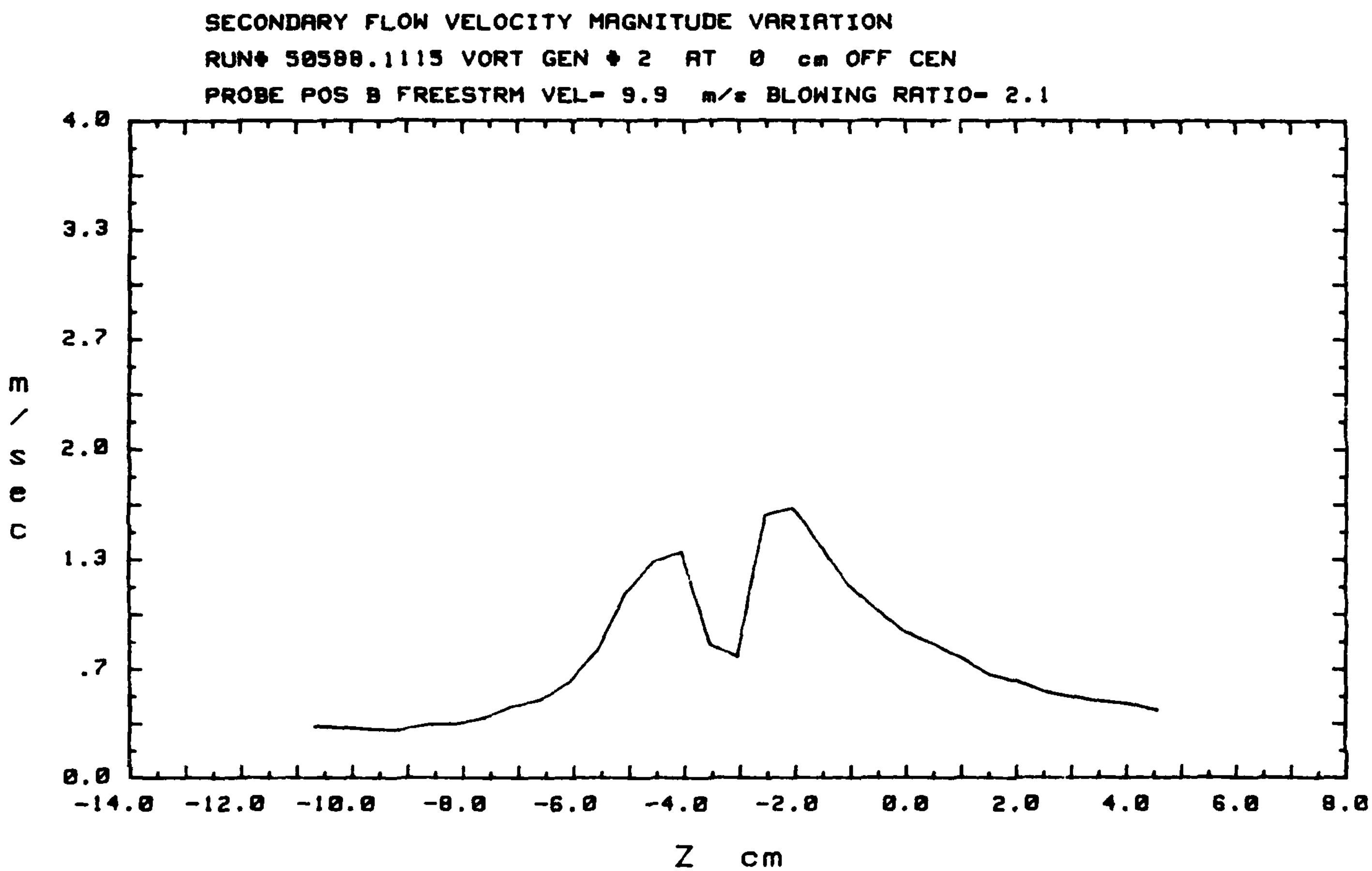

Figure 22. Secondary Flow Velocity (Radially)

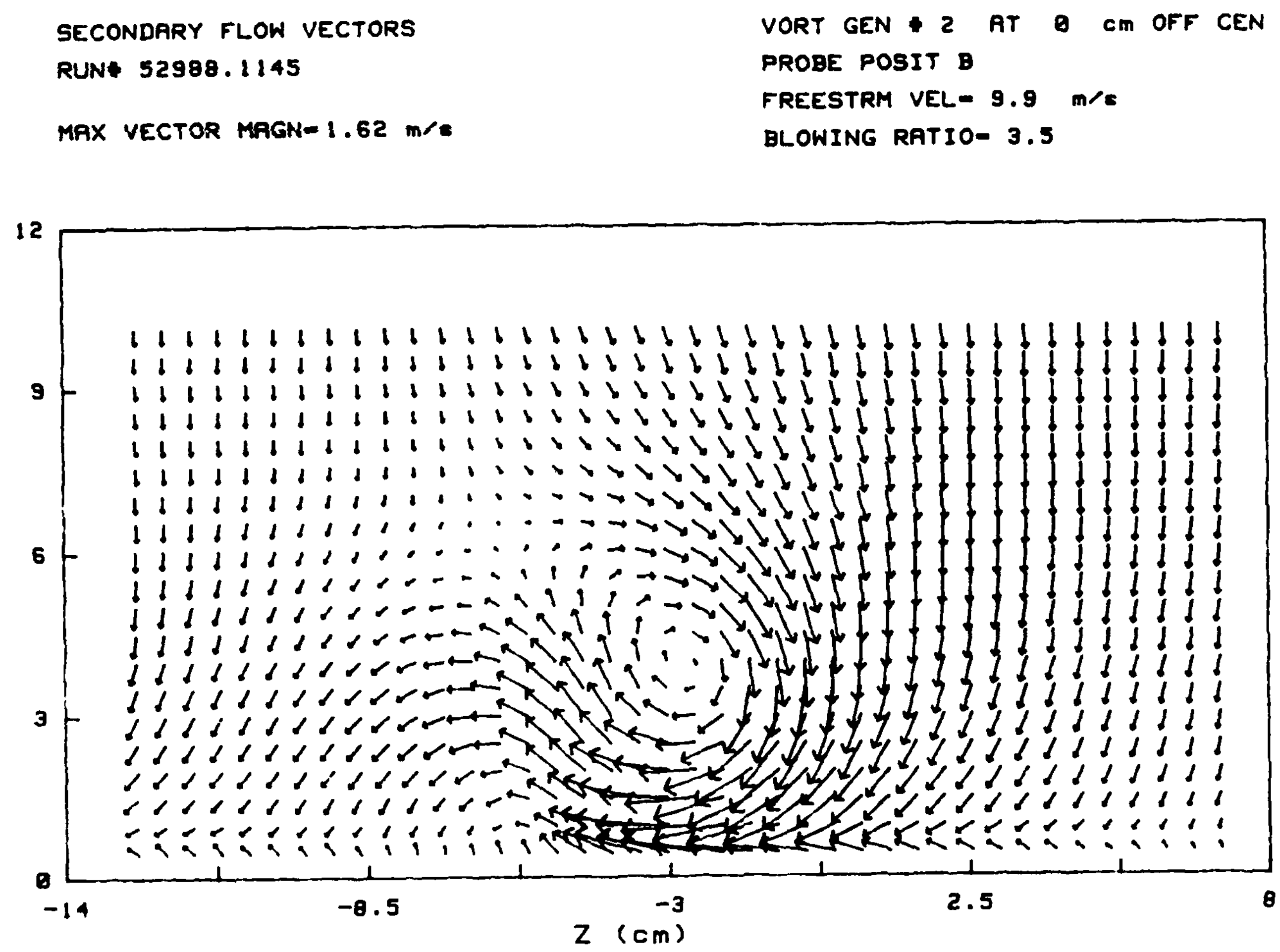

Figure 23. Secondary Flow Vectors

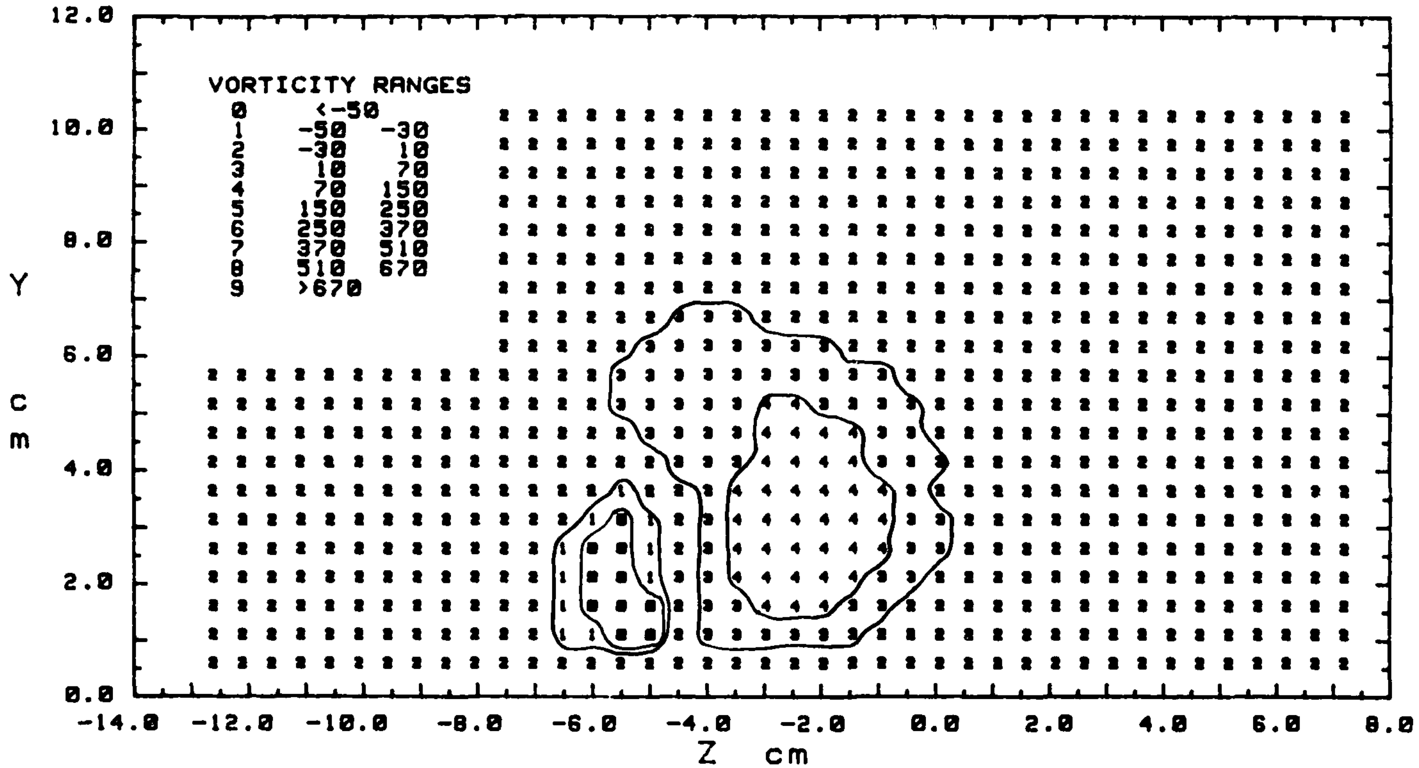

Figure 24. Streamwise Vorticity Contours

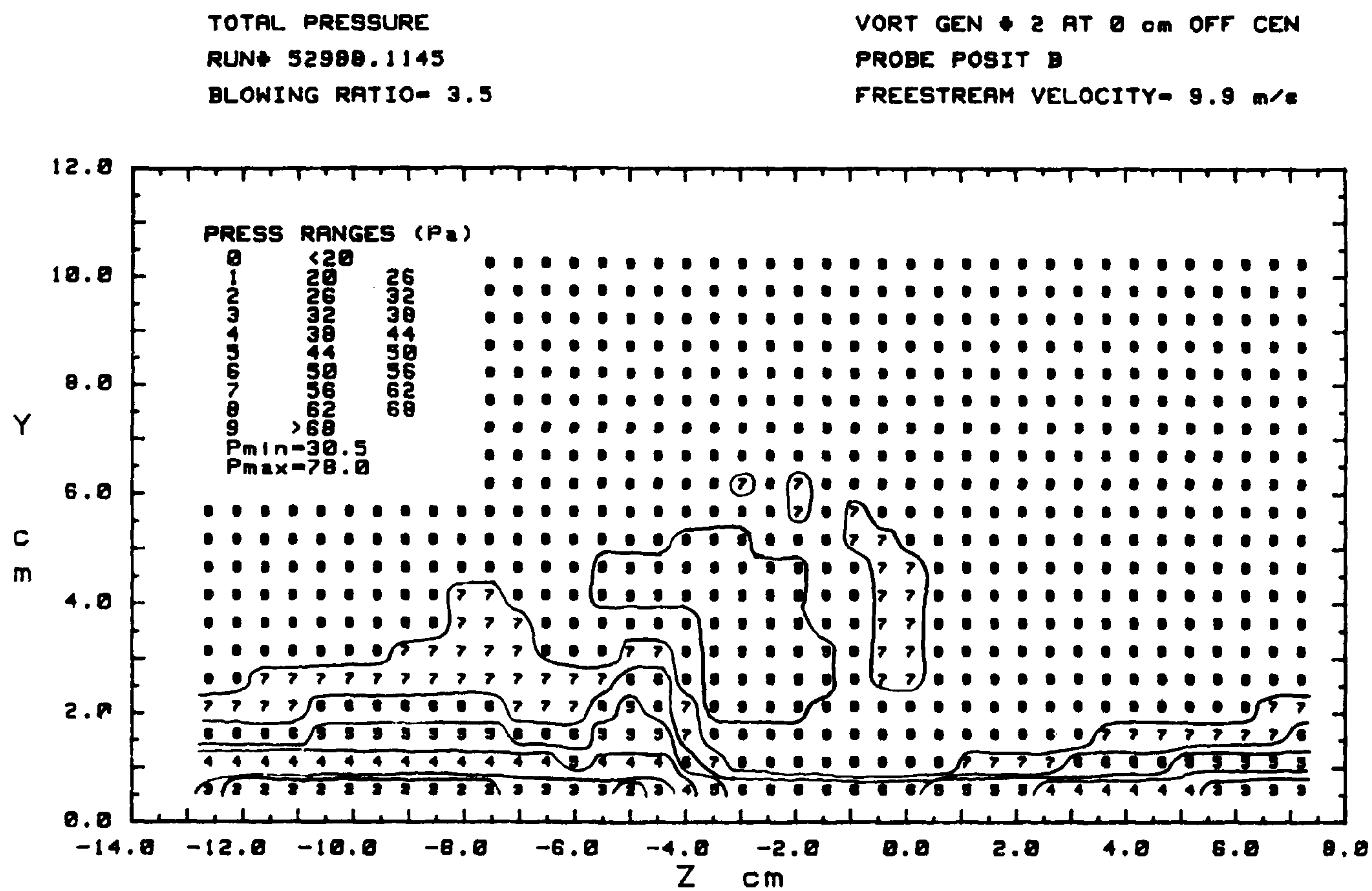

Figure 25. Total Pressure Contours

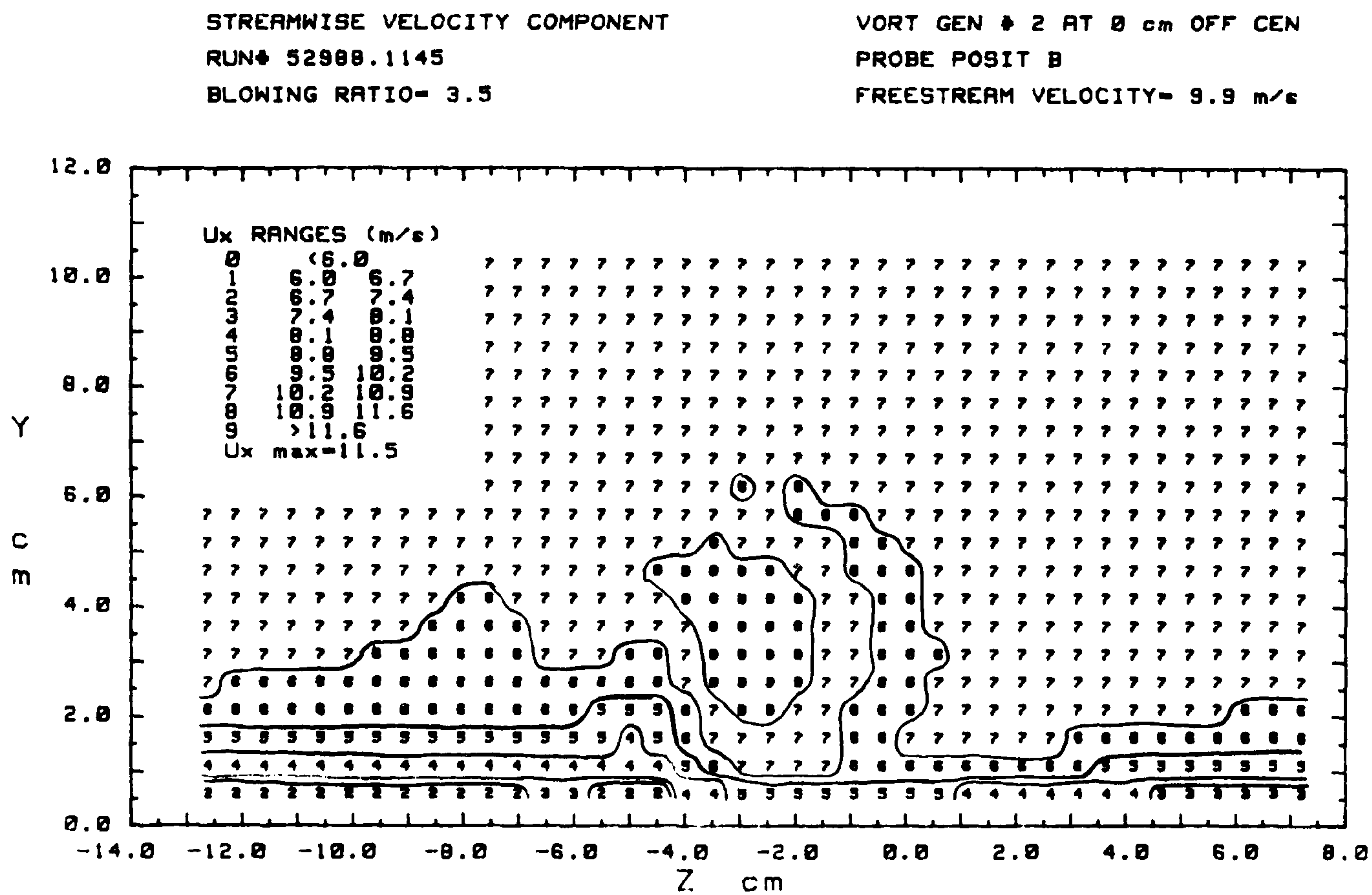

Figure 26. Streamwise Velocity Component Contours

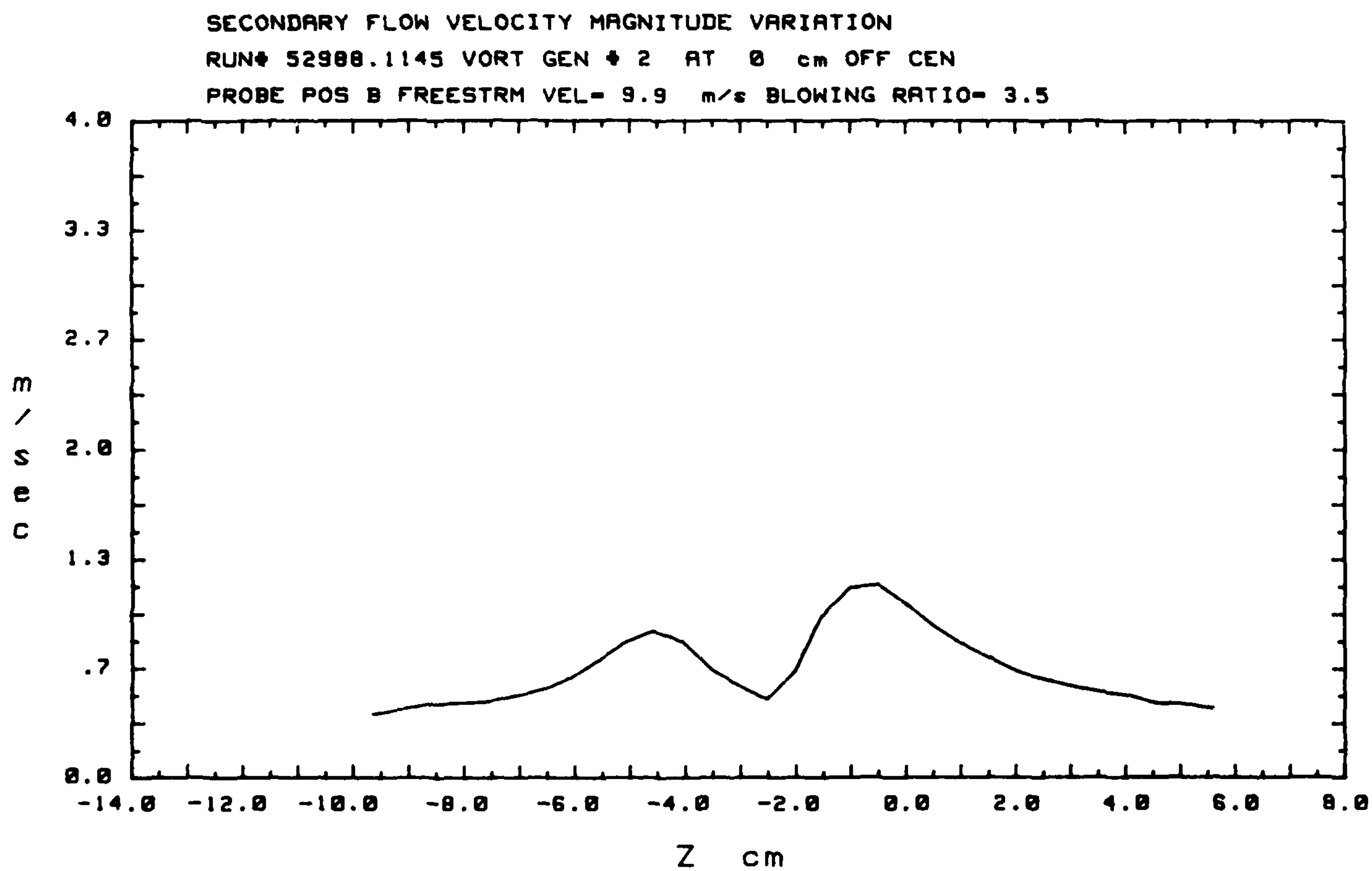

Figure 27. Secondary Flow Velocity (Radially)

$ND\Gamma_1, ND\Gamma_2$) and core dimensions up to blowing ratio 3.0; the jet induces little change beyond that blowing ratio. The effect of the jet opposing the downwash (hence opposing the rotation of secondary flow) is clear in Figures 4-8. Circulation, maximum streamwise vorticity, and maximum secondary flow vector magnitude all decrease considerably up to m = 3.0. Further decreases beyond this blowing ratio are less extreme. Structurally, the vortex core is observed to enlarge (Figure 9), while the vortex center moves first up, then down at m = 3.0 (Figure 10). It is thus apparent that a significant change in the trends of data occurs at m = 3.0. Figure 10 shows the vortex center moving toward the jet as blowing ratio increases. This is probably because the jet has lower local static pressure than the vortex. Figures 11 and 12 show that maximum streamwise velocity and maximum total pressure increase as blowing ratio increases. For m > 2.1 this maximum is due almost entirely to jet momentum.

Figures 13-27 provide clear visualization of the strong influence of the jet on the vortex. In the secondary flow vector plots (Figures 13, 18, 23) the vortex is seen to change from the circular flow pattern characterizing the familiar "swirling" conception of a vortex at m = 0, to an oval-shaped flow pattern with a large region of counter rotation to the left of the vortex at m = 3.5. Streamwise vorticity contour plots (Figures 14, 19, 24) show the growth

of the vortex core and the region of negative vorticity on the upwash (left) side with increasing m. Total pressure and streamwise velocity component contour plots (Figures 15, 16, 20, 21, 25, 26) show that the vortex becomes less clearly defined with increasing m. Beyond m = 3.0, the vortex becomes less similar to that described by the combined vortex model. This effect is especially evident from m = 4.8 data in Figures 109-113 in Appendix A. Figures 17, 22, and 27 show the maximum secondary flow velocity at horizontal (z) positions from the vortex center, indicating that the vortex "core" (region between secondary flow velocity peaks) is less distinguishable at high blowing ratio. This is made especially clear by comparing Figure 27 in this chapter with Figure 113 in Appendix A.

C. EXPERIMENTAL RESULTS FOR INJECTION AT VORTEX DOWNWASH: STREAMWISE DEVELOPMENT

For this experiment, vortex generator #2 was placed at the tunnel centerline and injection was through the center wall jet, so that the jet opposed the vortex downwash (as in the first experiment). Streamwise development measurements for blowing ratios of 0, 2.1, and 3.5 were obtained from the five-hole pressure probe at x/d = 5.2, 41.9, 82.9, and 109.2 (positions A, B, C, and D). Heat transfer measurements were made at 21 spanwise points for X = 1.15, 1.25, 1.4, 1.6, 1.8, and 2.0 meters (x/d = 7.37, 17.89, 33.68, 54.74, 75.79, 96.84). For the heat transfer observations, the average

wall (tunnel floor) temperature of the test plate was approximately 40°C, while the injection system provided injectant at approximately 47°C. Results of this experiment are summarized in Table 4 and in Figures 28-58 in this chapter, and in Figures 114-173 in Appendix A.

Figures 28-40 indicate that the wall jet significantly influences the streamwise development of vortex fluid mechanics parameters (ω_x, Γ, V, $ND\Gamma_1$, $ND\Gamma_2$) and core dimensions as blowing ratio increases. Figures 28-32 show that streamwise vorticity, circulation, and maximum secondary flow vector magnitude all decrease at a given blowing ratio as x/d increases. The effect of the jet opposing the vortex downwash (opposing secondary flow direction) is clear in these figures; as blowing ratio increases, the parameters at each streamwise position decrease.

Streamwise development of vortex structural effects is seen in Figures 33-38. The vortex center height above the wall (tunnel floor) rises nearly linearly downstream (Figure 33). This behavior is (rather surprising, considering results up to this point) essentially independent of blowing ratio. The center also moves in the negative z direction (Figures 34 and 35), which is a result of the angle of the vortex generator and lower local static pressure in the jet. Figures 36 and 37 show that the average vortex core radius increases with downstream development, and that this effect is greatly enhanced at m = 3.5. Figure 38 shows that ratios

TABLE 4

FLUID MECHANICS MEASUREMENTS FOR VORTEX GENERATOR #2
AT TUNNEL CENTERLINE, PROBE POSITIONS A, B, C, D

m	0				2.1				3.5			
Probe Position	A	B	C	D	A	B	C	D	A	B	C	D
Y_{max} (m/s)	3.34	2.94	2.12	1.79	3.88	2.38	1.93	1.54	4.60	1.76	1.46	1.31
U_{xmax} (m/s)	10.3	10.6	10.5	10.2	12.4	10.5	10.6	10.2	16.1	10.7	10.5	10.3
ω_{xmax} (s^{-1})	923.3	769.1	579.8	410.9	762.4	578.6	440.3	302.2	645.0	241.3	181.3	175.6
Y_{core} (cm)	1.02	1.02	0.76	1.27	1.02	0.76	1.02	1.27	0.76	2.29	1.52	1.52
Z_{core} (cm)	0.76	0.76	1.02	1.02	0.76	1.02	1.02	1.27	0.76	1.52	1.78	2.03
$\left(\frac{Y_{core}+Z_{core}}{2}\right)$ (cm)	0.89	0.89	0.89	1.15	0.89	0.89	1.02	1.27	0.76	1.90	1.65	1.77
Z_{core}/Y_{core}	0.745	0.745	1.34	0.803	0.745	1.34	1.0	1.0	1.0	0.664	1.17	1.34
Y_{cen} (cm)	2.48	2.98	3.49	4.0	2.48	3.49	3.49	4.0	2.48	3.49	3.49	4.0
Z_{cen} (cm)	-1.52	-3.56	-4.57	-5.59	-1.52	-3.05	-4.57	-5.59	-2.03	-3.05	-4.57	-5.08
Γ (m^2/s)	0.182	0.150	0.118	0.096	0.192	0.132	0.103	0.086	0.221	0.097	0.062	0.049
$ND\Gamma_1$	0.021	0.020	0.013	0.008	0.022	0.015	0.010	0.007	0.029	0.005	0.004	0.003
$ND\Gamma_2$	-	-	-	-	0.074	0.670	0.523	0.436	0.672	0.30	0.188	0.149
P_{max} (Pa)	65.3	66.7	65.2	64.7	95.7	65.8	65.7	64.6	162.3	67.0	64.9	64.7

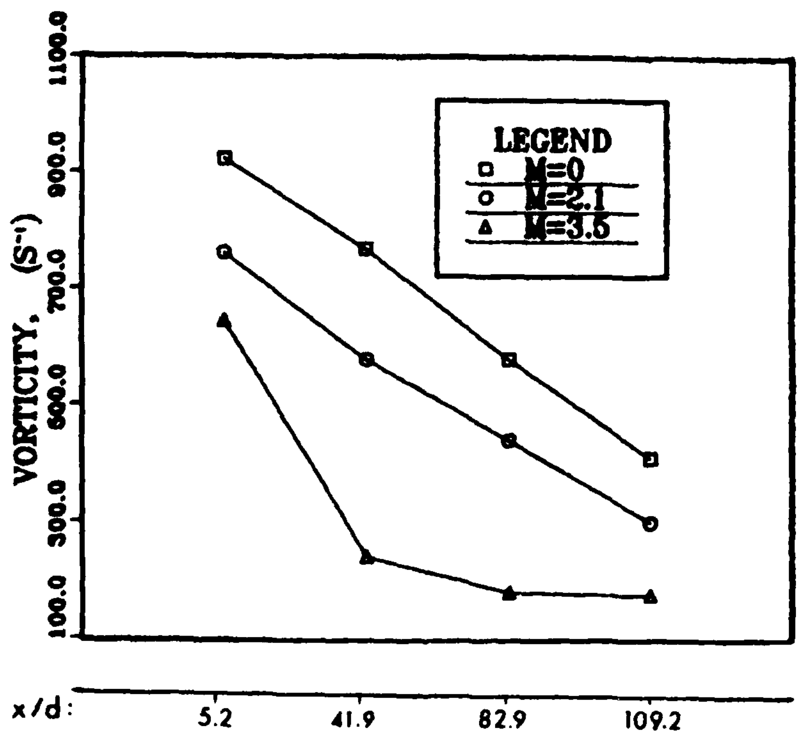

Figure 28. Streamwise Development of Maximum Streamwise Vorticity (ω_{xmax})

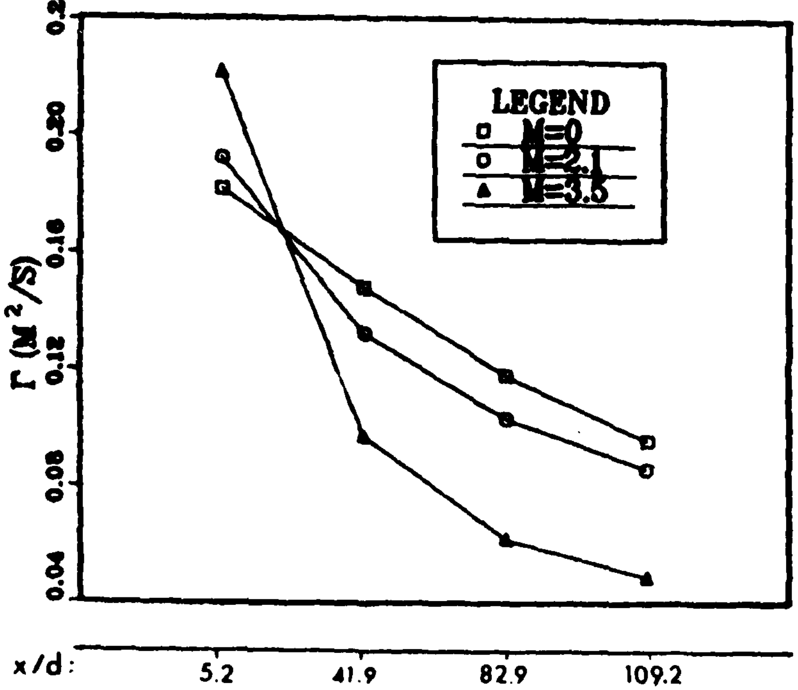

Figure 29. Streamwise Development of Circulation (Γ)

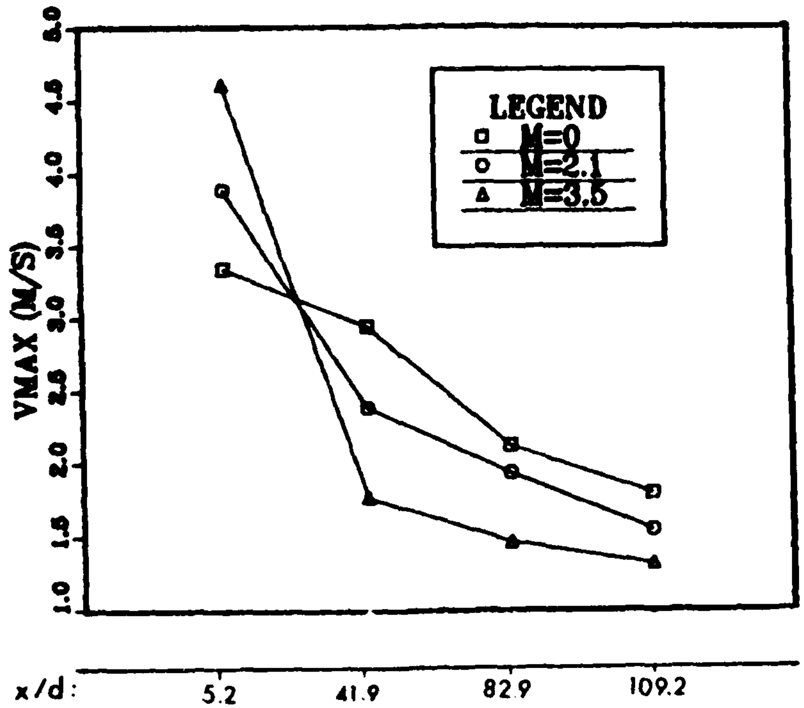

Figure 30. Streamwise Development of Maximum Secondary Flow Vector Magnitude (V_{max})

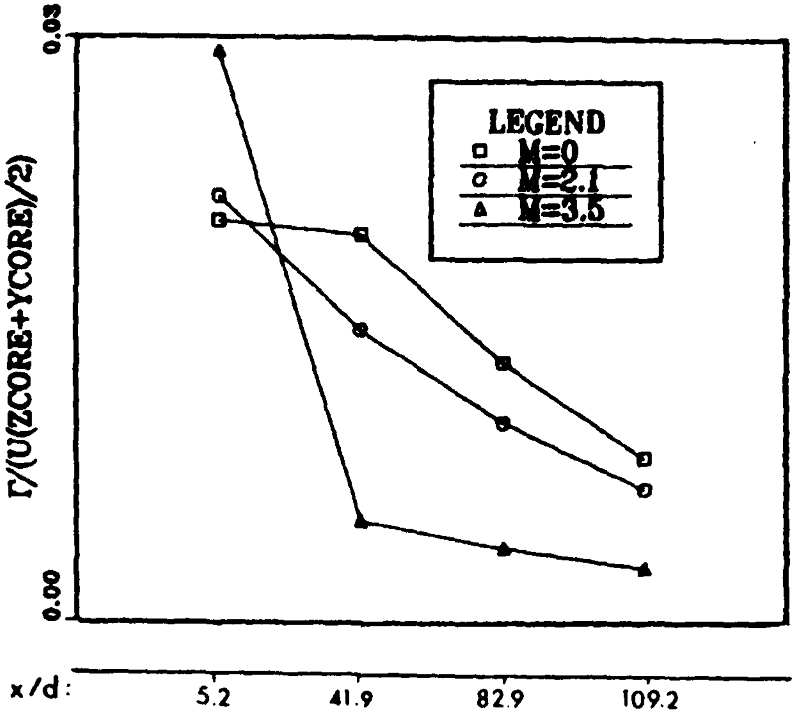

Figure 31. Streamwise Development of $ND\Gamma_1$

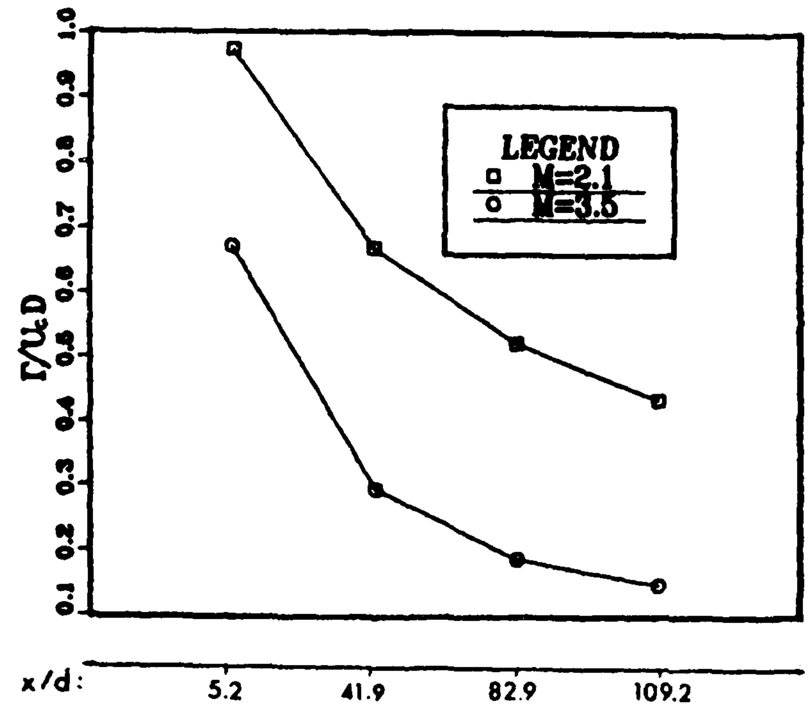

Figure 32. Streamwise Development of $ND\Gamma_2$

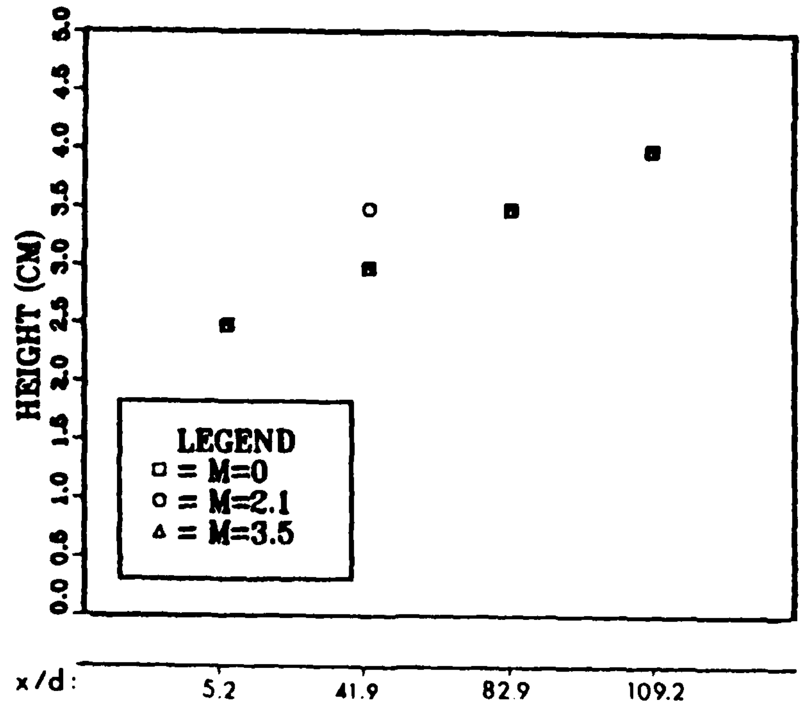

Figure 33. Streamwise Development of Vortex Center Height Above Tunnel Floor (Y_{cen})

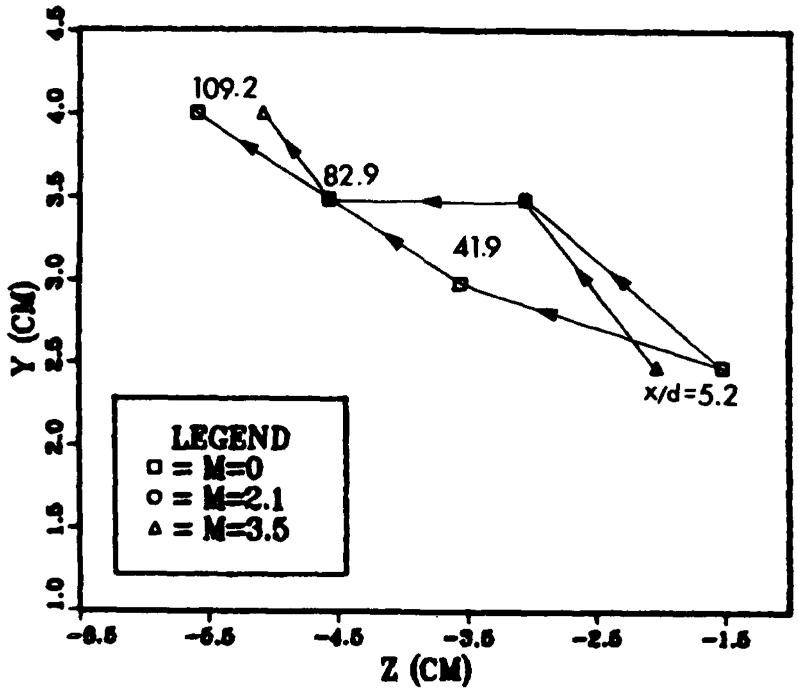

Figure 34. Streamwise Development of Vortex Center (Y_{cen},Z_{cen}) Position

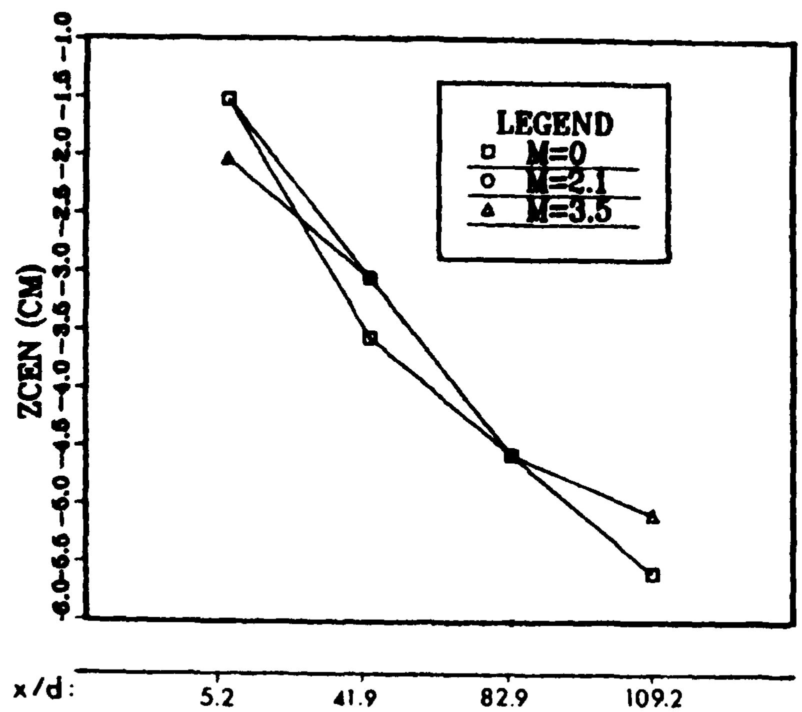

Figure 35. Streamwise Development of Vortex Center Z Coordinate

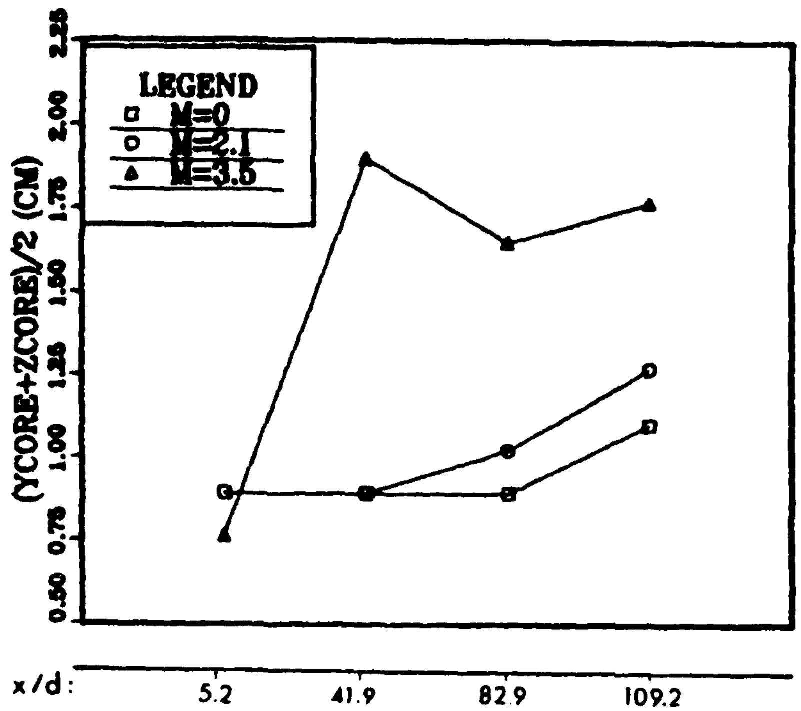

Figure 36. Streamwise Development of Average Vortex Core Radius

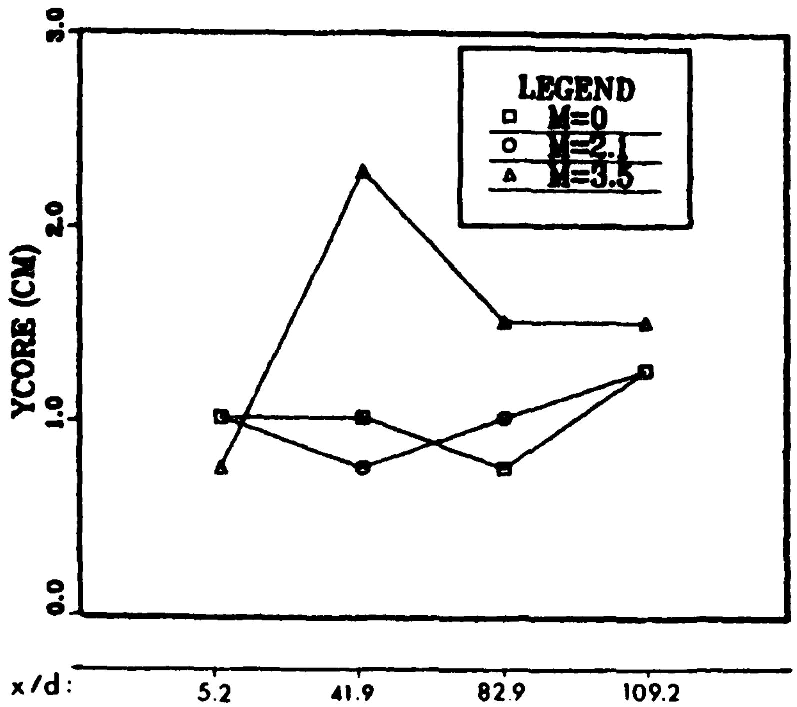

Figure 37. Streamwise Development of Average Vortex Core Radius in Vertical (Y) Direction

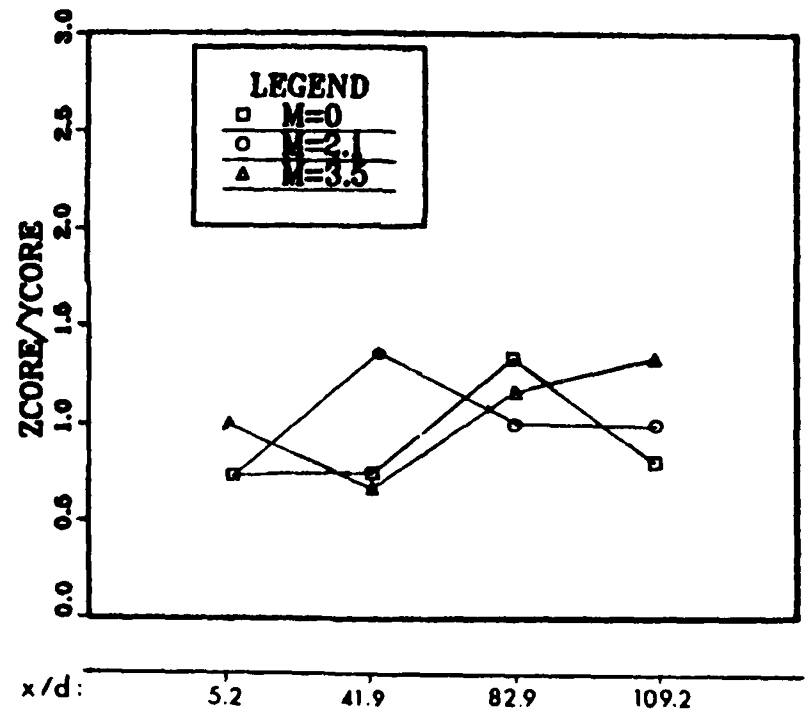

Figure 38. Streamwise Development of Average Vortex Core Y and Z Radius Ratio

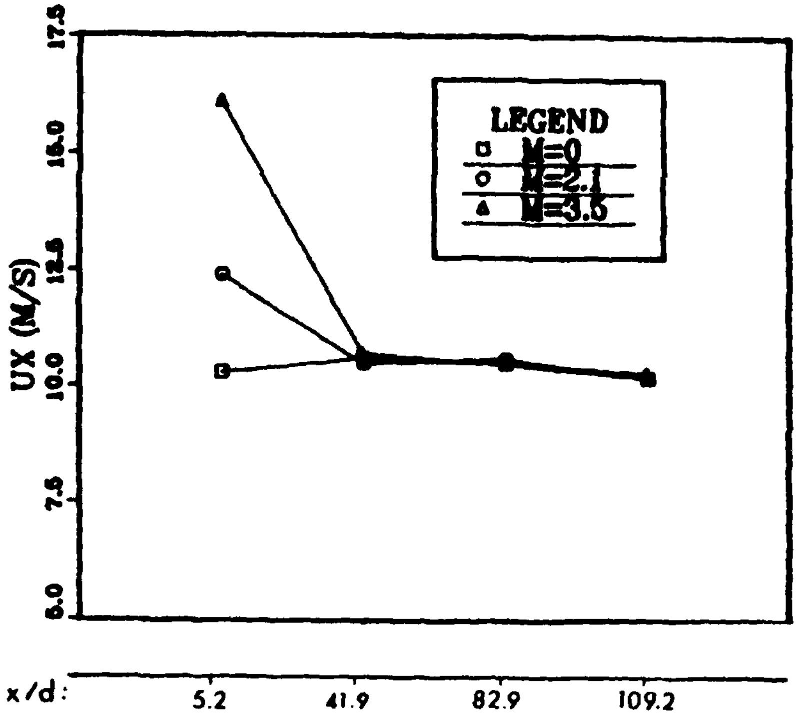

Figure 39. Streamwise Development of Maximum Streamwise Velocity Component (U_{xmax})

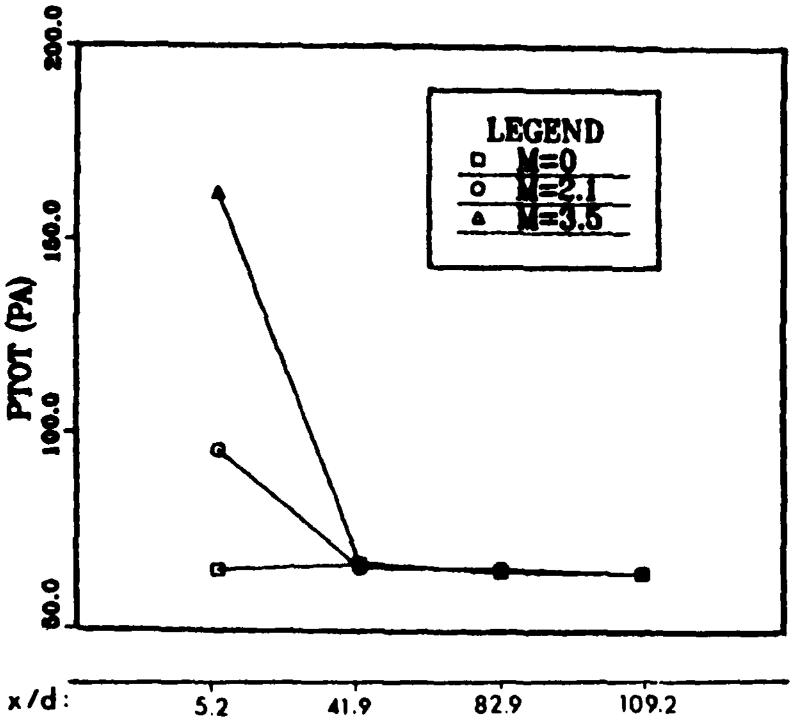

Figure 40. Streamwise Development of Maximum Total Pressure (P_{tot})

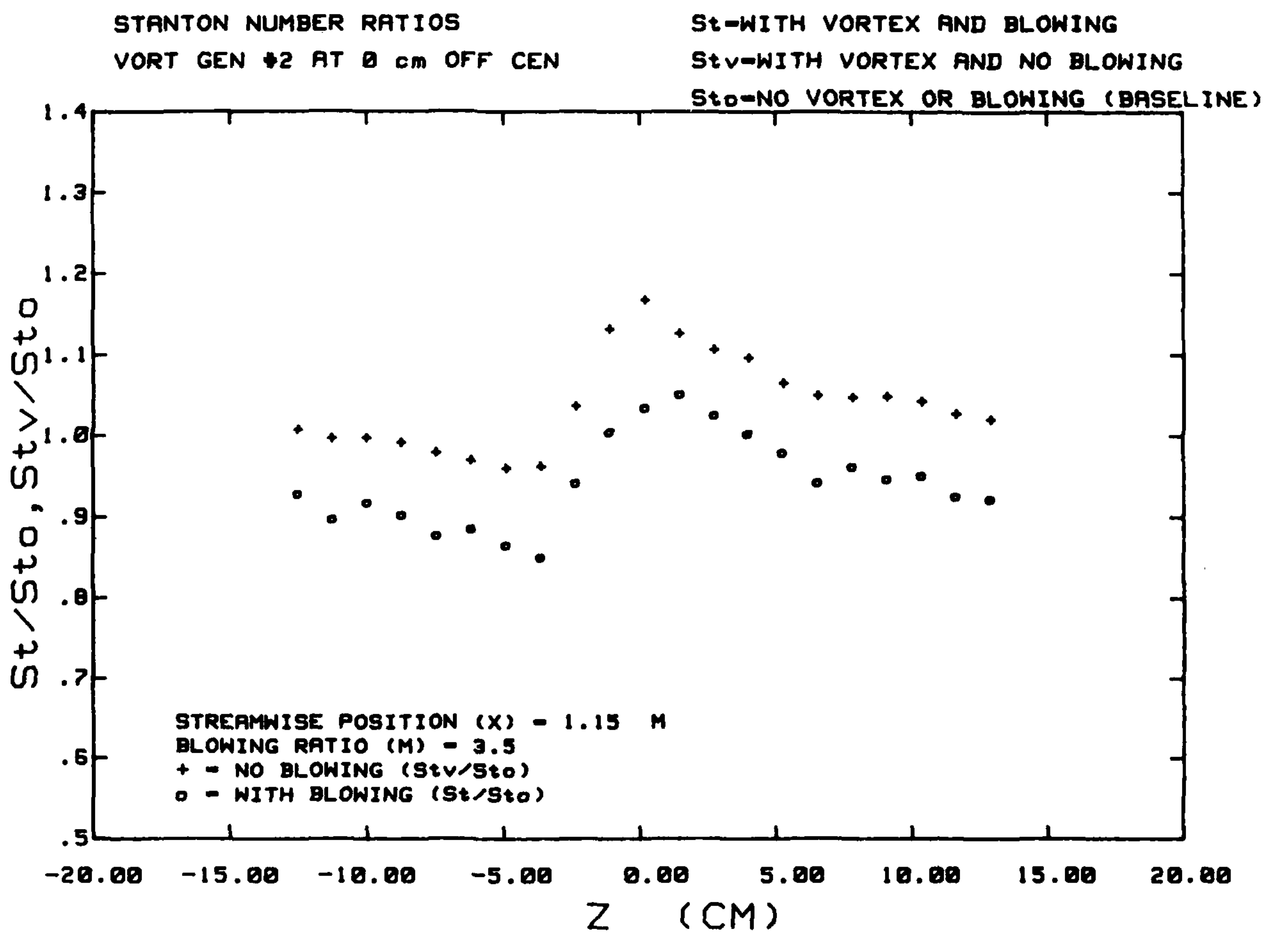

Figure 41. Stanton Number Ratios

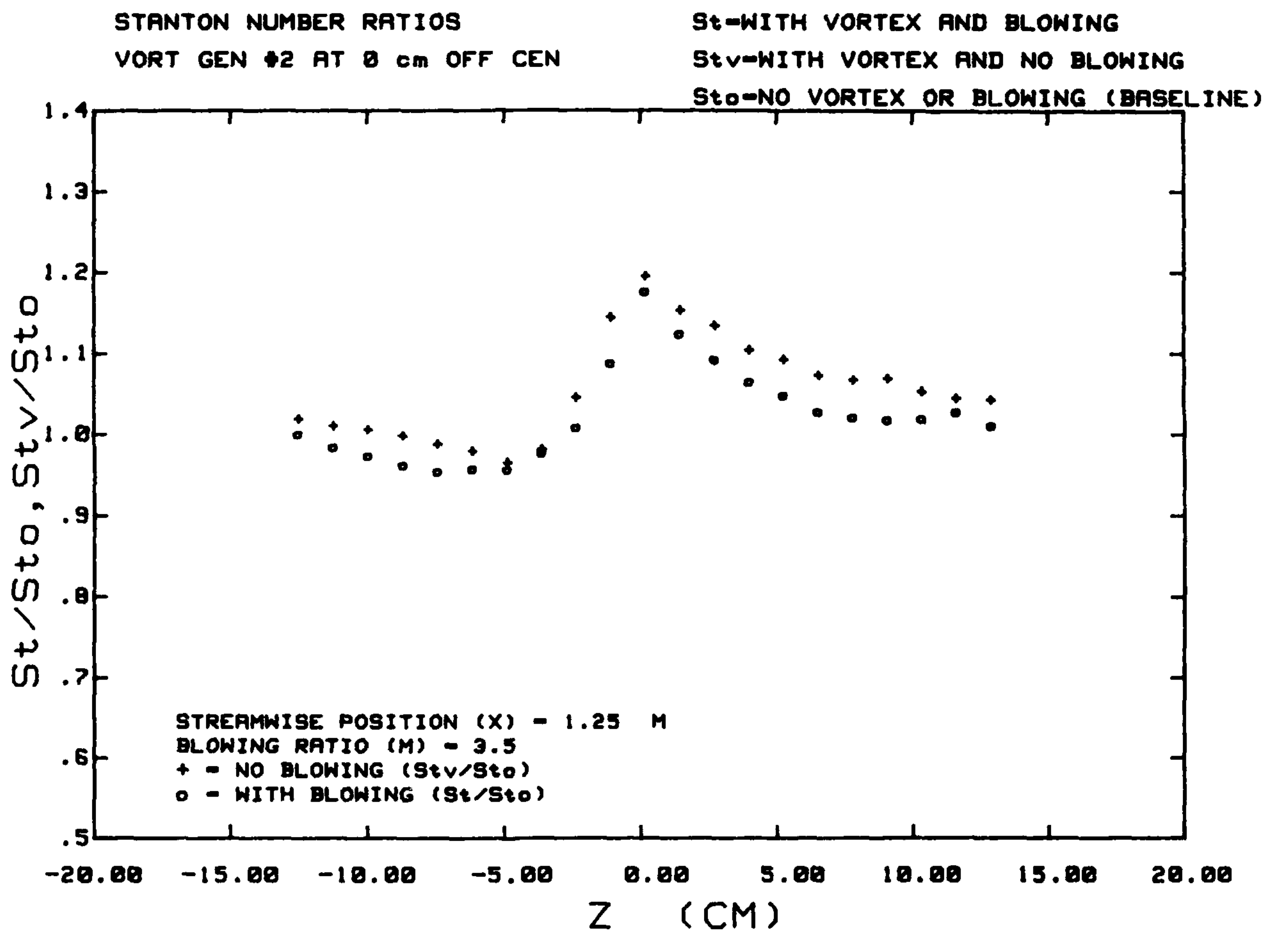

Figure 42. Stanton Number Ratios

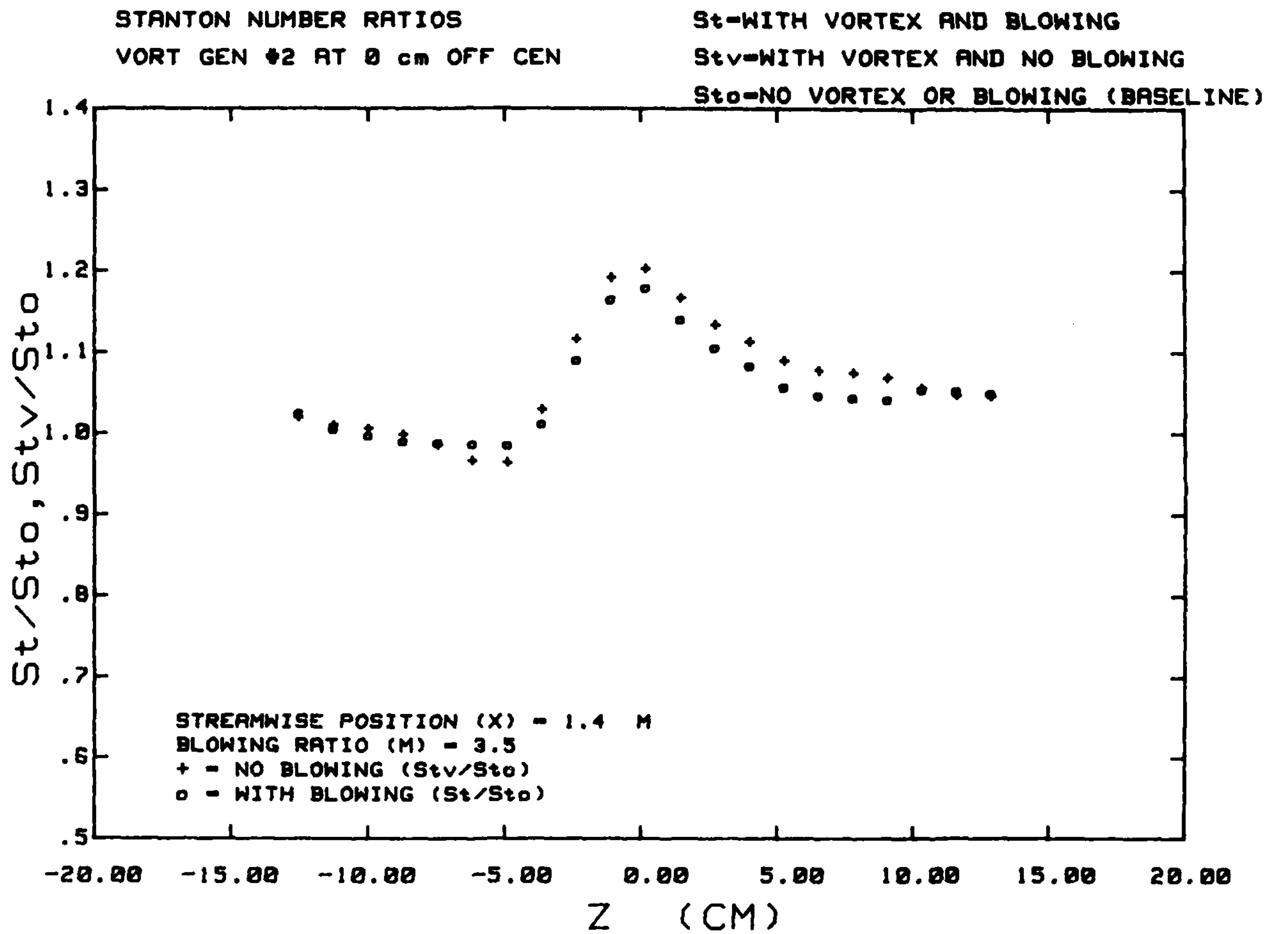

Figure 43. Stanton Number Ratios

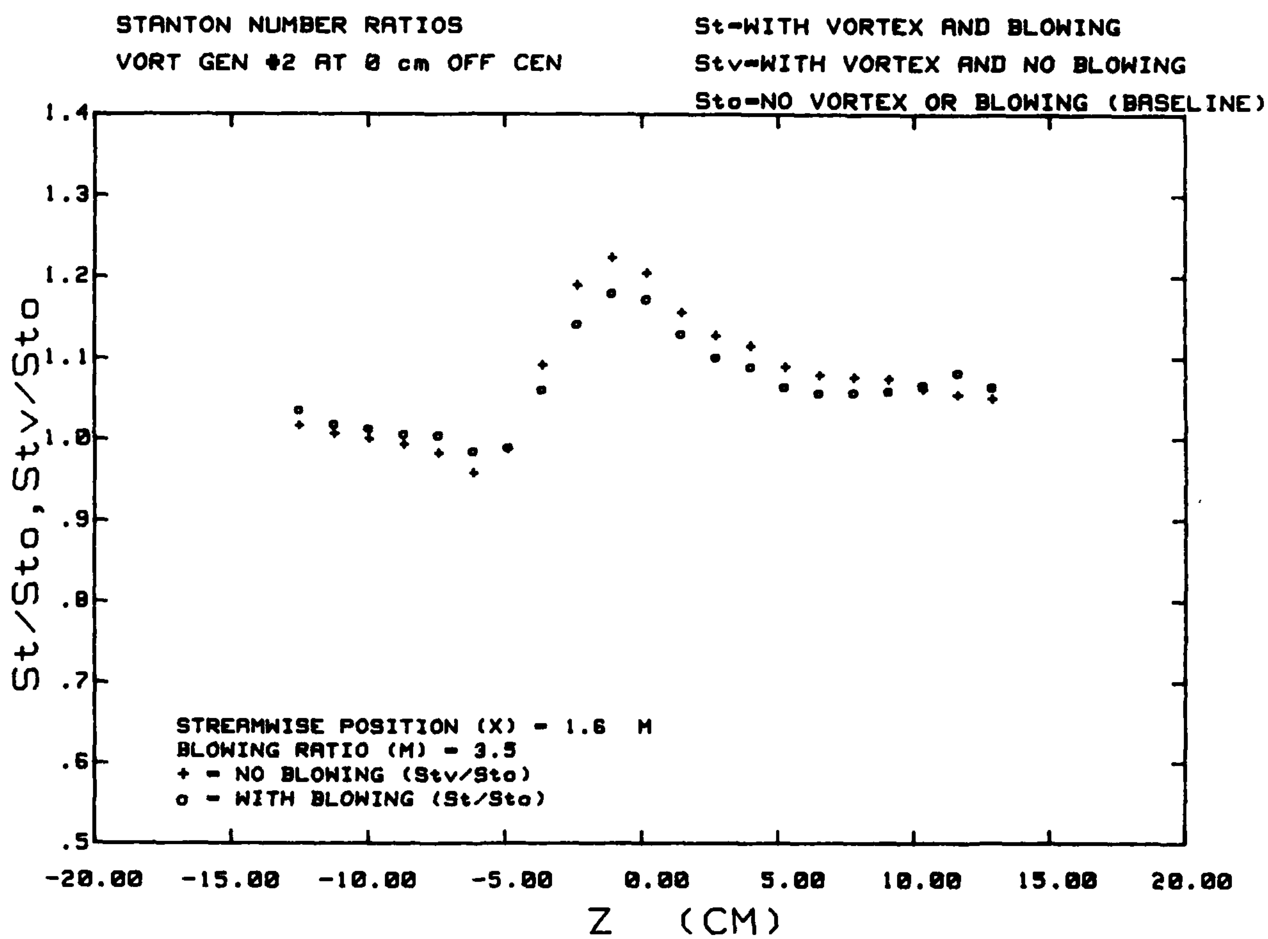

Figure 44. Stanton Number Ratios

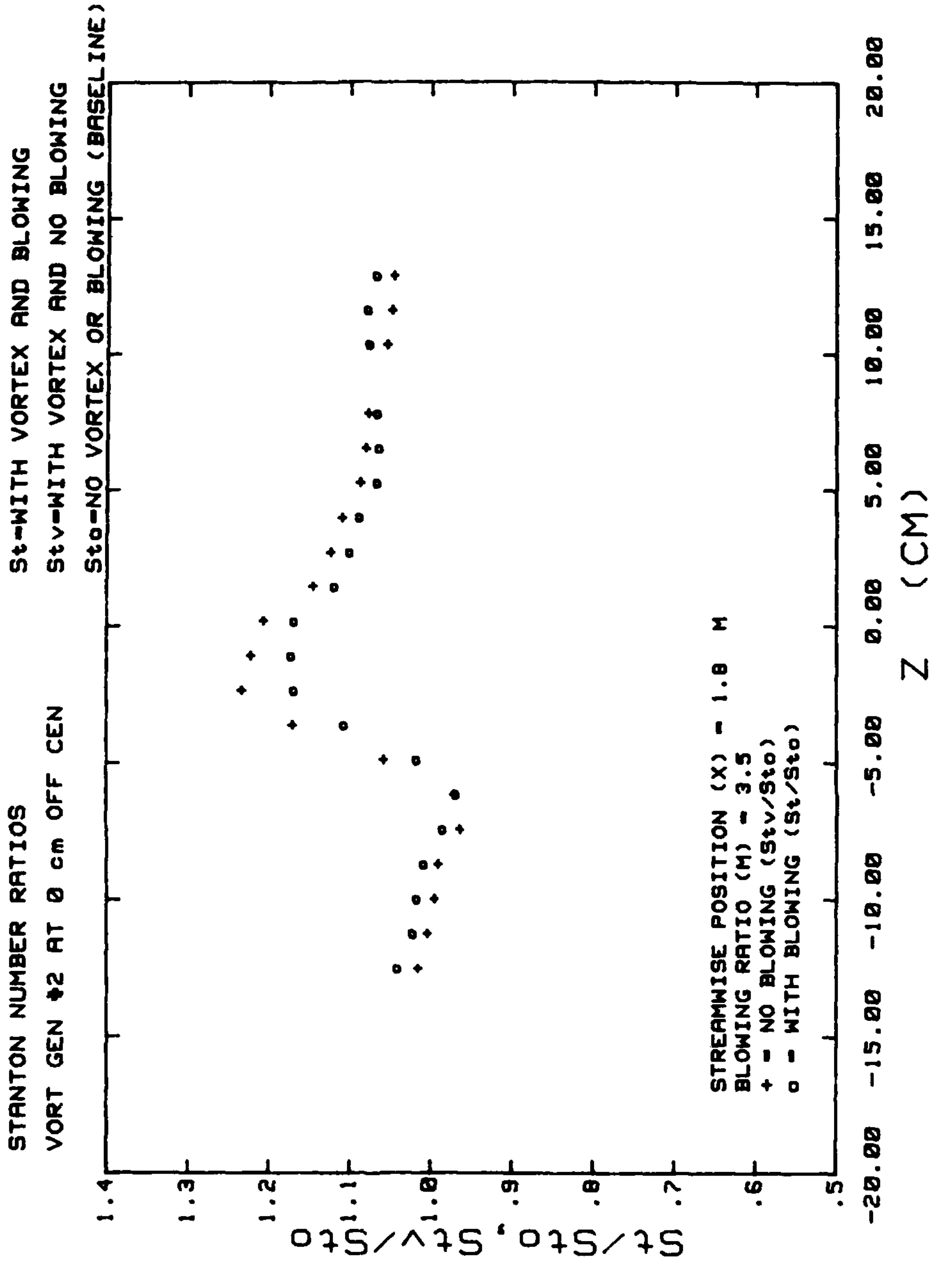

Figure 45. Stanton Number Ratios

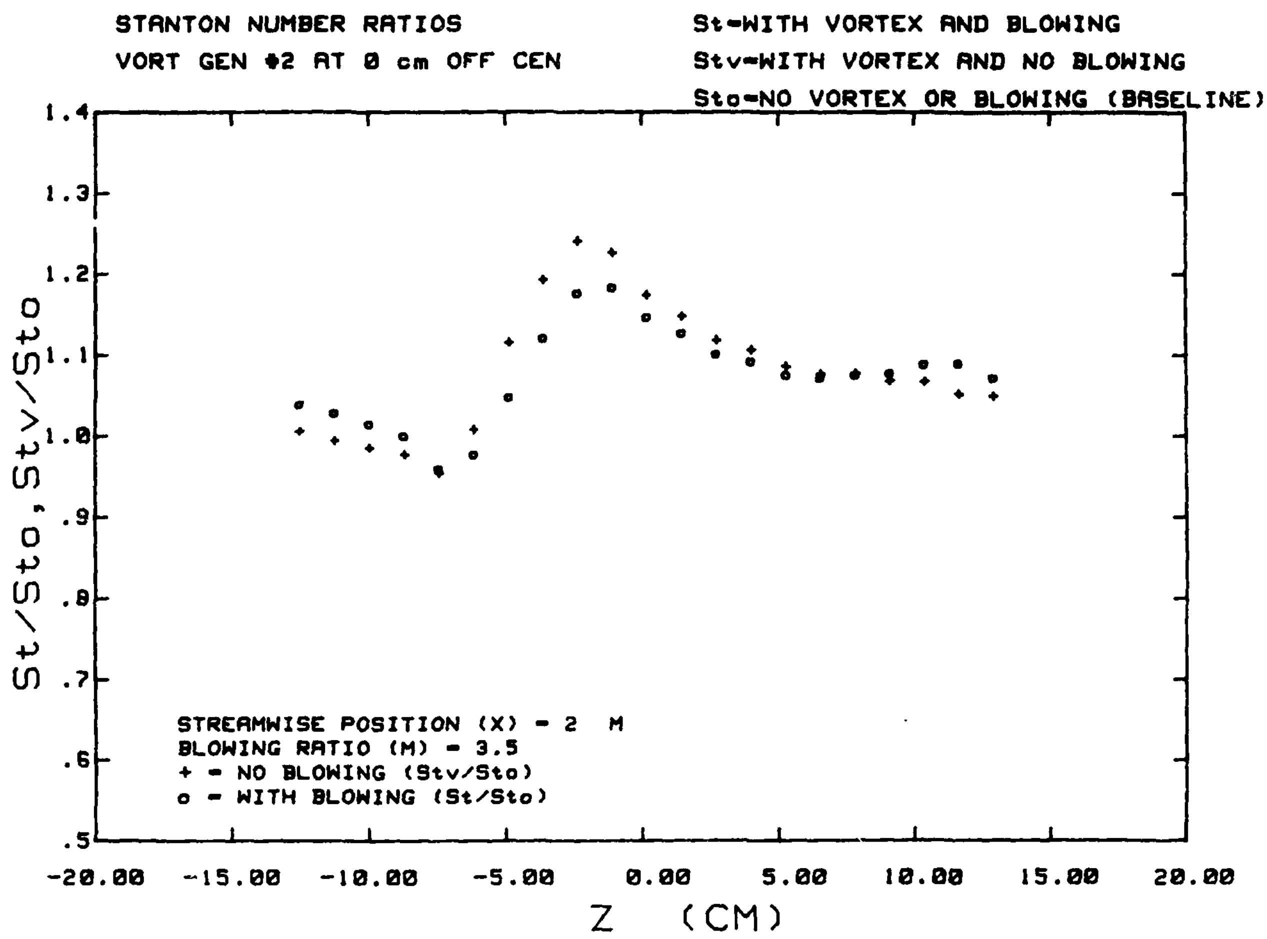

Figure 46. Stanton Number Ratios

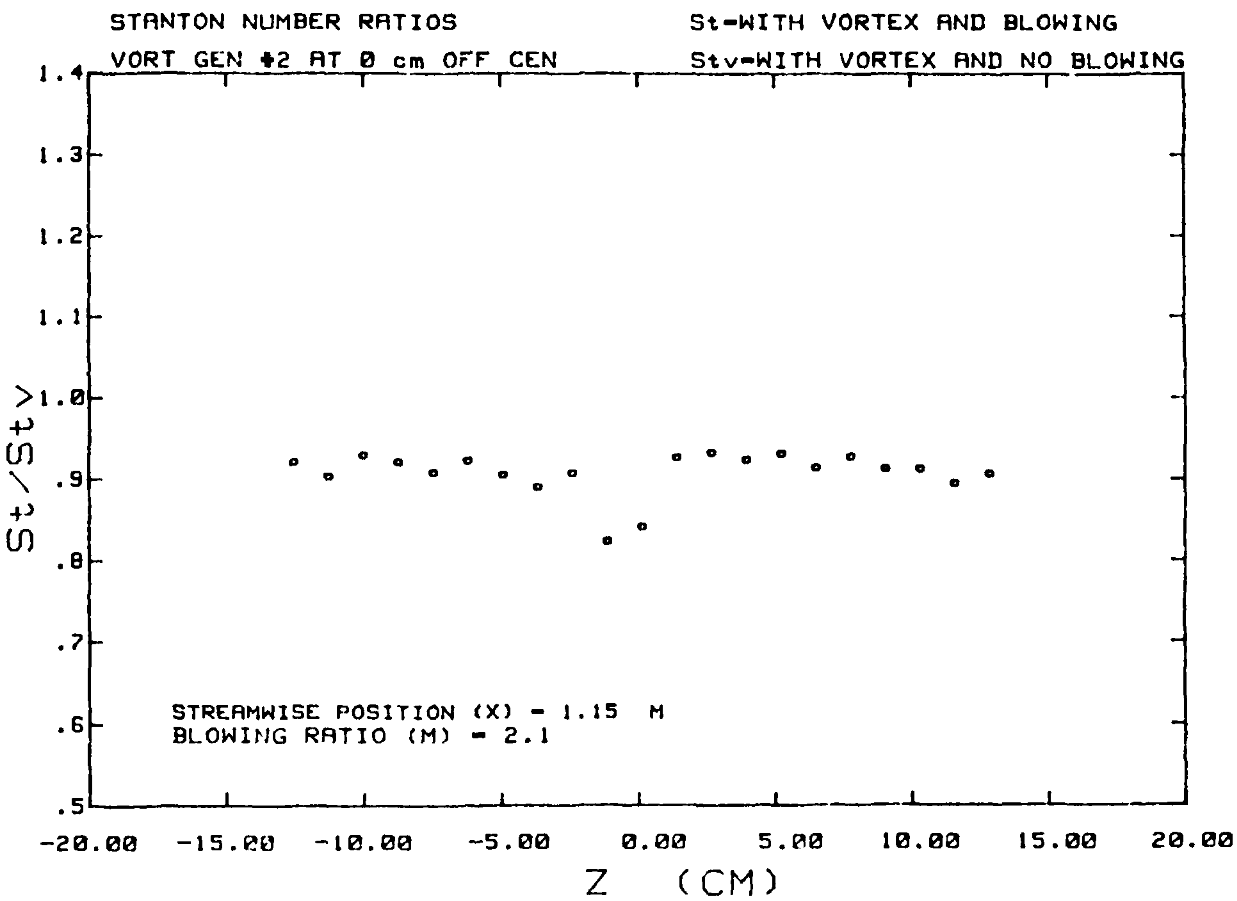

Figure 47. Stanton Number Ratios

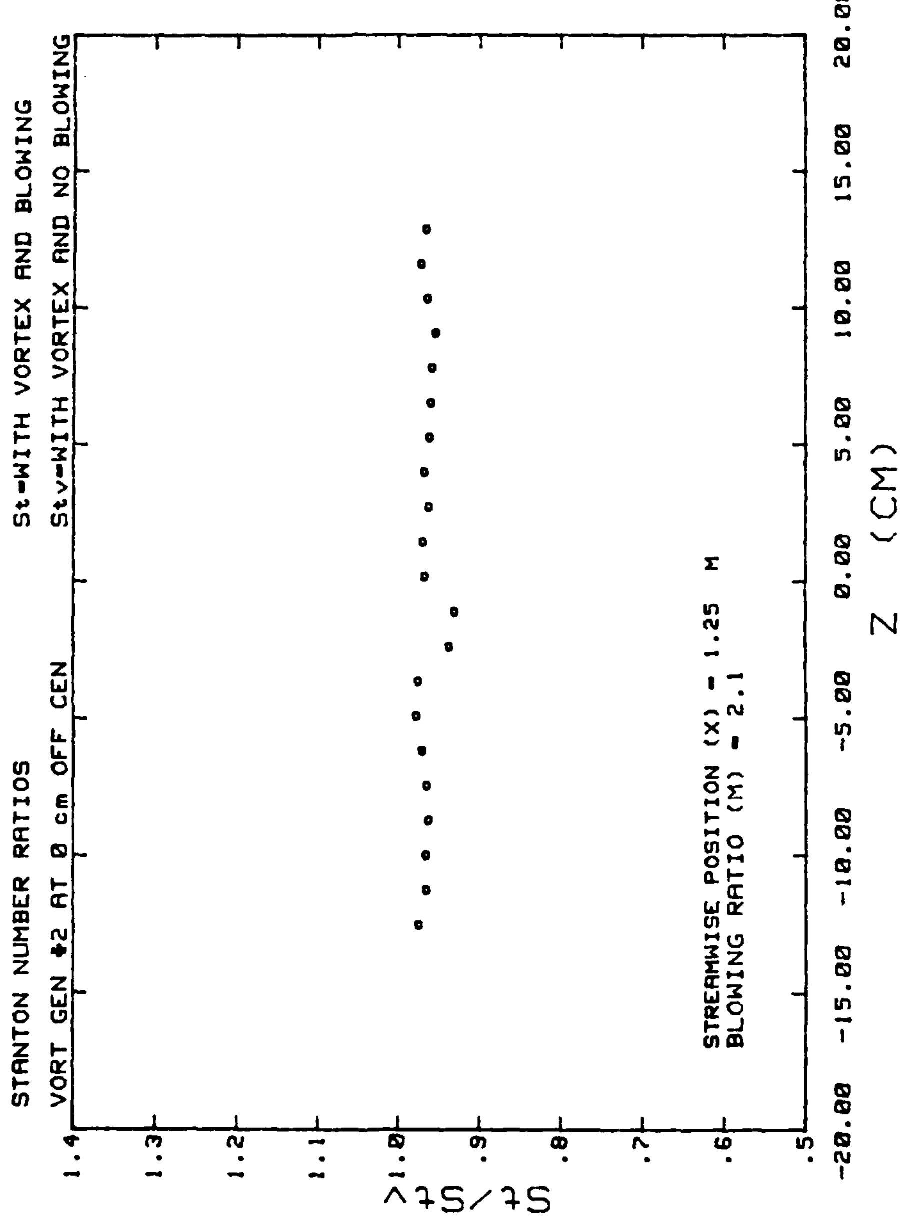

Figure 48. Stanton Number Ratios

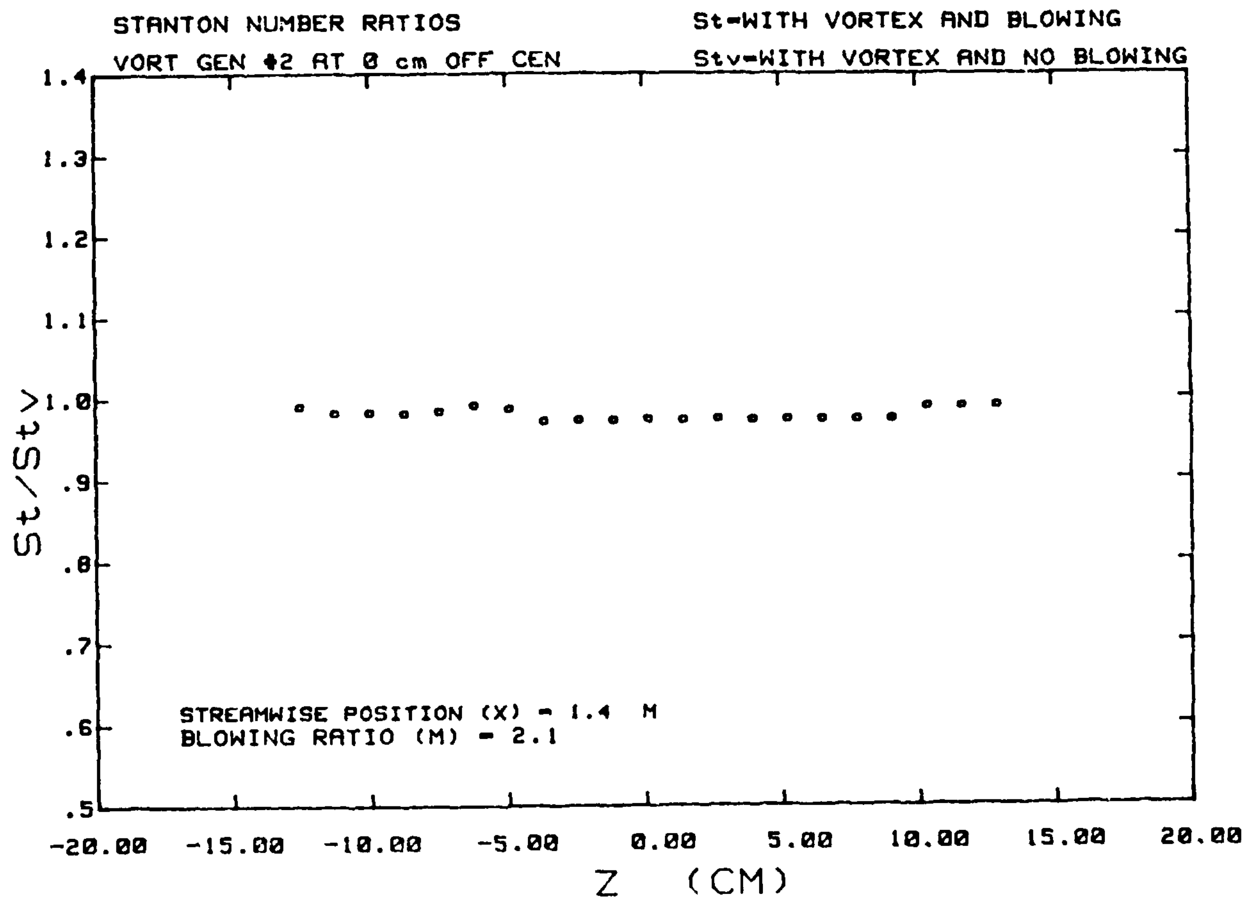

Figure 49. Stanton Number Ratios

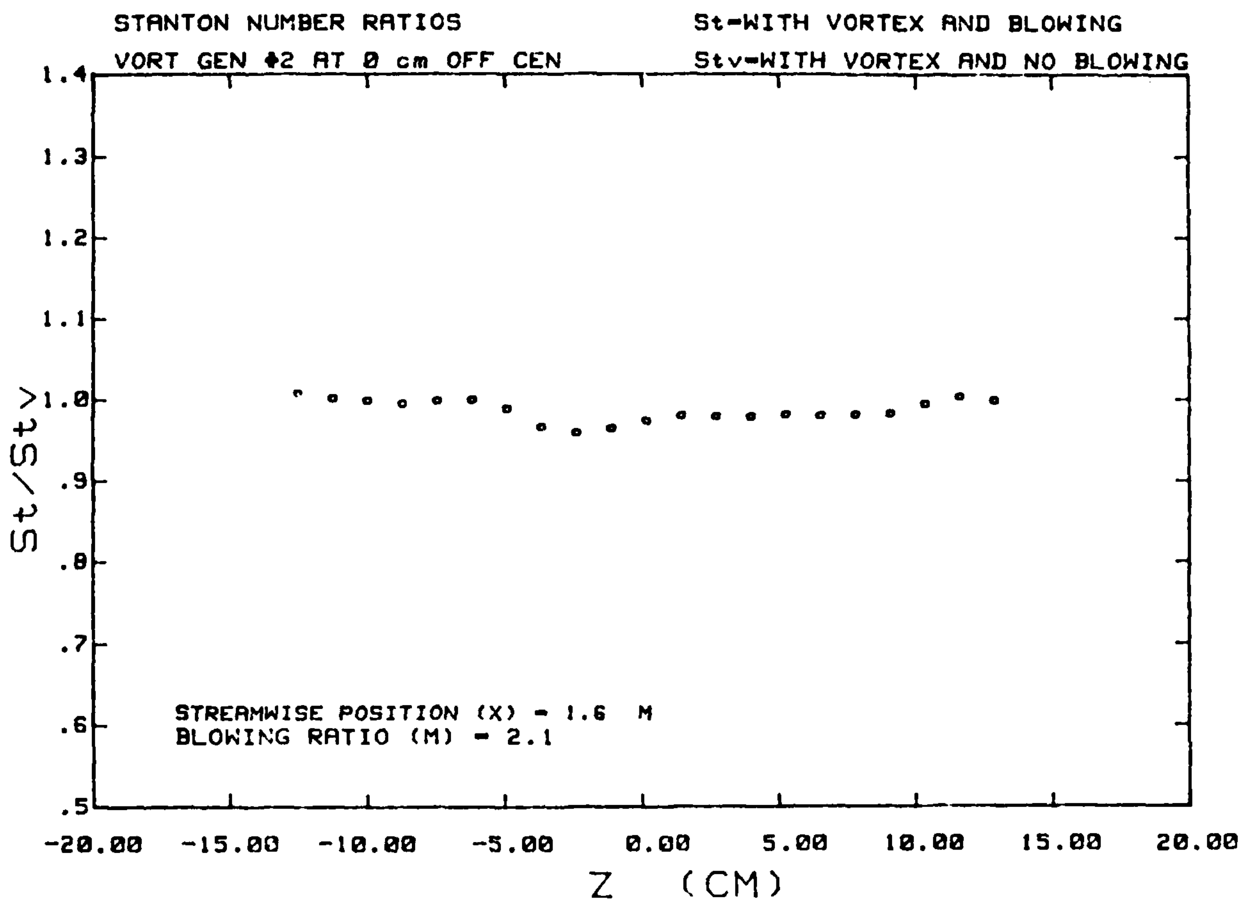

Figure 50. Stanton Number Ratios

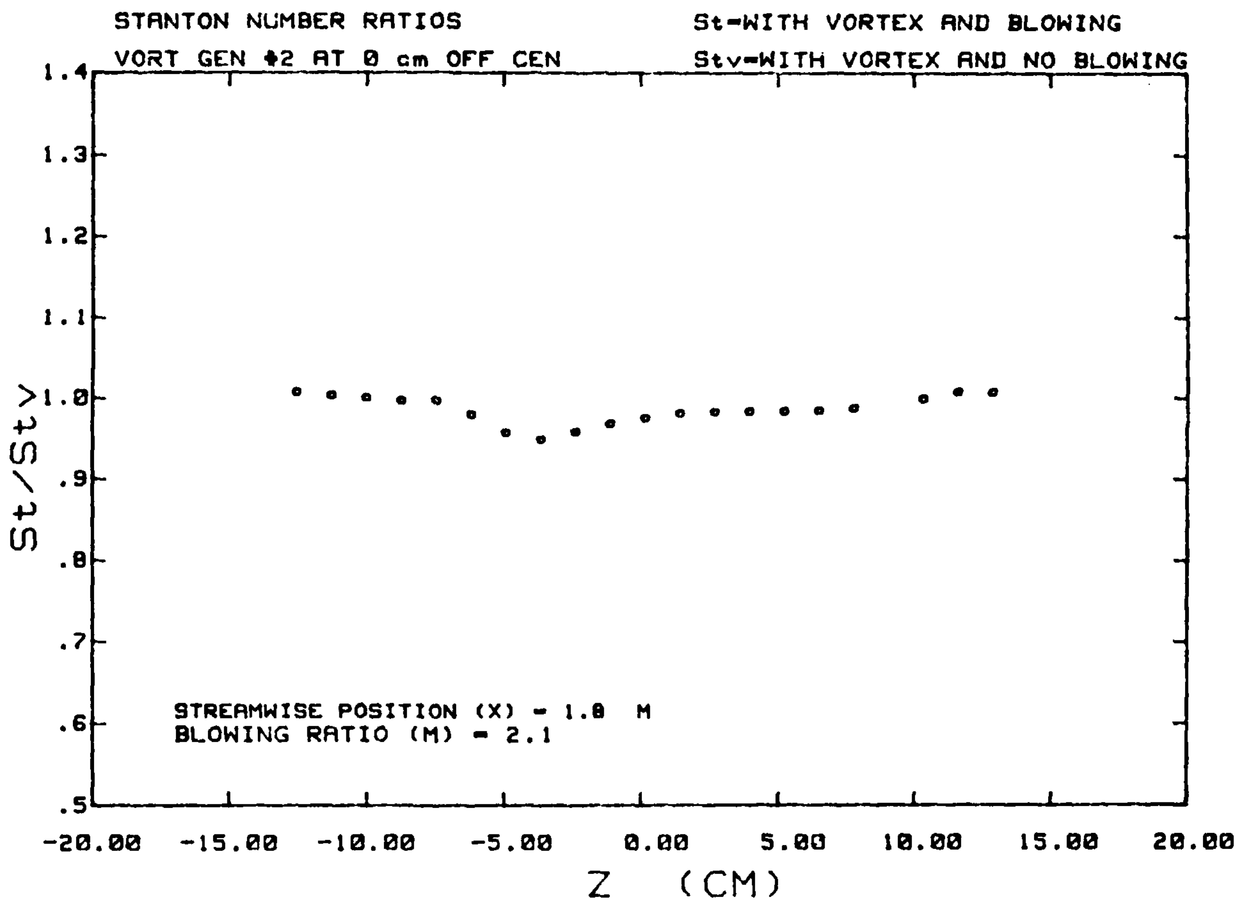

Figure 51. Stanton Number Ratios

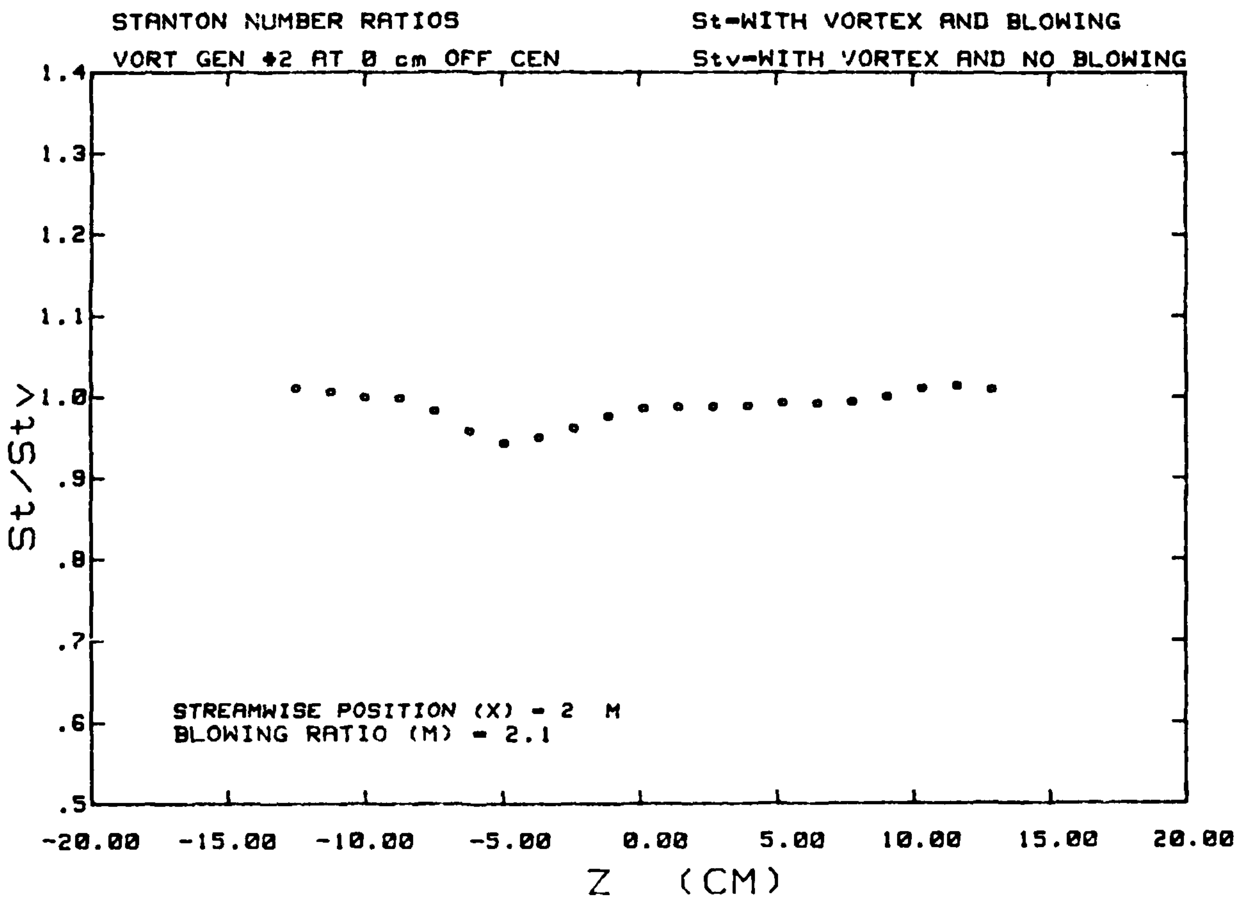

Figure 52. Stanton Number Ratios

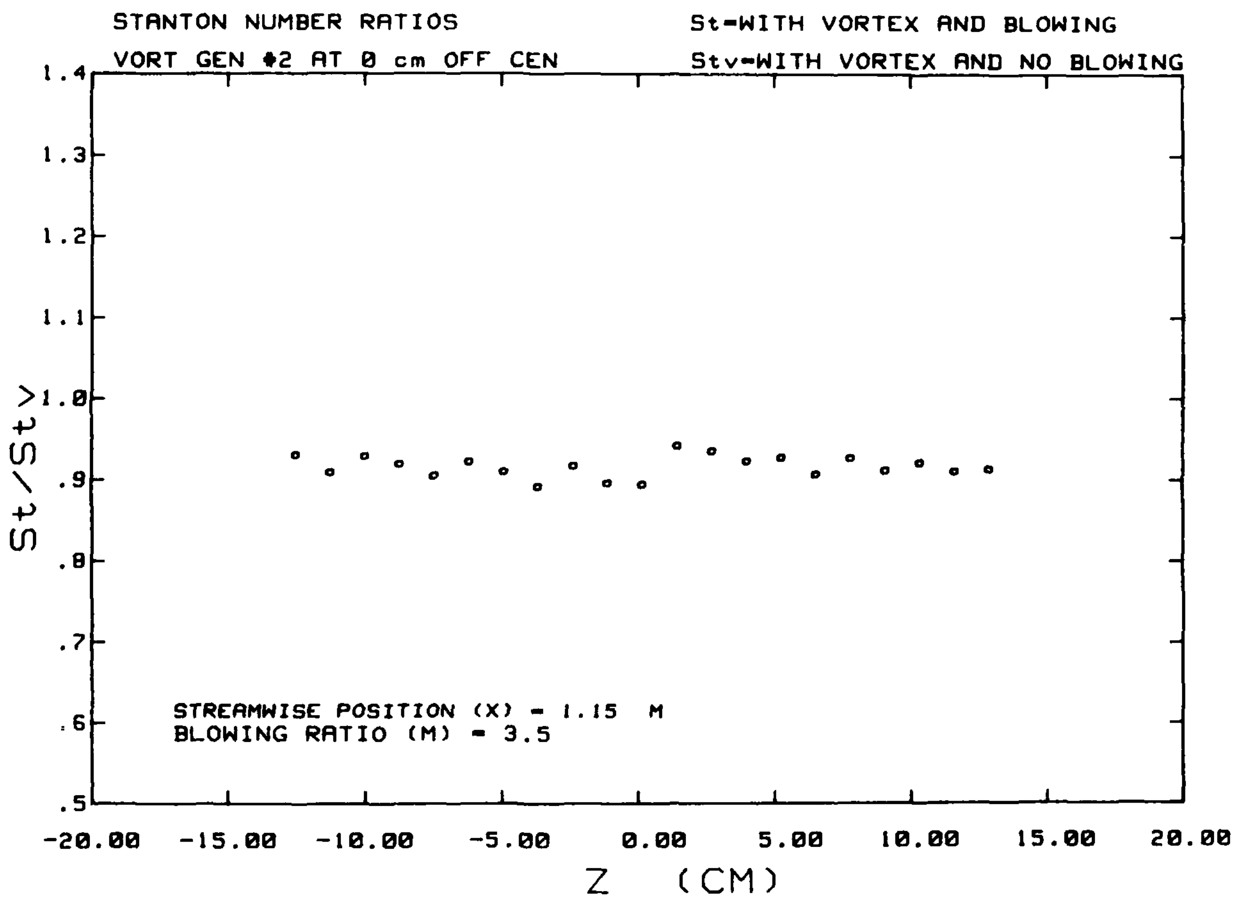

Figure 53. Stanton Number Ratios

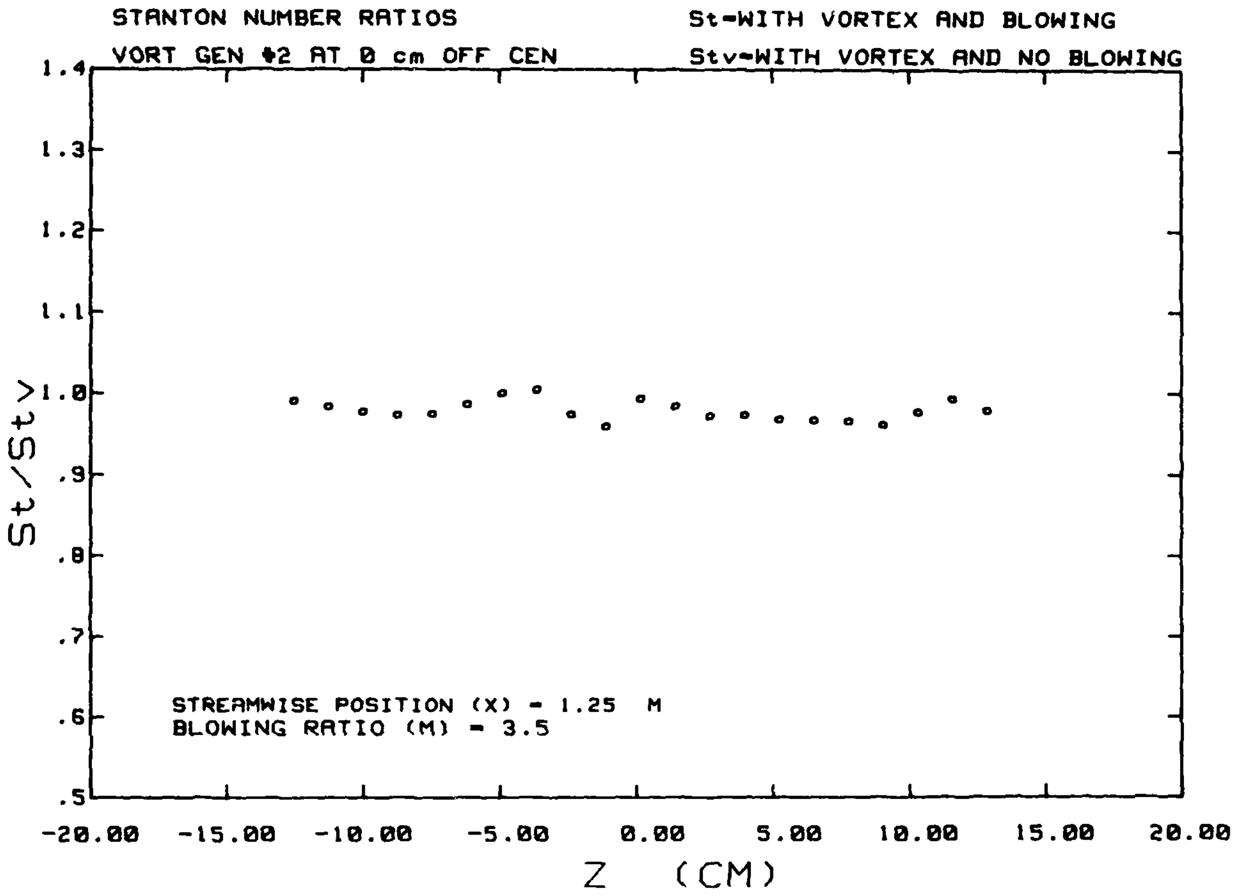

Figure 54. Stanton Number Ratios

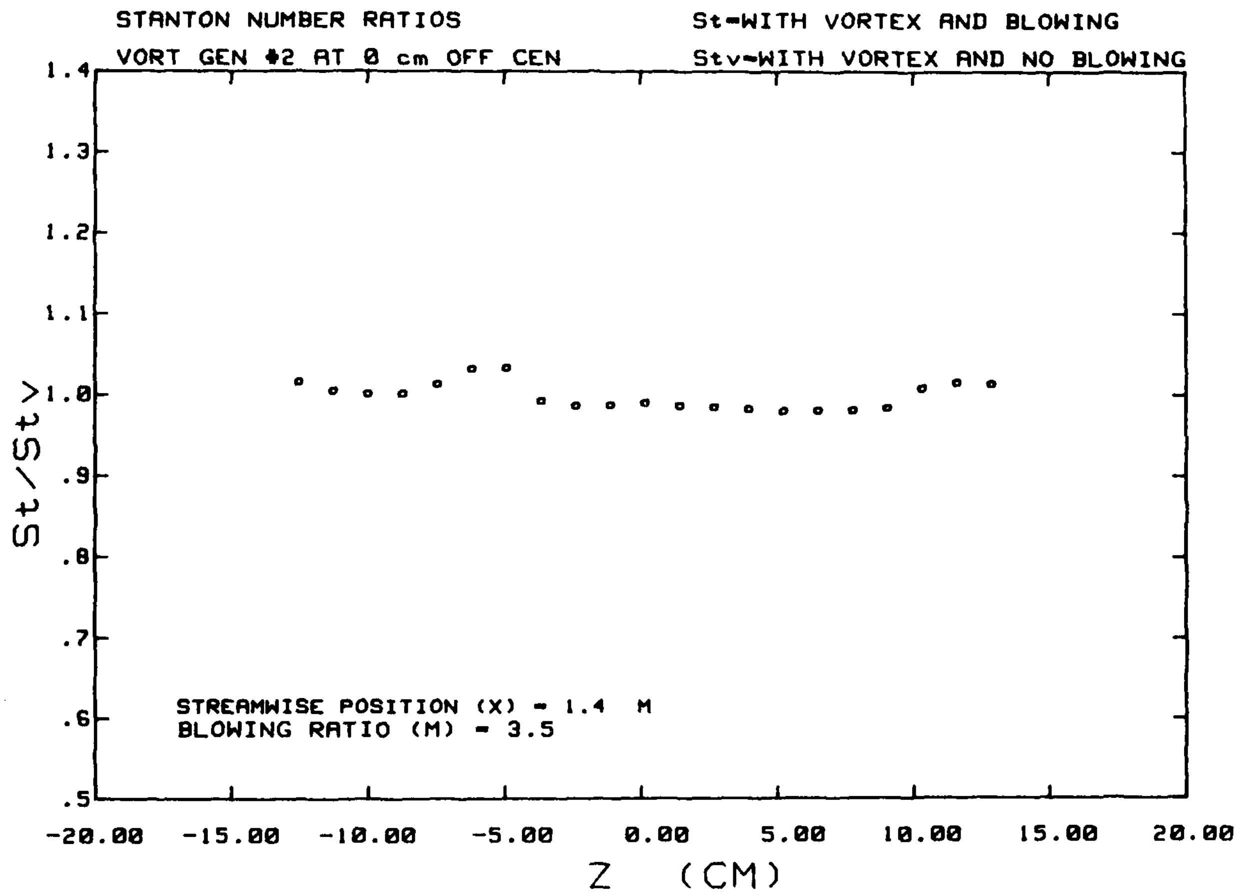

Figure 55. Stanton Number Ratios

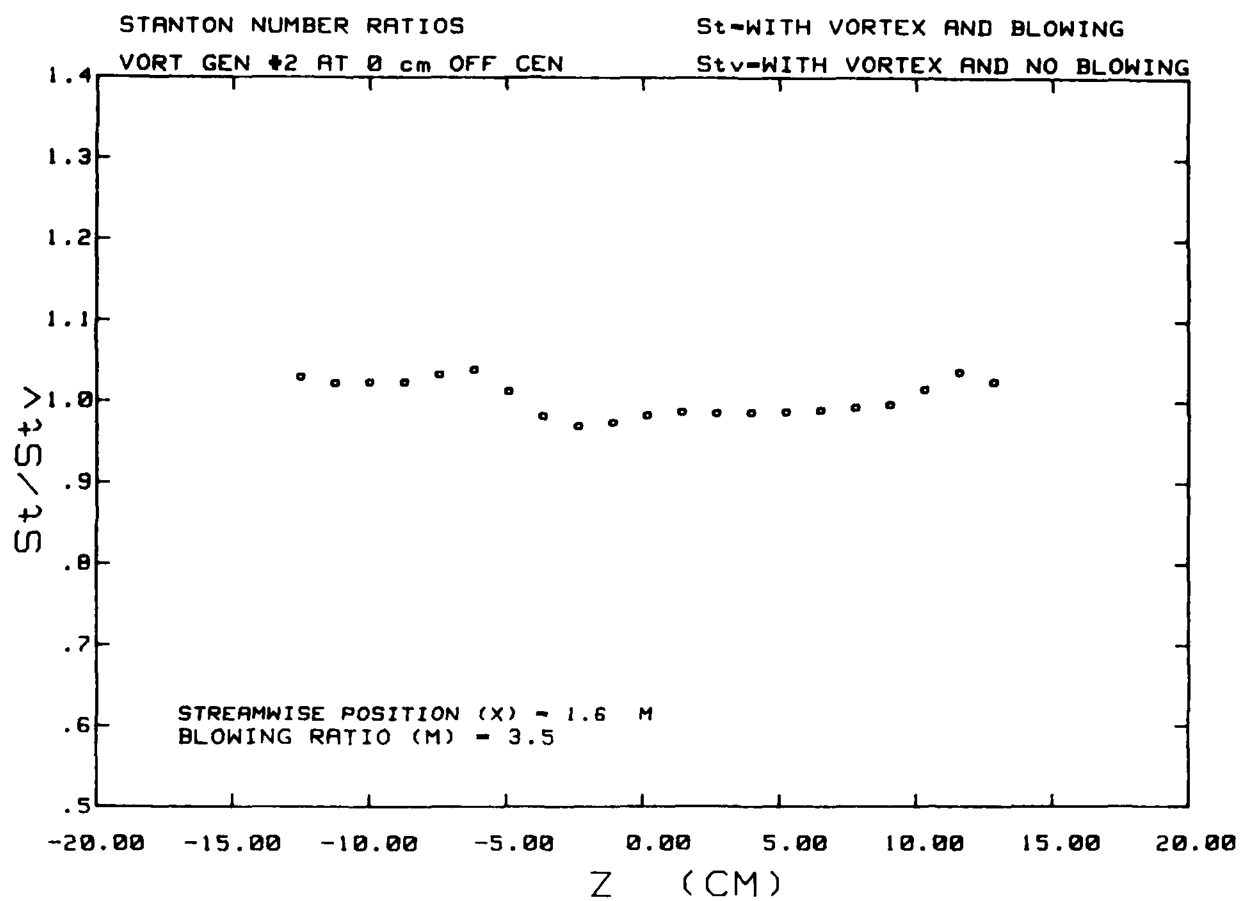

Figure 56. Stanton Number Ratios

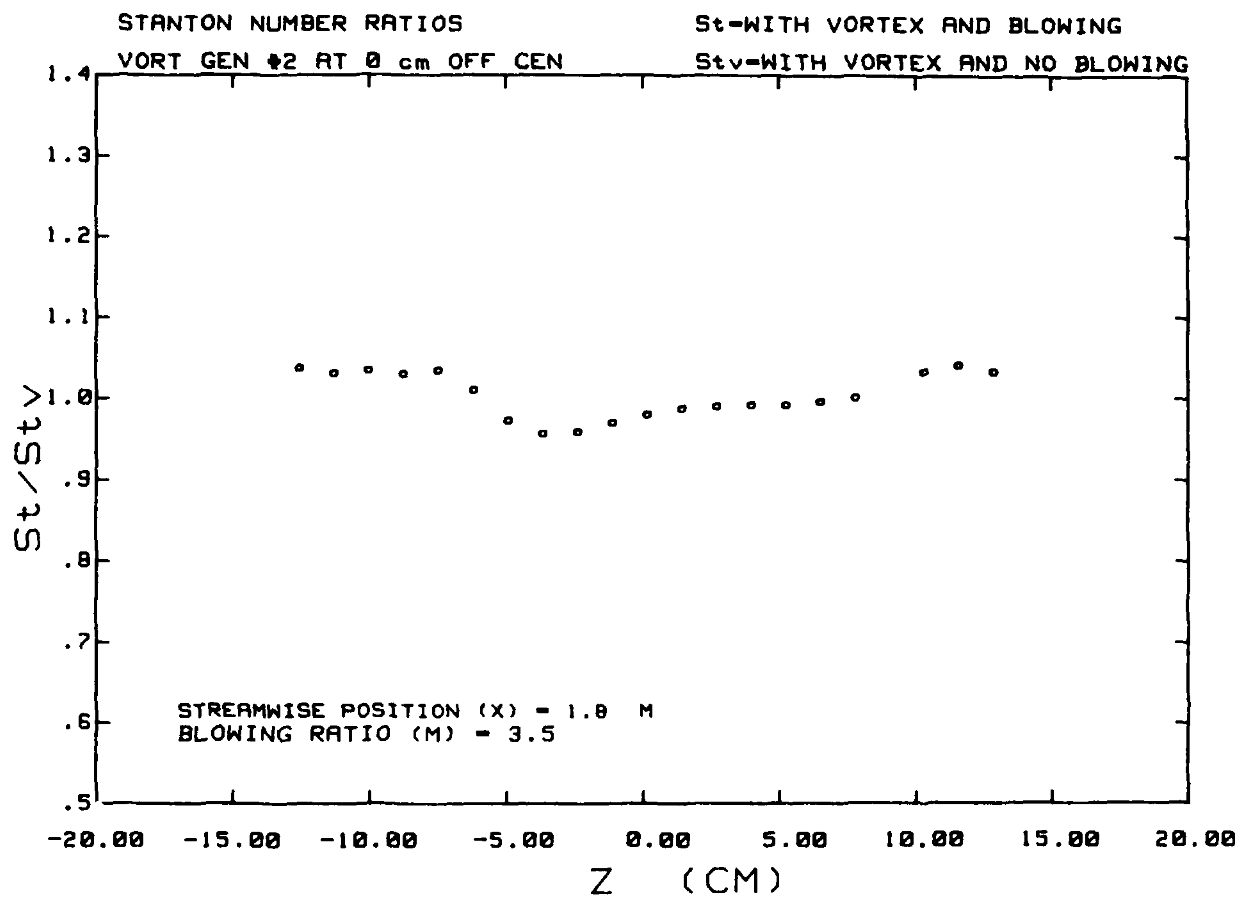

Figure 57. Stanton Number Ratios

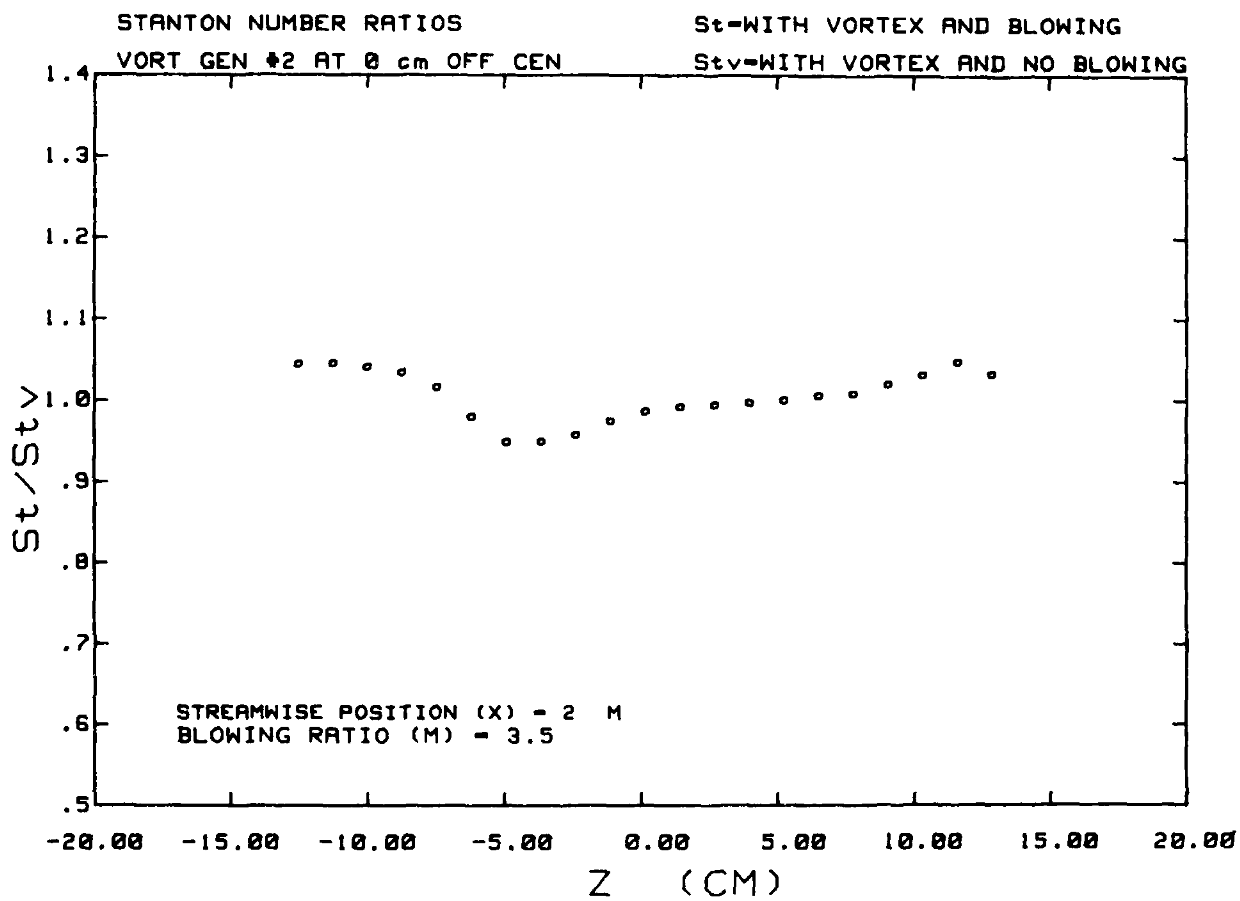

Figure 58. Stanton Number Ratios

of the average core radii in the y and z directions remain relatively equal downstream for all blowing ratios.

Figures 39 and 40 show that maximum streamwise velocity and maximum total pressure increase near the origin of the jet as blowing ratio increases. A large reduction in both then occurs between the injection hole and x/d = 41.9. Further downstream, the parameters remain relatively constant at the same values which exist with no blowing. From these figures, it is evident that the majority of the jet momentum is expended between x/d = 0 and 41.9. The greatest reductions in vorticity, circulation, and secondary flow velocity are also within this range of x/d.

The results of the heat transfer measurements in this experiment were somewhat unexpected. In Figures 41-46 (Stv/Sto at m = 0 and St/Sto at m = 3.5, where St is Stanton number with vortex and blowing, Stv is Stanton number with vortex and no blowing, Sto is Stanton number without vortex or blowing), the peak in Stv/Sto is due to the vortex downwash. The downwash causes thinning of the boundary layer. This is clearly evident in the contour plot of total pressure and streamwise velocity component. The thinning of the boundary layer increases the wall heat transfer rate at the downwash.

Reference 6, using the same apparatuses and experimental set-up as the present study, reported that St/Sto is lower than Stv/Sto with the vortex downwash opposing the jet and

m < 1.0. In contrast, the present results for m = 3.5 and X > 1.25 m (x/d > 17.89) show that there is little difference between Stv/Sto and St/Sto. This is because for m > 1.0, the injection jet lifts off the wall, causing little change to the near wall region of the boundary layer already altered by the vortex.

Figures 47-58 show St/Stv for m = 2.1 and 3.5. Again it is seen that the wall heat transfer rate is relatively unaffected by high blowing ratio.

D. EXPERIMENTAL RESULTS FOR INJECTION AT VORTEX UPWASH: x/d = 41.9 (PROBE POSITION B); UNDISTURBED VORTEX CIRCULATION = 1.67 x 10^{-1} m^2/s

For this experiment, vortex generator #2 was placed at z = +5.08 cm (2 inches) and injection was through the center wall jet, so that the jet was in the same direction as the vortex upwash. The five-hole pressure probe was placed at x/d = 41.9 (position B), blowing ratio was varied between 0 and 6.7. Fluid mechanics results are summarized in Table 5 and Figures 59-67 in this chapter, and in Figures 174-203 in Appendix A. Additionally, with this vortex/jet configuration and m = 3.0, heat transfer measurements at X = 1.15, 1.25, 1.4, 1.6, 1.8, and 2.0 meters (x/d = 7.37, 17.89, 33.68, 54.74, 75.79, 96.84) were made as presented in Figures 68-79.

Prior to conducting the experiment, it was expected that the variation of results with m would be opposite to the results in the first experiment. That is, it was thought

TABLE 5

COMPARISON: WALL JET AT VORTEX DOWNWASH OR UPWASH

	Parameter	m = 0	m = 4.8	% Decrease
Jet Opposing Vortex Downwash	ω_{xmax} (s^{-1})	725.9	128.3	82
	Γ (m^2/s)	0.148	0.047	68
	V_{max} (m/s)	2.63	1.52	42
	$ND\Gamma_1$	0.0168	0.0029	83
	Parameter	**m = 0**	**m = 5.0**	**% Decrease**
Jet at Vortex Upwash	ω_{xmax} (s^{-1})	857.6	677.0	21
	Γ (m^2/s)	0.167	0.151	9.6
	V_{max} (m/s)	3.06	2.57	16
	$ND\Gamma_1$	0.022	0.015	32
		m = 1.5	**m = 4.8**	**% Decrease**
Jet Opp. Downwash	$ND\Gamma_2$	0.955	0.103	89
		m = 1.0	**m = 5.0**	**% Decrease**
Jet at Upwash:	$ND\Gamma_2$	1.60	0.24	85

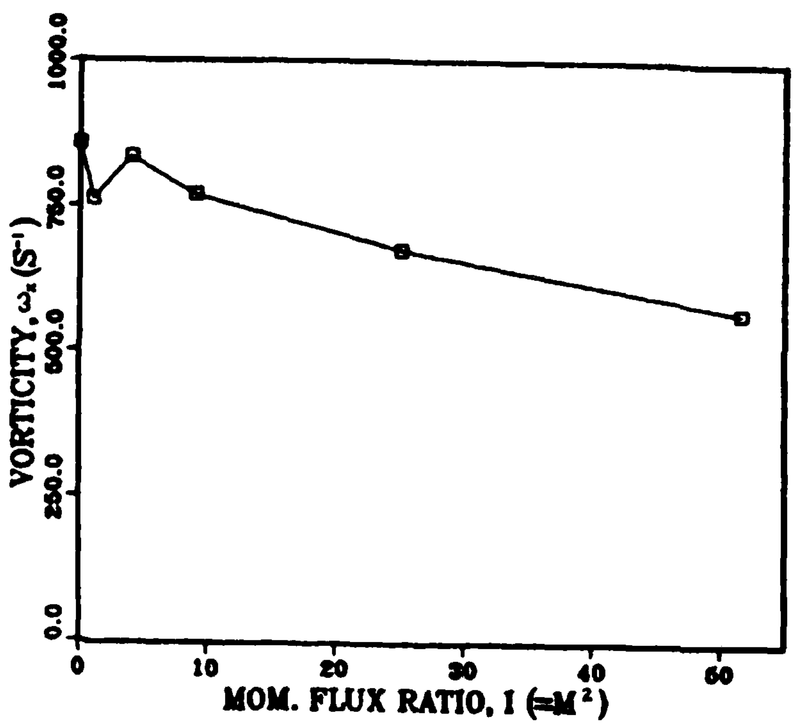

Figure 59. Maximum Streamwise Vorticity (ω_{xmax}) vs. Momentum Flux Ratio

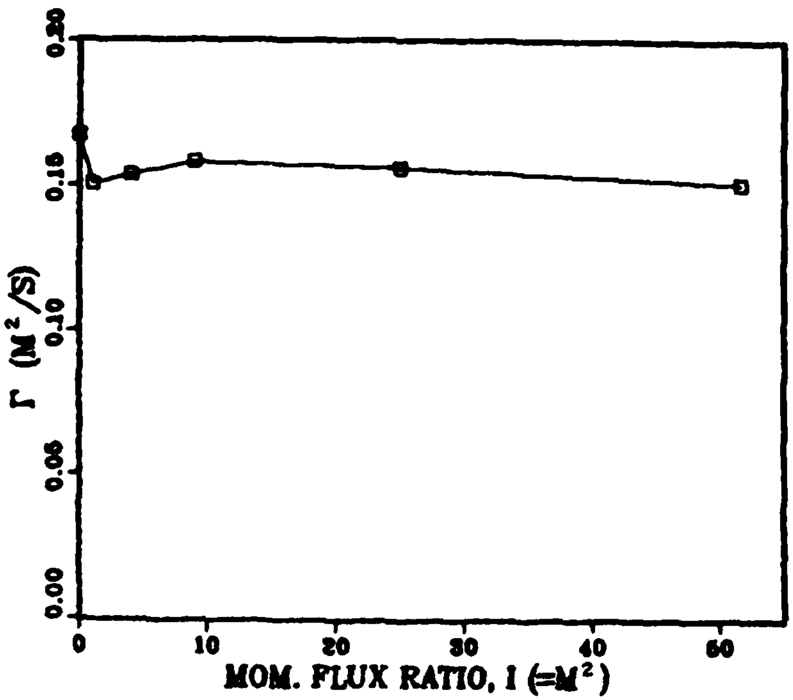

Figure 60. Circulation (Γ) vs. Momentum Flux Ratio

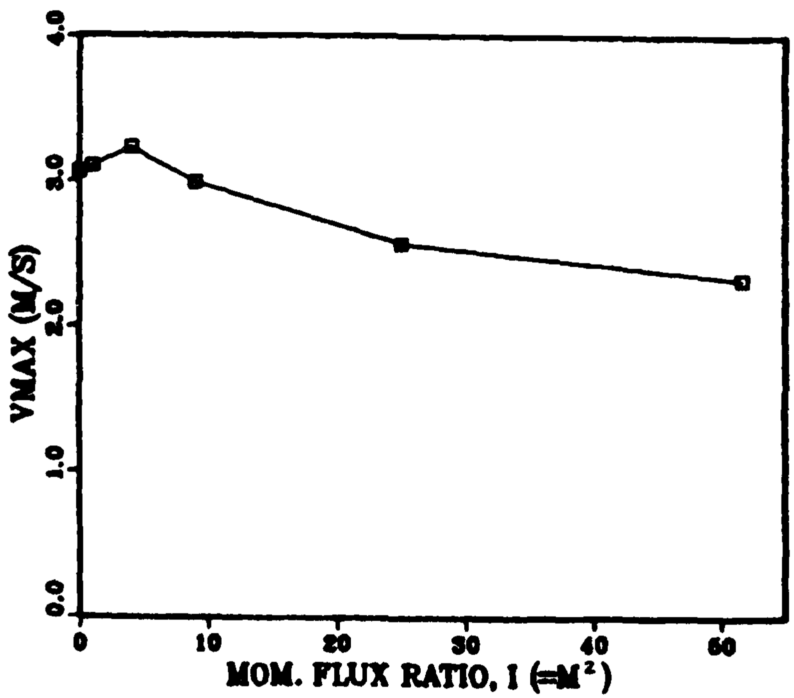

Figure 61. Maximum Secondary Flow Vector Magnitude (v_{max}) vs. Momentum Flux Ratio

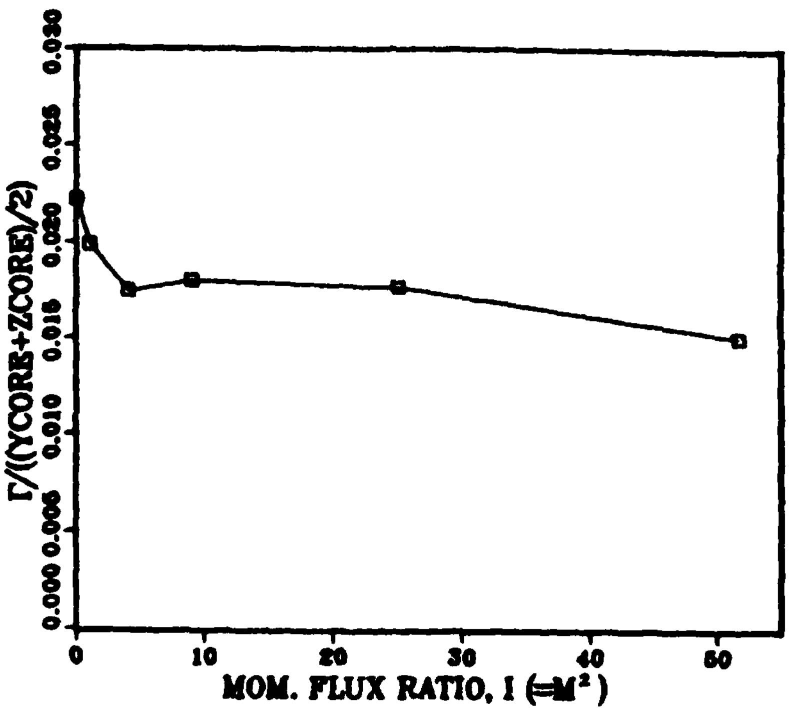

Figure 62. $ND\Gamma_1$ vs. Momentum Flux Ratio

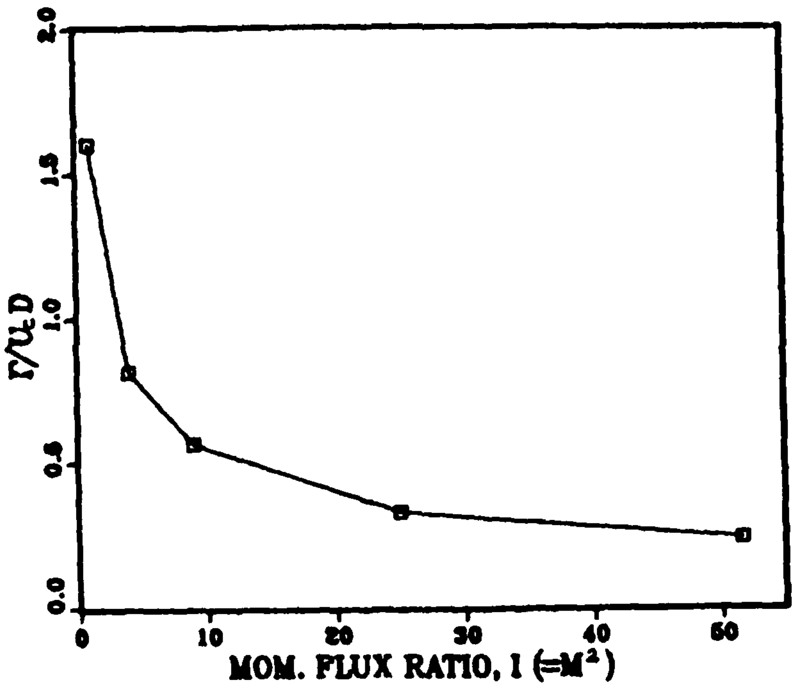

Figure 63. $ND\Gamma_2$ vs. Momentum Flux Ratio

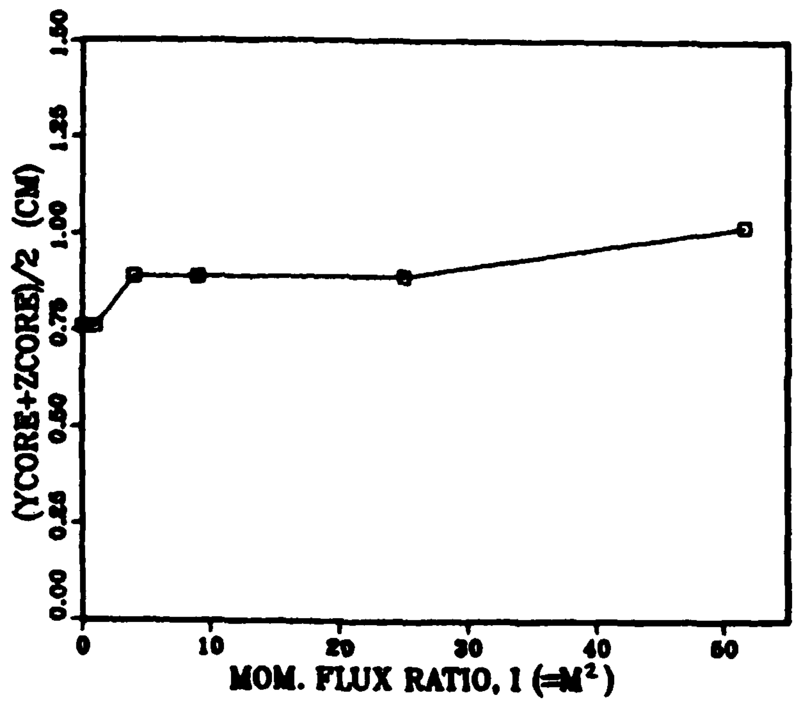

Figure 64. Average Vortex Core Radius vs. Momentum Flux Ratio

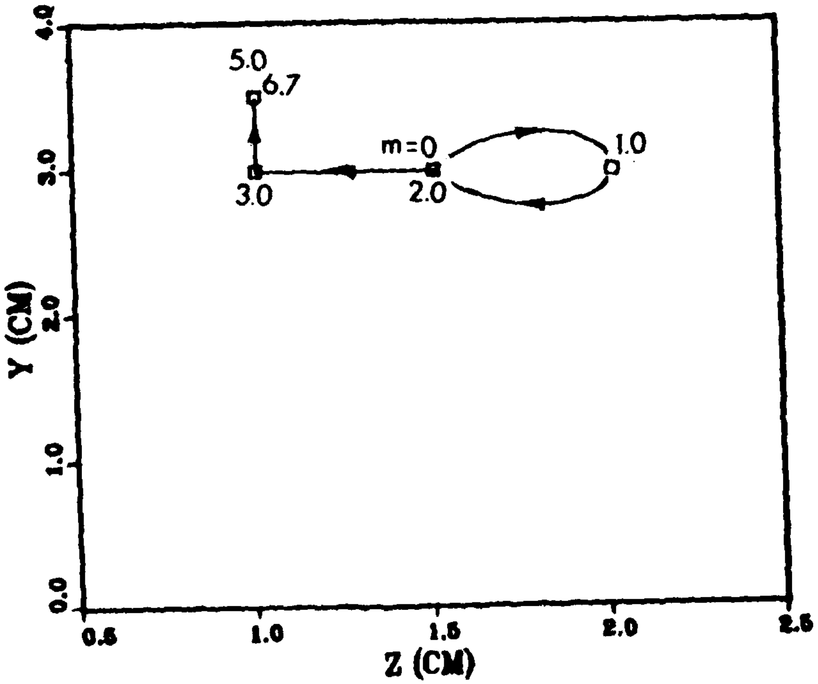

Figure 65. Vortex Center (Y_{cen}, Z_{cen}) Position

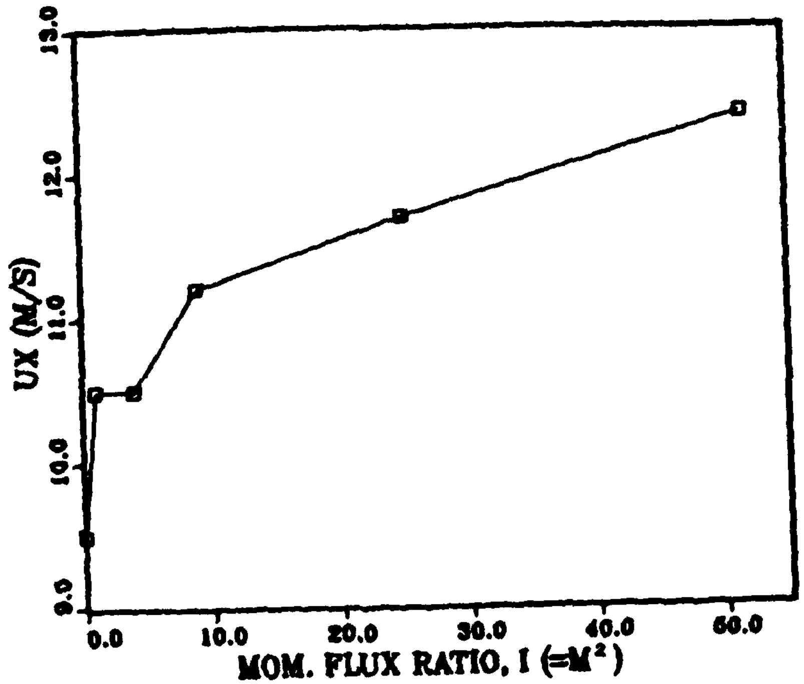

Figure 66. Maximum Streamwise Velocity Component (U_{xmax}) vs. Momentum Flux Ratio

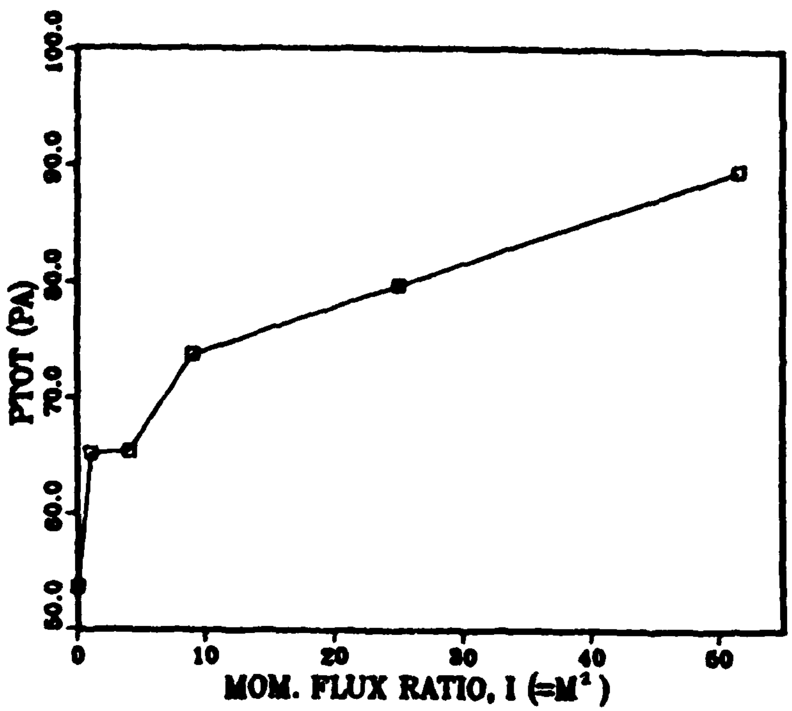

Figure 67. Maximum Total Pressure (P_{tot}) vs. Momentum Flux Ratio

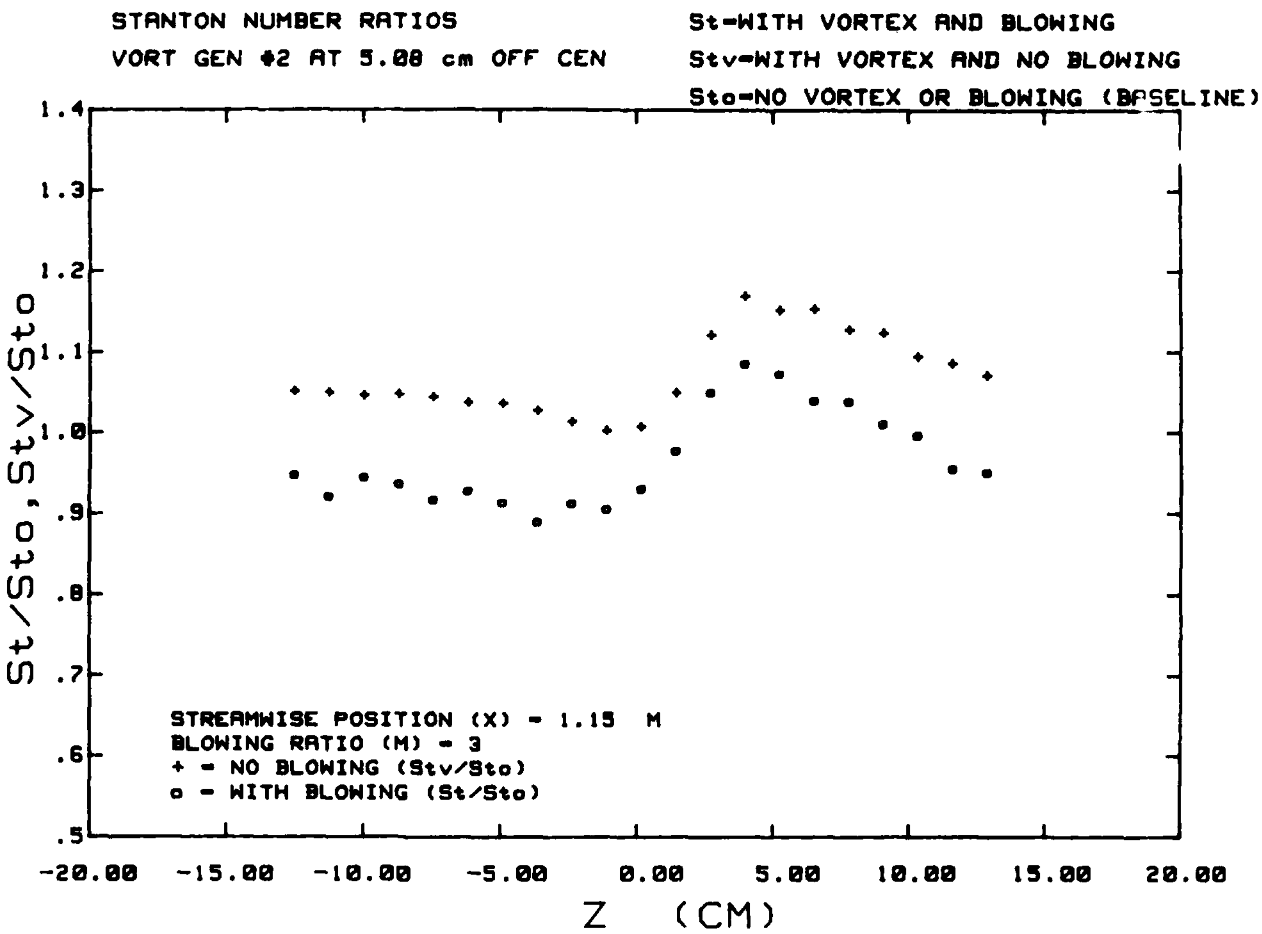

Figure 68. Stanton Number Ratios

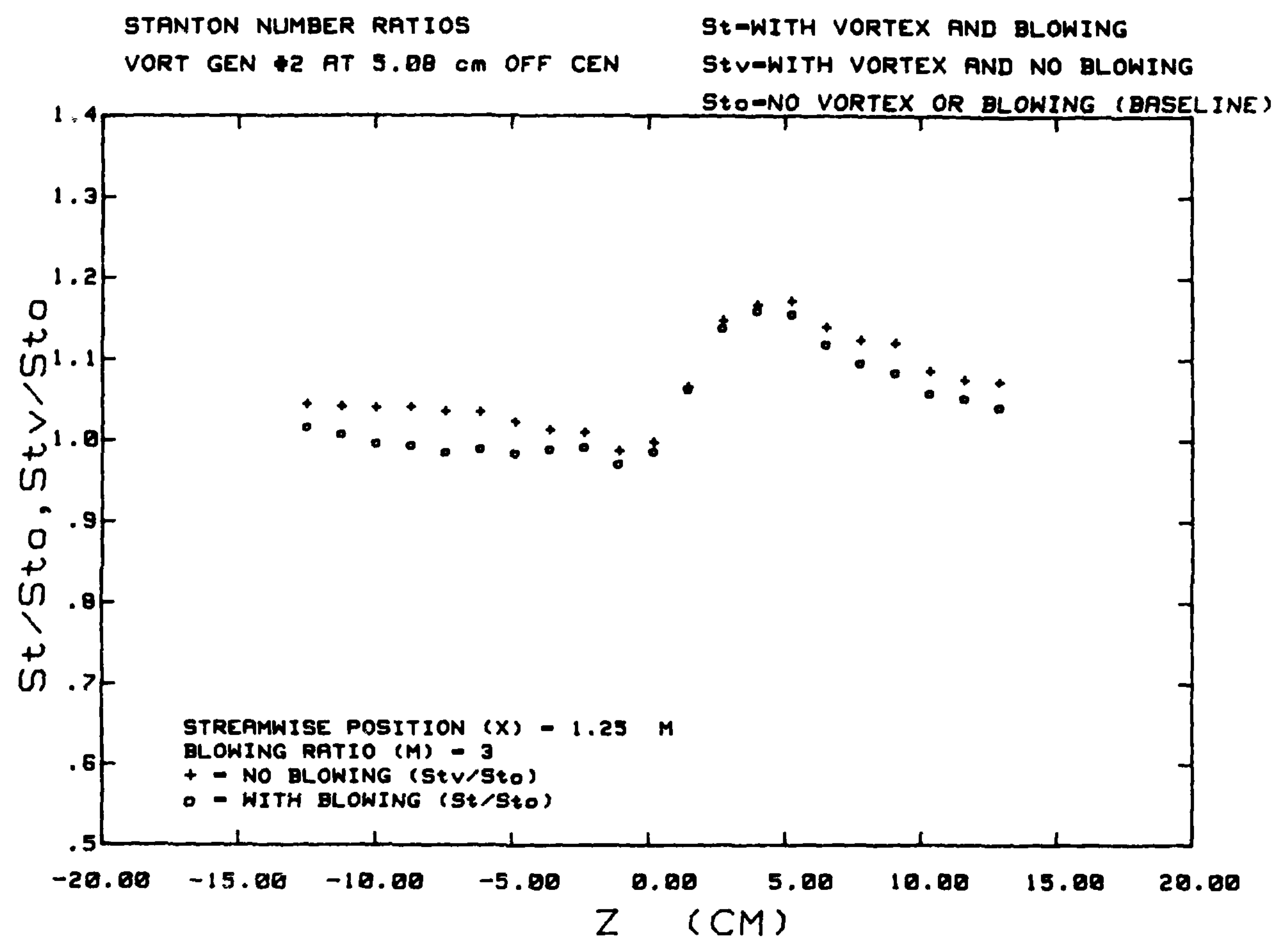

Figure 69. Stanton Number Ratios

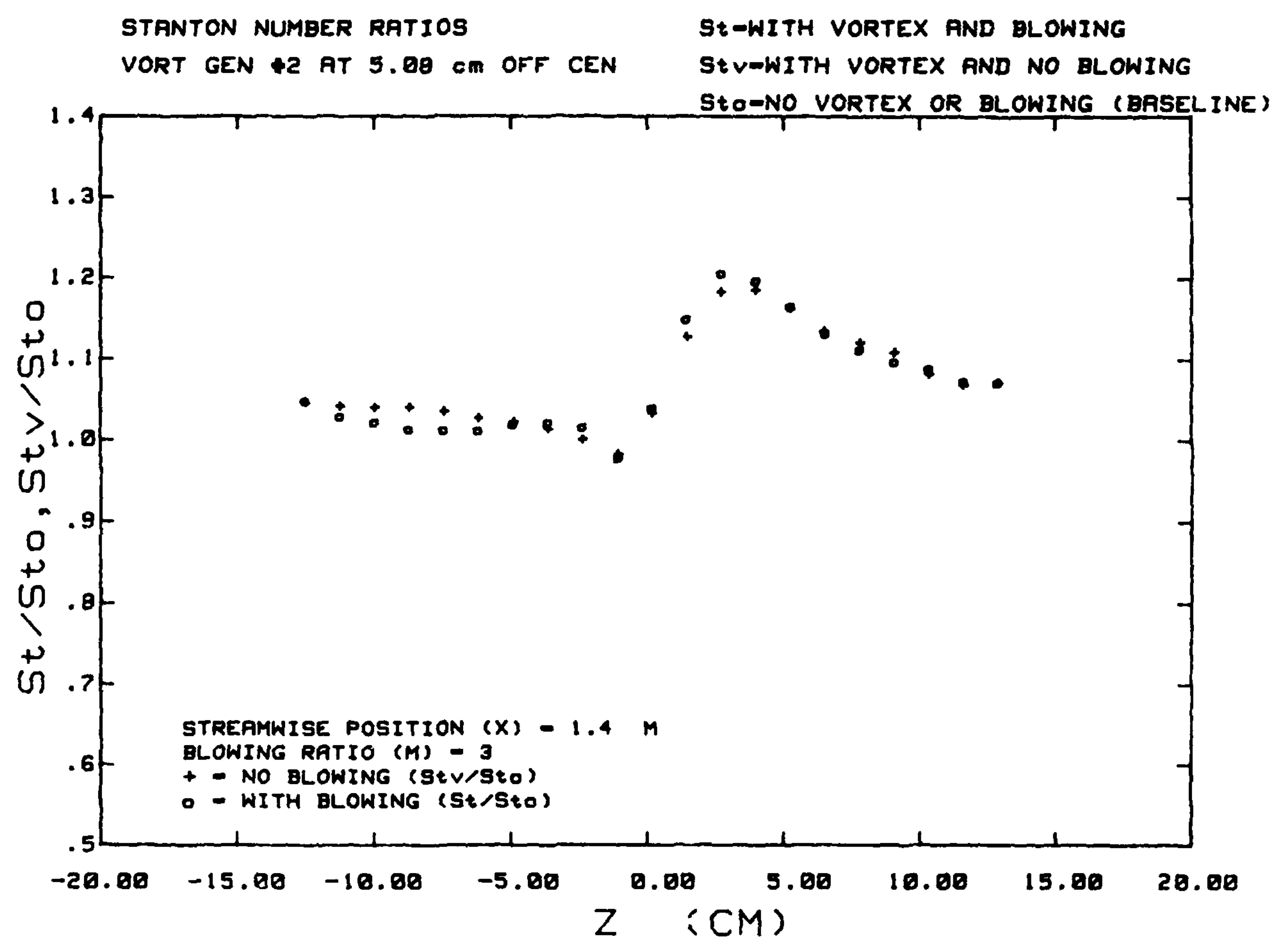

Figure 70. Stanton Number Ratios

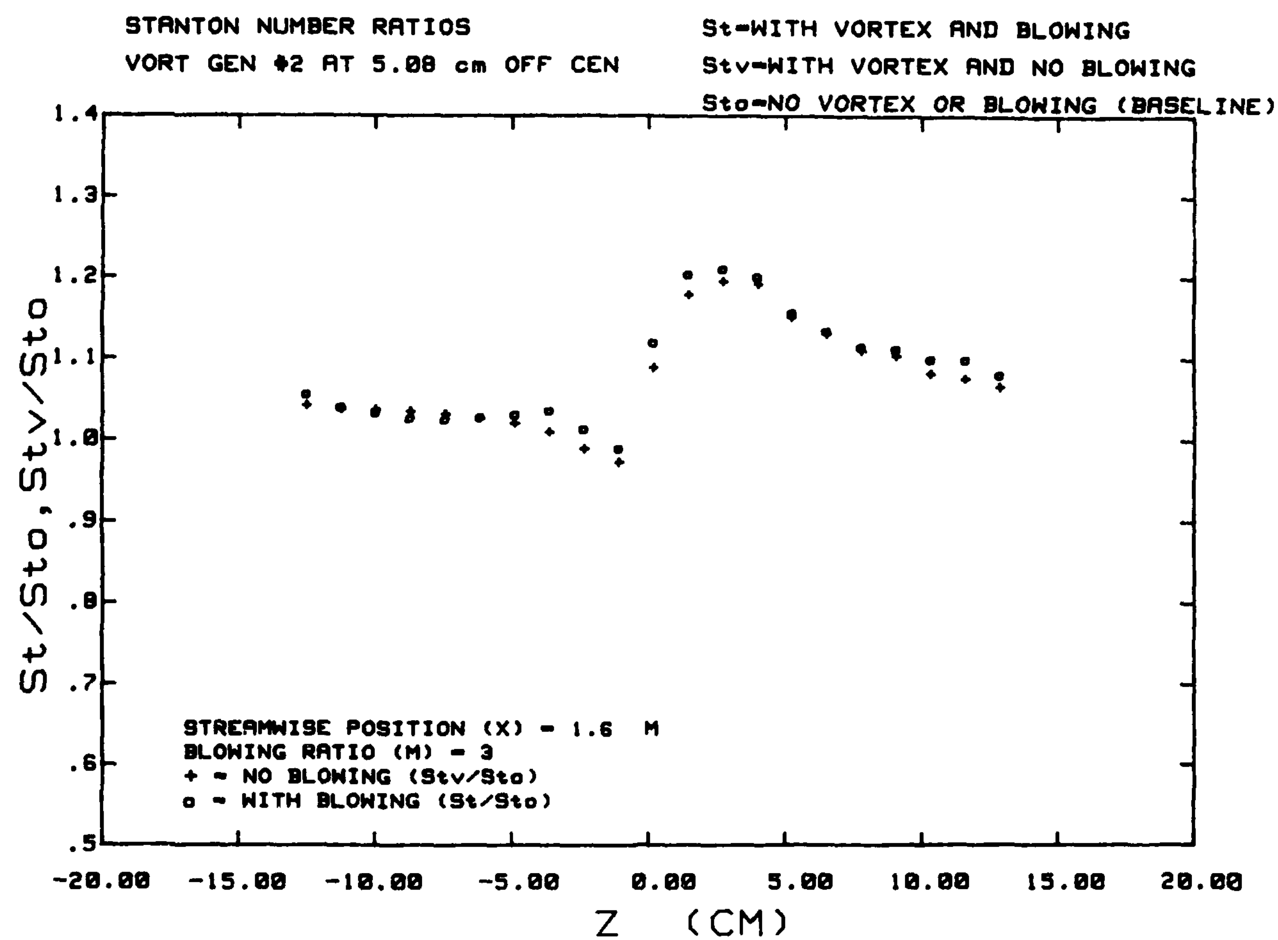

Figure 71. Stanton Number Ratios

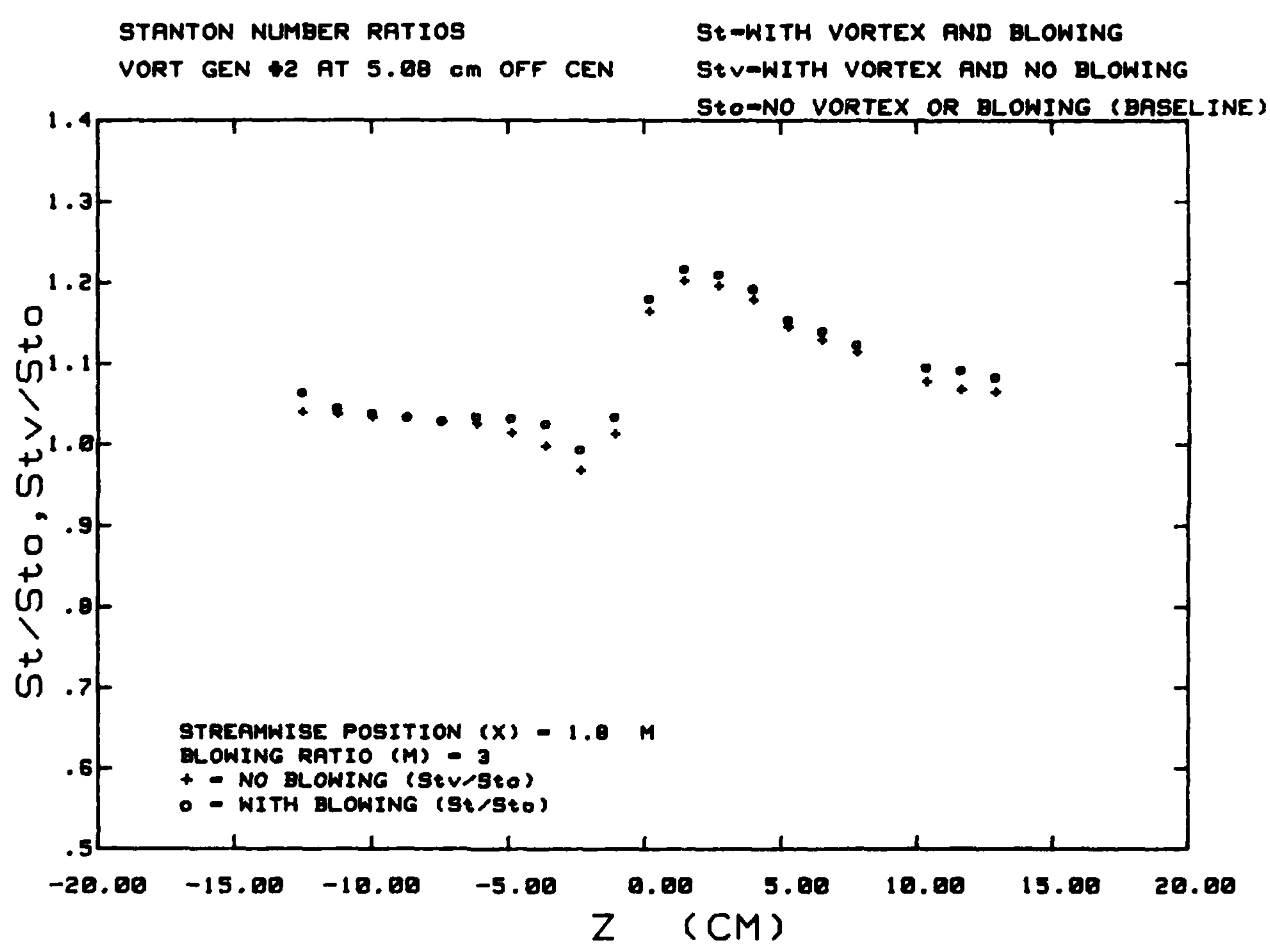

Figure 72. Stanton Number Ratios

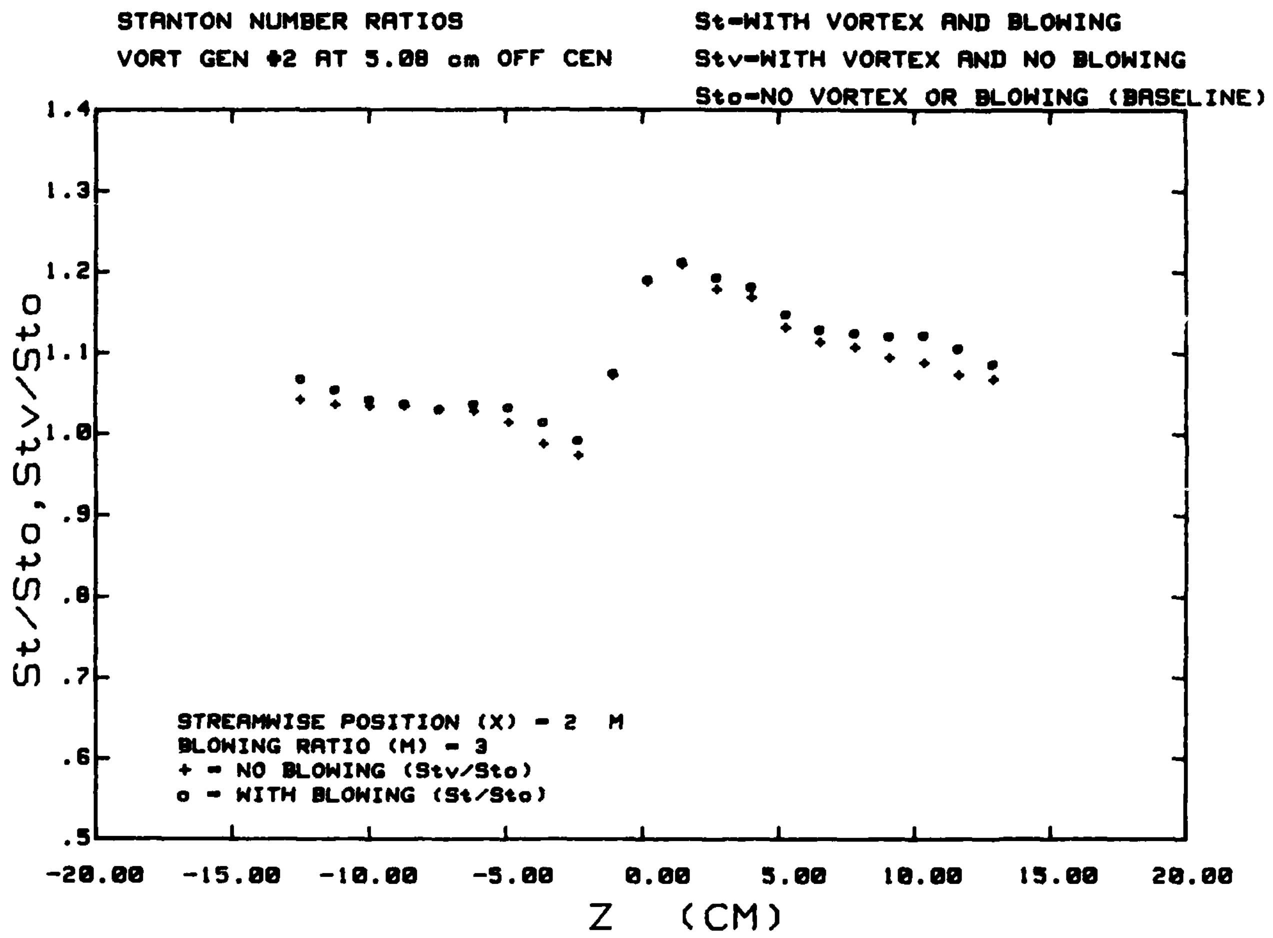

Figure 73. Stanton Number Ratios

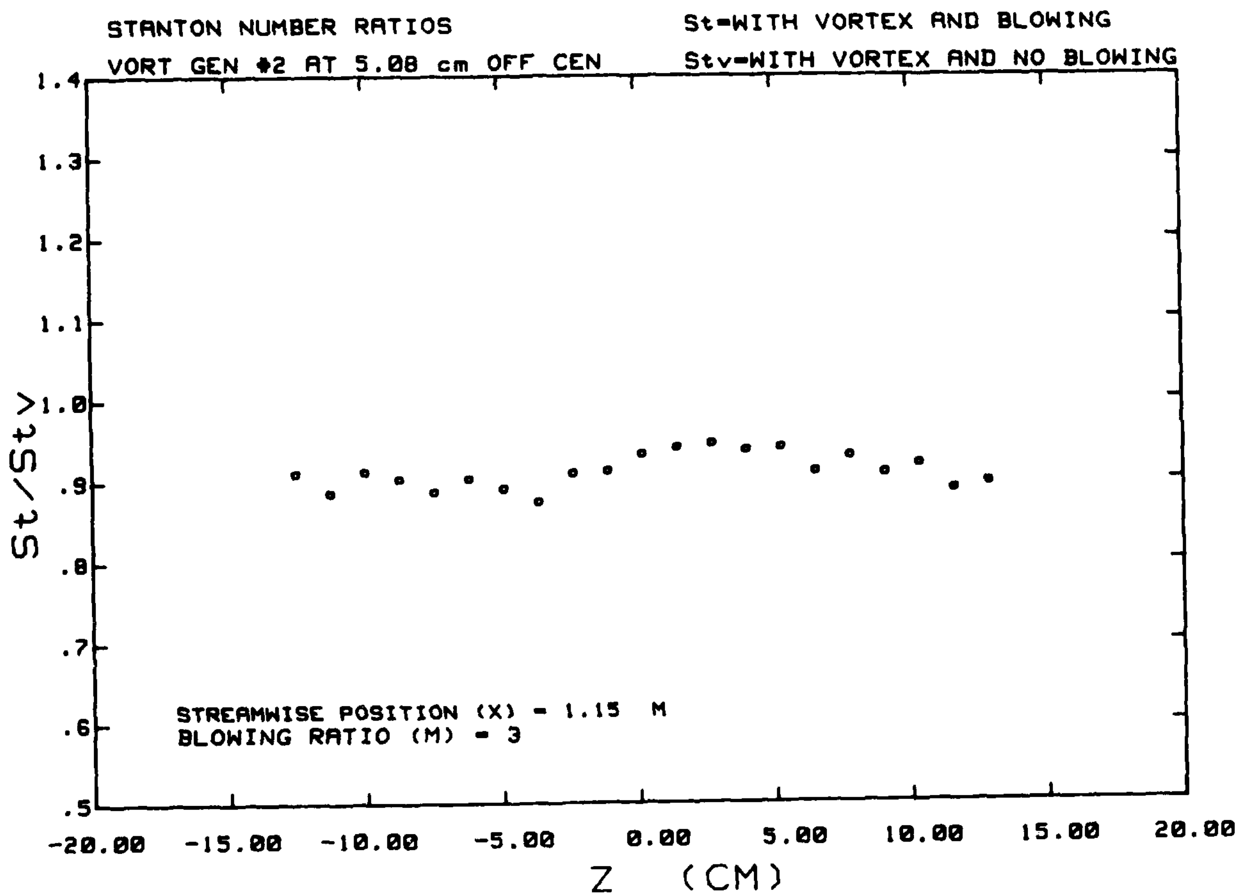

Figure 74. Stanton Number Ratios

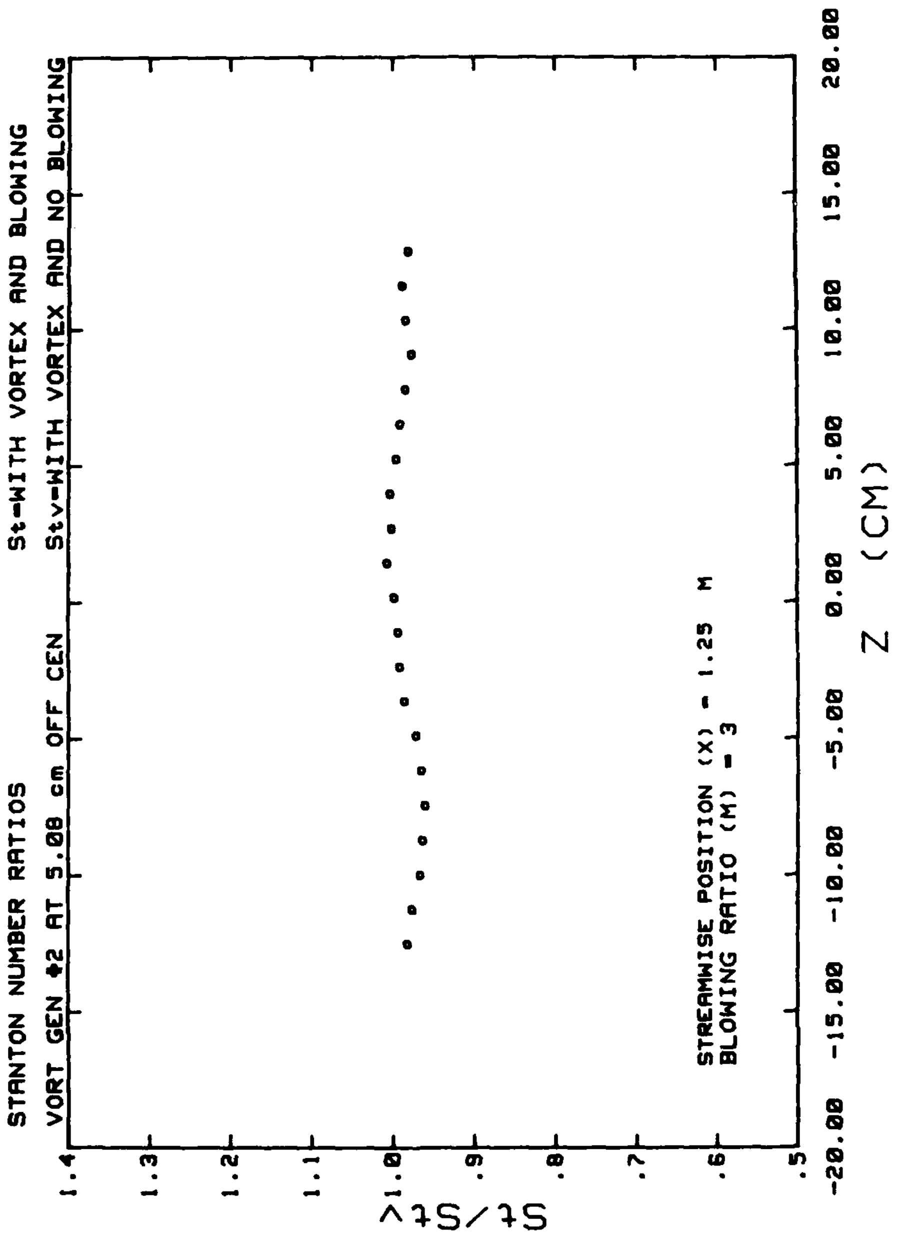

Figure 75. Stanton Number Ratios

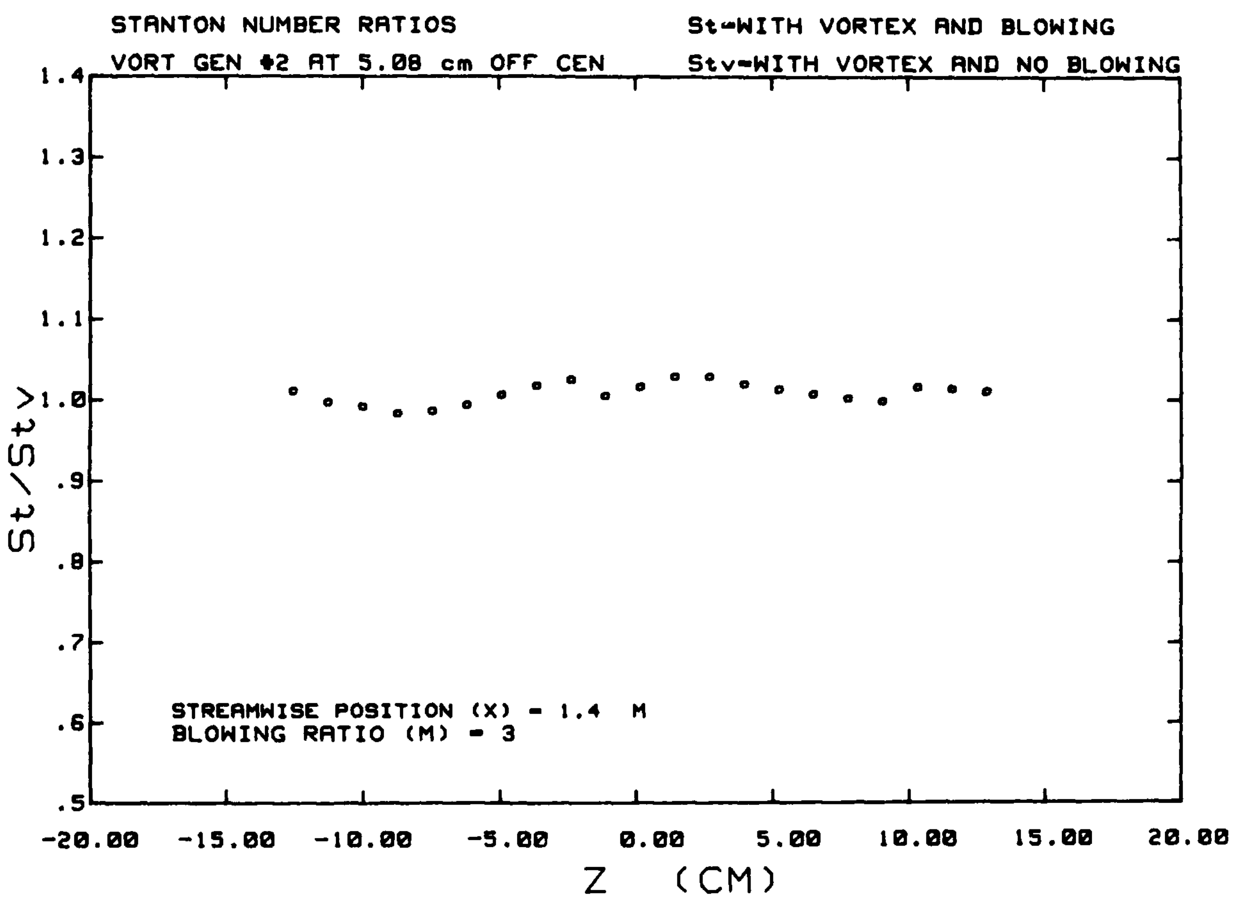

Figure 76. Stanton Number Ratios

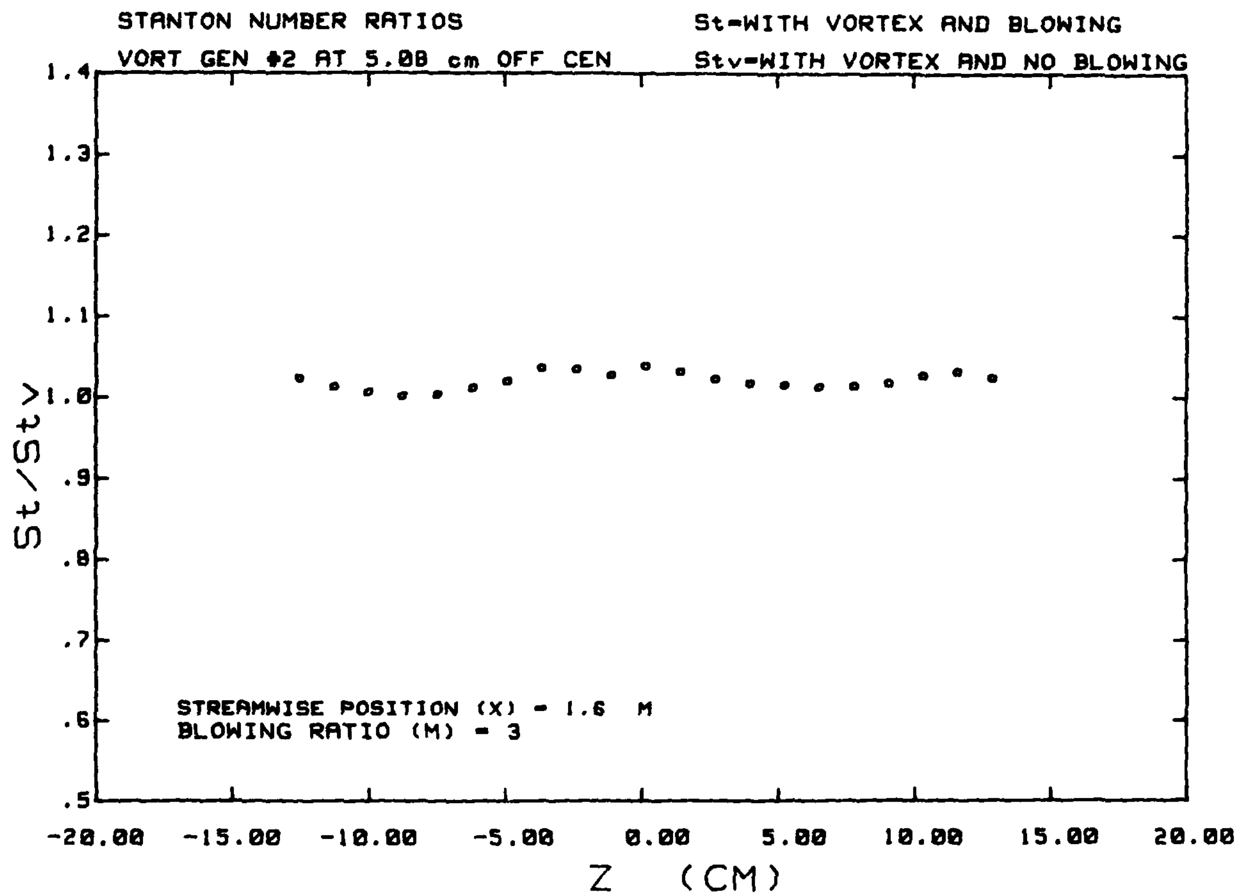

Figure 77. Stanton Number Ratios

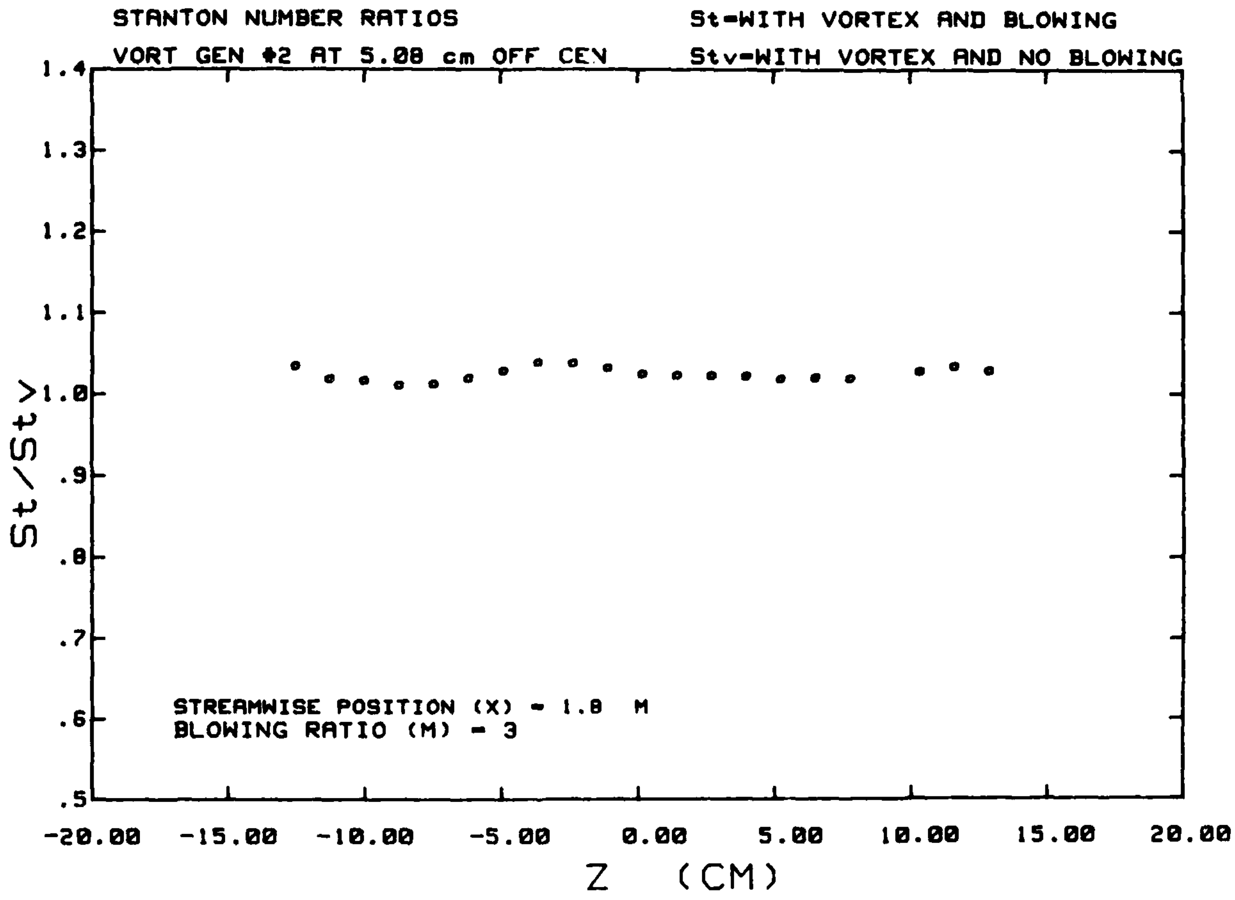

Figure 78. Stanton Number Ratios

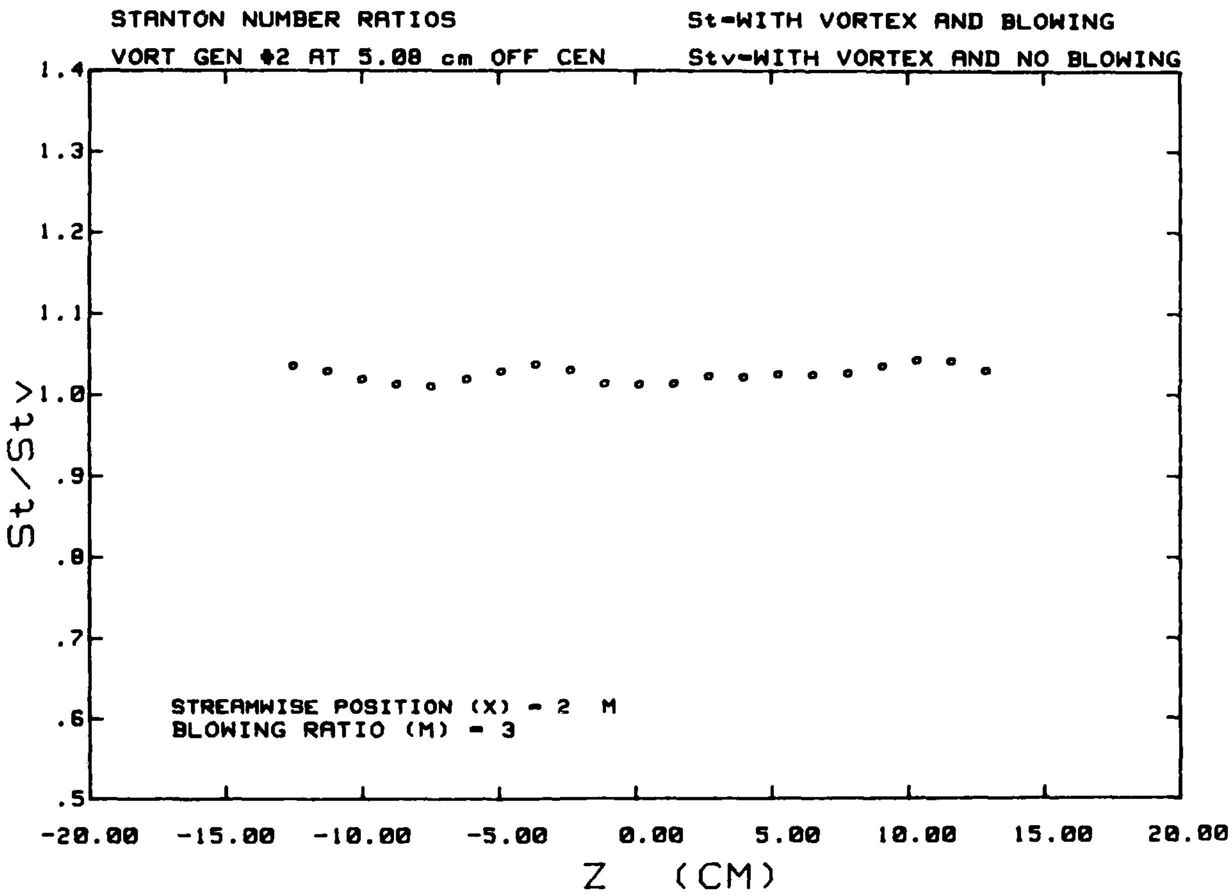

Figure 79. Stanton Number Ratios

that the jet would "augment" the vortex as m increases. This was the case only for m < 2.0, where some augmentation of fluid mechanics parameters (ω_x, Γ, V, $ND\Gamma_1$, $ND\Gamma_2$) did occur. However, higher blowing ratios resulted in reductions in parameters and structural alterations that were similar, but less extreme, to those obtained with the jet opposing the downwash. This is evident from Figures 59-63. Table 5 compares results with injection located at the downwash and at the upwash of the vortex. With the jet in the same direction as the upwash, the average vortex core size increases with blowing ratio and the vortex moves toward the jet (Figures 64, 65). Figures 66 and 67 show that the maximum total pressure and maximum streamwise velocity increase with increasing jet momentum.

Several interesting effects are visualized in the plots corresponding to this experiment in Appendix A (Figures 174-203). The secondary flow vector plots show that at very high blowing ratio a second, counter-rotating vortex is produced to the left and above the main vortex upwash. This evidences a blockage effect at high blowing ratios which opposes the secondary flow. With the jet in the same direction as the upwash, the vortex resembles a combined vortex at high blowing ratio, in contrast to the vortex interacting with a jet opposing the downwash.

Figures 68-73 present St/Sto and Stv/Sto at m = 3.0, while Figures 74-79 present St/Stv. As with the jet

TABLE 6

FLUID MECHANICS MEASUREMENTS FOR VORTEX GENERATOR #2
AT Z = +5.08 CM (+2 IN), PROBE POSITION B*

m	V_{max} (m/s)	U_{xmax} (m/s)	ω_{xmax} (1/s)	$(\frac{Y_{core}+Z_{core}}{2})$ (cm)	Y_{cen} (cm)	Z_{cen} (cm)	Γ (m^2/s)	$ND\Gamma_1$	$ND\Gamma_2$	P_{max} (Pa)
0	3.06	9.5	857.6	0.76	2.98	1.52	0.167	0.0022	-	53.6
1.0	3.10	10.5	762.1	0.76	2.98	2.03	0.150	0.02	1.60	65.2
2.0	3.23	10.5	834.2	0.89	2.98	1.52	0.154	0.017	0.816	65.4
3.0	2.99	11.2	770.0	0.89	2.98	1.02	0.158	0.018	0.57	73.8
5.0	2.57	11.7	677.0	0.89	3.49	1.02	0.156	0.0177	0.331	79.7
6.7	2.33	12.4	572.1	1.02	3.49	1.02	0.151	0.015	0.24	89.6

*x/d = 41.9

opposing the vortex downwash, high blowing ratio has little effect on wall heat transfer for X = 1.25 m (x/d = 17.89) and beyond. The explanation for this is the same as in the case of the jet opposing the vortex downwash.

E. EXPERIMENTAL RESULTS FOR INJECTION AT VORTEX DOWNWASH: x/d = 41.9 (PROBE POSITION B); UNDISTURBED VORTEX CIRCULATION = 34.2 x 10^{-1} m^2/s

For this experiment, vortex generator #3 was placed at the tunnel centerline and injection was through the center wall jet, so that the jet opposed the vortex downwash. The five-hole pressure probe was placed at x/d = 41.9 (position B). Vortex generator #3 is larger than vortex generator #2 (Figure 3), and thus produces a vortex with greater (~1.3x) undisturbed circulation of streamwise vorticity.

Results of this experiment, in which blowing ratio was increased from 0 to 3.0, are summarized in Table 8 and Figures 80-88 in this chapter, and Figures 204-228 in Appendix A. Prior to conducting the experiment, it was expected that since the undisturbed vortex was stronger and structurally larger, the results would be similar but less extreme to those with the weaker, smaller vortex in the first experiment. This was in fact the case. A comparison of fluid mechanics parameters (ω_x, Γ, V, NDΓ_1, NDΓ_2) in the two experiments is given in Table 7. No heat transfer measurements were made in this experiment.

TABLE 7

COMPARISON: VORTEX GENERATORS #2 AND #3, WALL JET AT VORTEX DOWNWASH

	Parameter	m = 0	m = 3.0	% Decrease
Generator #2	ω_{xmax} (s^{-1})	725.9	128.3	82
	Γ (m^2/s)	0.148	0.047	68
	V_{max} (m/s)	2.63	1.52	42
	$ND\Gamma_1$	0.0168	0.0029	83
Generator #3	ω_{xmax}	1001.5	705.6	30
	Γ	0.342	0.271	21
	V_{max}	4.2	3.3	21
	$ND\Gamma_1$	0.025	0.022	12
		m = 1.5	m = 3.0	% Decrease
Gen. #2:	$ND\Gamma_2$	0.955	0.273	71
		m = 1.5	m = 3.0	
Gen. #3:	$ND\Gamma_2$	2.4	0.96	60

TABLE 8

FLUID MECHANICS MEASUREMENTS FOR VORTEX GENERATOR #3
AT TUNNEL CENTERLINE, PROBE POSITION B*

m	V_{max} (m/s)	U_{xmax} (m/s)	ω_{xmax} (1/s)	$(\frac{Y_{core}+Z_{core}}{2})$ (cm)	Y_{cen} (cm)	Z_{cen} (cm)	Γ (m^2/s)	$ND\Gamma_1$	$ND\Gamma_2$	P_{max} (Pa)
0	4.2	10.2	1001.5	1.4	4.0	-4.06	0.342	0.025	-	64.3
1.5	4.31	10.3	1112.3	1.4	4.51	-4.06	0.338	0.024	2.4	65.0
2.1	3.94	10.4	909.7	1.27	4.51	-3.56	0.33	0.026	1.67	64.3
2.6	3.55	10.8	816.3	1.4	5.02	-3.56	0.293	0.021	1.2	69.1
3.0	3.3	11.1	705.6	1.27	5.02	-3.05	0.271	0.022	0.96	72.4

*x/d = 41.9

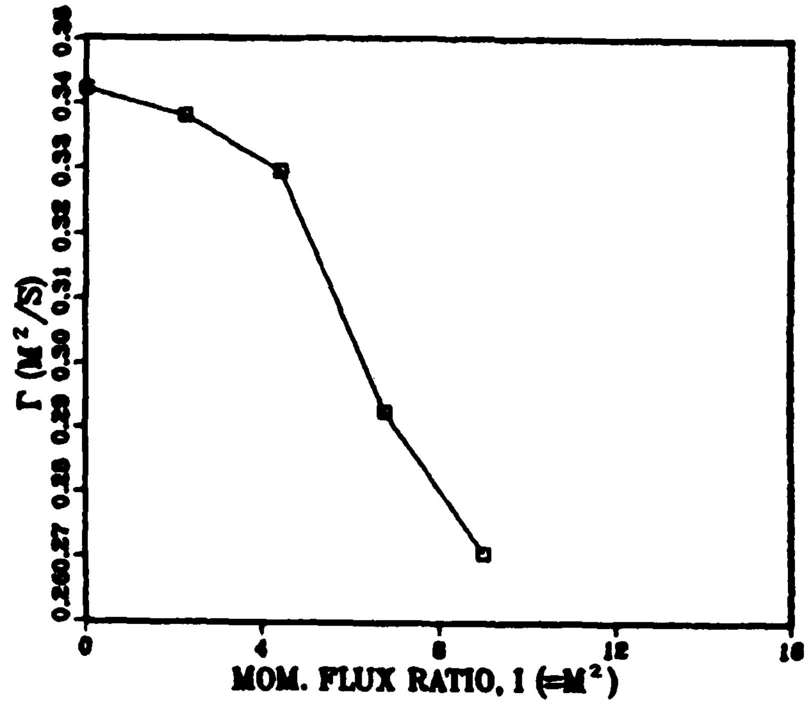

Figure 80. Circulation (Γ) vs. Momentum Flux Ratio

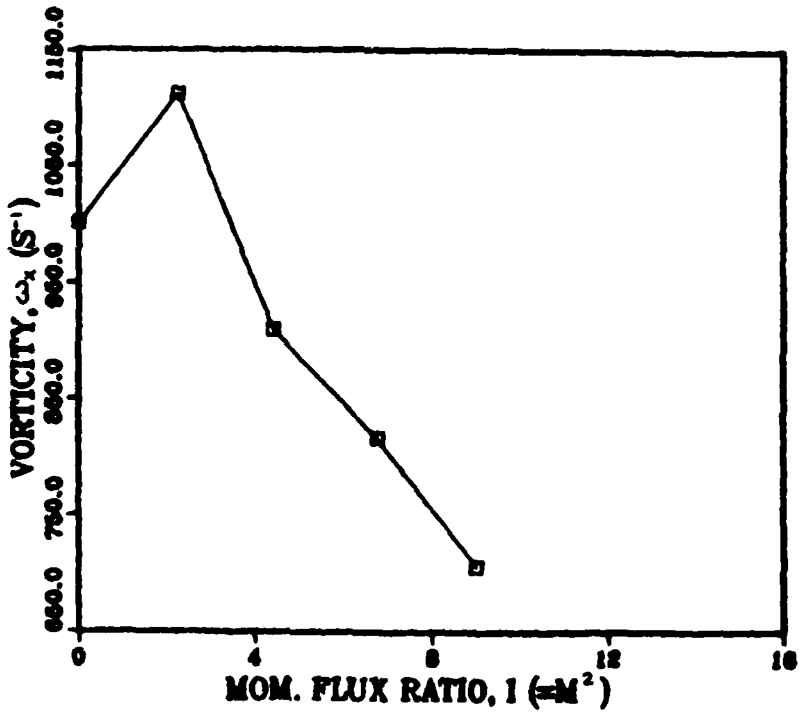

Figure 81. Maximum Streamwise Vorticity (ω_{xmax}) vs. Momentum Flux Ratio

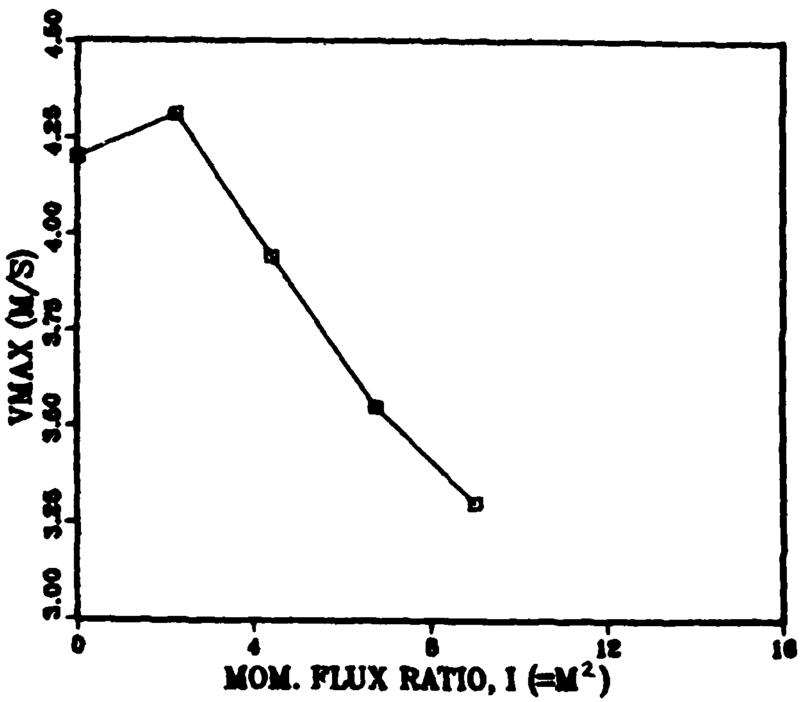

Figure 82. Maximum Secondary Flow Vector Magnitude (V_{max}) vs. Momentum Flux Ratio

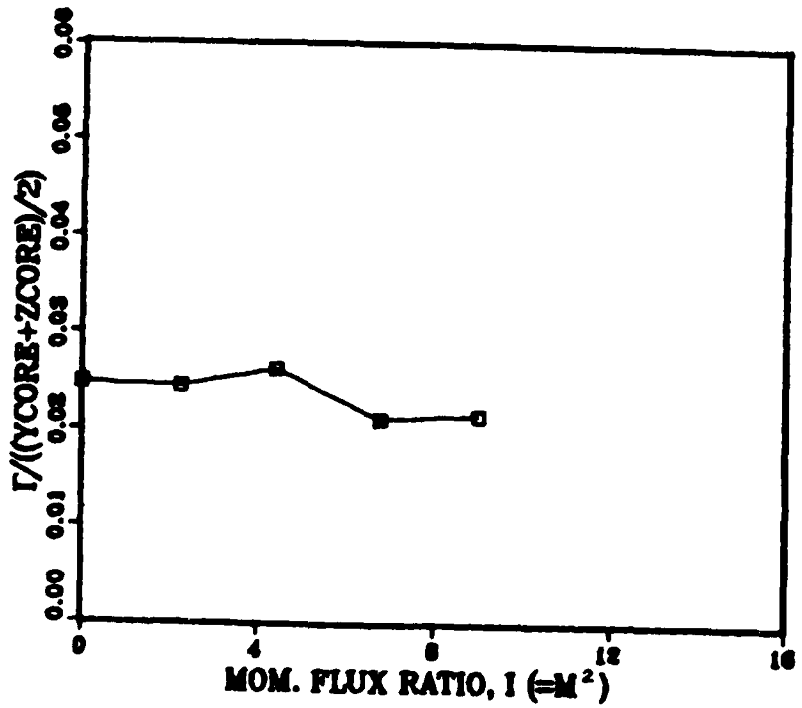

Figure 83. $ND\Gamma_1$ vs. Momentum Flux Ratio

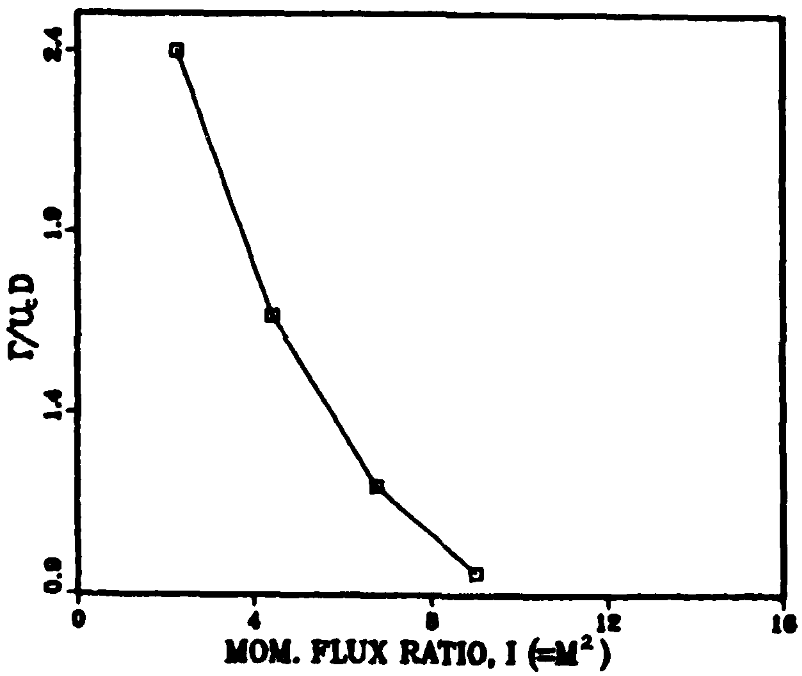

Figure 84. $ND\Gamma_2$ vs. Momentum Flux Ratio

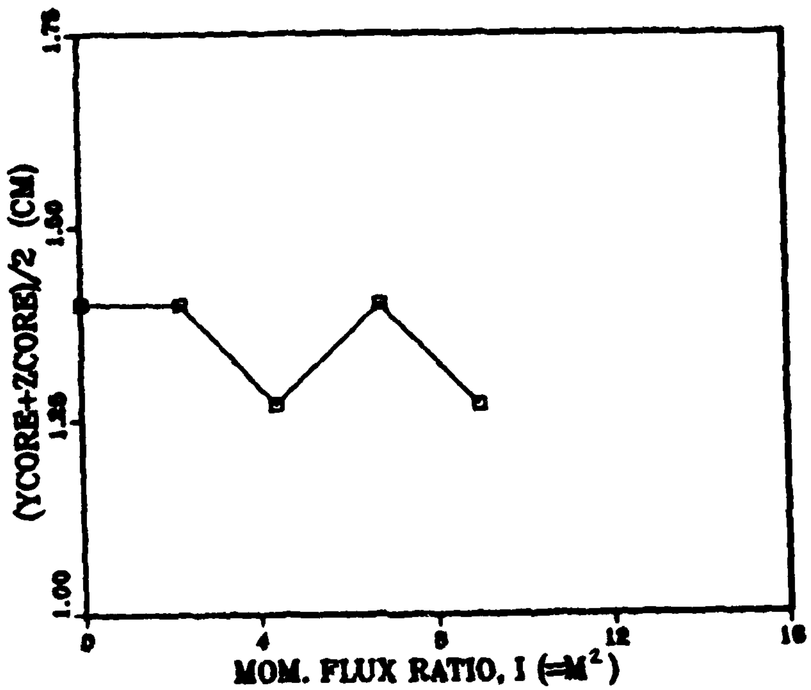

Figure 85. Average Vortex Core Radius vs. Momentum Flux Ratio

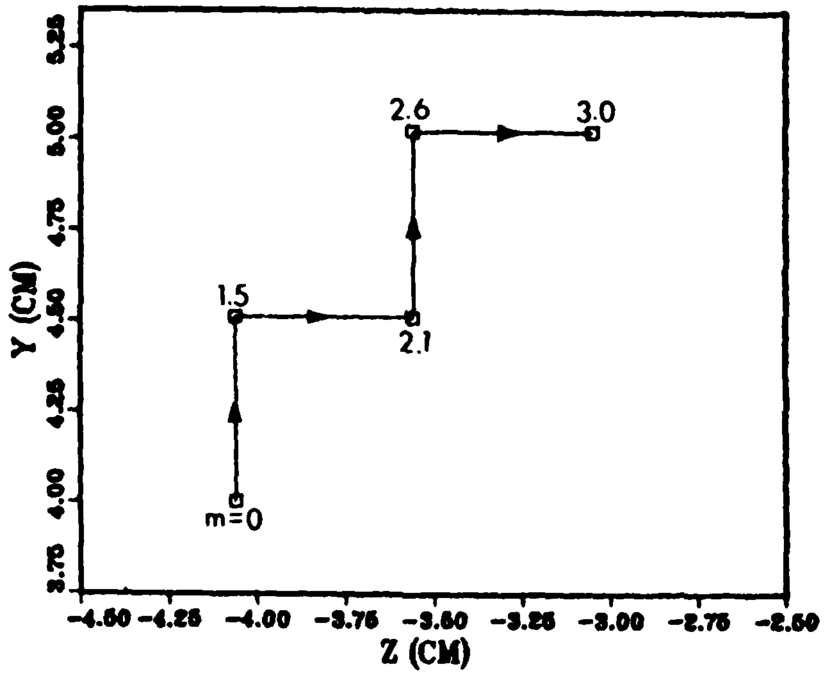

Figure 86. Vortex Center (Y_{cen},Z_{cen}) Position

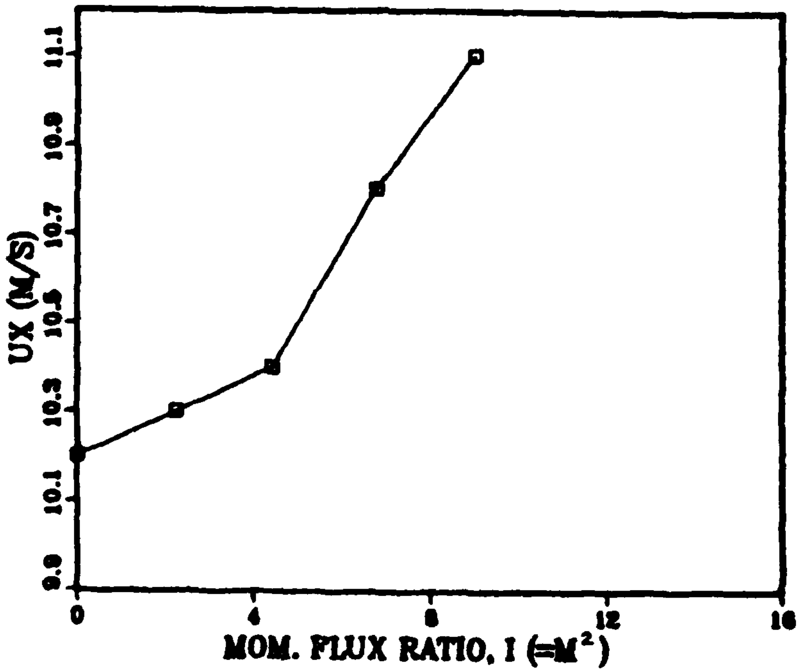

Figure 87. Maximum Streamwise Velocity Component (U_{xmax}) vs. Momentum Flux Ratio

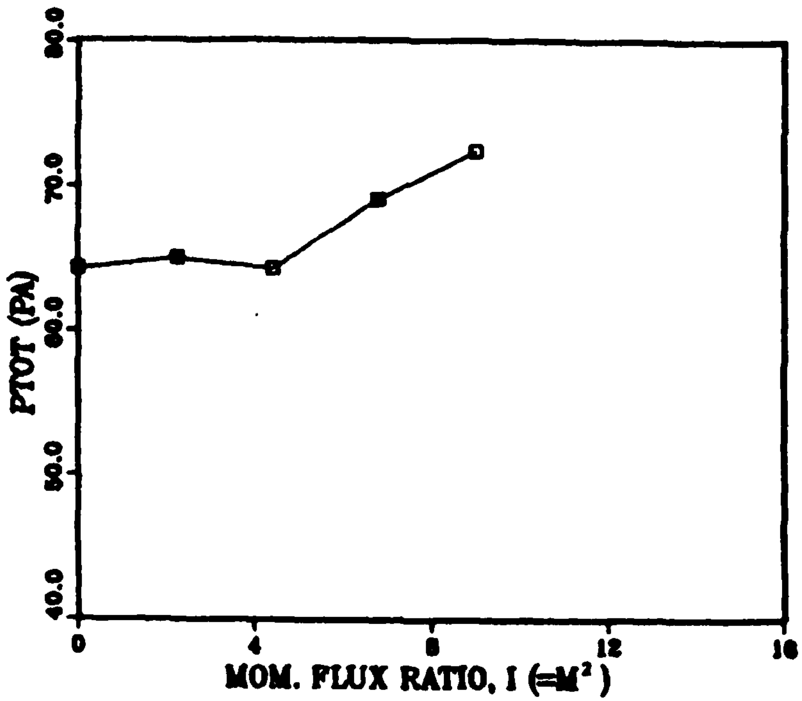

Figure 88. Maximum Total Pressure vs. Momentum Flux Ratio

IV. SUMMARY AND CONCLUSIONS

Observations were made of streamwise vortices embedded in a turbulent boundary layer. The vortices were generated with a half delta wing attached to the floor of a wind tunnel with zero pressure gradient. The wind tunnel floor was capable of being heated and was fitted with wall jets and an injection system. The heated wall was instrumented with thermocouples for making heat transfer measurements (spanwise Stanton numbers and Stanton number ratios). Fluid mechanics measurements (pressure, mean velocity components, streamwise vorticity, circulation) were made using a five-hole pressure probe. Four experiments were conducted, each with a number of experimental runs, to determine if the properties and structure of a vortex can be influenced and controlled with a wall jet.

Wall jets significantly influence the behavior and structural characteristics of streamwise vortices embedded in turbulent boundary layers. By placing a jet in opposition to a vortex downwash, blowing ratio above 1.0 reduces streamwise vorticity and circulation, and causes the secondary flow velocity magnitude in the vortex "core" (combined vortex model) to become nearly uniform. Similar but less significant effects on vorticity and circulation may be obtained with the jet at the vortex upwash as a result of a

blockage effect. In contrast, however, wall heat transfer rates with an embedded vortex are not significantly altered for blowing ratios greater than 1.0. The heat transfer peak at the vortex downwash with $m = 0$, which is reduced for $0 < m < 1.0$, remains intact at $m > 2.0$. This is because for $m > 2.0$ the jet lifts off the wall and has minimal influence on the near wall region of the boundary layer already altered by the vortex. It is recommended that further study be conducted on the turbulence characteristics of embedded vortex and wall jet interactions.

Highlights of the four experiments conducted in this study follow. x = streamwise distance from wall jet hole; d = wall jet hole diameter (0.95 cm); X = streamwise distance from origin of velocity boundary layer; m = blowing ratio.

1. Experiment 1

Jet opposing vortex downwash, $x/d = 41.9$, $m = 0$ to 4.8: streamwise vorticity decreased from ~750 to ~150 s^{-1}, while circulation of streamwise vorticity decreased from ~0.15 to ~0.05 m^2/s. The average core radius increased from ~0.9 to ~2.4 cm, while the vortex moved ~3.0 cm toward the jet. $m = 3.0$ was a significant blowing ratio, beyond which further influences on the vortex by the jet were minimal.

2. Experiment 2

Jet opposing vortex downwash, streamwise development; $m = 0, 2.1, 3.5$: streamwise vorticity and circulation decreased with downstream distance. This effect was

enhanced by increasing blowing ratio. Vortex average core radius increased with downstream distance, and this effect was also augmented by increasing blowing ratio. Interestingly, blowing ratio had no effect on streamwise development of vortex center height above the tunnel floor. Beyond X = 1.25 m (x/d = 17.89) wall heat transfer rates were nearly the same for m = 0, 2.1, and 3.5 (all with a vortex).

3. Experiment 3

Jet a vortex upwash, x/d = 41.9, m = 0 to 6.7: prior to conducting the experiment, results were expected to be opposite to Experiment 1 above. In contrast, for m > 2.0 results were similar due to blockage effect. Streamwise vorticity decreased from ~860 to ~570 s^{-1}, while circulation decreased from ~0.17 to 0.15 m^2/s. For m = 3.0 with a vortex it was again found that wall heat transfer rates were nearly the same as for m = 0 with a vortex.

4. Experiment 4

Jet opposing vortex downwash, x/d = 41.9, m = 0 to 3.0, stronger vortex: with a larger vortex, having greater circulation, fluid mechanics and vortex structural trends were the same as for Experiment 1 above, but results were less extreme numerically.

APPENDIX A

WIND TUNNEL FLUID MECHANICS PLOTS

This appendix contains fluid mechanics plots as listed below in Table 9.

TABLE 9

WIND TUNNEL FLUID MECHANICS PLOTS

Figures	Jet at	Generator #	x/d (Probe Posit.)	m
89-93	Downwash	2	41.9 (B)	1.5
94-98	Downwash	2	41.9 (B)	2.6
99-103	Downwash	2	41.9 (B)	3.0
104-108	Downwash	2	41.9 (B)	4.375
109-113	Downwash	2	41.9 (B)	4.8
114-118	Downwash	2	5.2 (A)	0
119-123	Downwash	2	5.2 (A)	2.1
124-128	Downwash	2	5.2 (A)	3.5
129-133	Downwash	2	41.9 (B)	0
134-138	Downwash	2	41.9 (B)	2.1
139-143	Downwash	2	41.9 (B)	3.5
144-148	Downwash	2	82.9 (C)	0
149-153	Downwash	2	82.9 (C)	2.1
154-158	Downwash	2	82.9 (C)	3.5
159-163	Downwash	2	109.2 (D)	0
164-168	Downwash	2	109.2 (D)	2.1
169-173	Downwash	2	109.2 (D)	3.5
174-178	Upwash	2	41.9 (B)	0
179-183	Upwash	2	41.9 (B)	1.0
184-188	Upwash	2	41.9 (B)	2.0
189-193	Upwash	2	41.9 (B)	3.0
194-198	Upwash	2	41.9 (B)	5.0
199-203	Upwash	2	41.9 (B)	6.7
204-208	Downwash	3	41.9 (B)	0
209-213	Downwash	3	41.9 (B)	1.5
214-218	Downwash	3	41.9 (B)	2.1
219-223	Downwash	3	41.9 (B)	2.6
224-228	Downwash	3	41.9 (B)	3.0

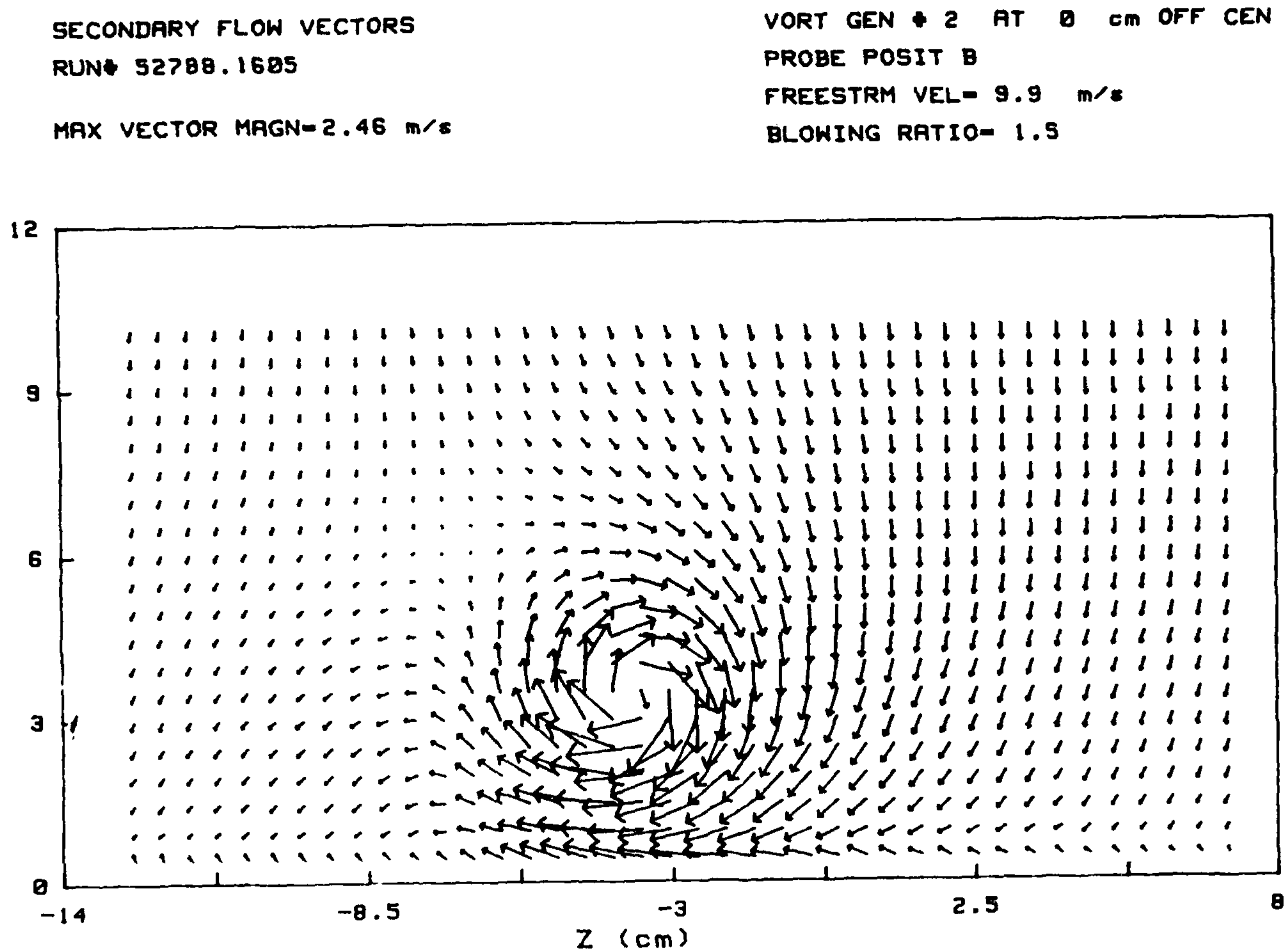

Figure 89. Secondary Flow Vectors

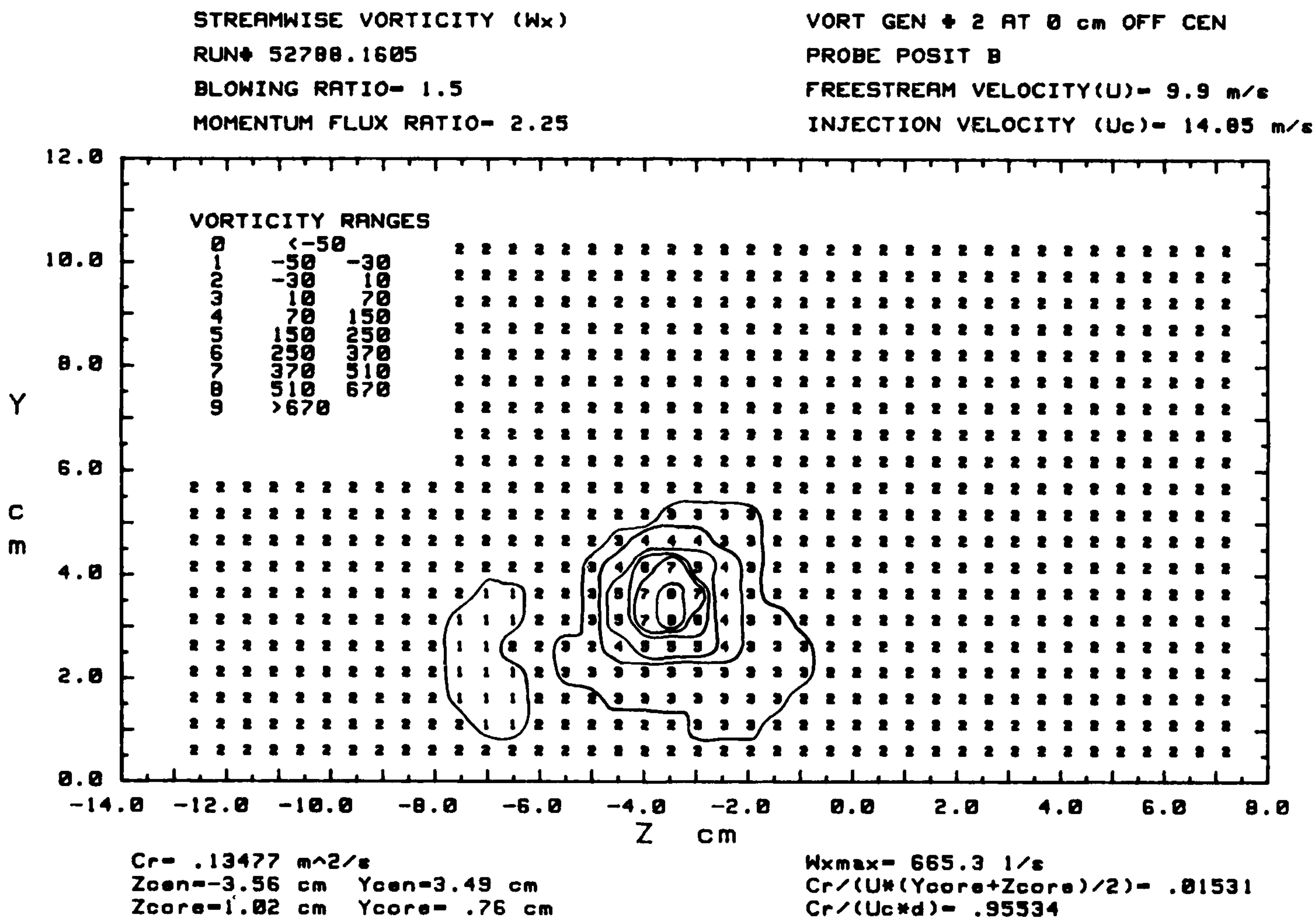

Figure 90. Streamwise Vorticity Contours

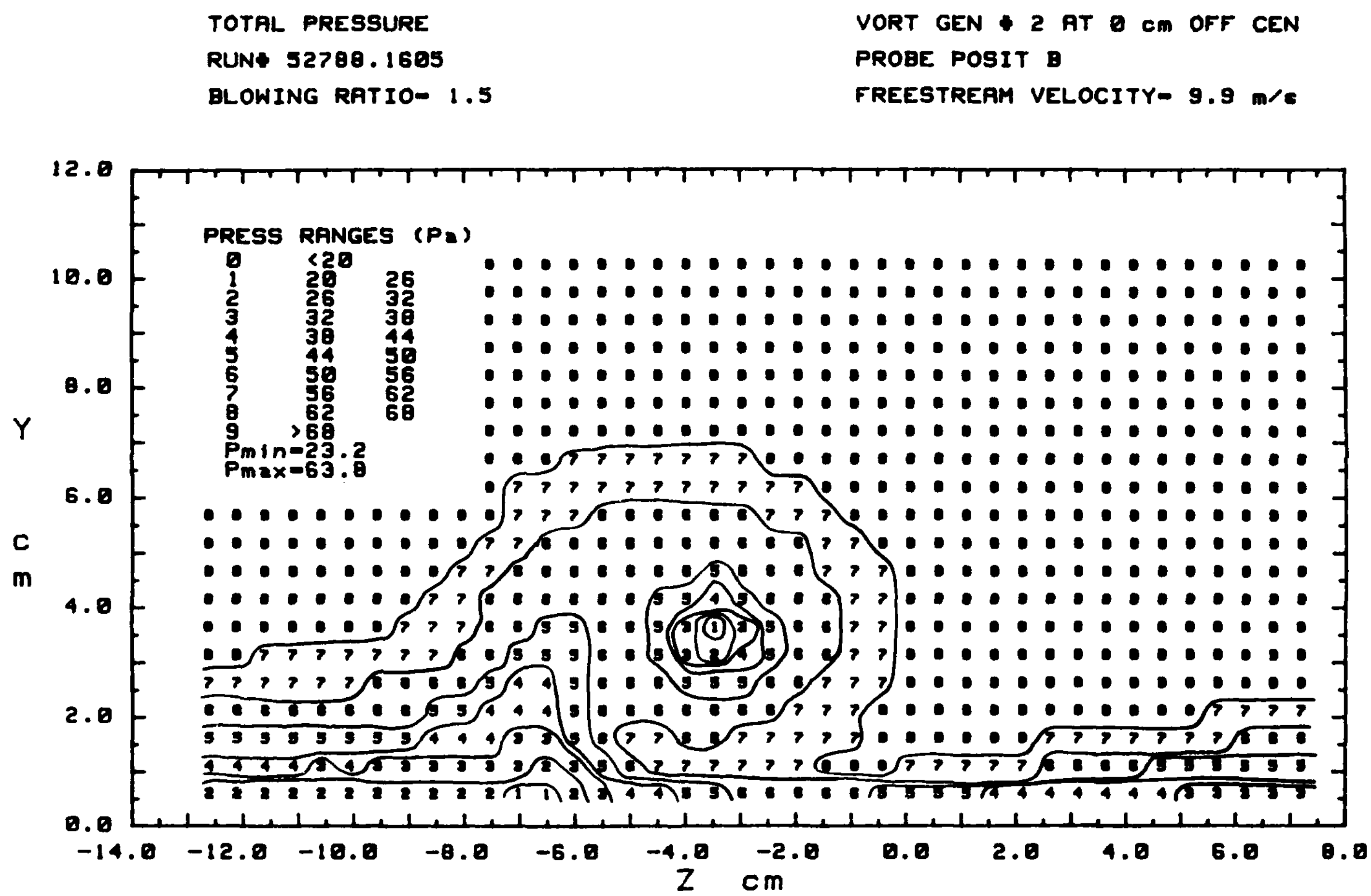

Figure 91. Total Pressure Contours

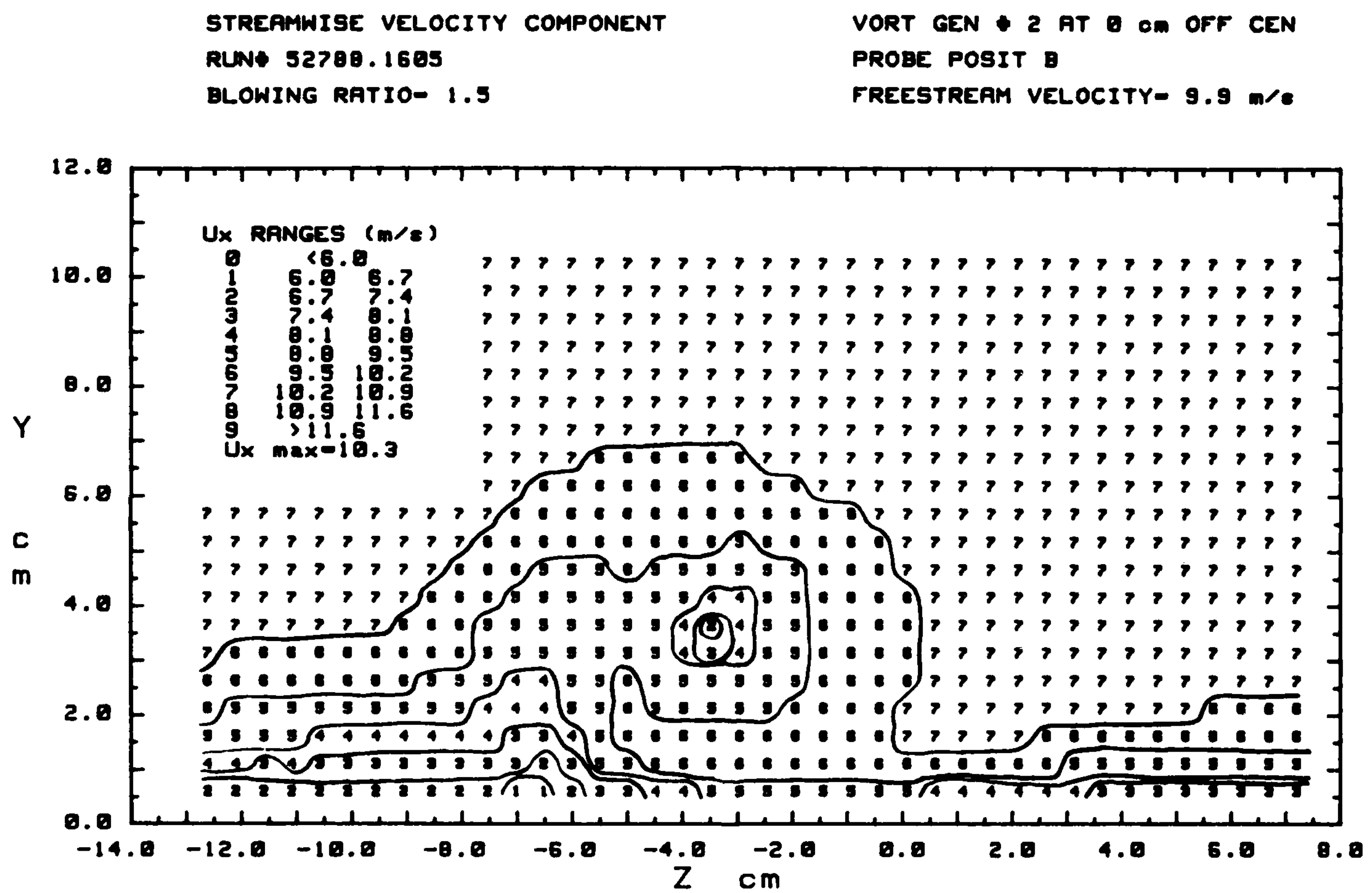

Figure 92. Streamwise Velocity Contours

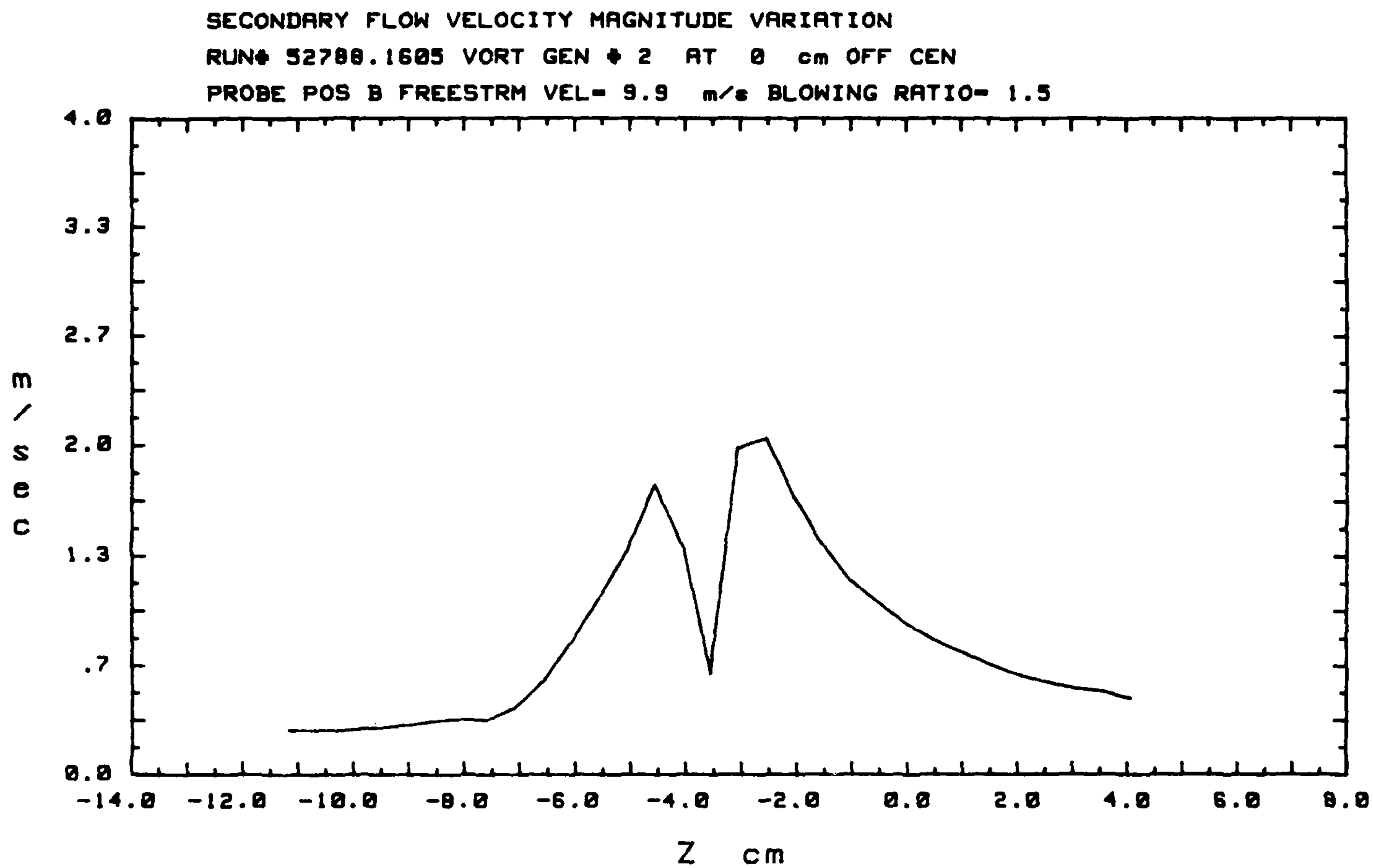

Figure 93. Secondary Flow Velocity (Radially)

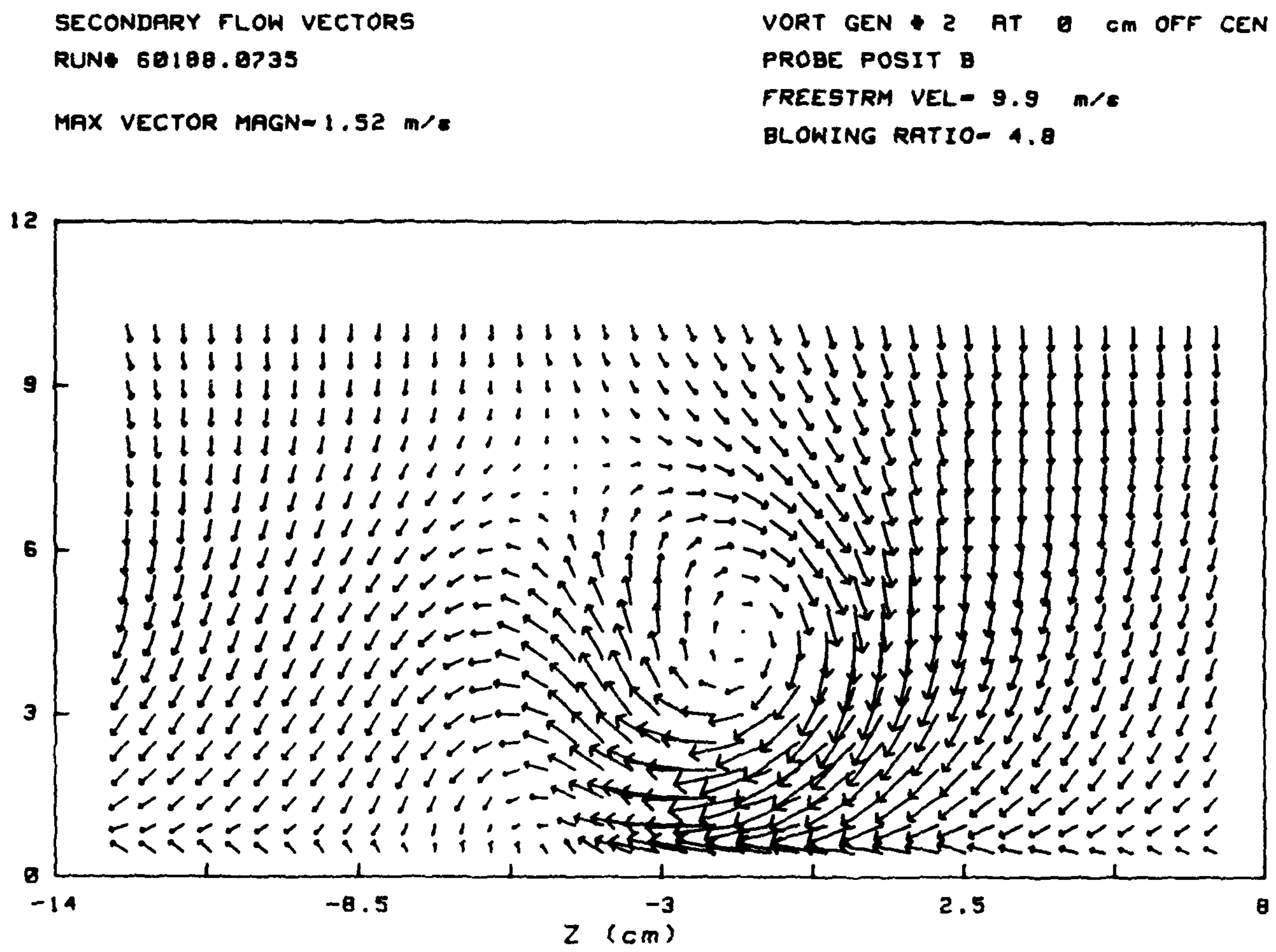

Figure 94. Secondary Flow Vectors

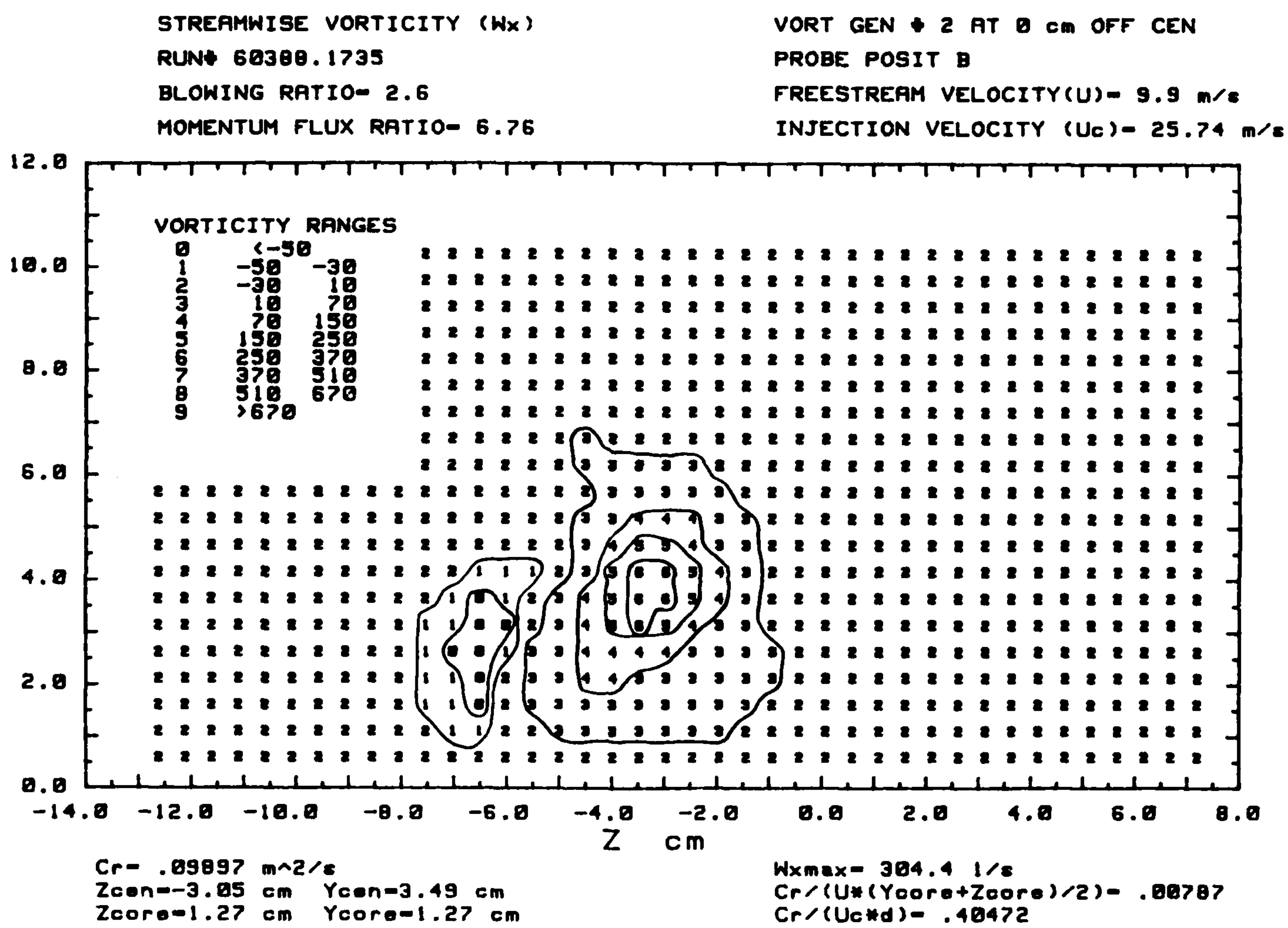

Figure 95. Streamwise Vorticity Contours

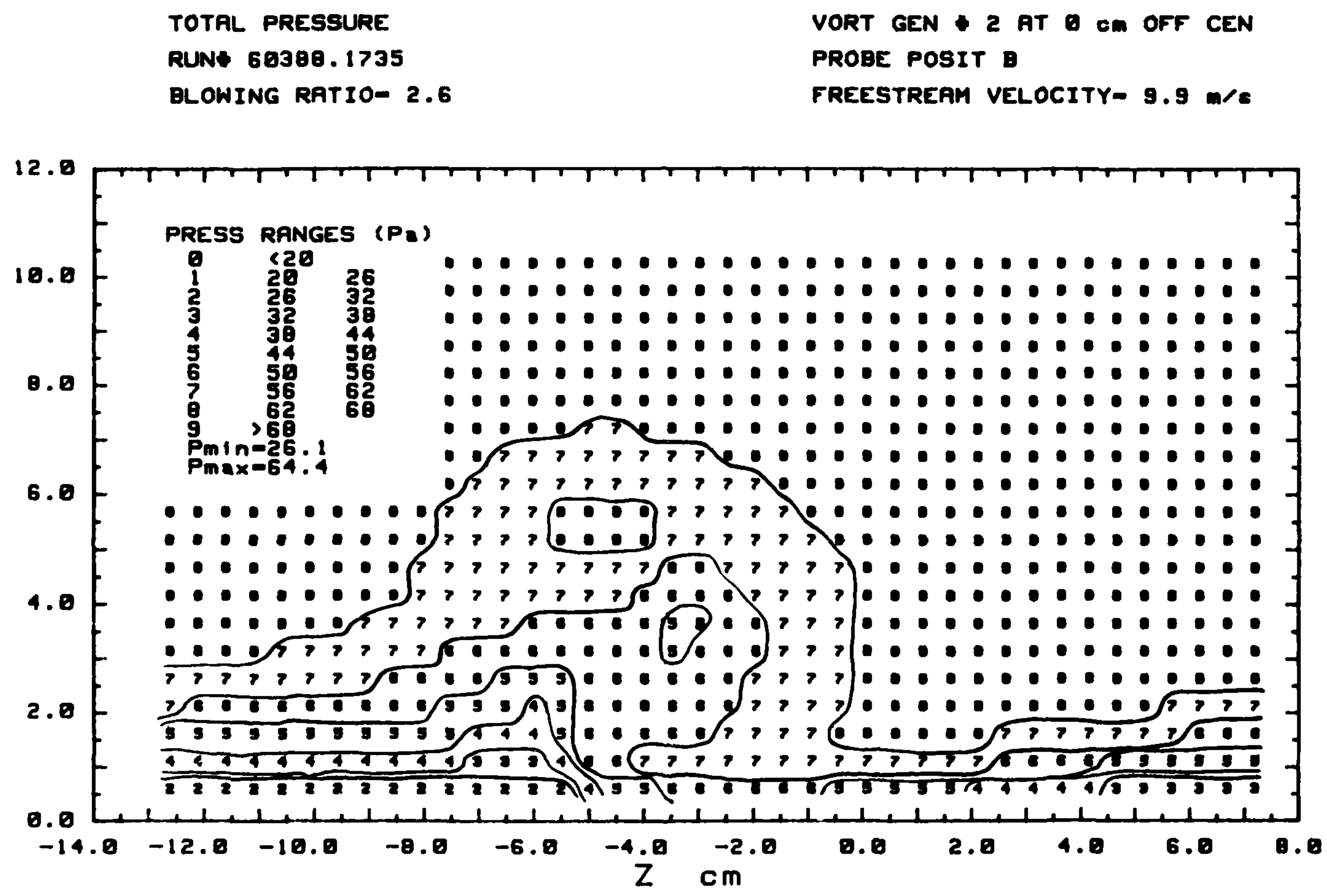

Figure 96. Total Pressure Contours

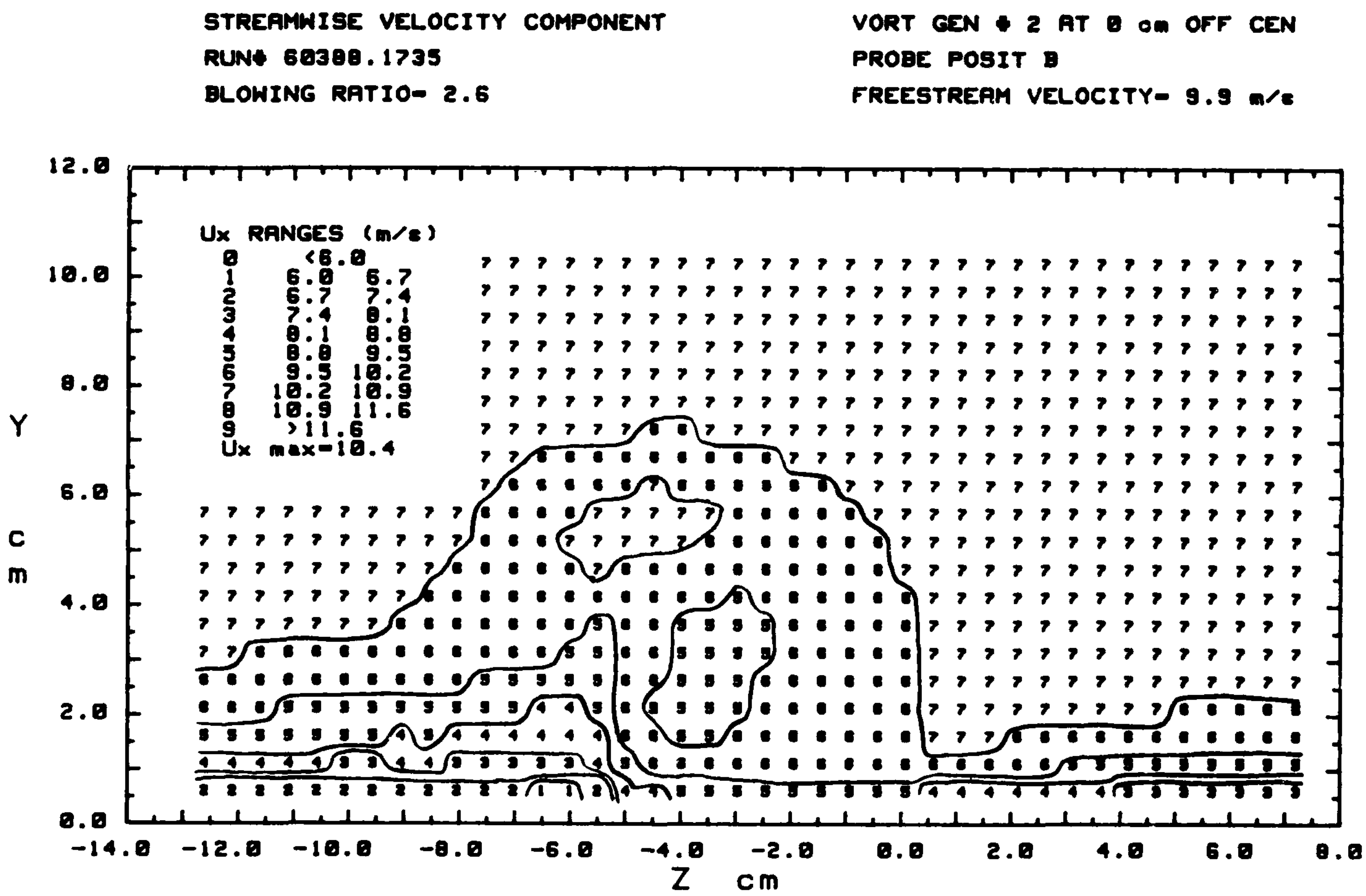

Figure 97. Streamwise Velocity Contours

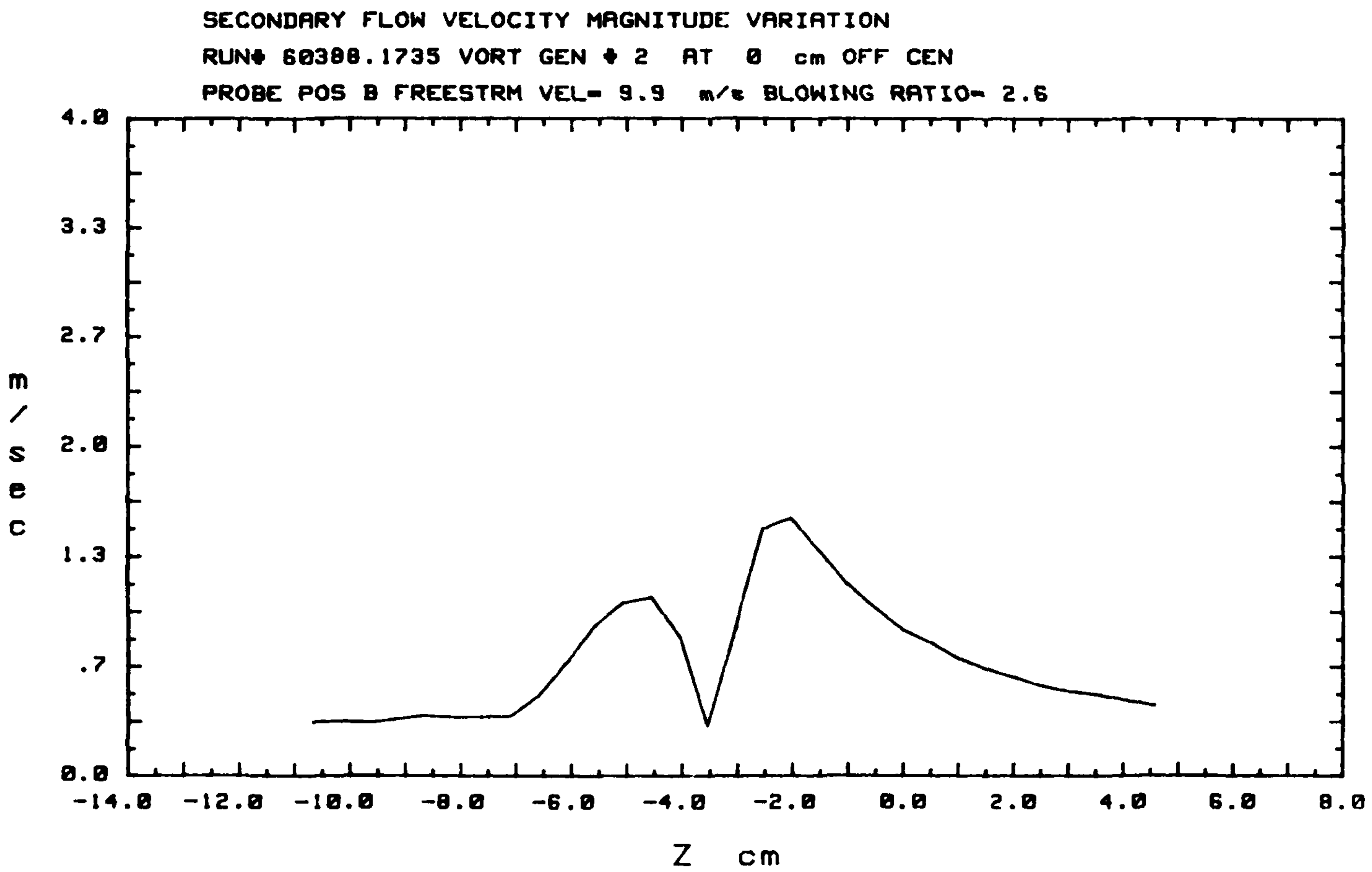

Figure 98. Secondary Flow Velocity (Radially)

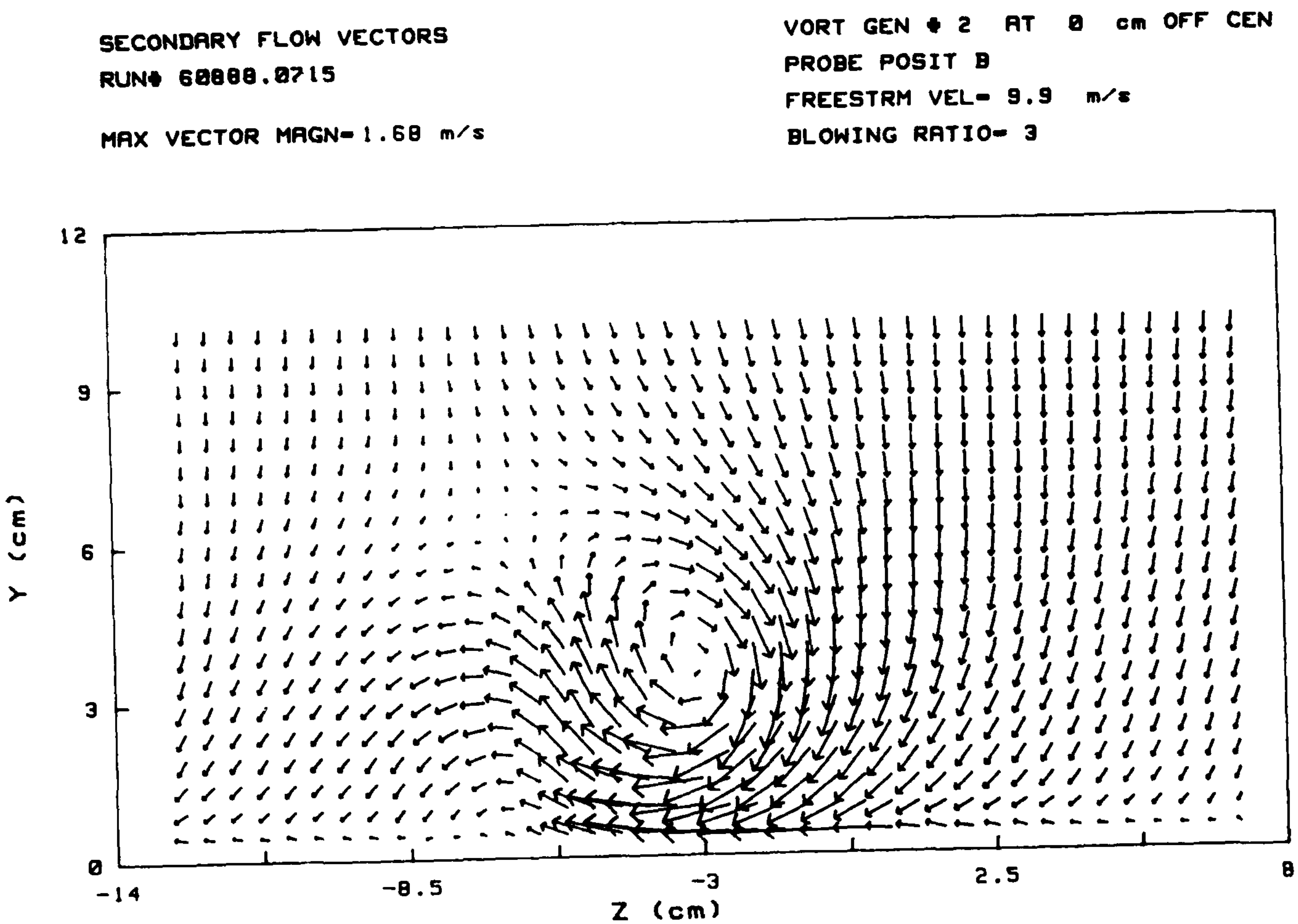

Figure 99. Secondary Flow Vectors

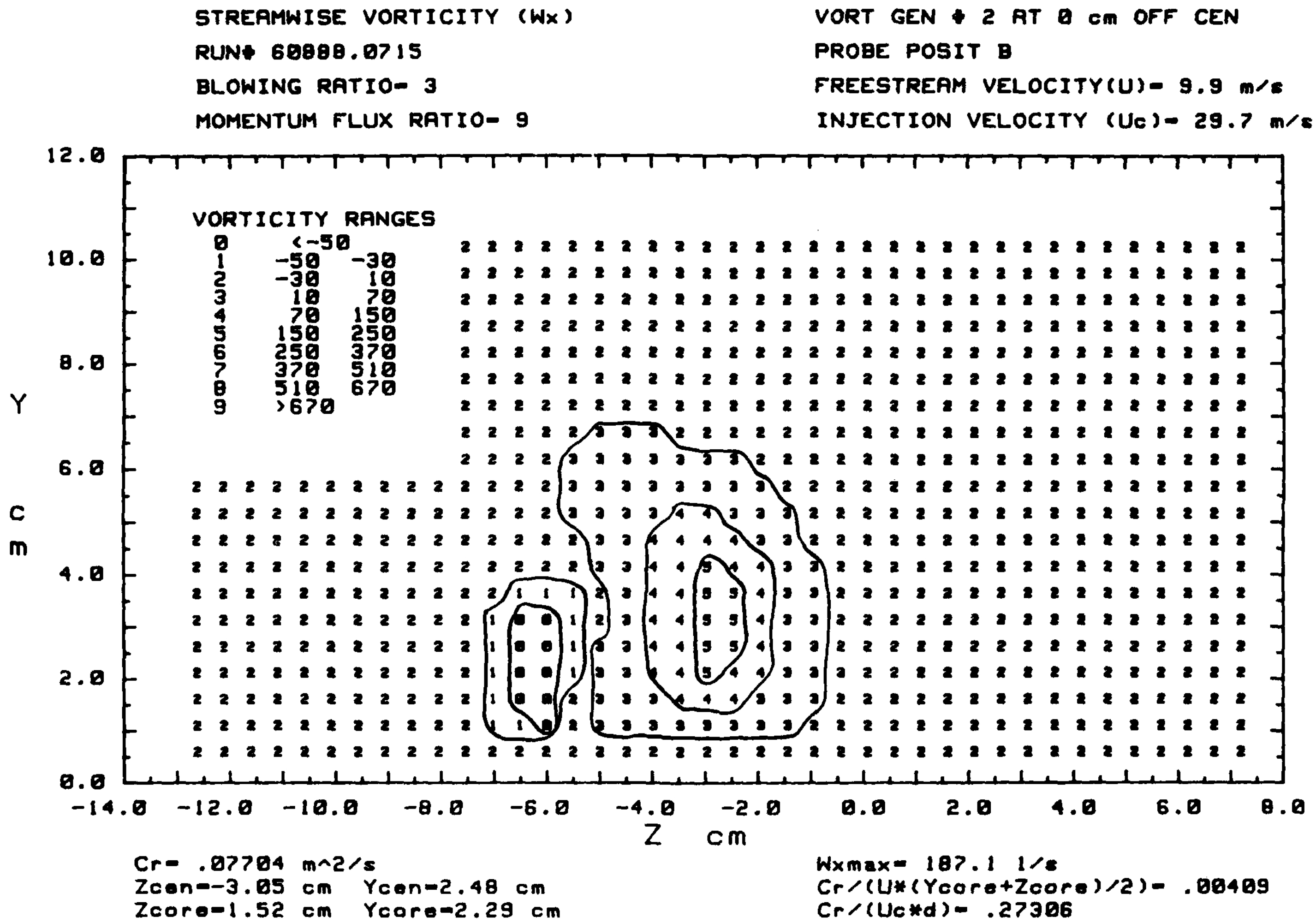

Figure 100. Streamwise Vorticity Contours

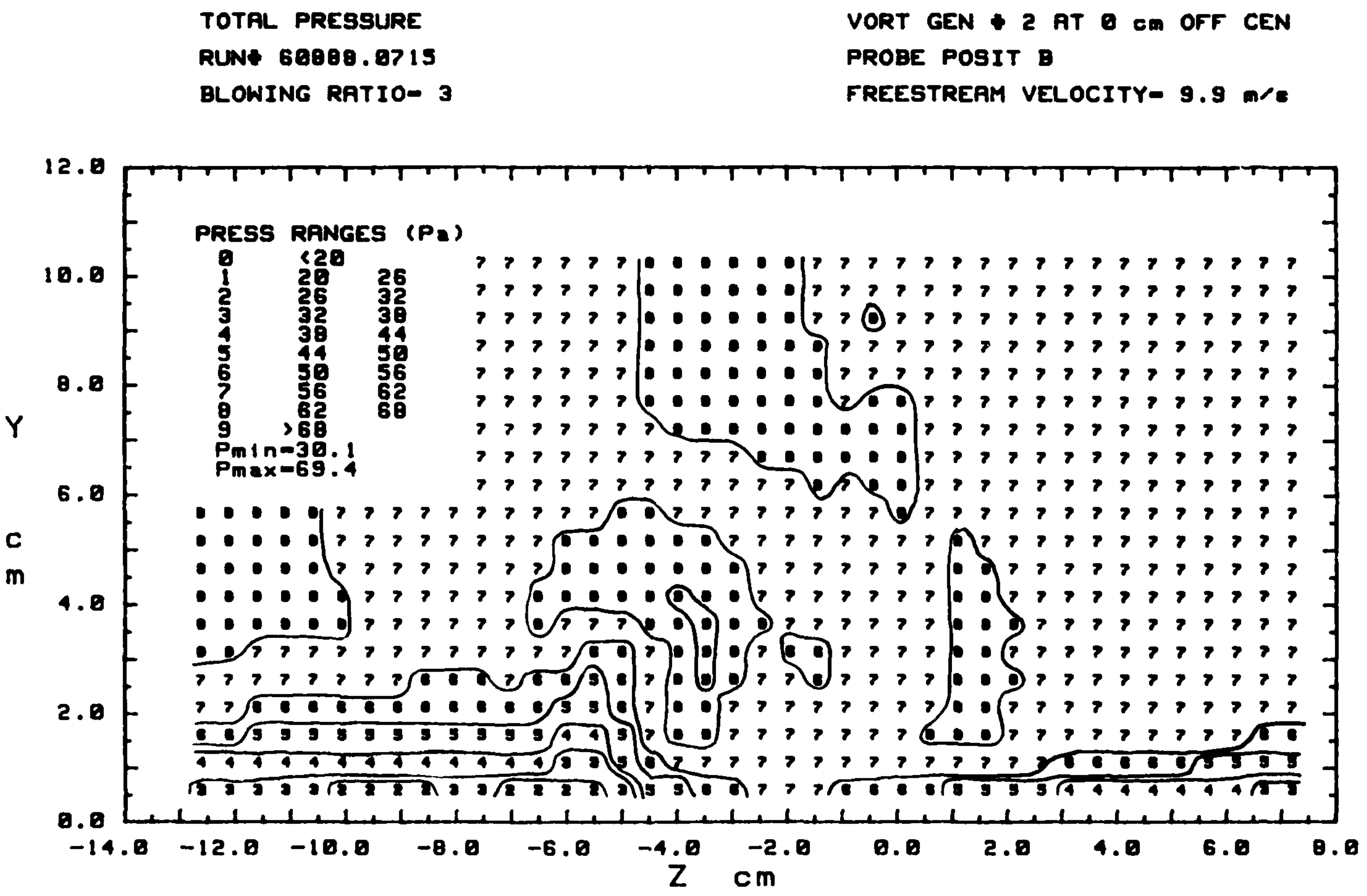

Figure 101. Total Pressure Contours

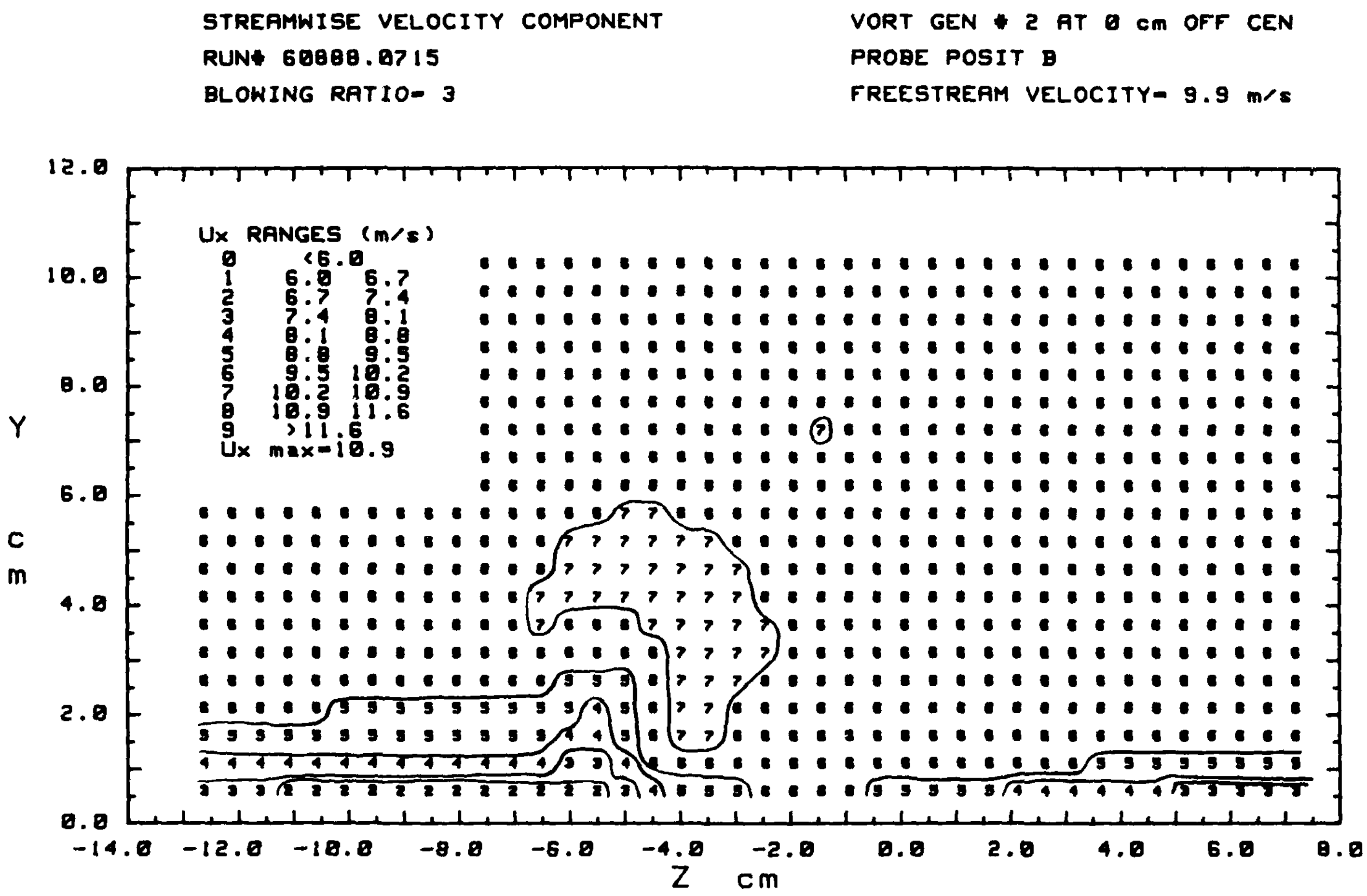

Figure 102. Streamwise Velocity Contours

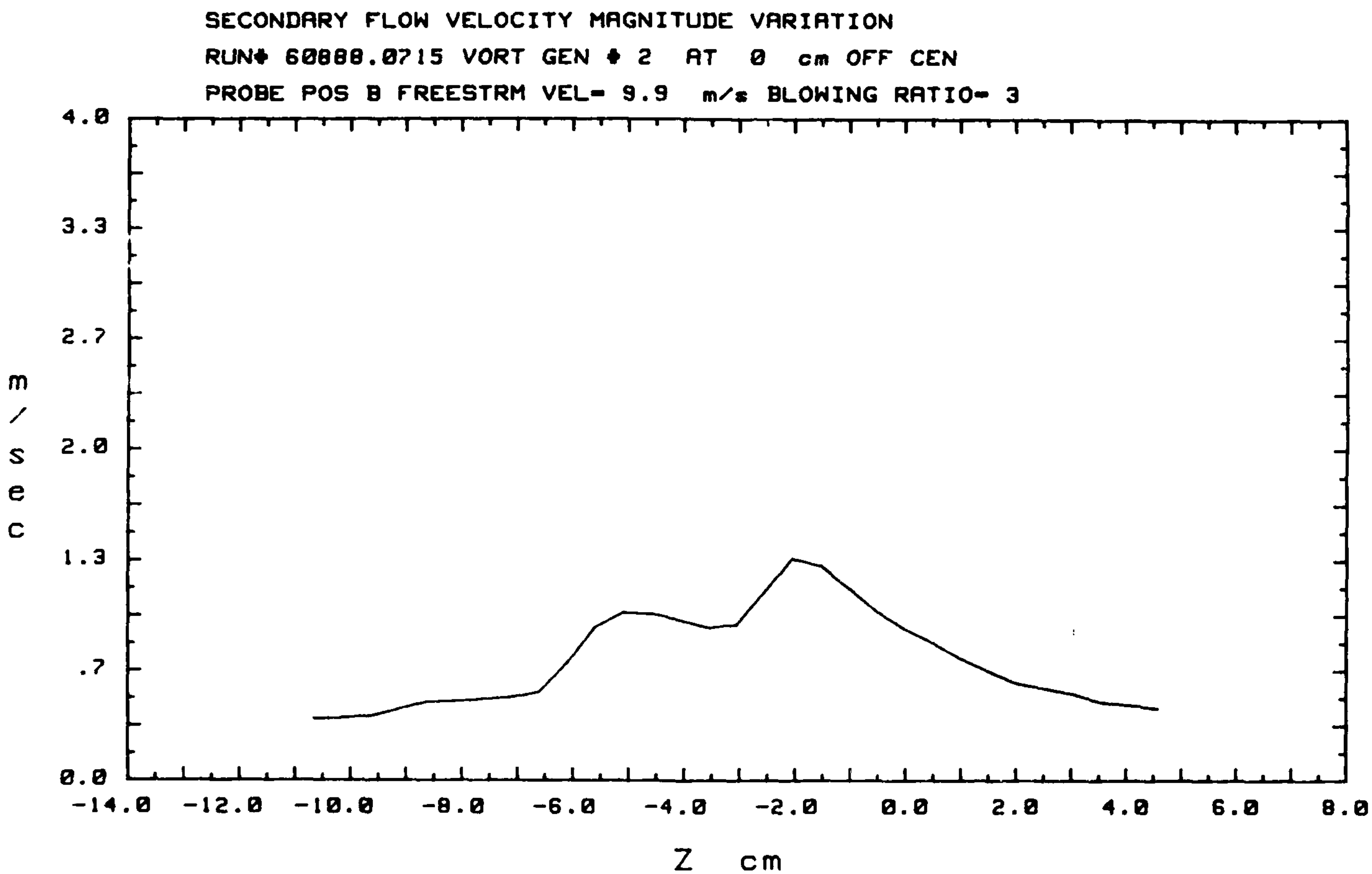

Figure 103. Secondary Flow Velocity (Radially)

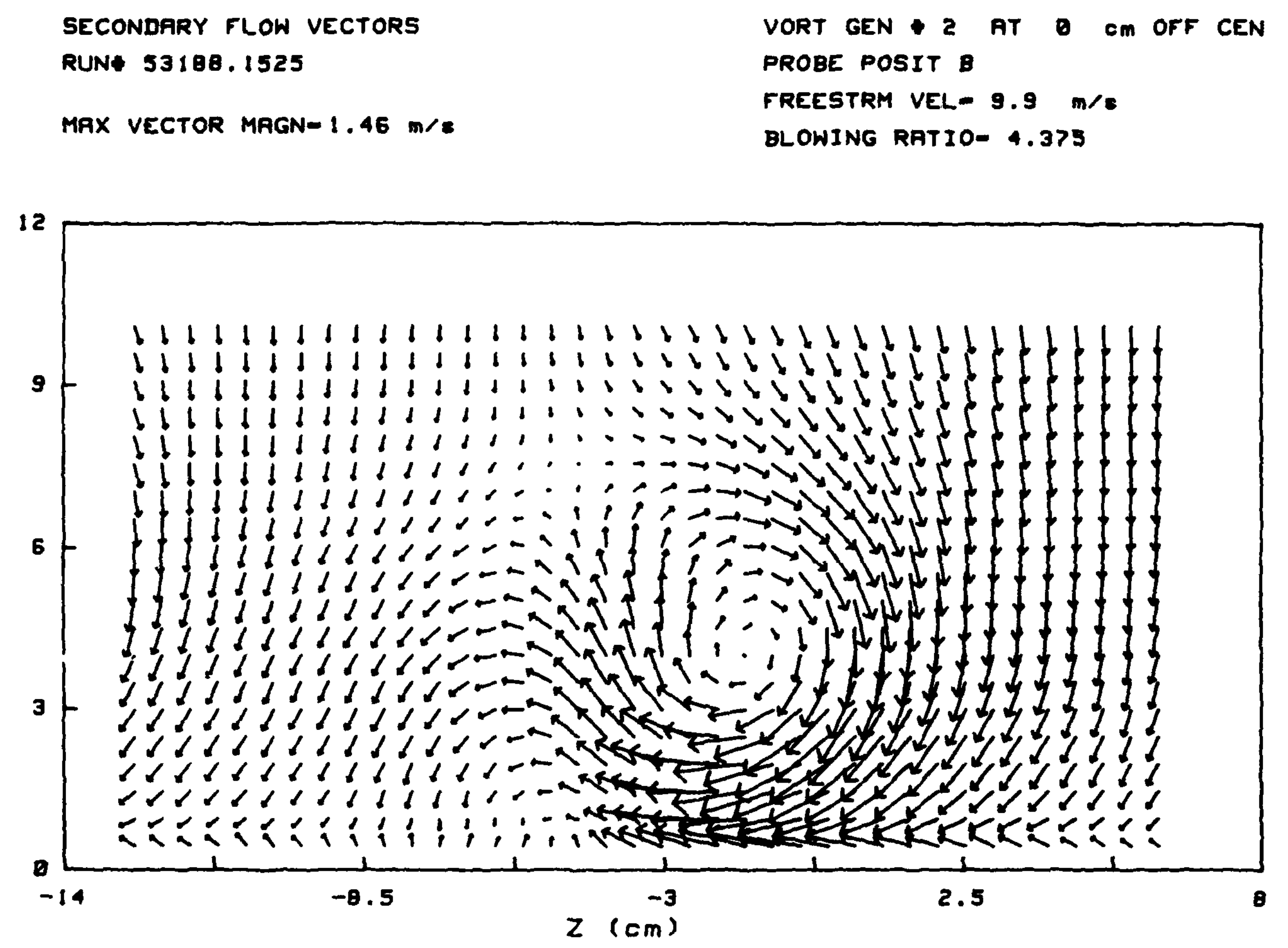

Figure 104. Secondary Flow Vectors

STREAMWISE VORTICITY (Wx)
RUN# 53188.1525
BLOWING RATIO= 4.375
MOMENTUM FLUX RATIO= 19.140625

VORT GEN # 2 AT 0 cm OFF CEN
PROBE POSIT B
FREESTREAM VELOCITY(U)= 9.9 m/s
INJECTION VELOCITY (Uc)= 43.3125 m/s

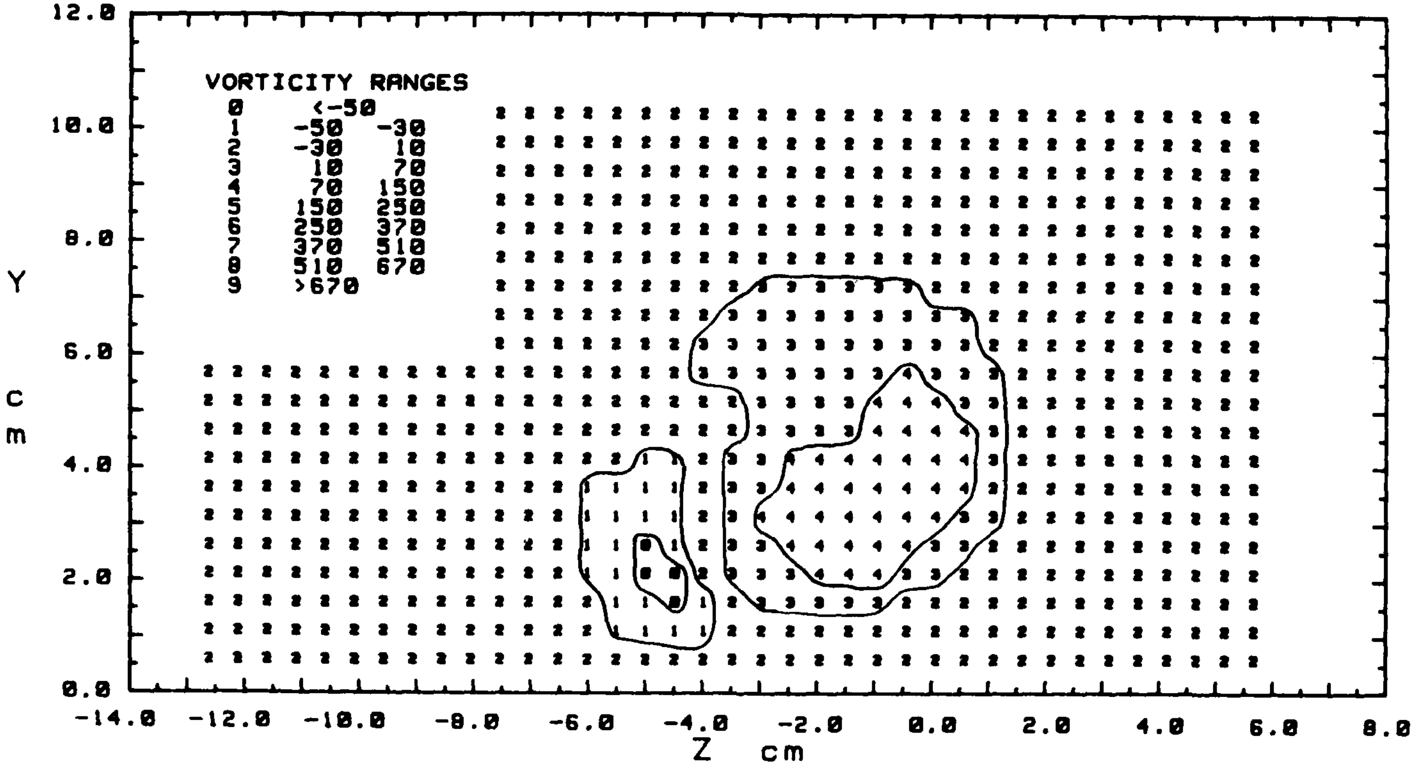

Cr= .04802 m^2/s
Zcen=-1.52 cm Ycen=2.98 cm
Zcore=2.03 cm Ycore=2.79 cm

Wxmax= 136.5 1/s
Cr/(U*(Ycore+Zcore)/2)= .00201
Cr/(Uc*d)= .11671

Figure 105. Streamwise Vorticity Contours

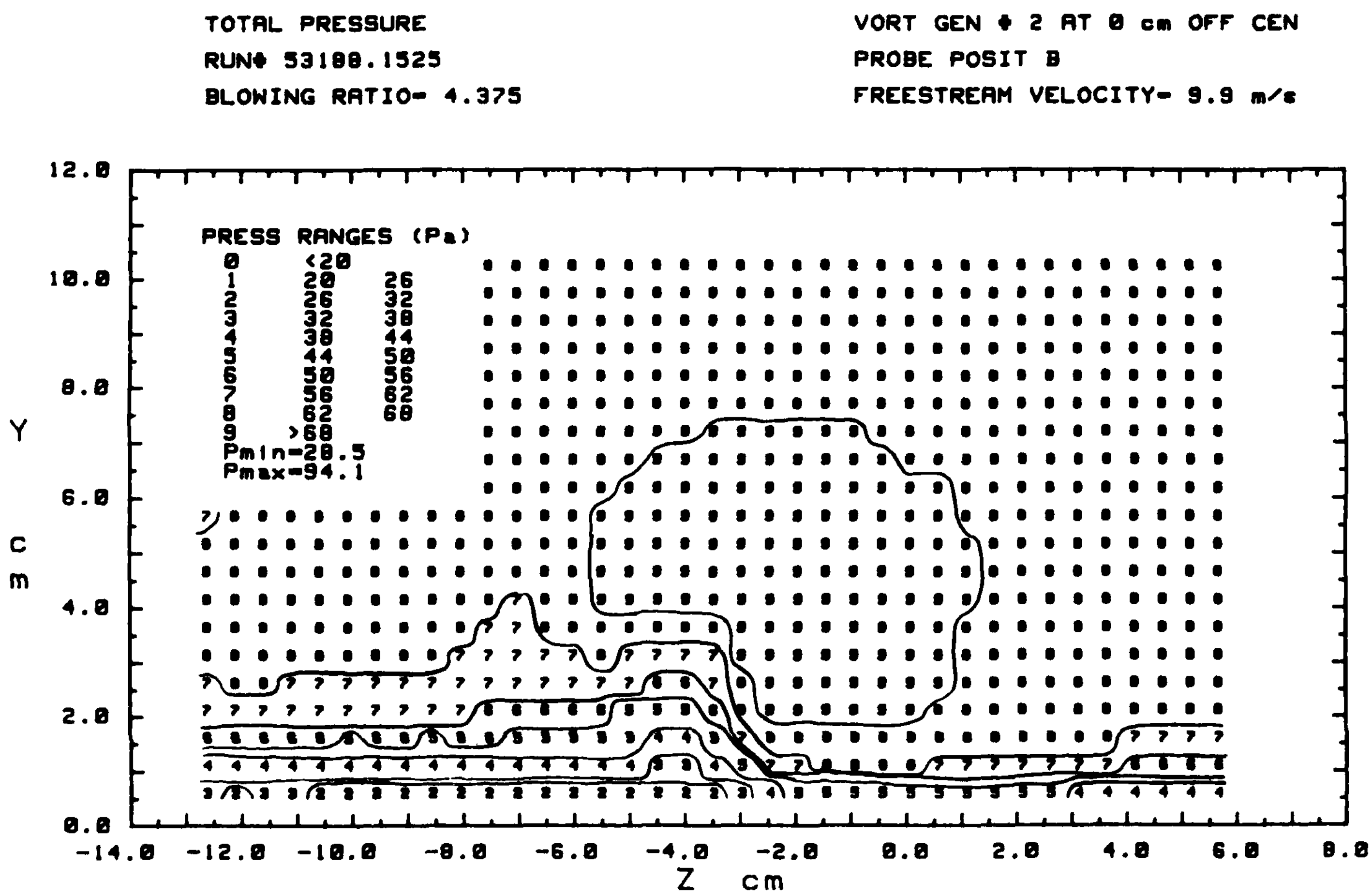

Figure 106. Total Pressure Contours

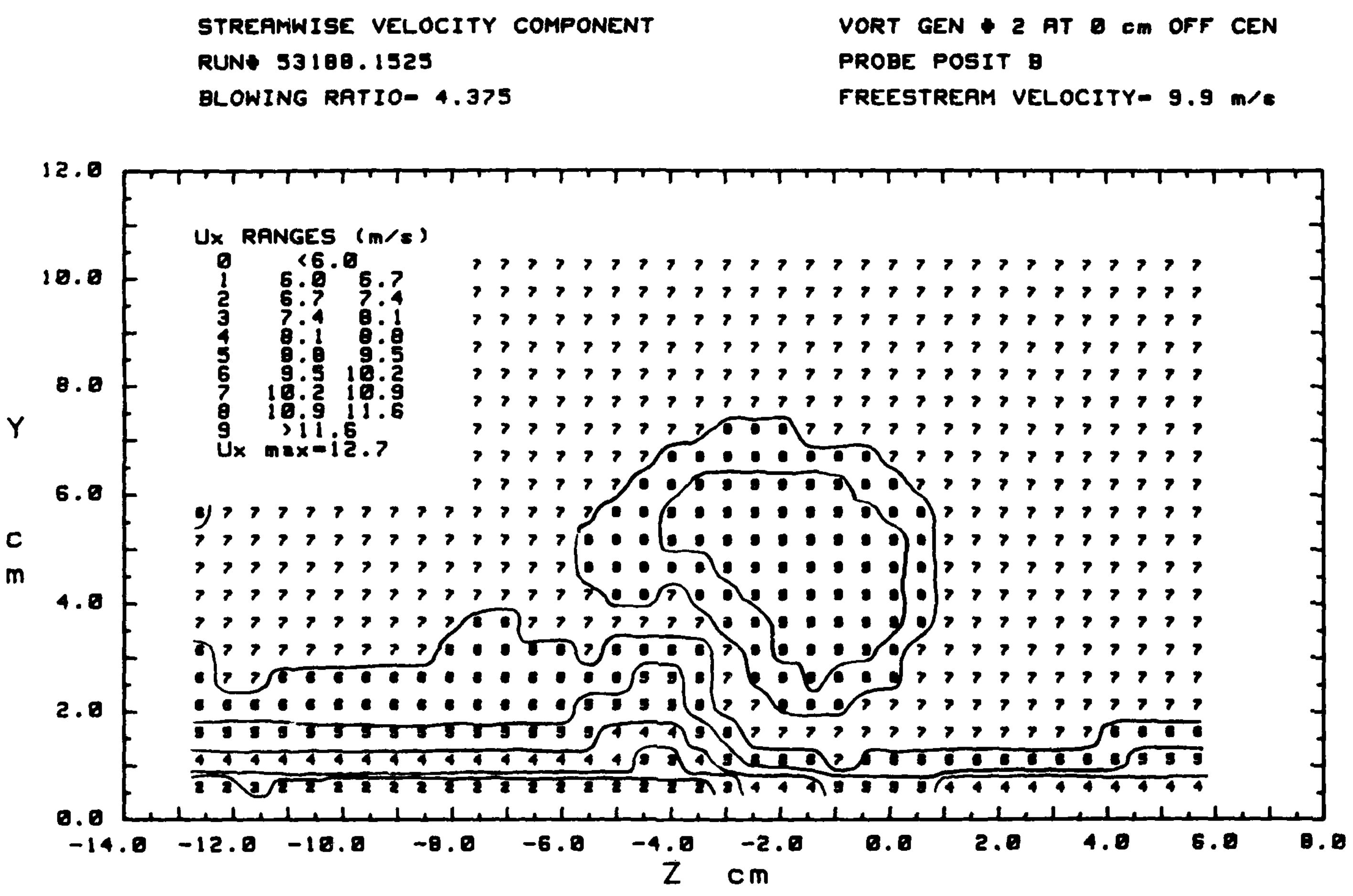

Figure 107. Streamwise Velocity Contours

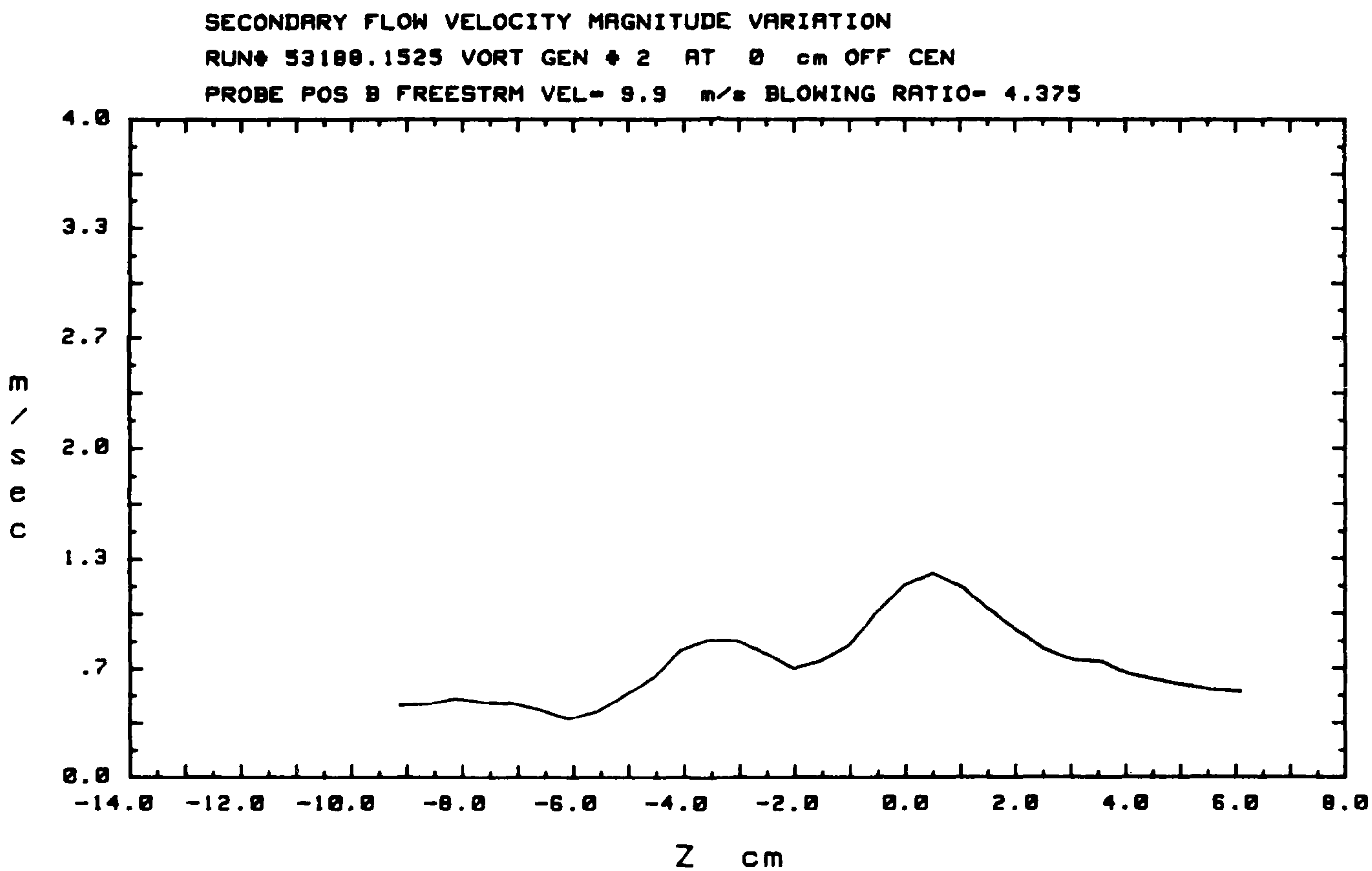

Figure 108. Secondary Flow Velocity (Radially)

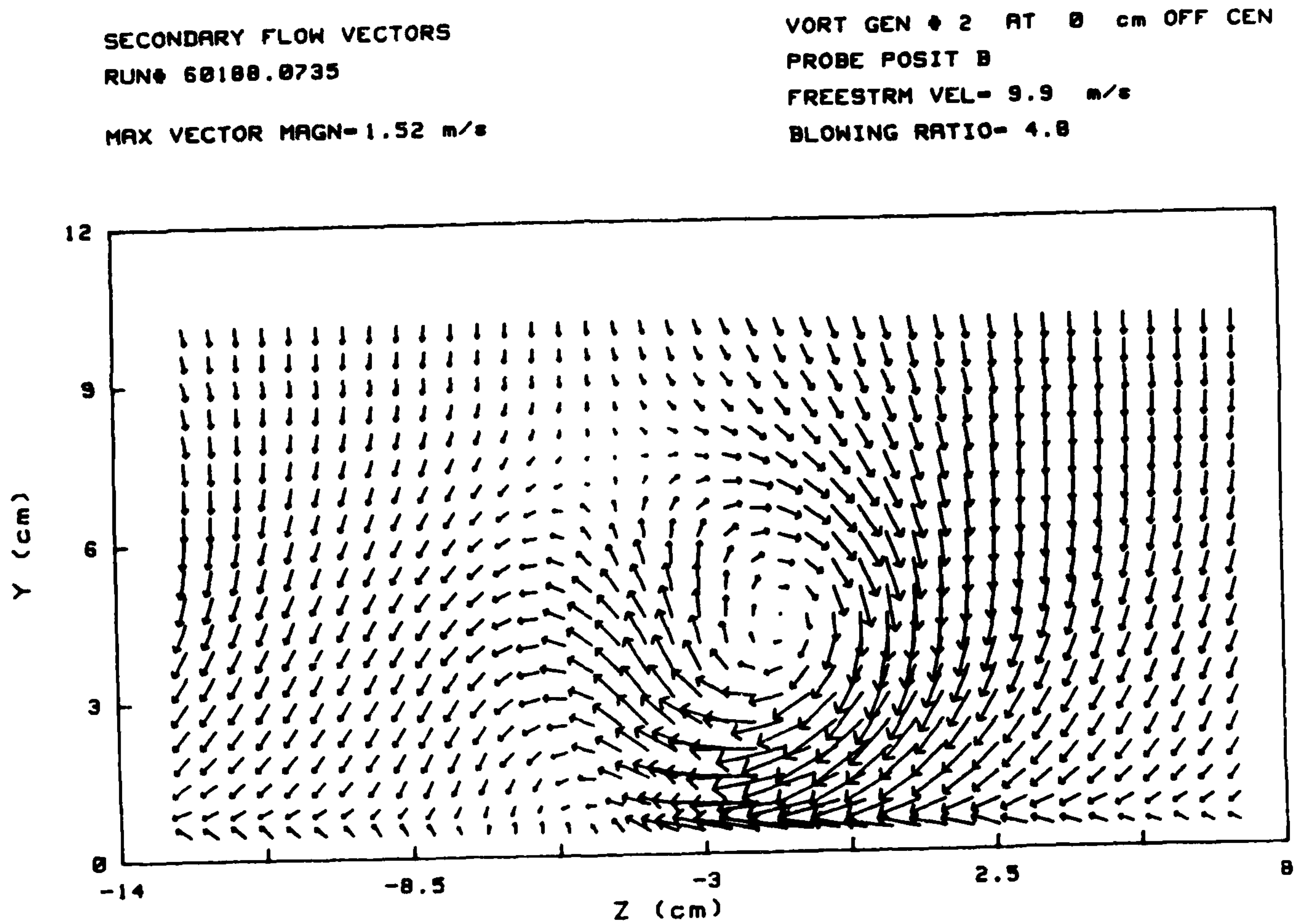

Figure 109. Secondary Flow Vectors

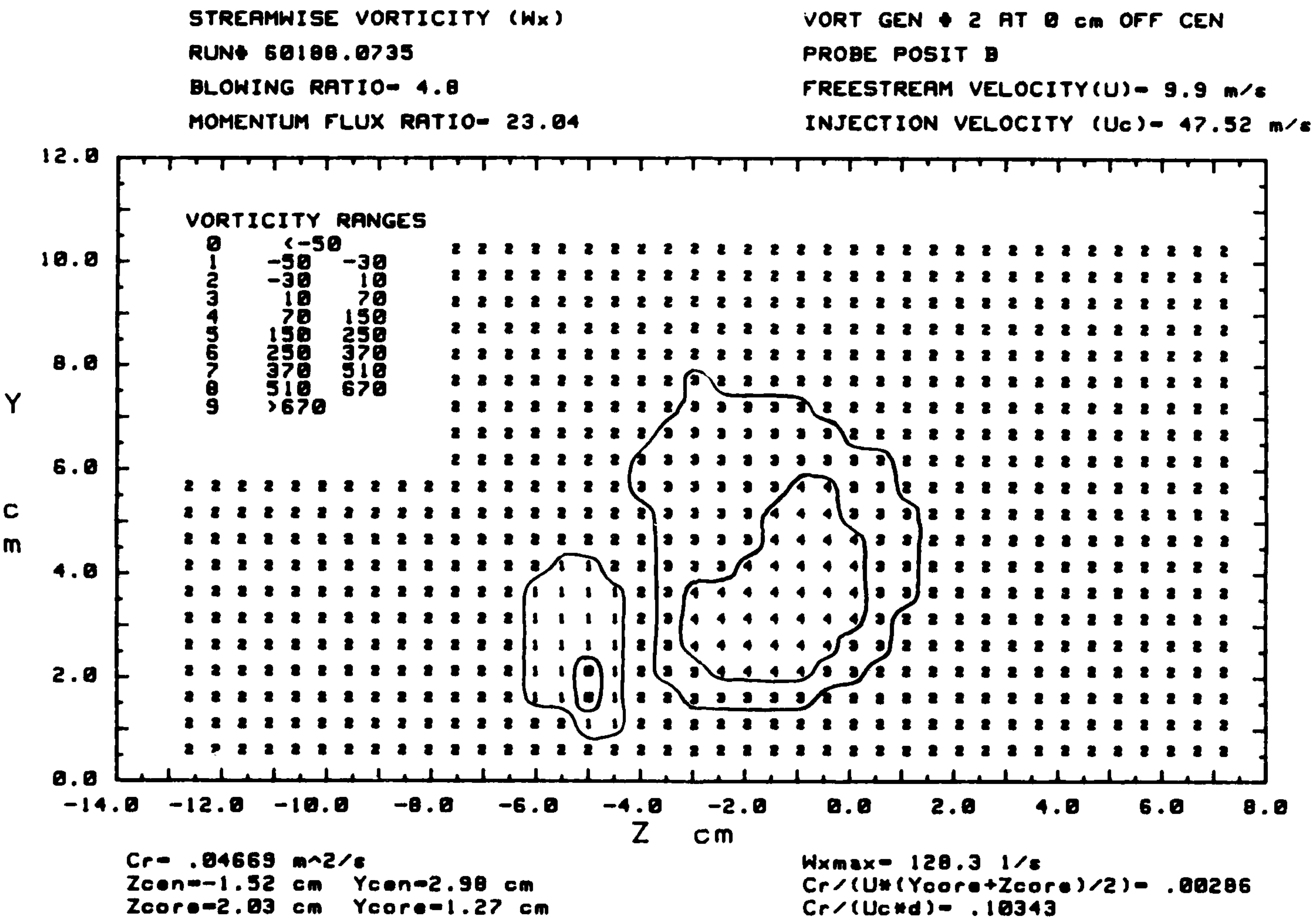

Figure 110. Streamwise Vorticity Contours

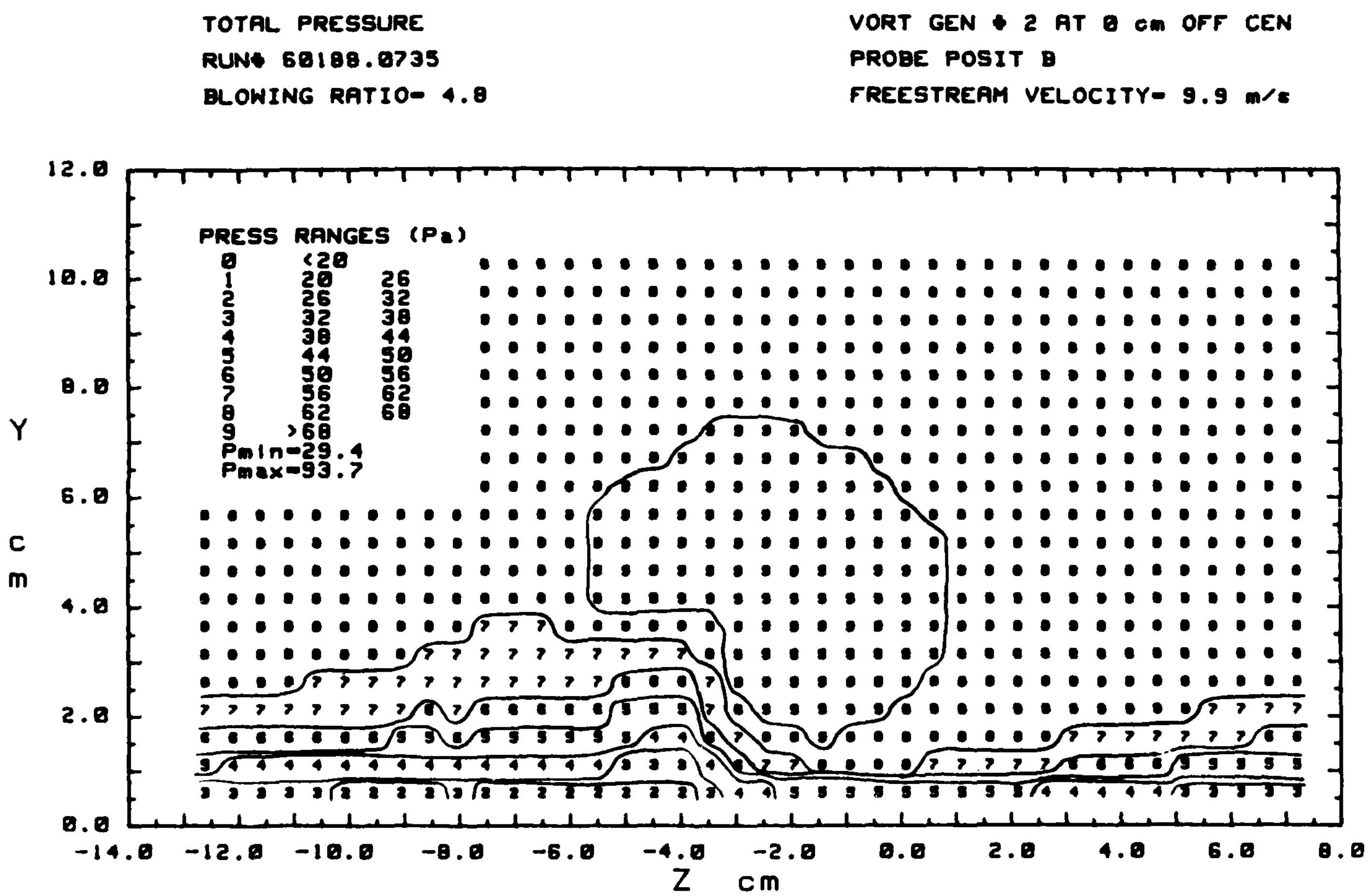

Figure 111. Total Pressure Contours

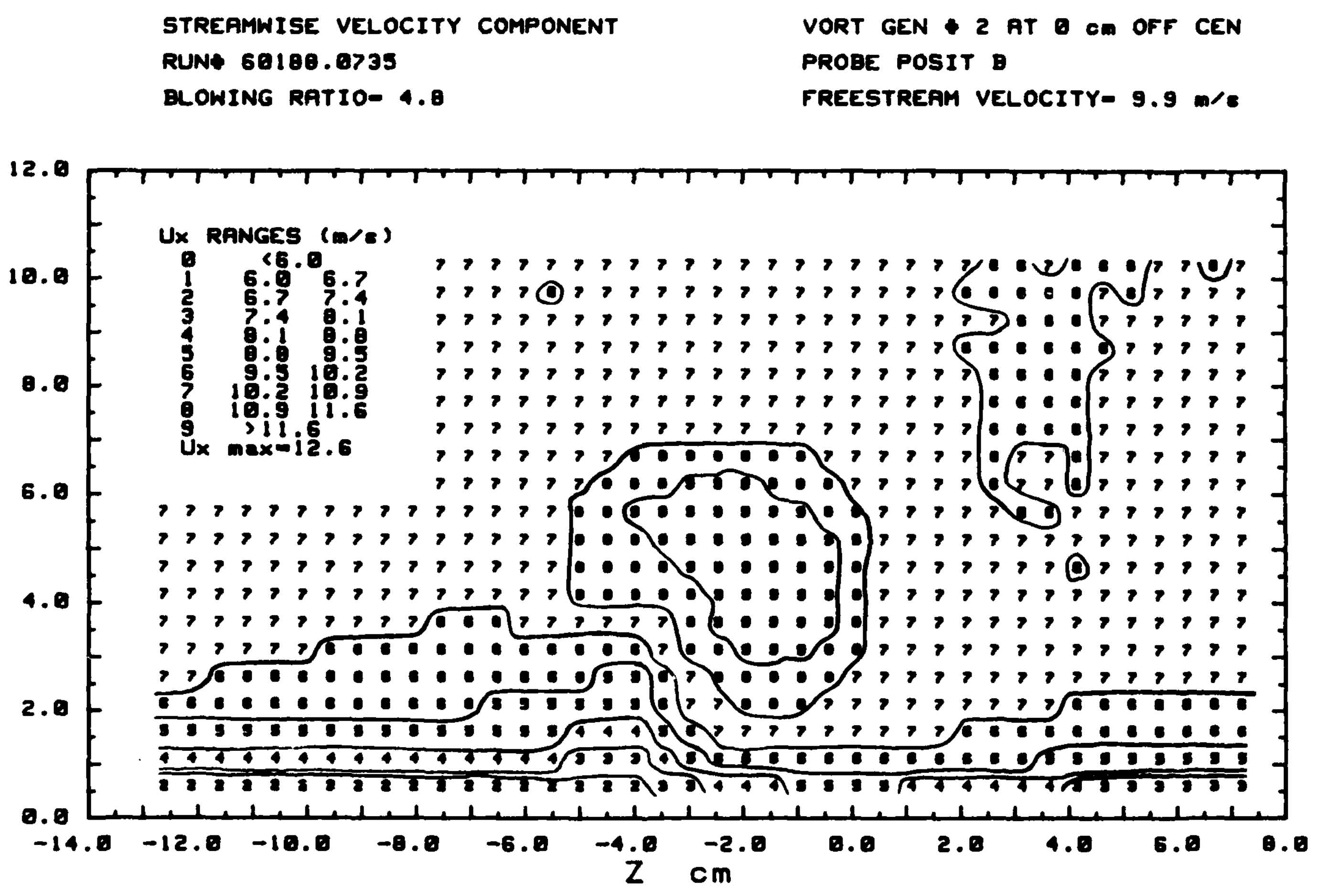

Figure 112. Streamwise Velocity Contours

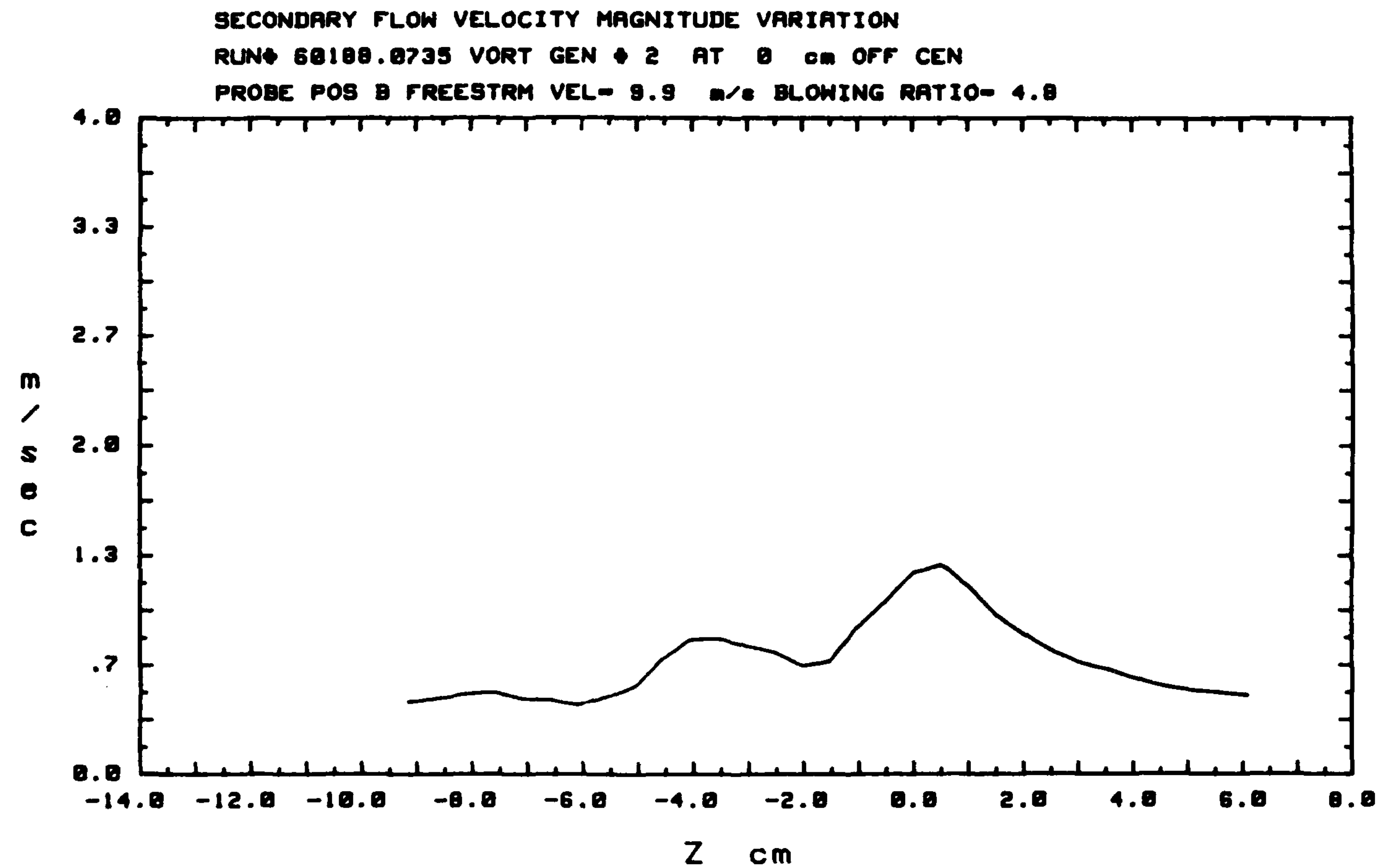

Figure 113. Secondary Flow Velocity (Radially)

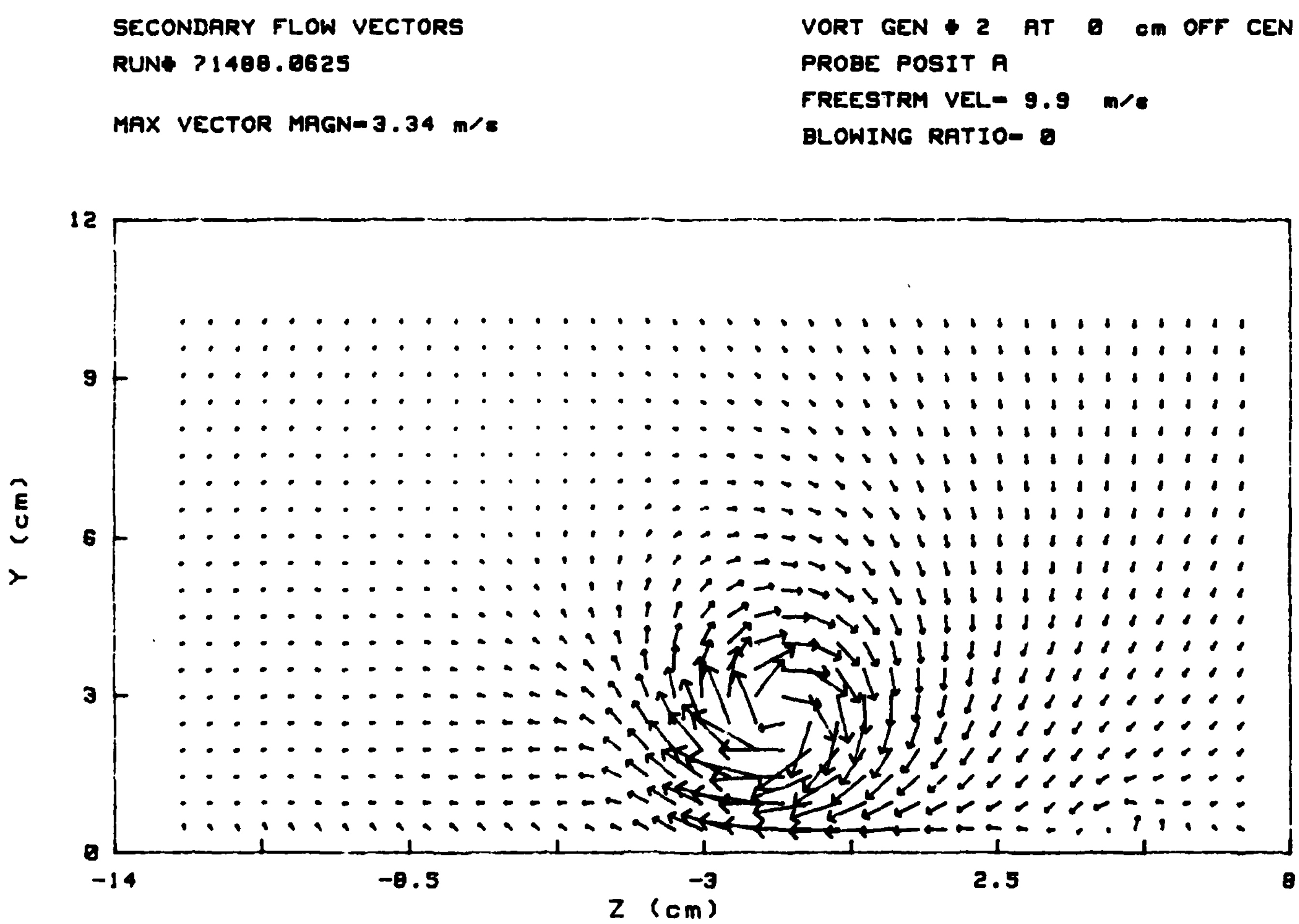

Figure 114. Secondary Flow Vectors

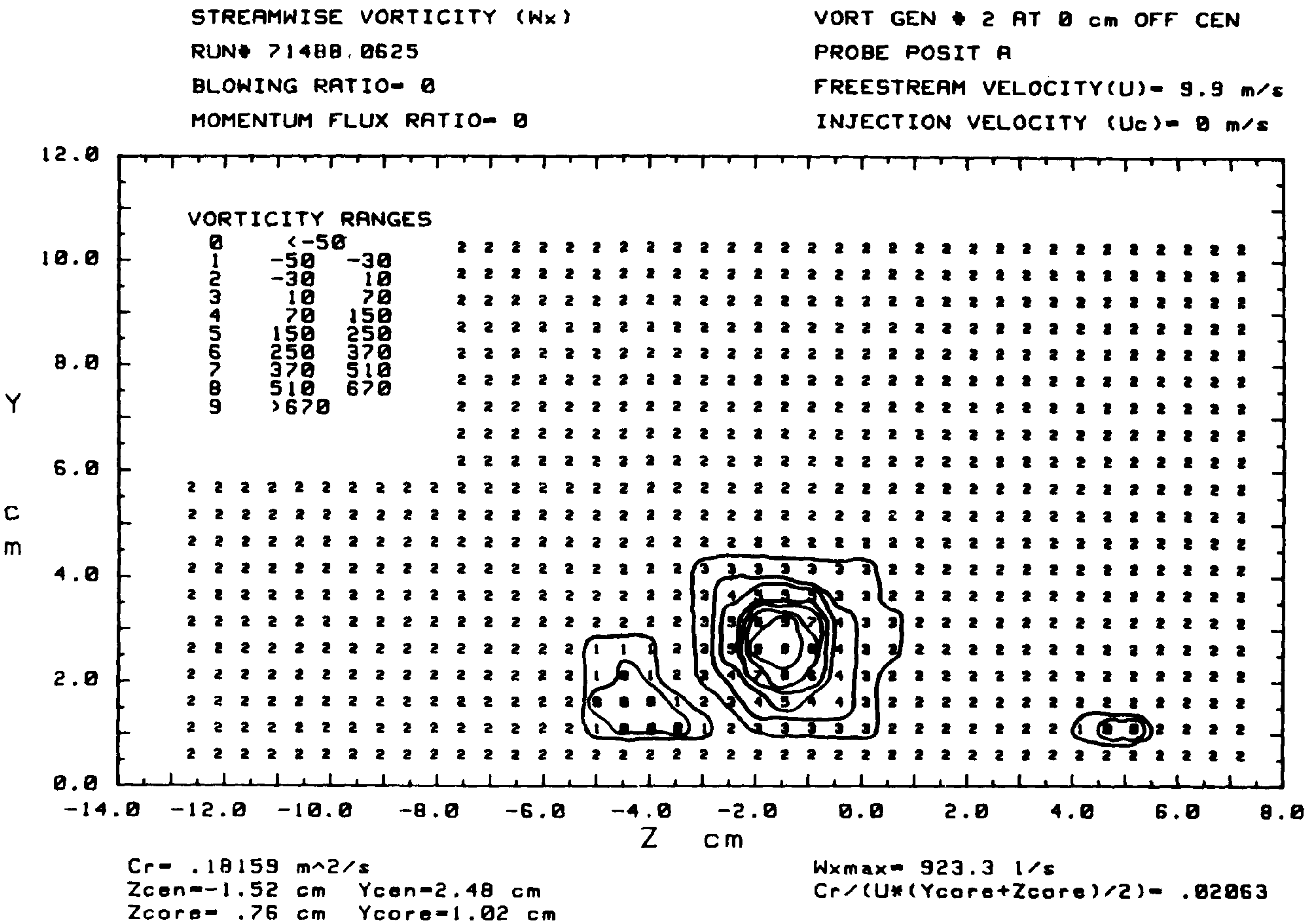

Figure 115. Streamwise Vorticity Contours

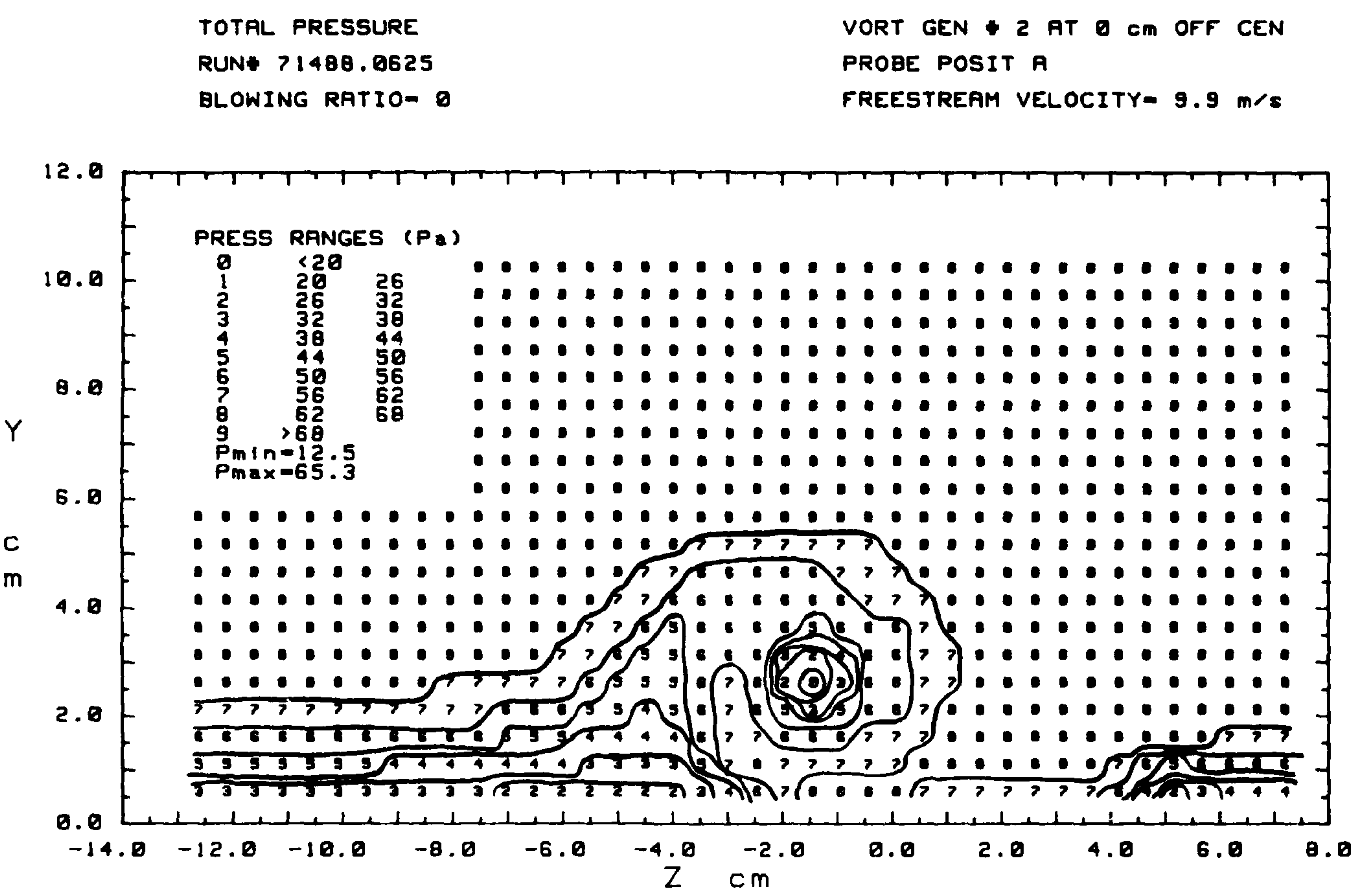

Figure 116. Total Pressure Contours

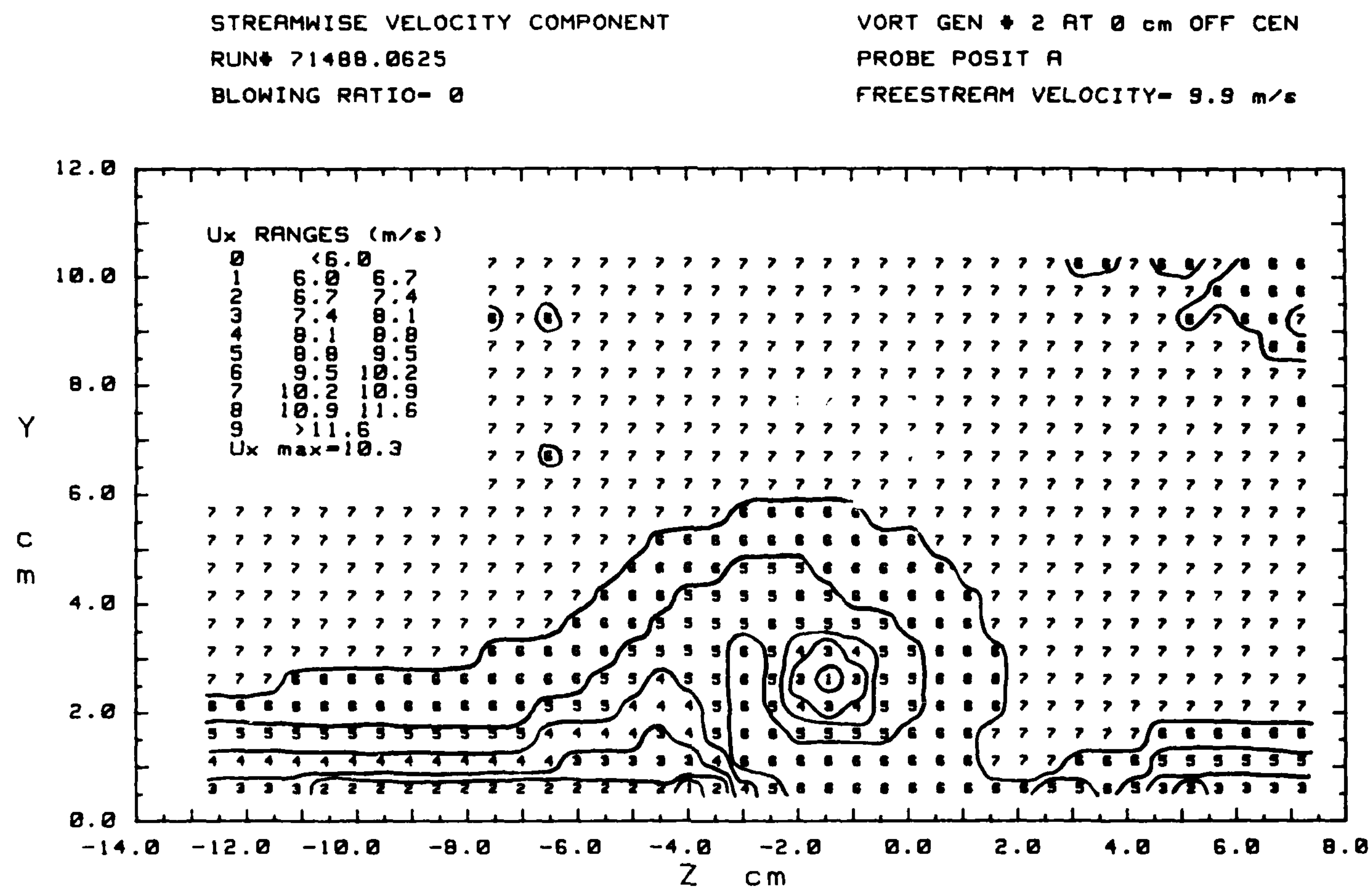

Figure 117. Streamwise Velocity Contours

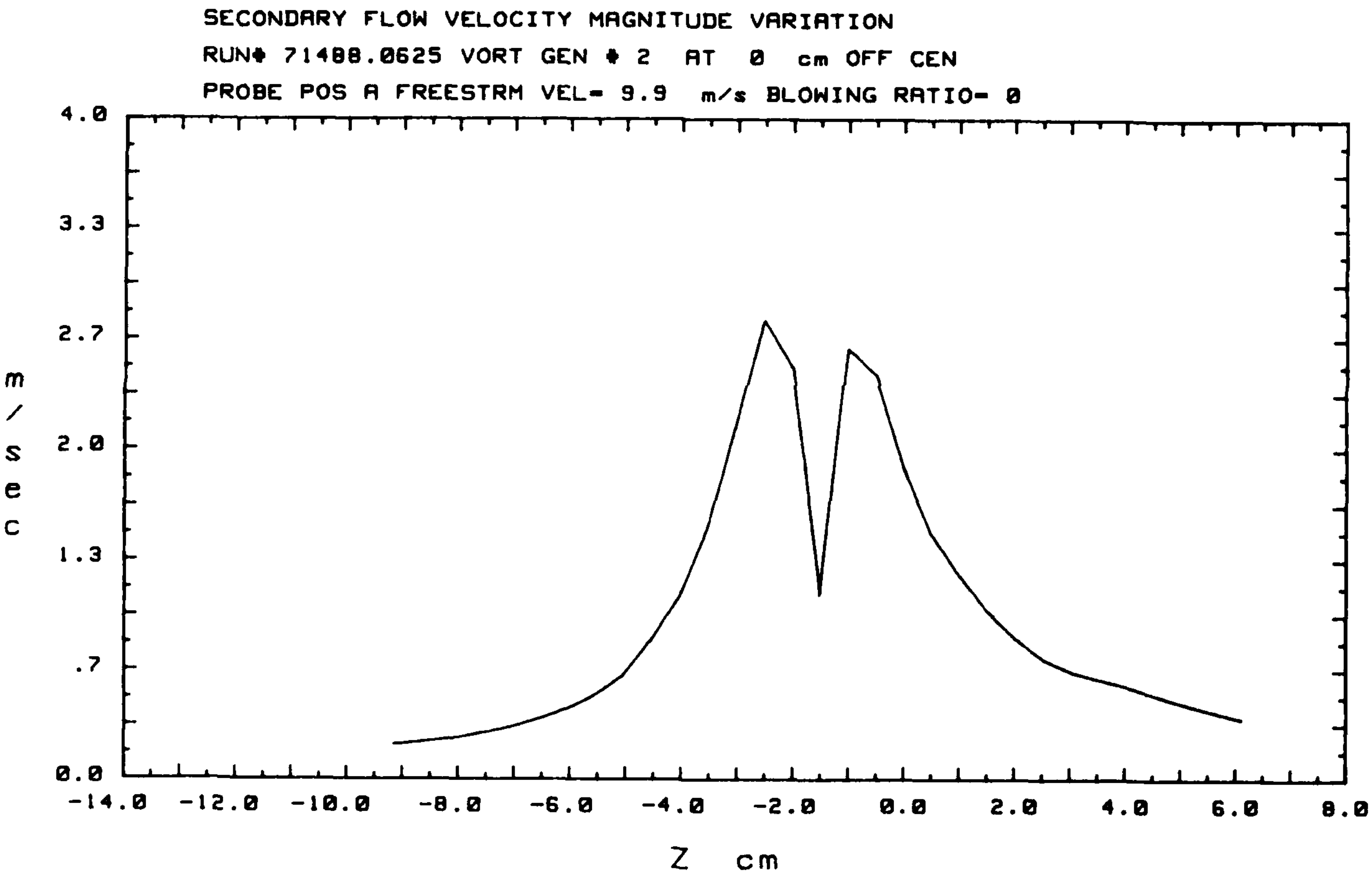

Figure 118. Secondary Flow Velocity (Radially)

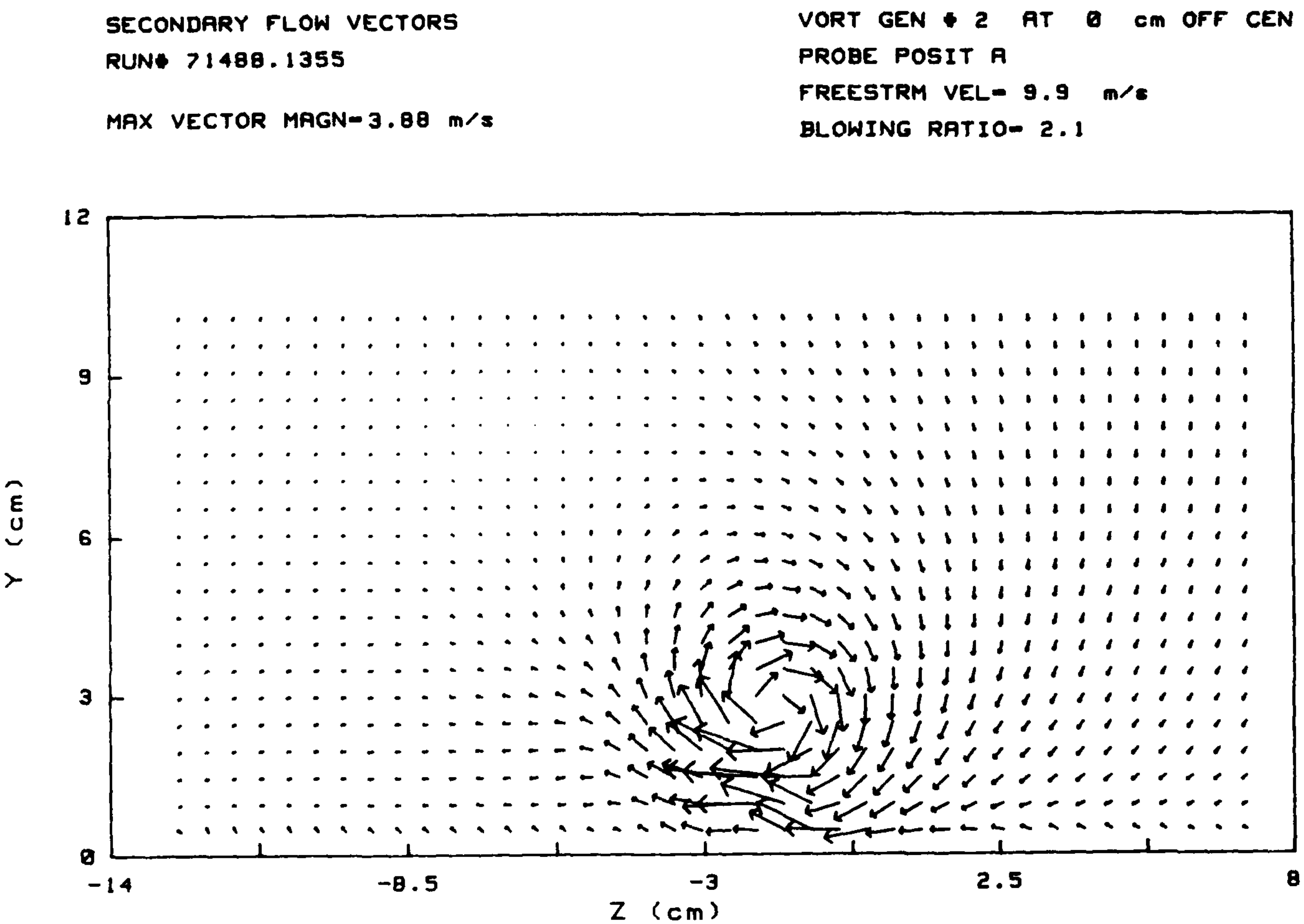

Figure 119. Secondary Flow Vectors

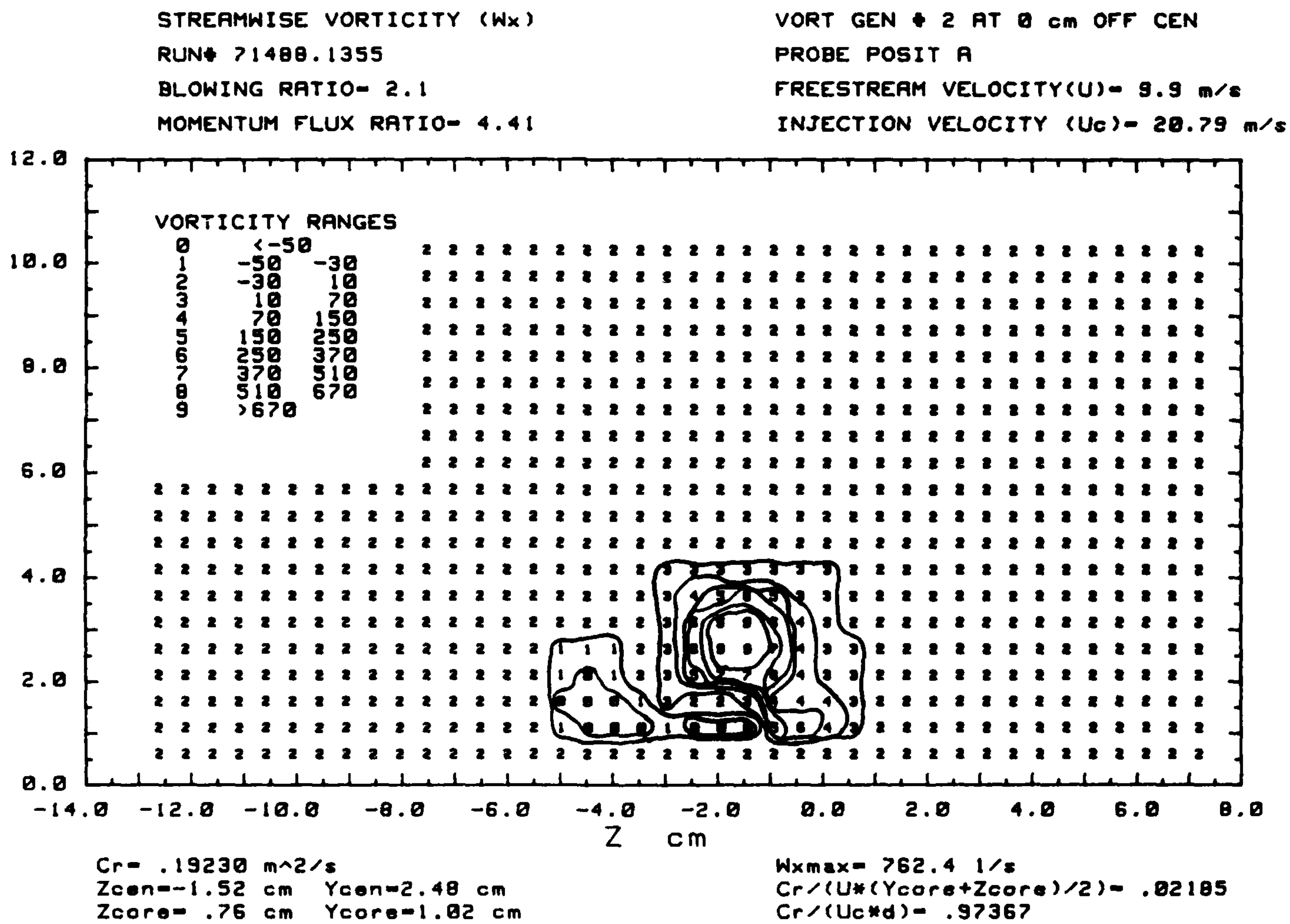

Figure 120. Streamwise Vorticity Contours

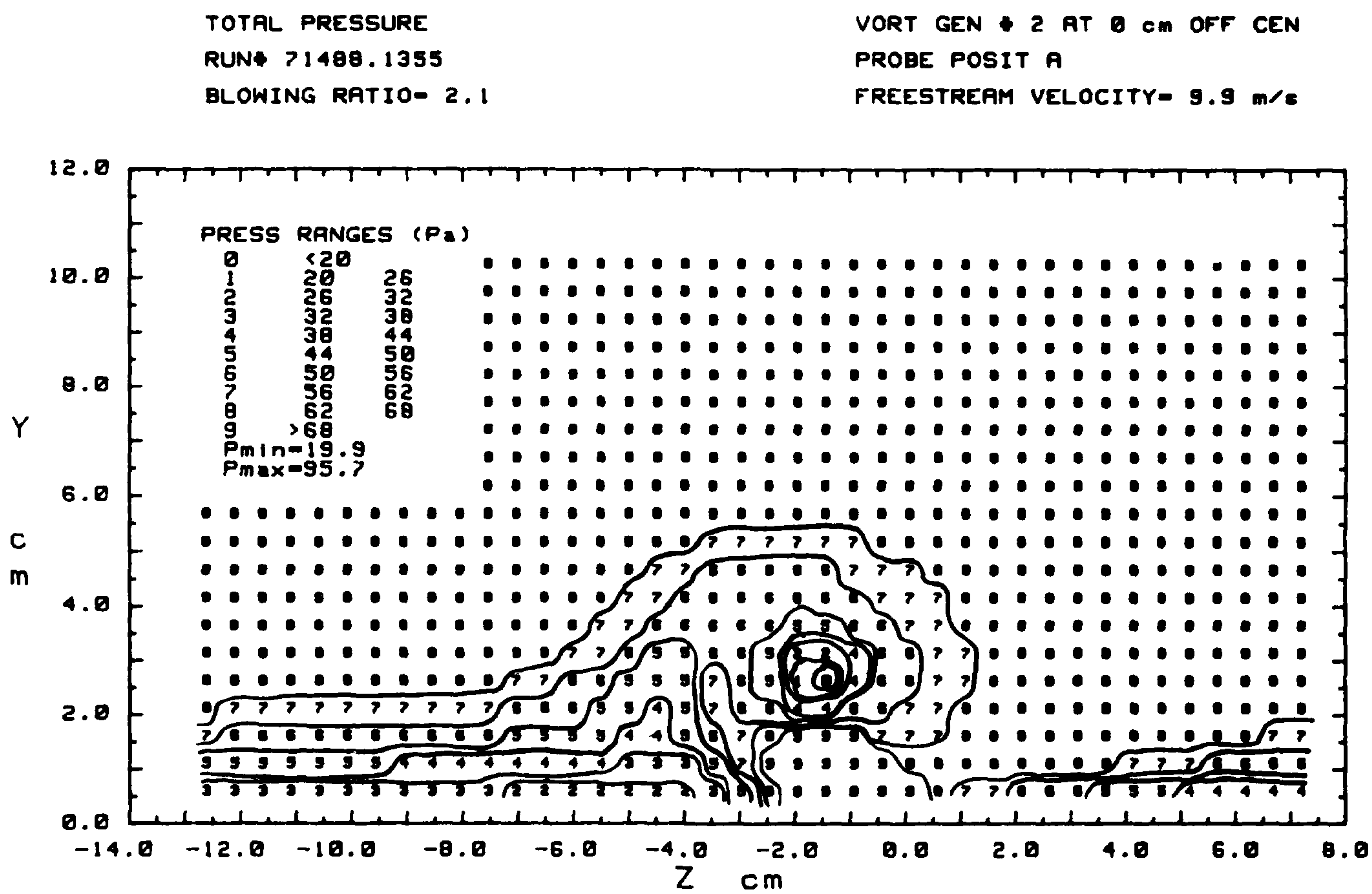

Figure 121. Total Pressure Contours

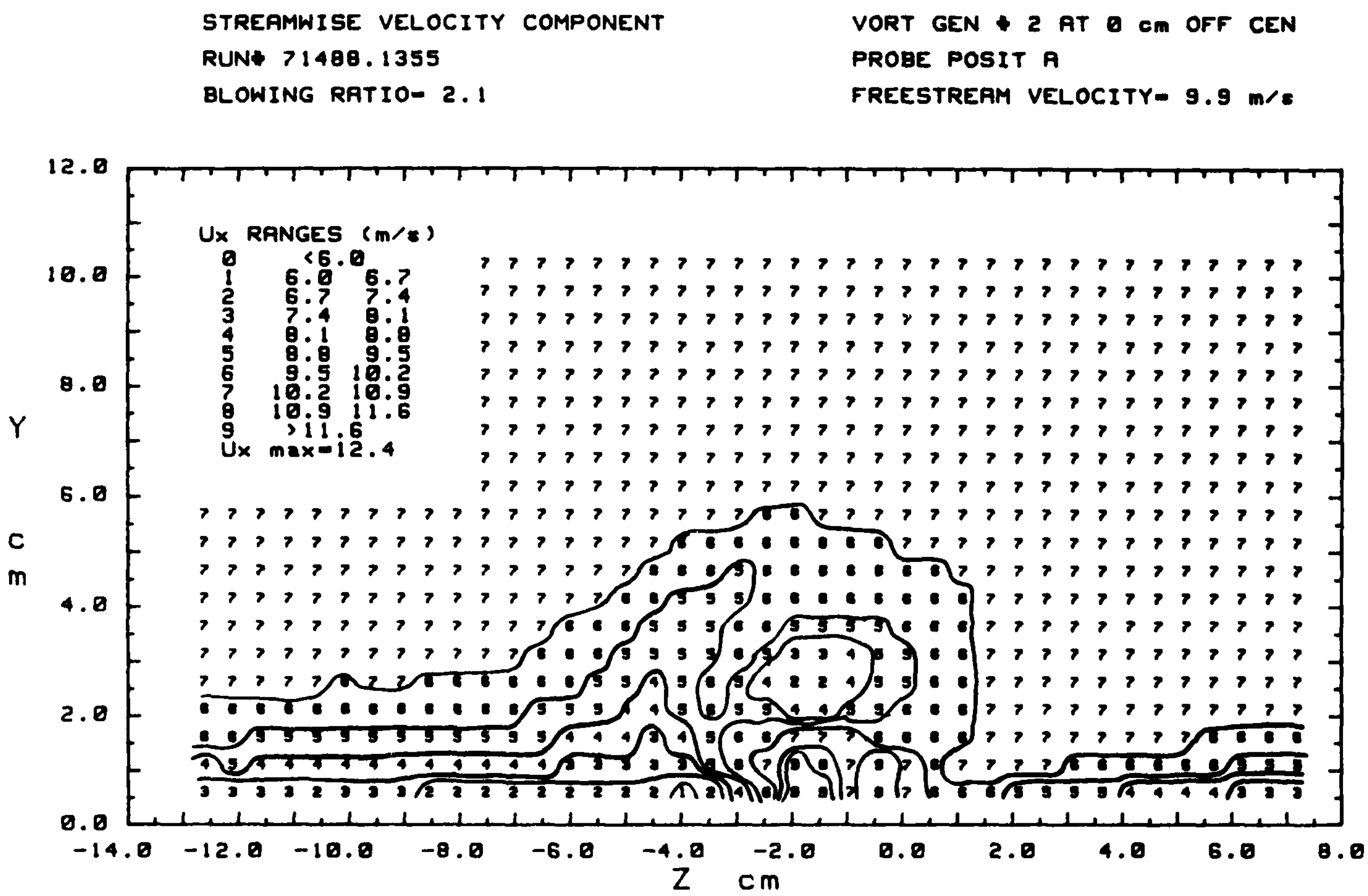

Figure 122. Streamwise Velocity Contours

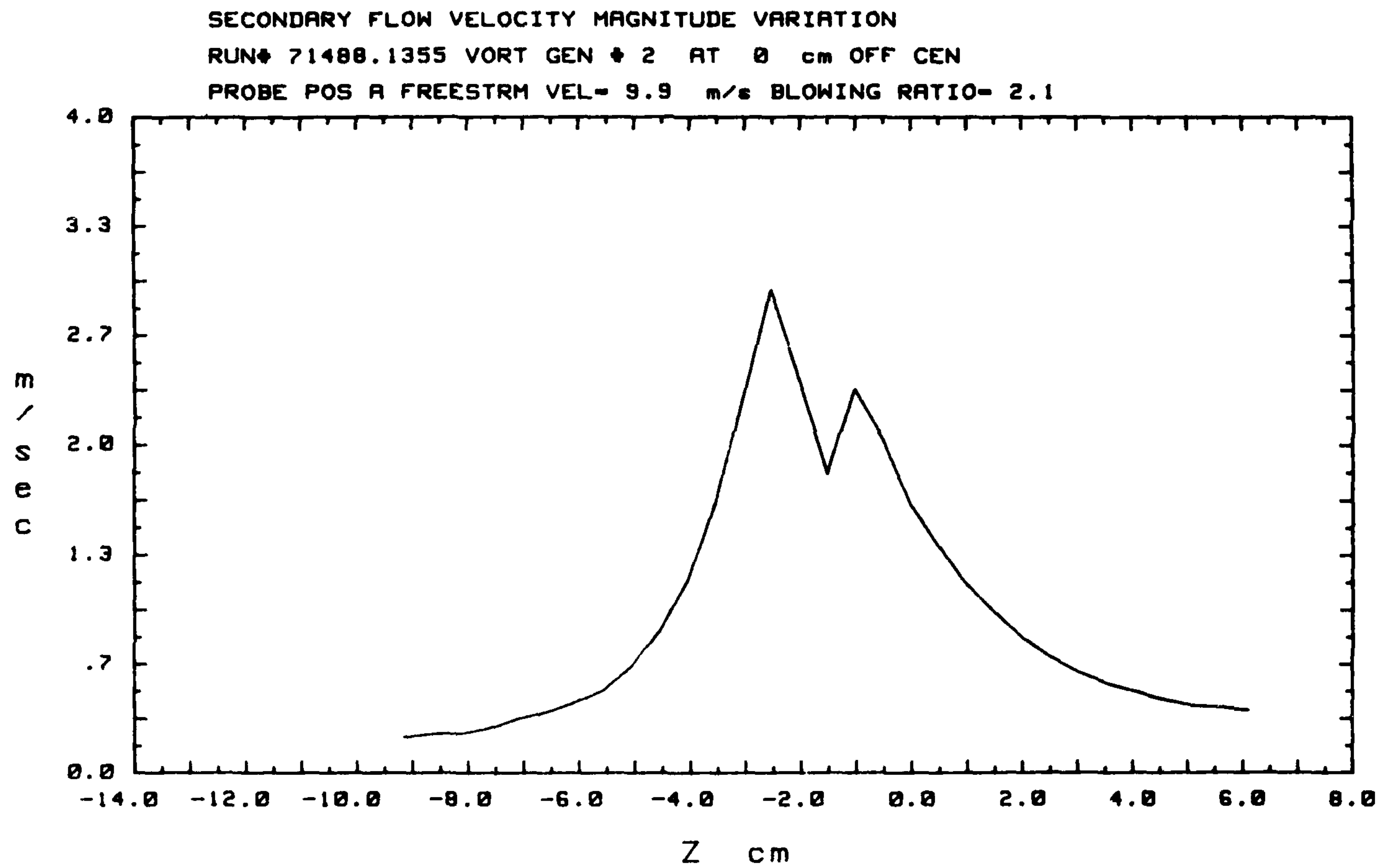

Figure 123. Secondary Flow Velocity (Radially)

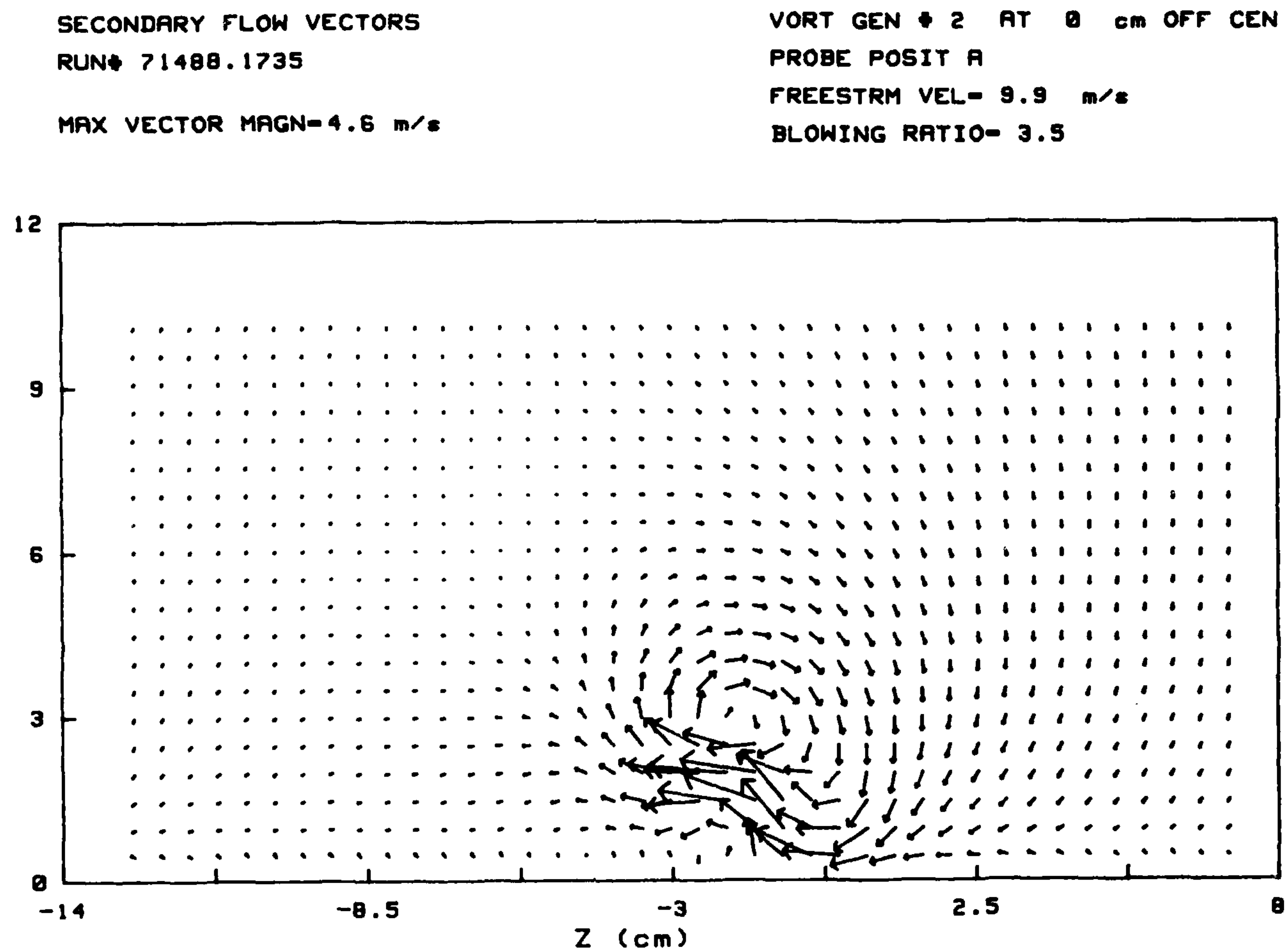

Figure 124. Secondary Flow Vectors

STREAMWISE VORTICITY (Wx)
RUN# 71488.1735
BLOWING RATIO= 3.5
MOMENTUM FLUX RATIO= 12.25

VORT GEN # 2 AT 0 cm OFF CEN
PROBE POSIT A
FREESTREAM VELOCITY(U)= 9.9 m/s
INJECTION VELOCITY (Uc)= 34.65 m/s

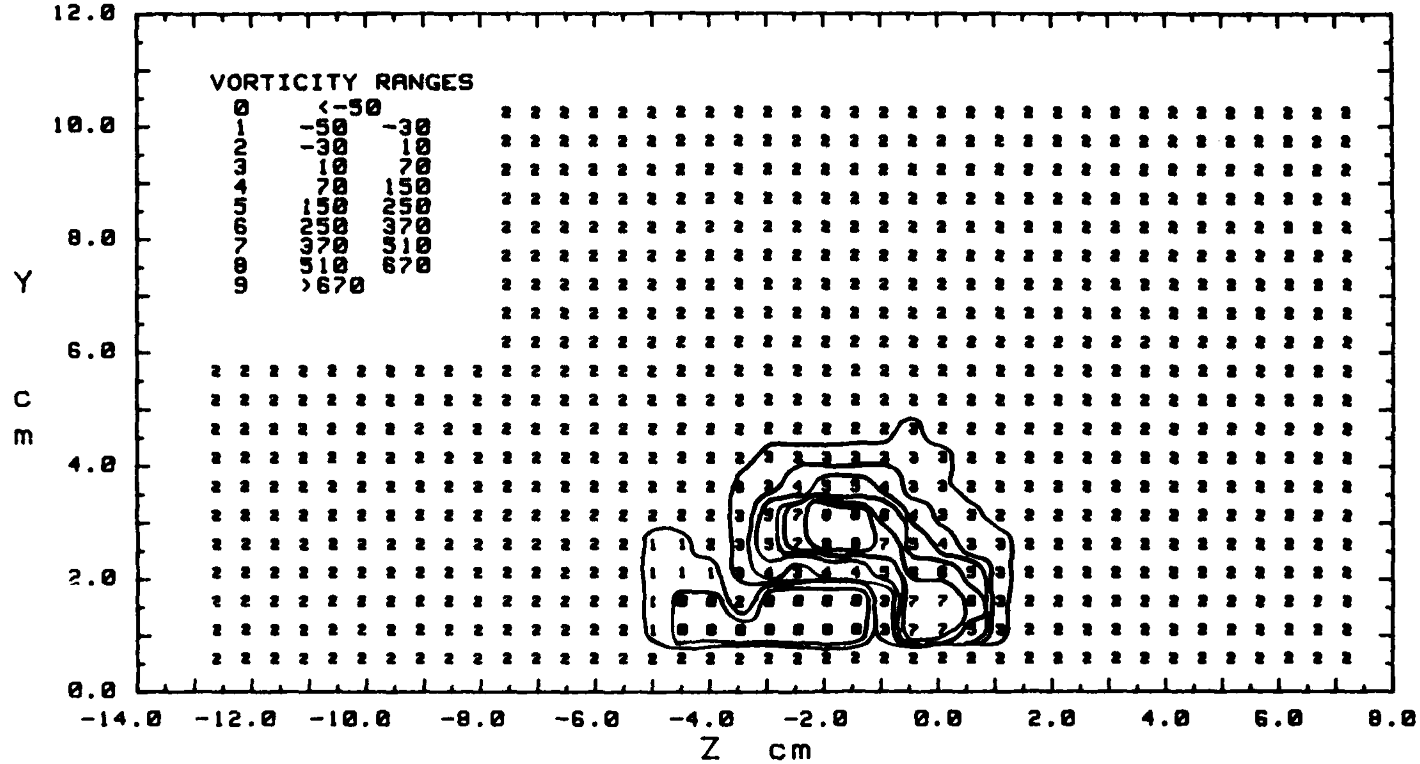

Cr= .22134 m^2/s
Zcen=-2.03 cm Ycen=2.48 cm
Zcore= .76 cm Ycore= .76 cm

Wxmax= 645.0 1/s
Cr/(U*(Ycore+Zcore)/2)= .02934
Cr/(Uc*d)= .67241

Figure 125. Streamwise Vorticity Contours

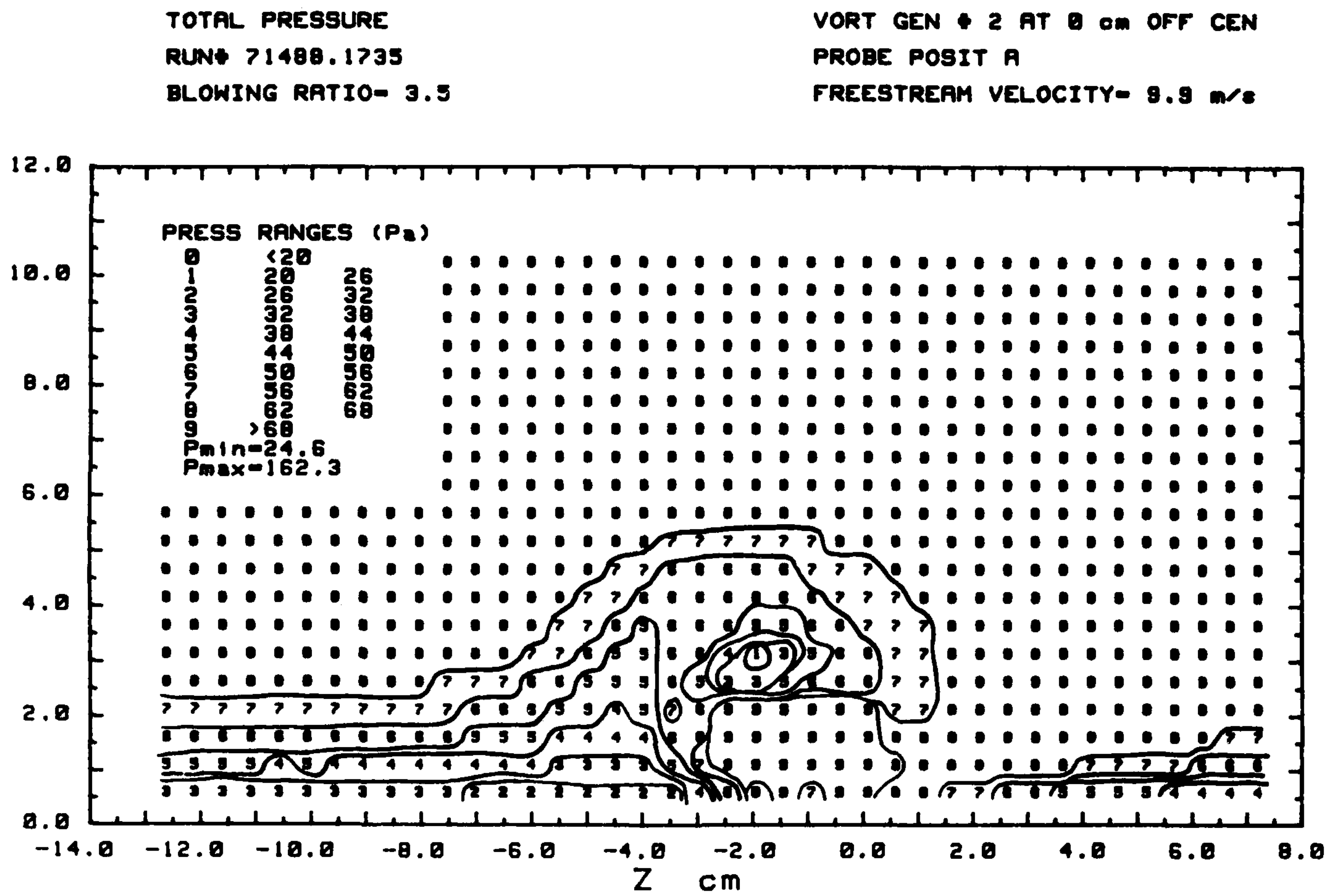

Figure 126. Total Pressure Contours

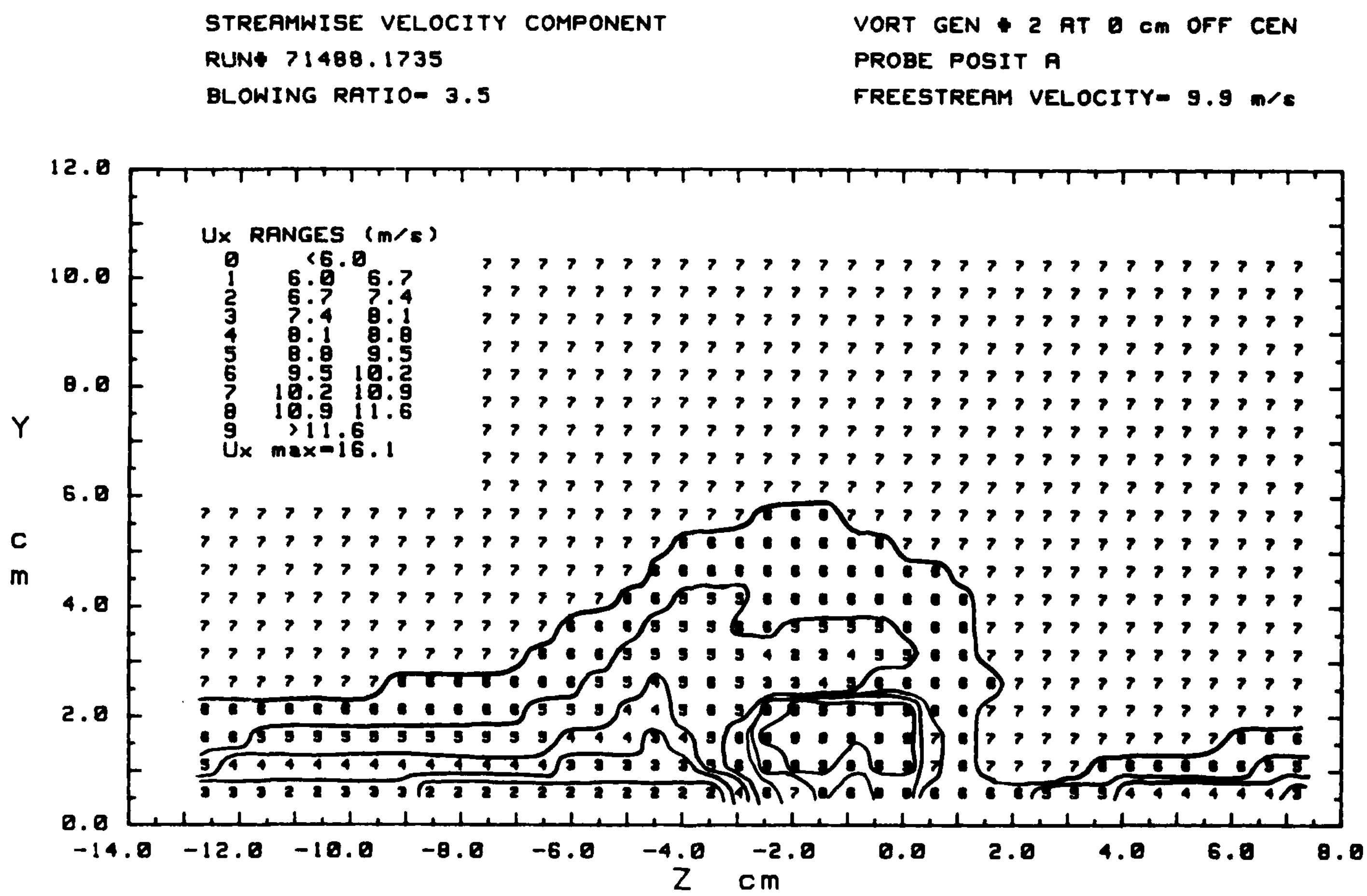

Figure 127. Streamwise Velocity Contours

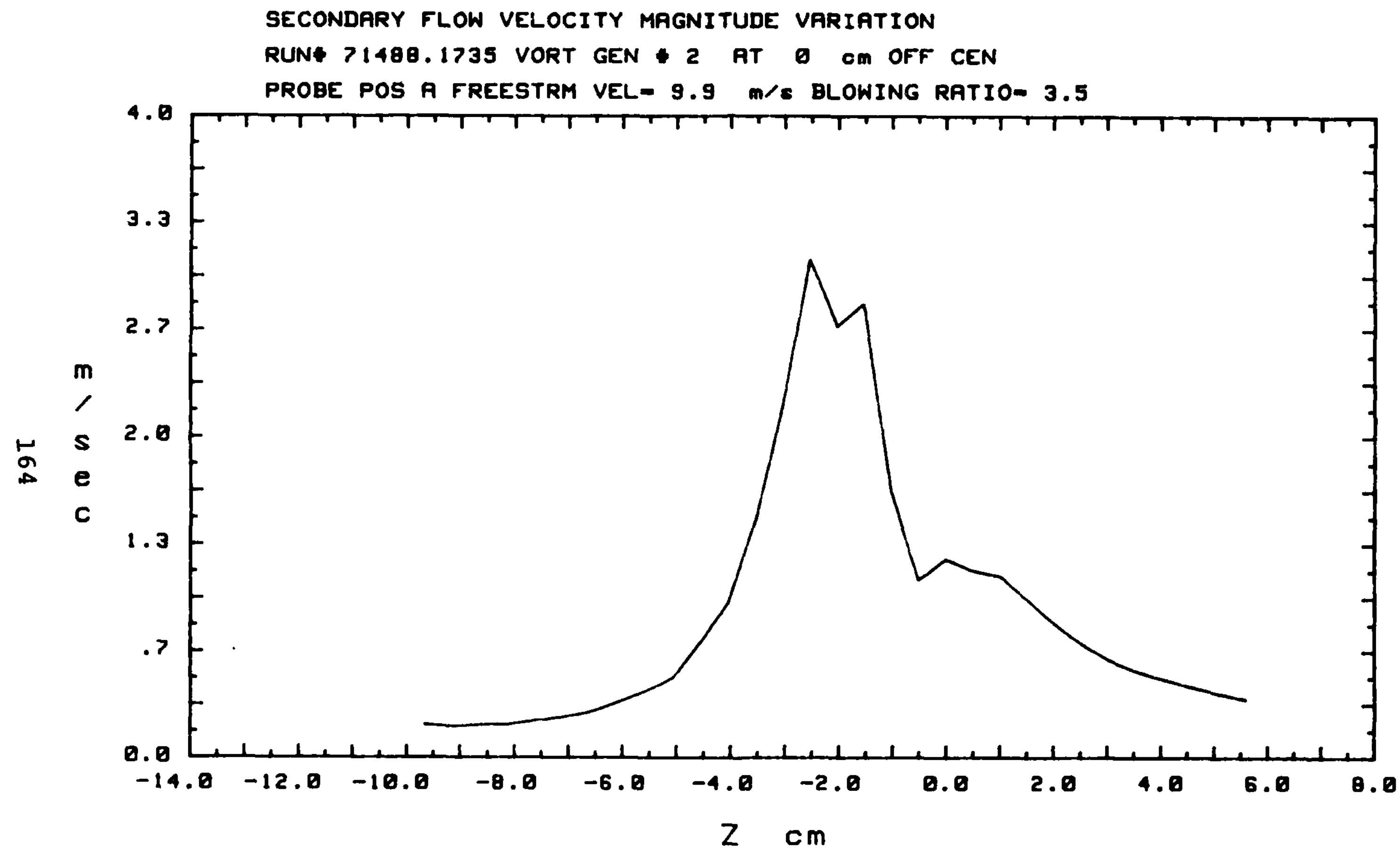

Figure 128. Secondary Flow Velocity (Radially)

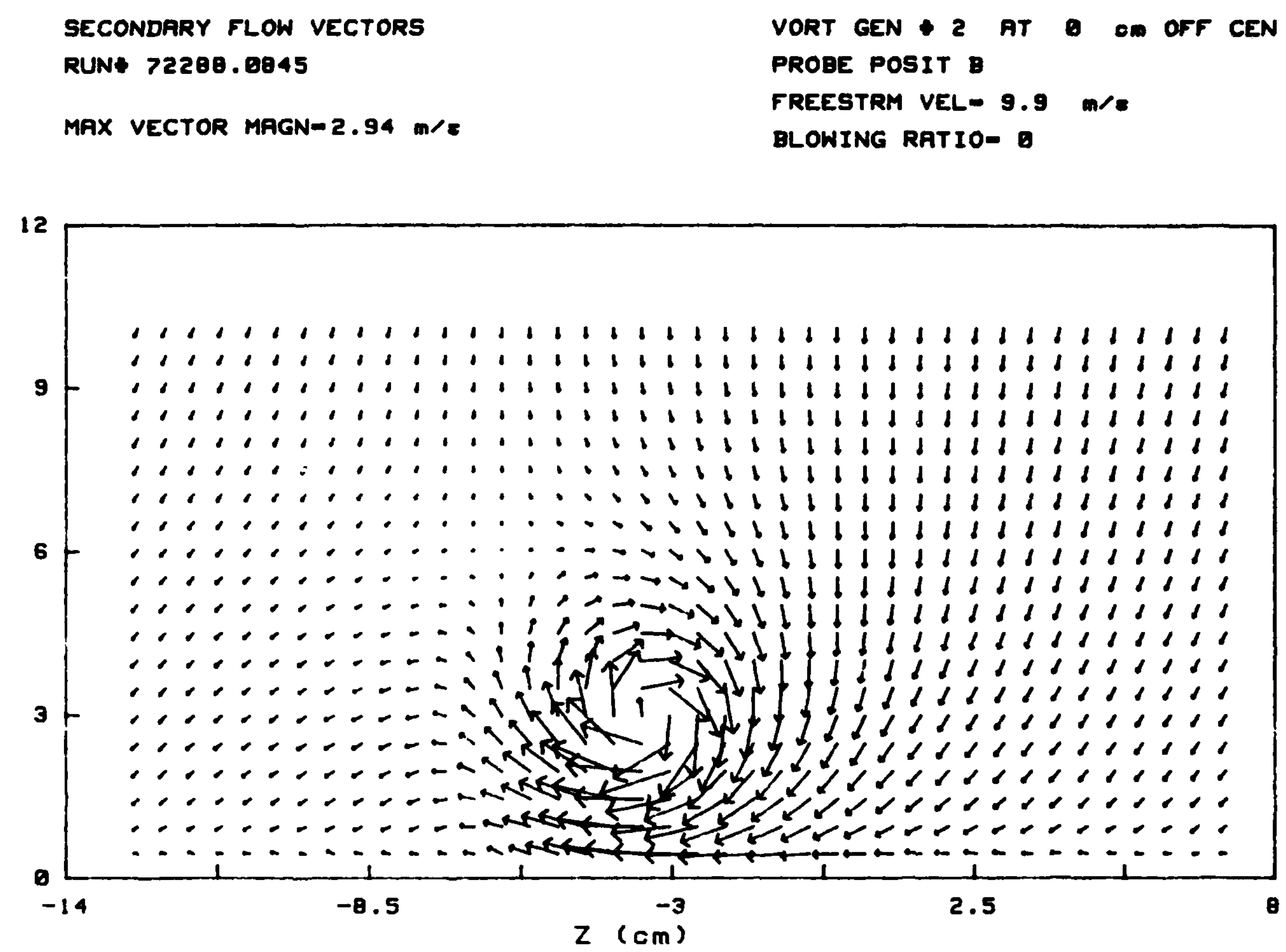

Figure 129. Secondary Flow Vectors

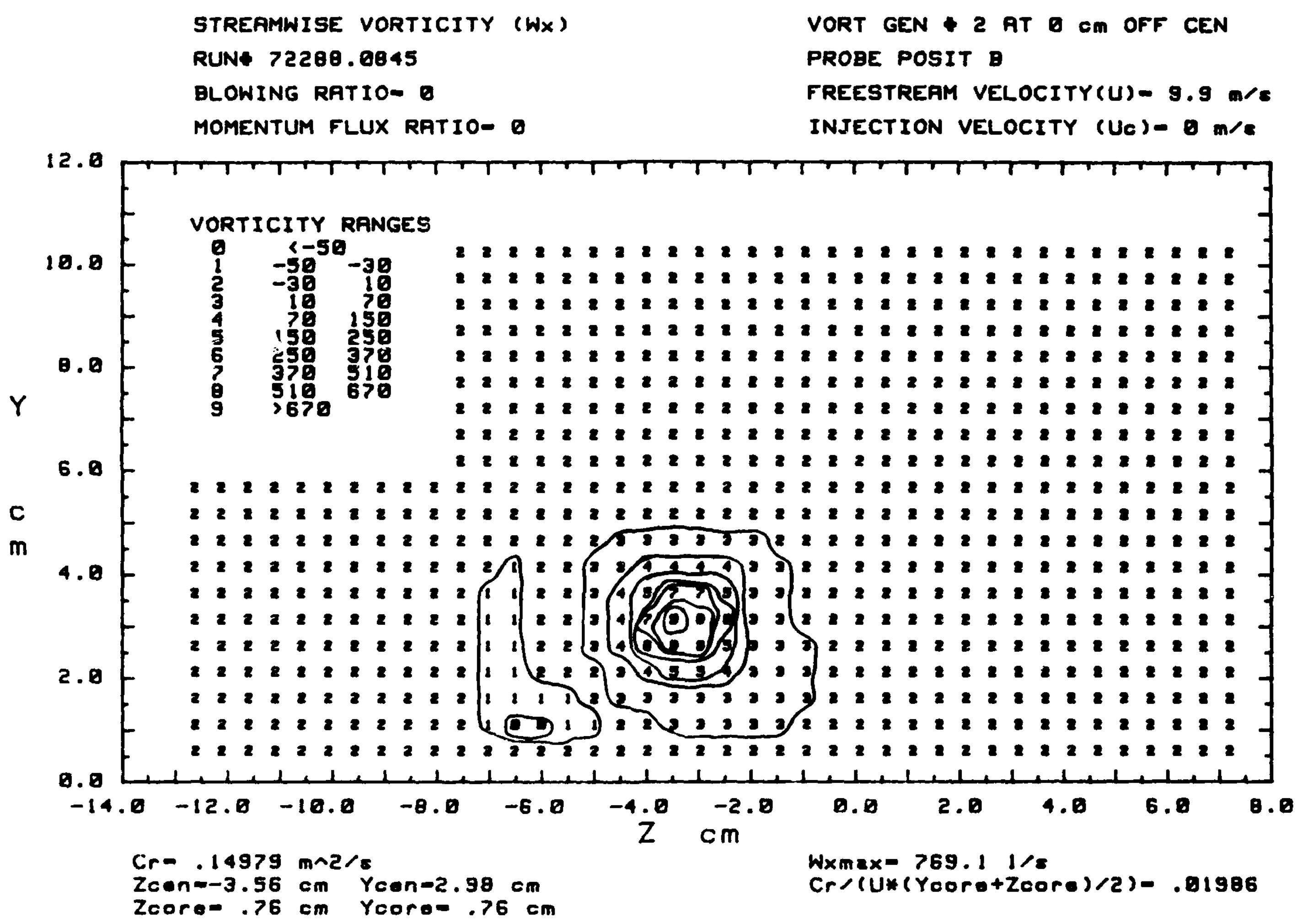

Figure 130. Streamwise Vorticity Contours

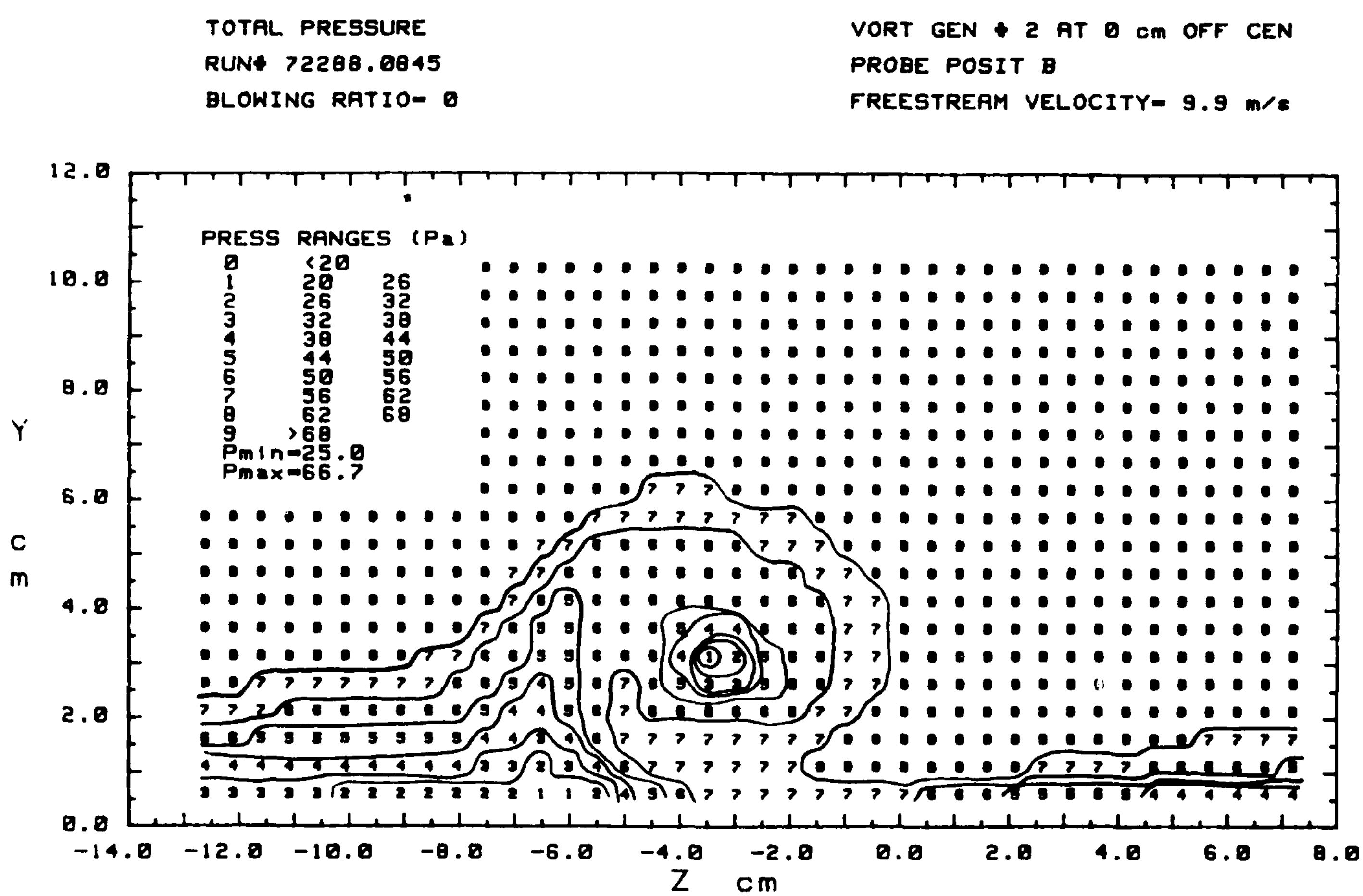

Figure 131. Total Pressure Contours

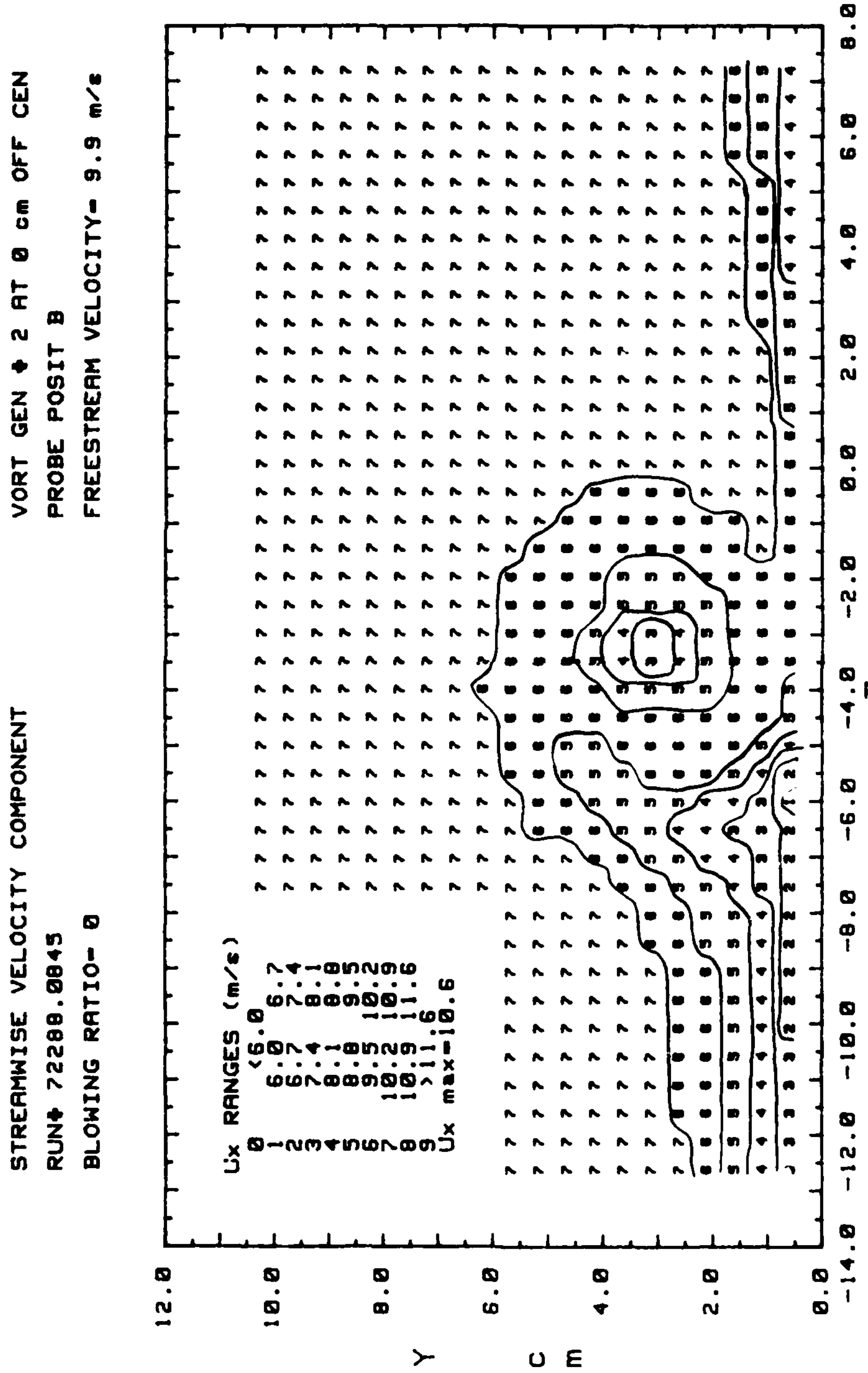

Figure 132. Streamwise Velocity Contours

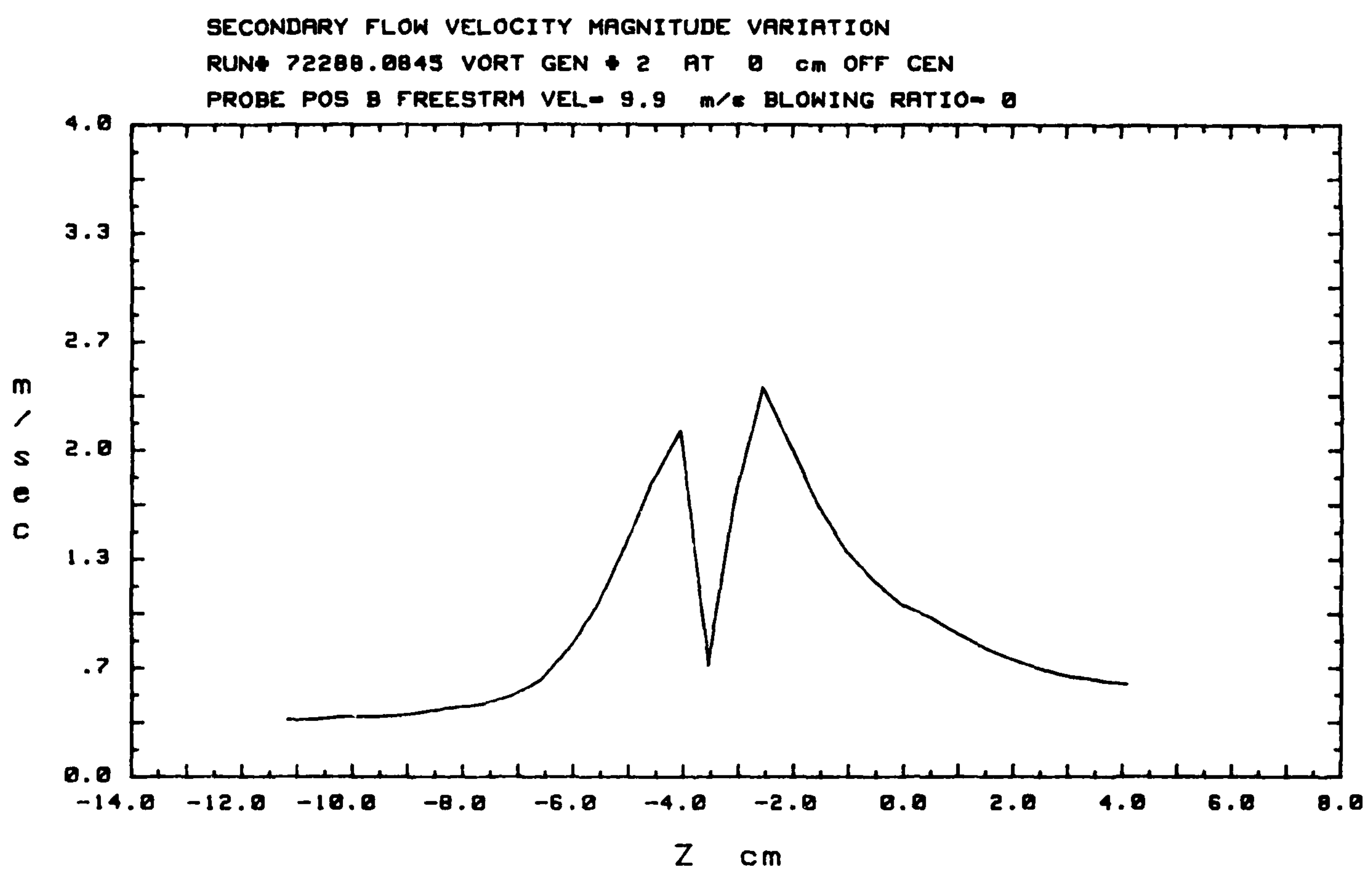

Figure 133. Secondary Flow Velocity (Radially)

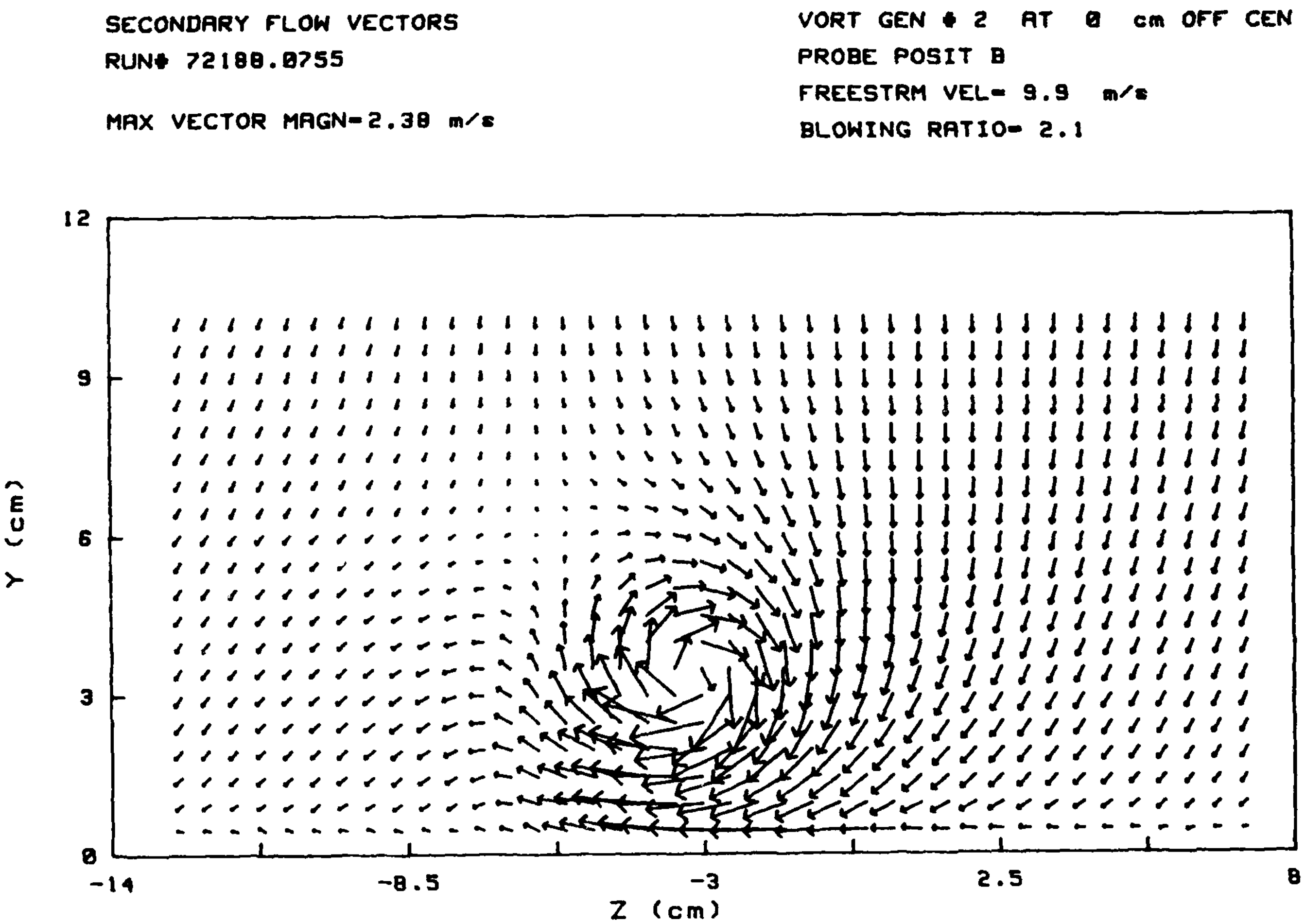

Figure 134. Secondary Flow Vectors

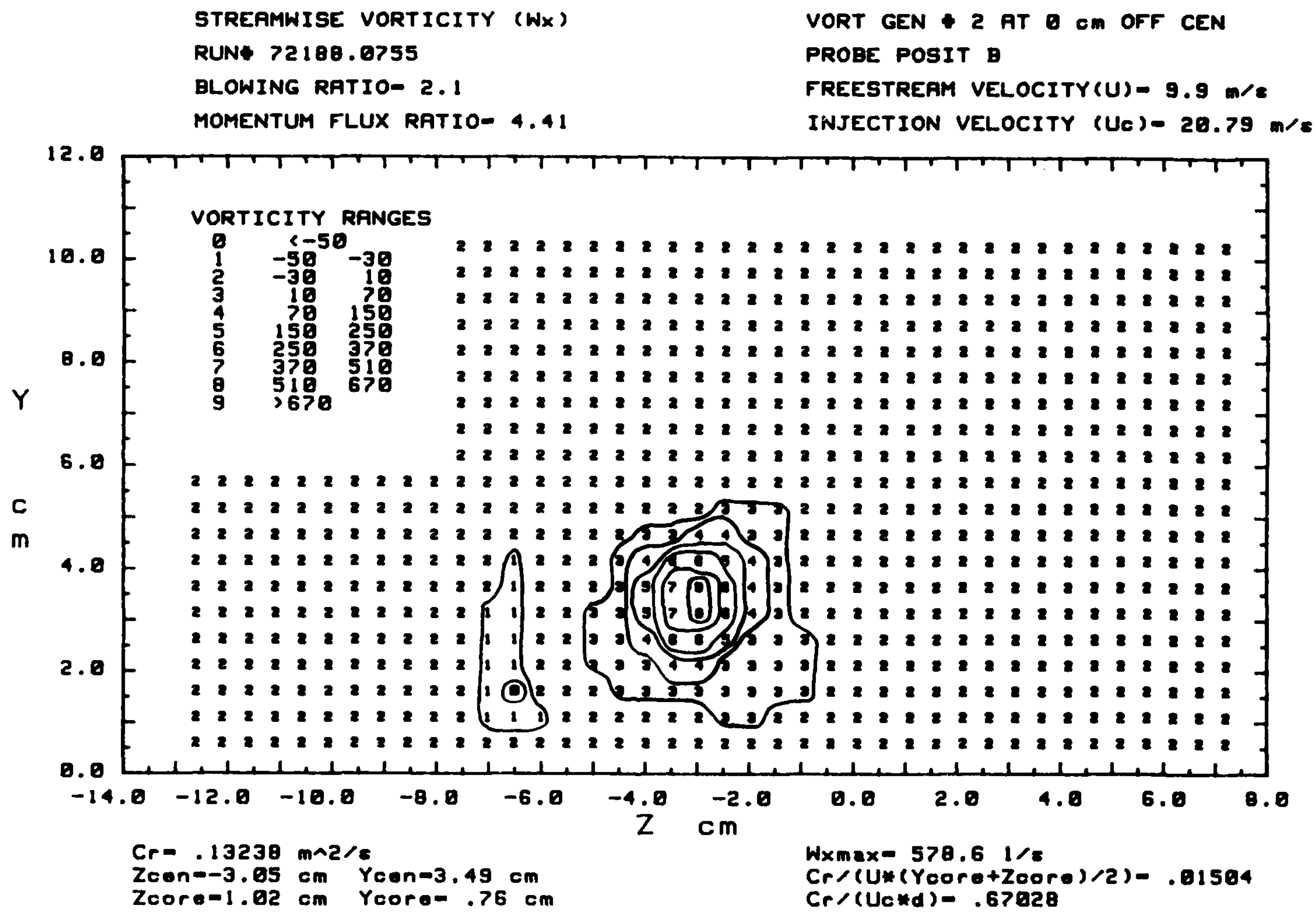

Figure 135. Streamwise Vorticity Contours

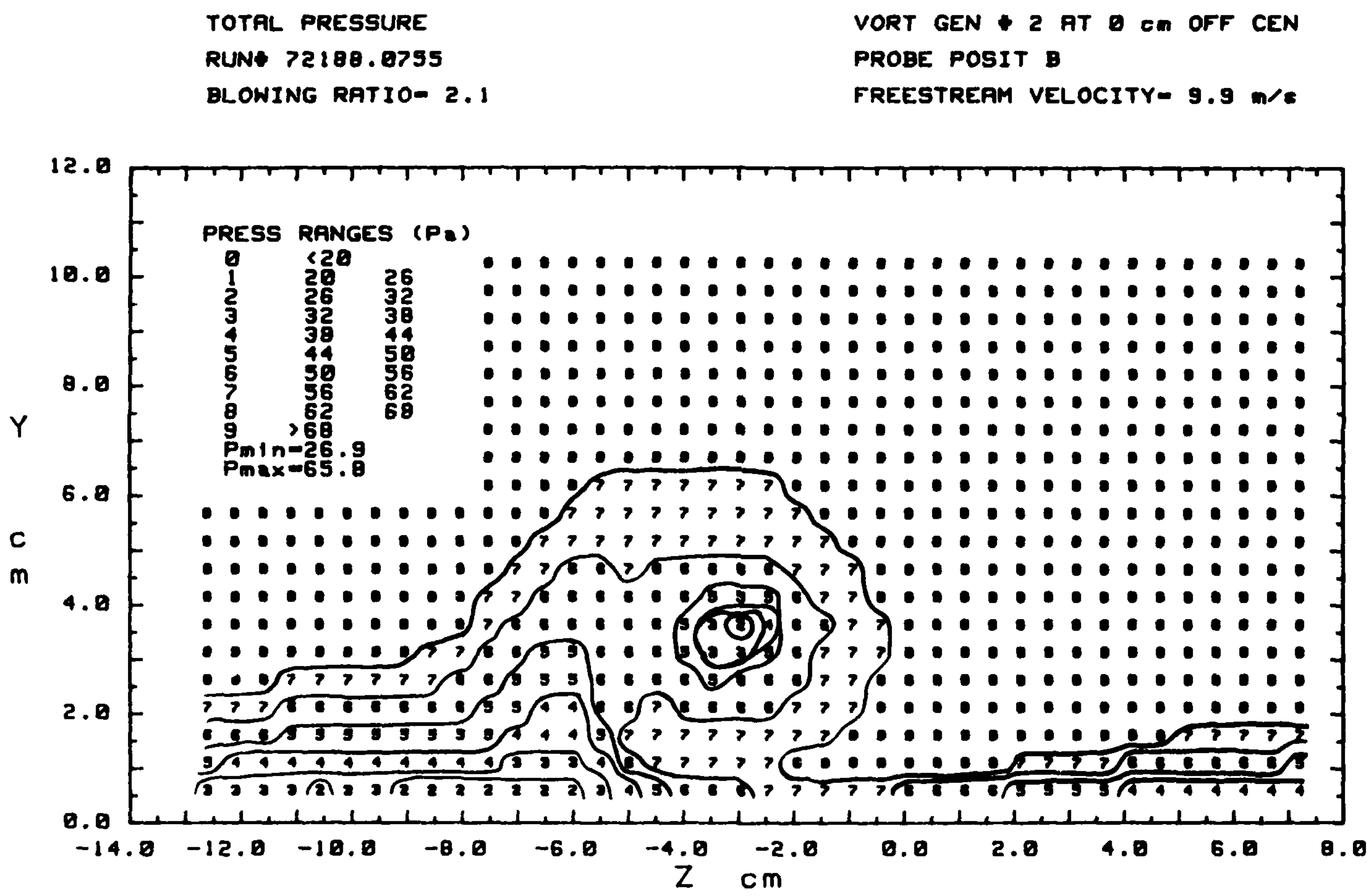

Figure 136. Total Pressure Contours

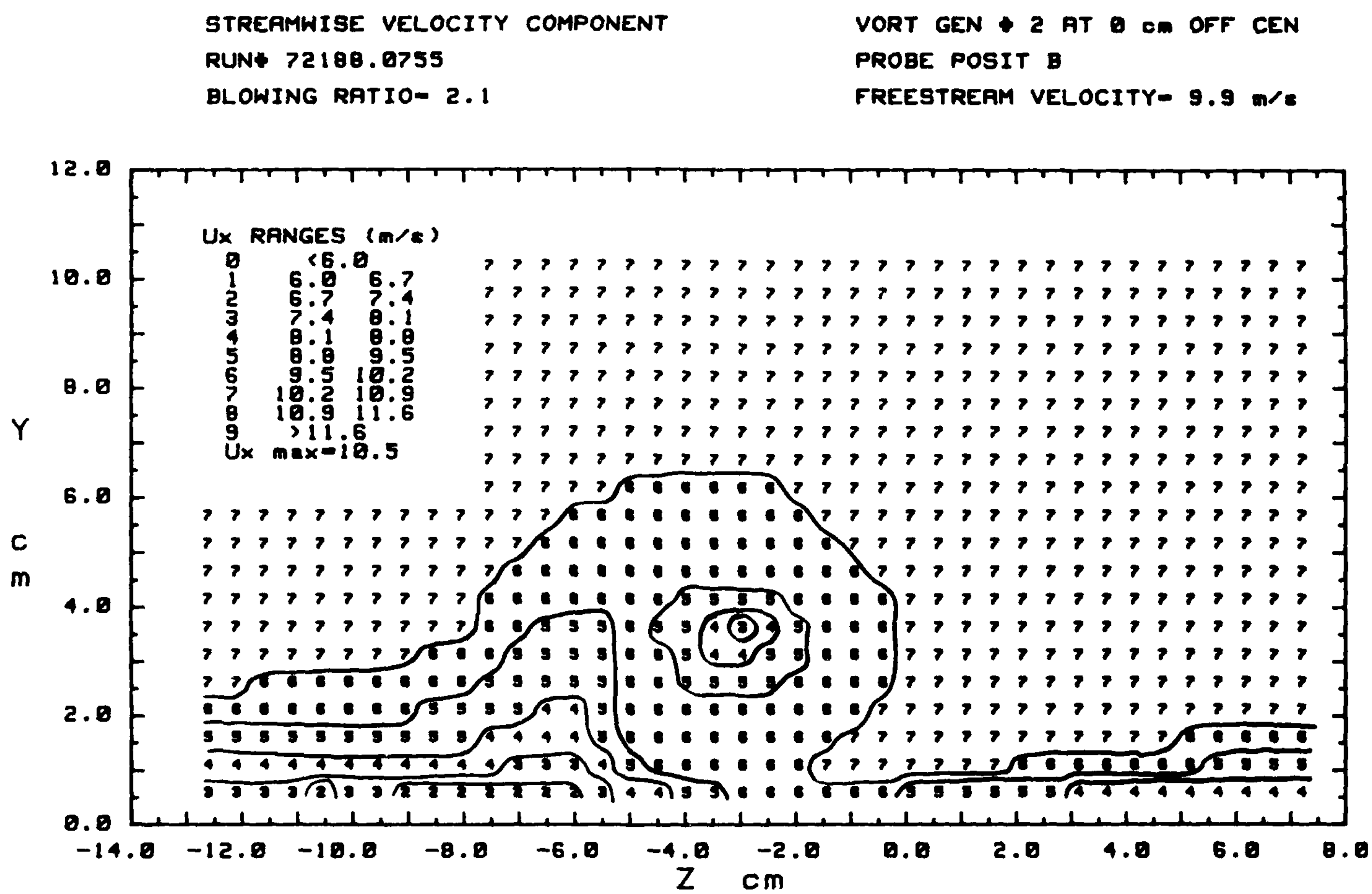

Figure 137. Streamwise Velocity Contours

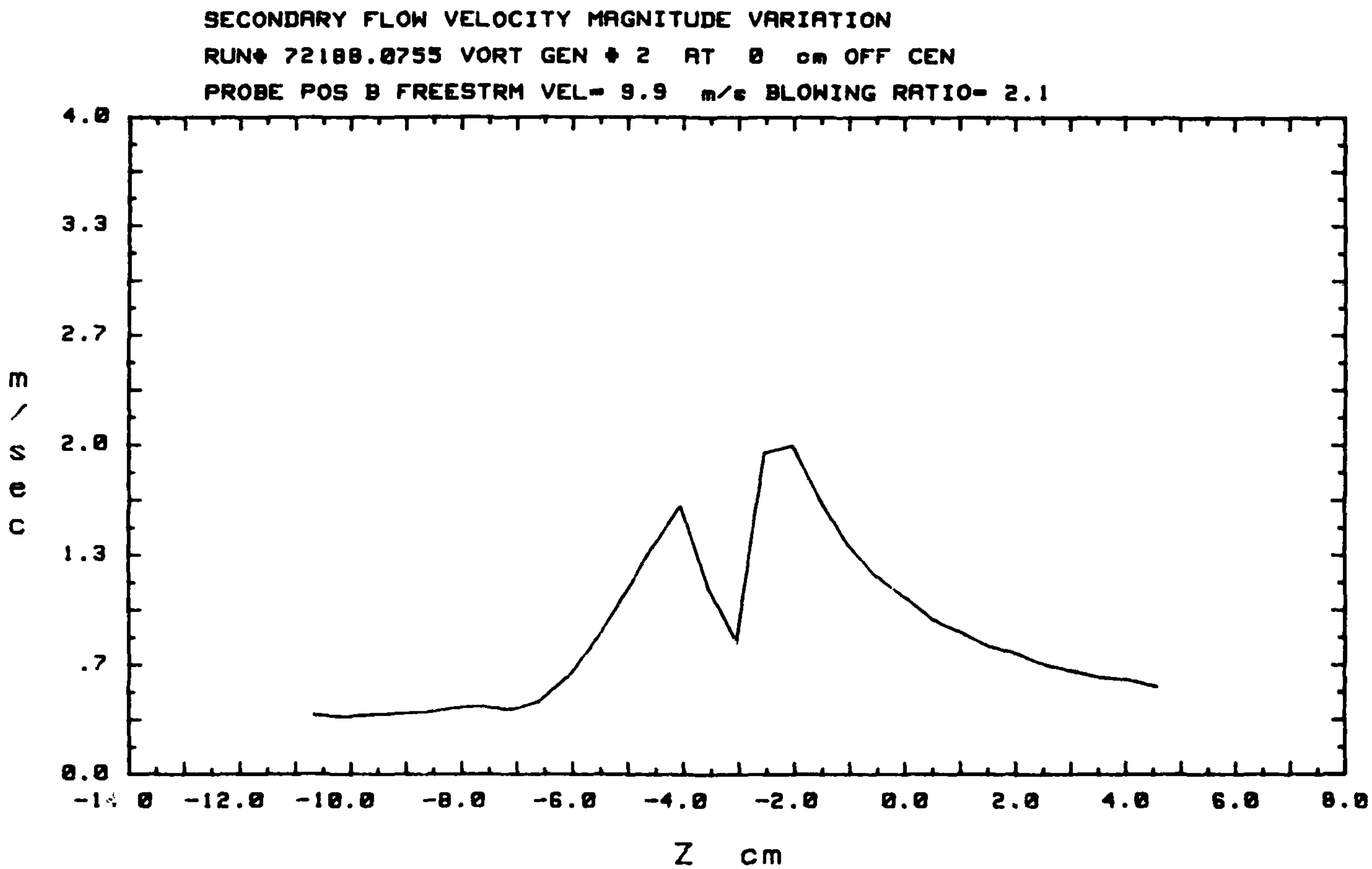

Figure 138. Secondary Flow Velocity (Radially)

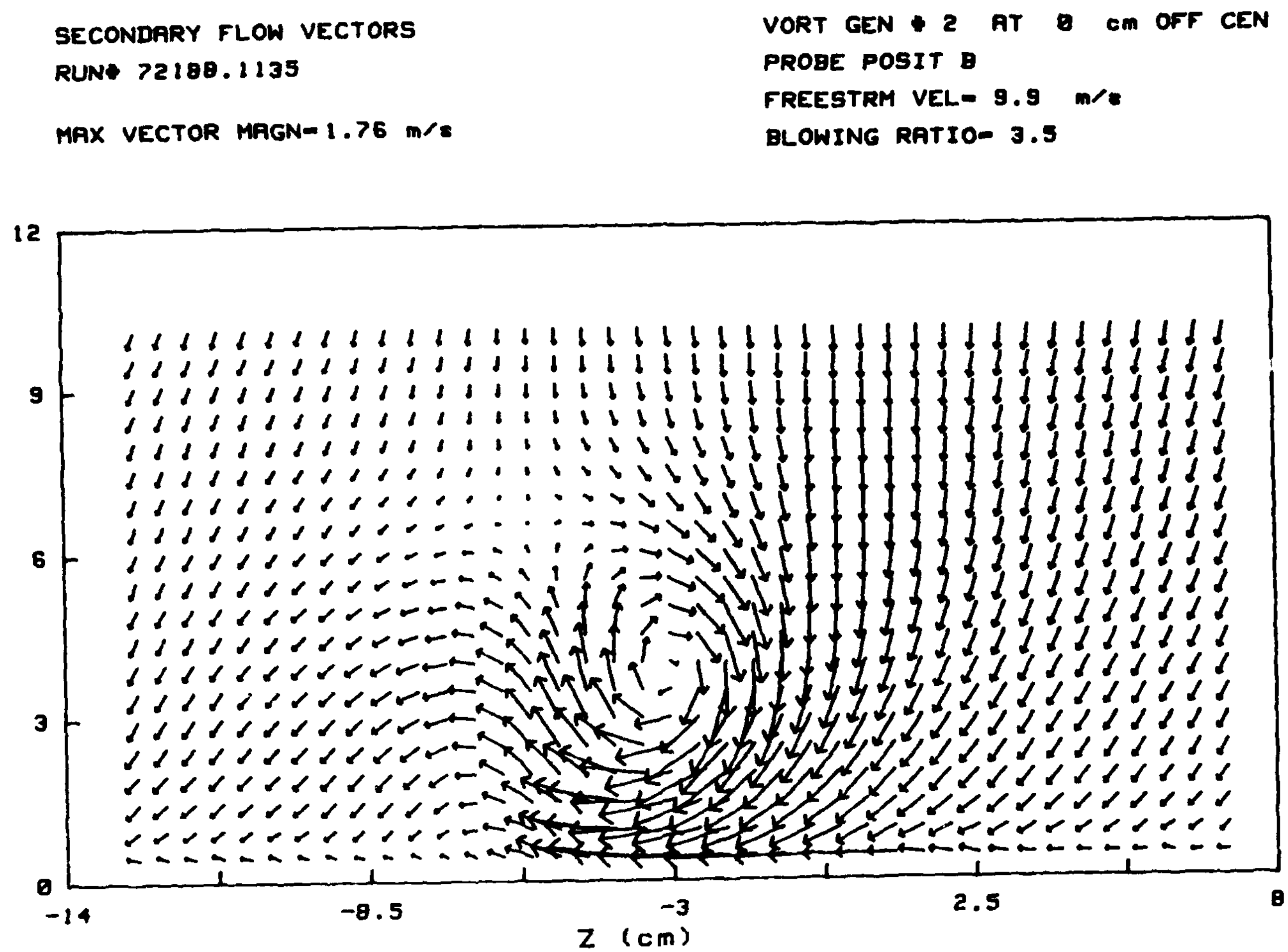

Figure 139. Secondary Flow Vectors

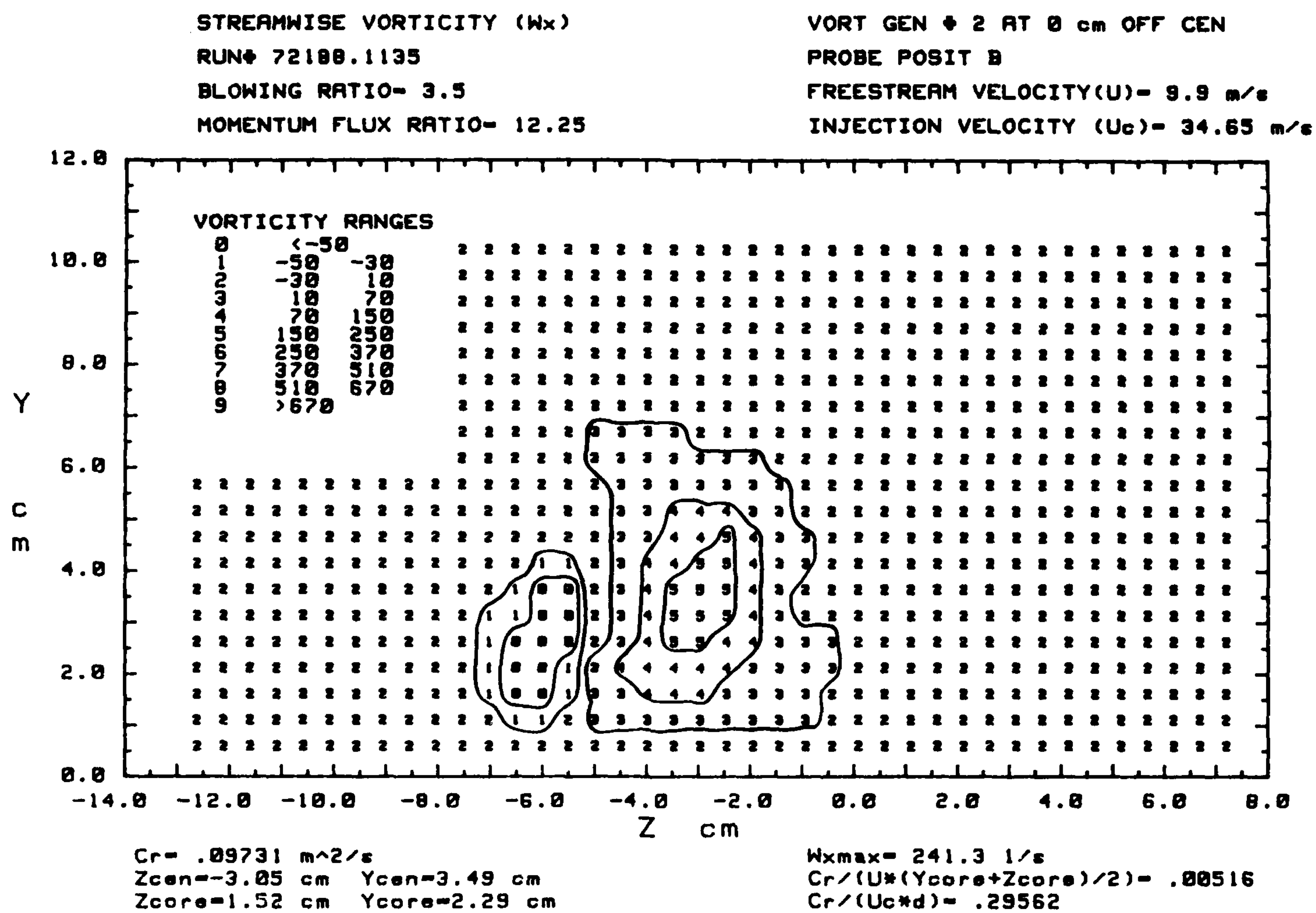

Figure 140. Streamwise Vorticity Contours

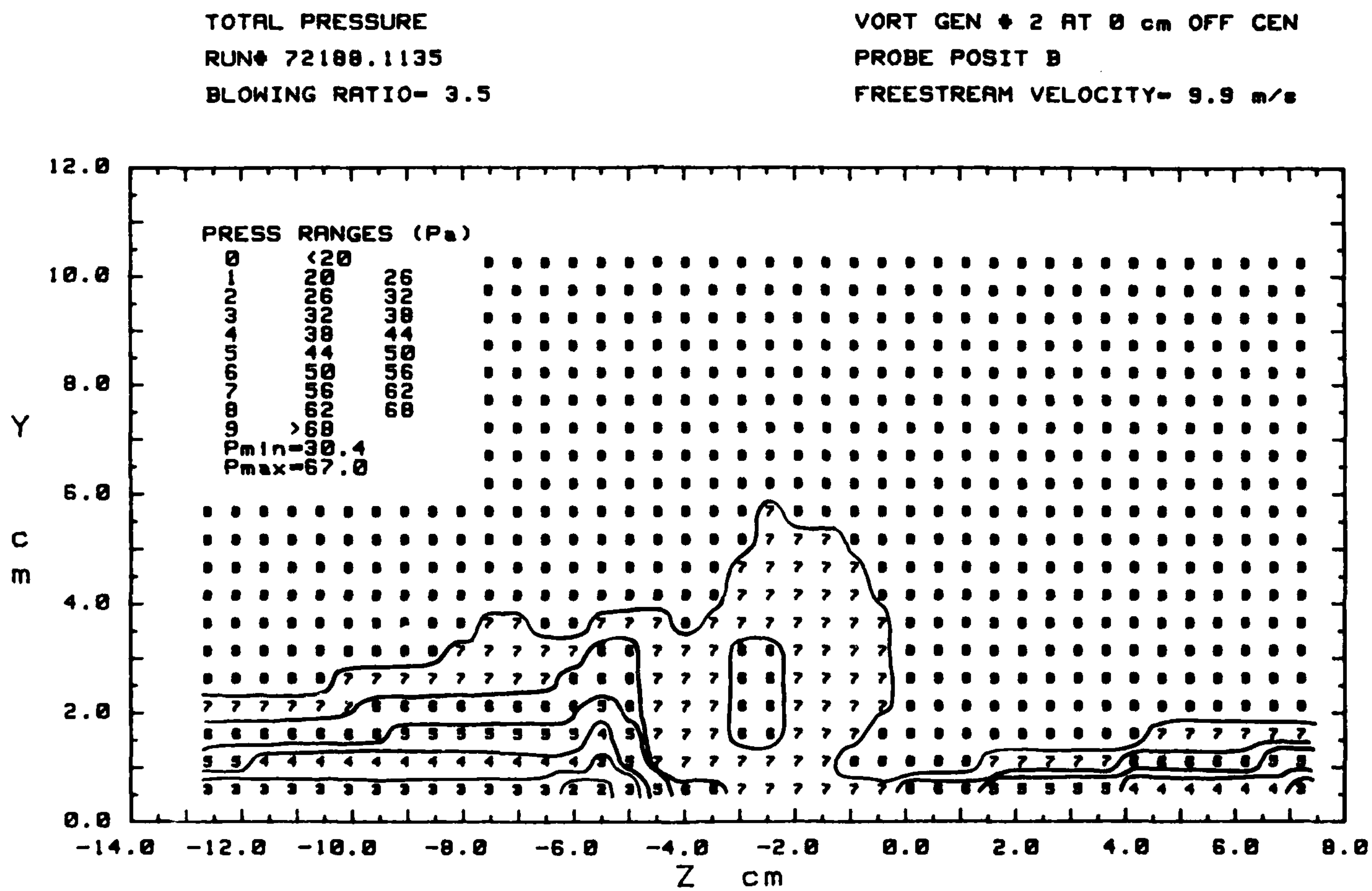

Figure 141. Total Pressure Contours

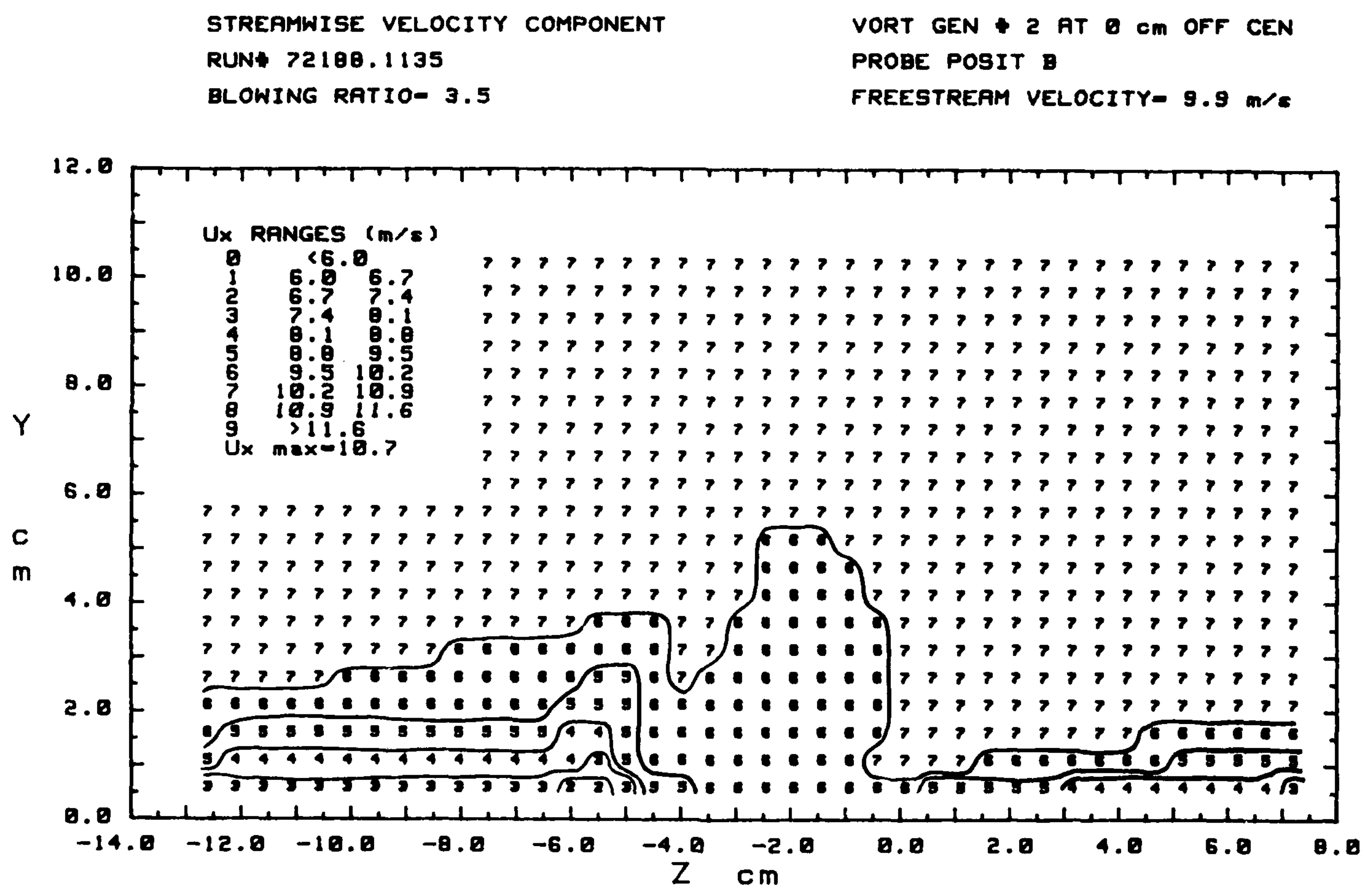

Figure 142. Streamwise Velocity Contours

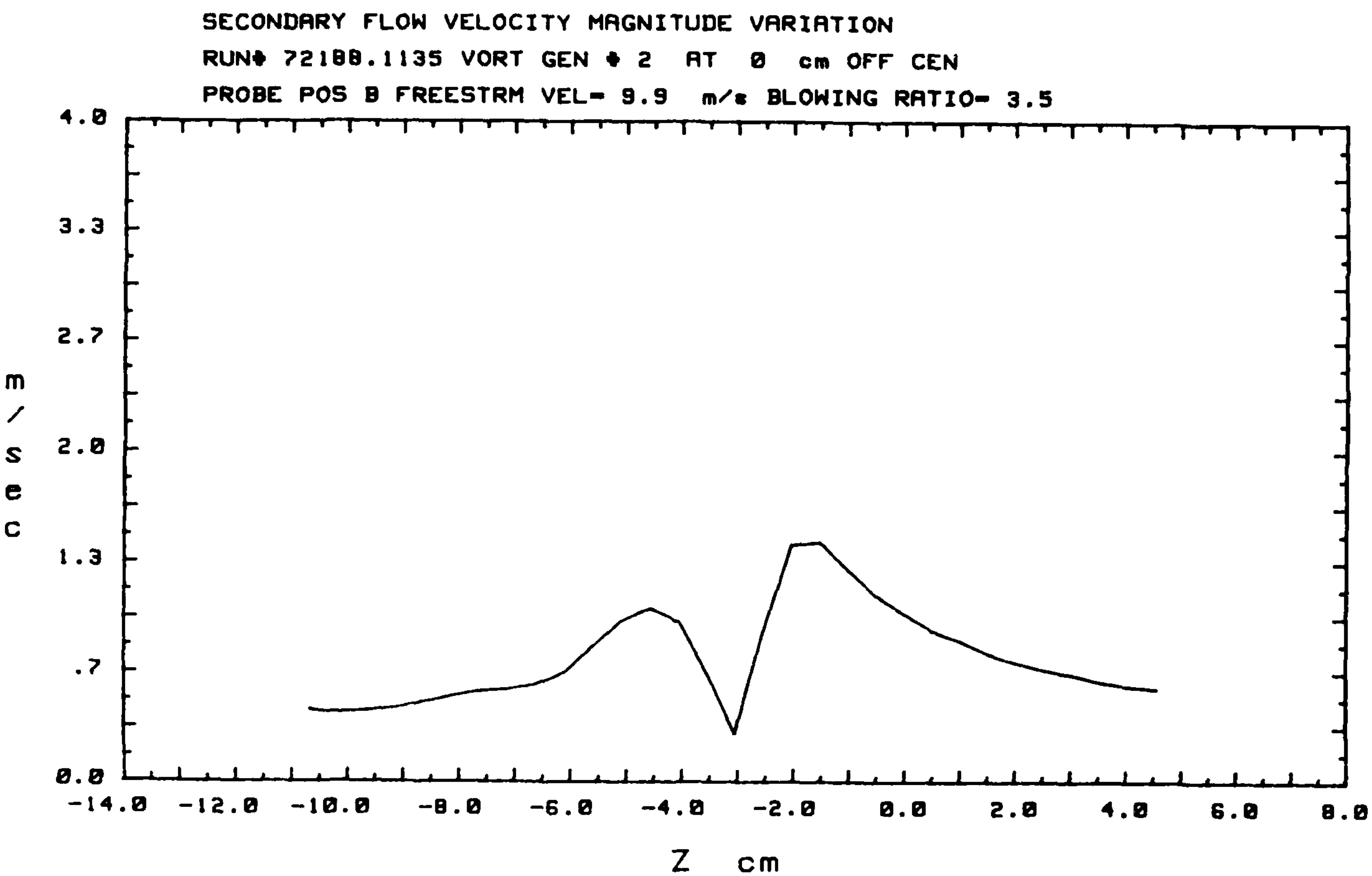

Figure 143. Secondary Flow Velocity (Radially)

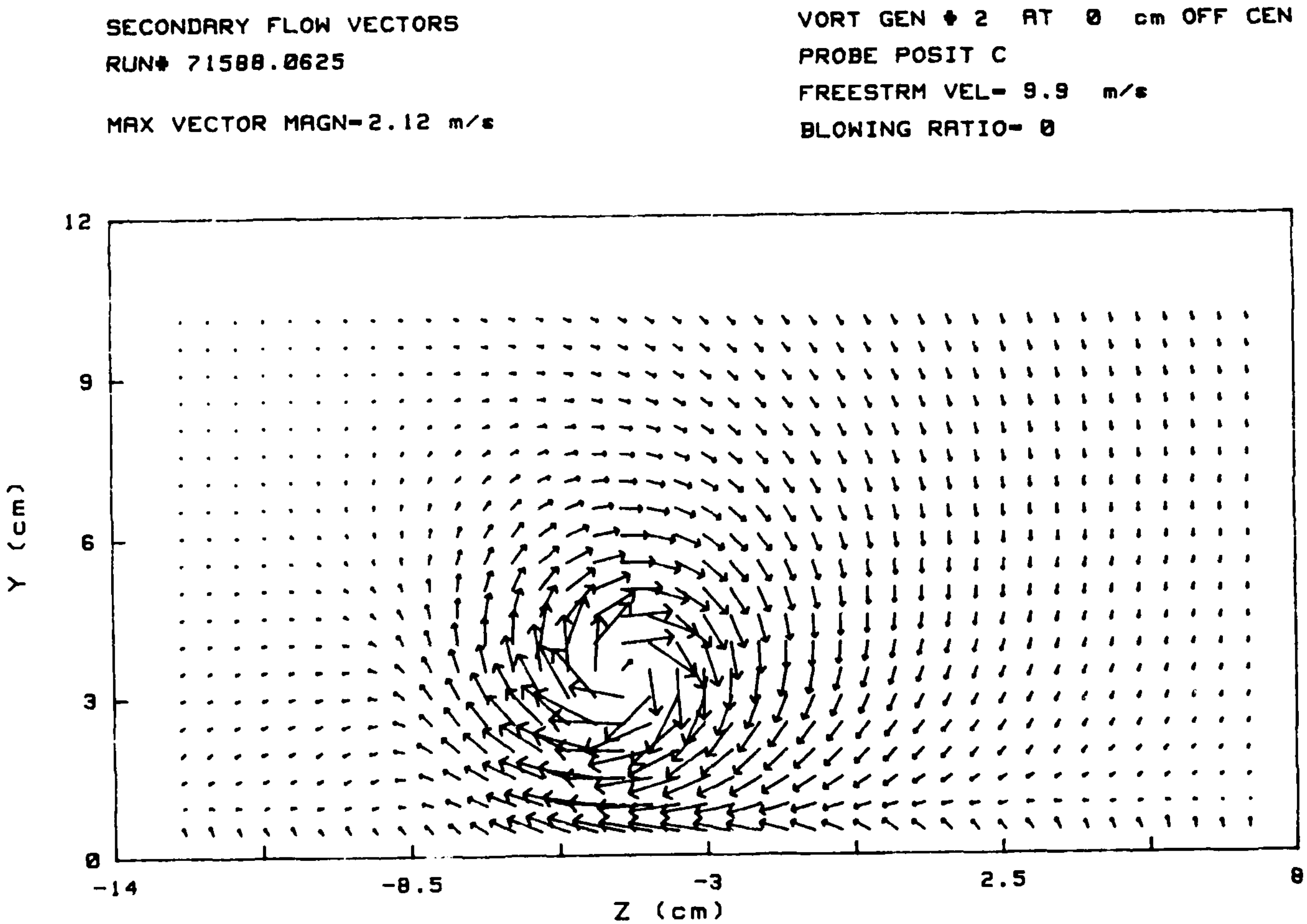

Figure 144. Secondary Flow Vectors

STREAMWISE VORTICITY (Wx)
RUN# 71588.0625
BLOWING RATIO= 0
MOMENTUM FLUX RATIO= 0

VORT GEN # 2 AT 0 cm OFF CEN
PROBE POSIT C
FREESTREAM VELOCITY(U)= 9.9 m/s
INJECTION VELOCITY (Uc)= 0 m/s

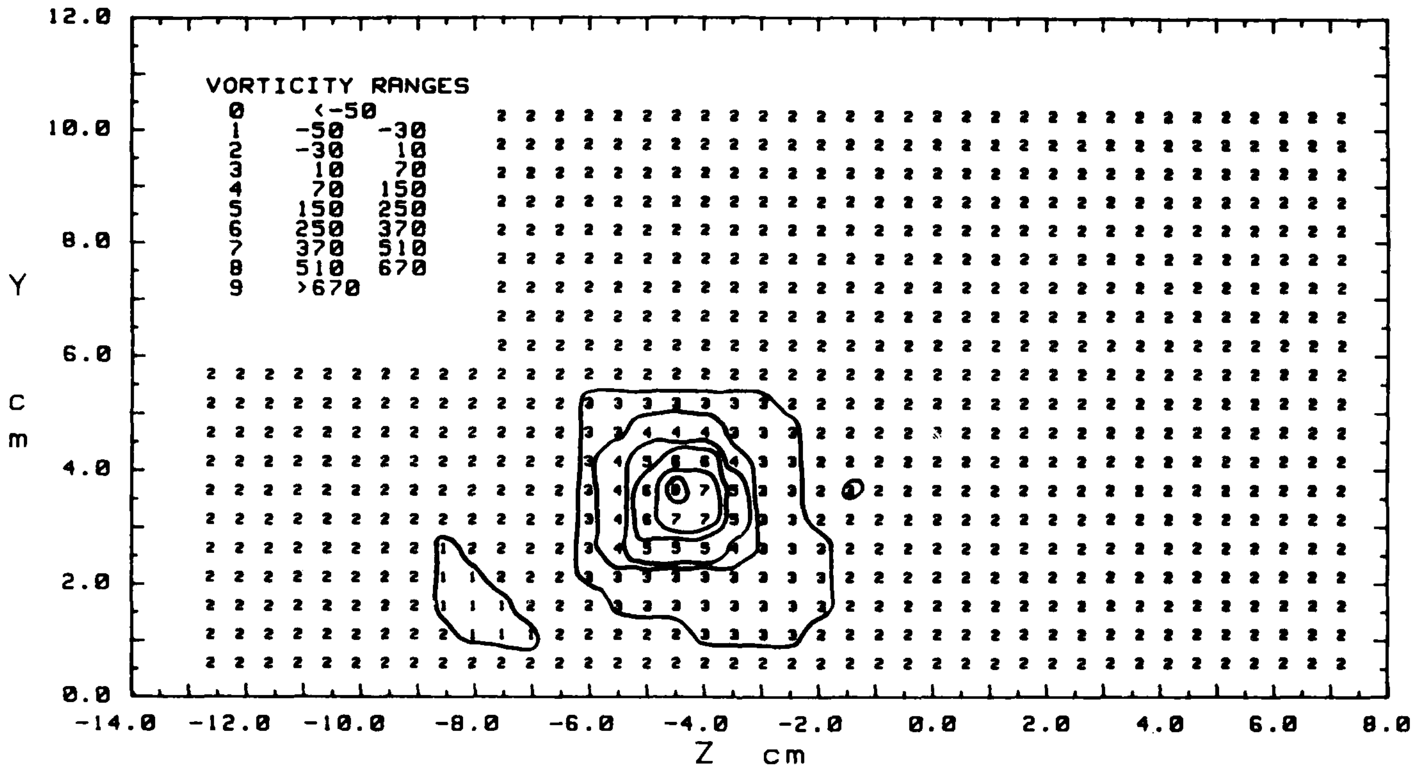

Cr= .11827 m^2/s
Zcen=-4.57 cm Ycen=3.49 cm
Zcore=1.02 cm Ycore= .76 cm

Wxmax= 579.8 1/s
Cr/(U*(Ycore+Zcore)/2)= .01344

Figure 145. Streamwise Vorticity Contours

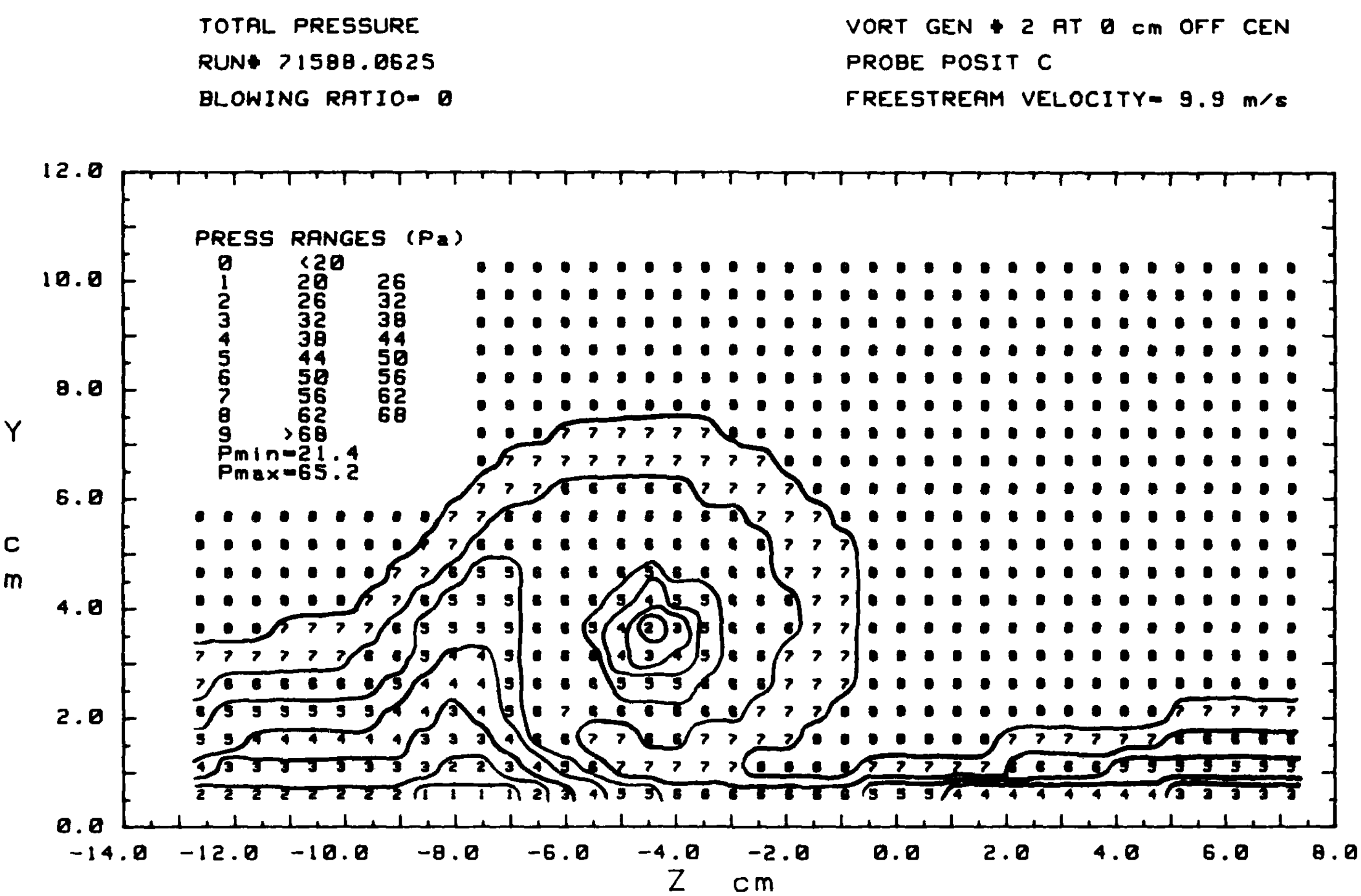

Figure 146. Total Pressure Contours

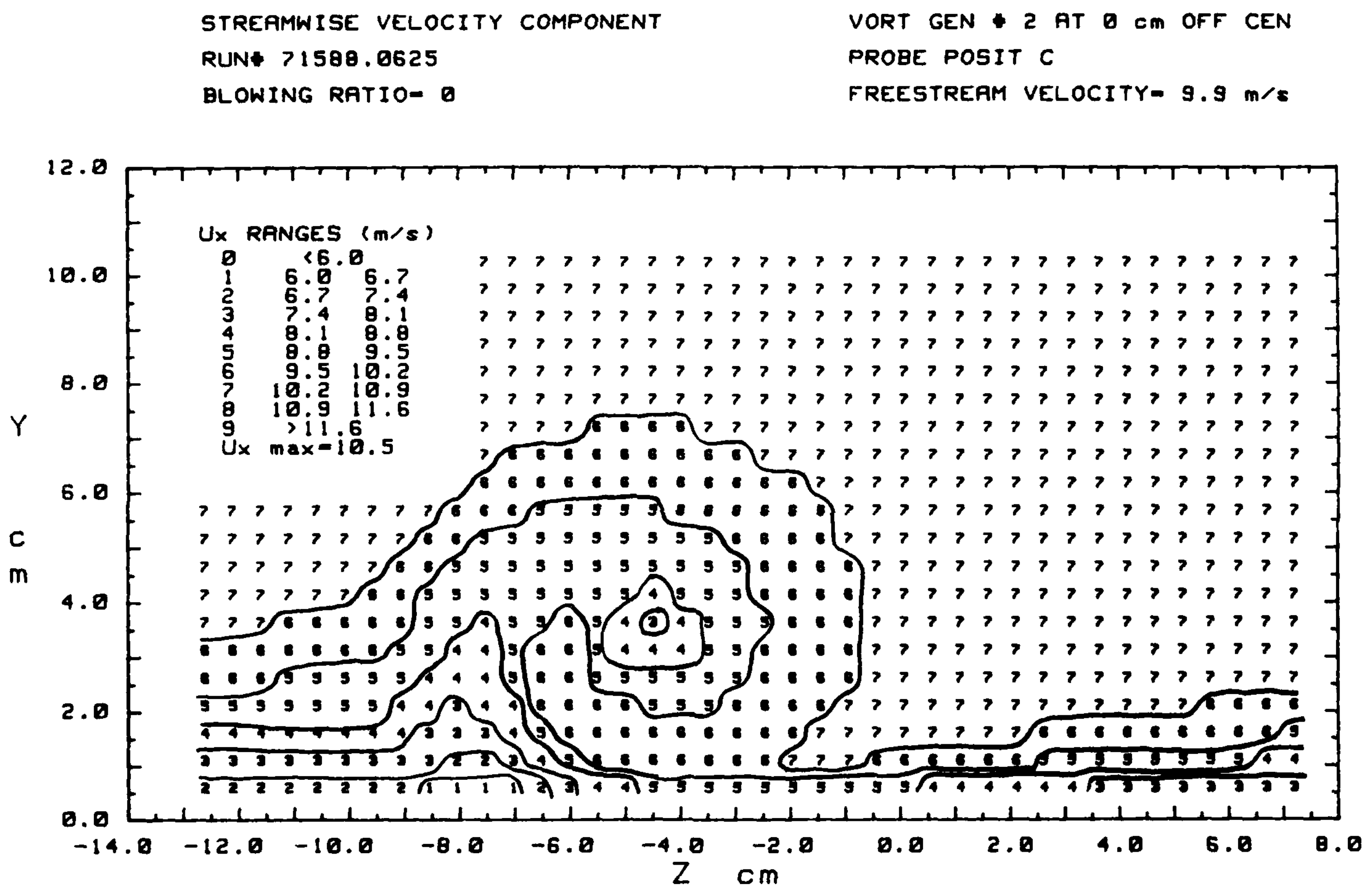

Figure 147. Streamwise Velocity Contours

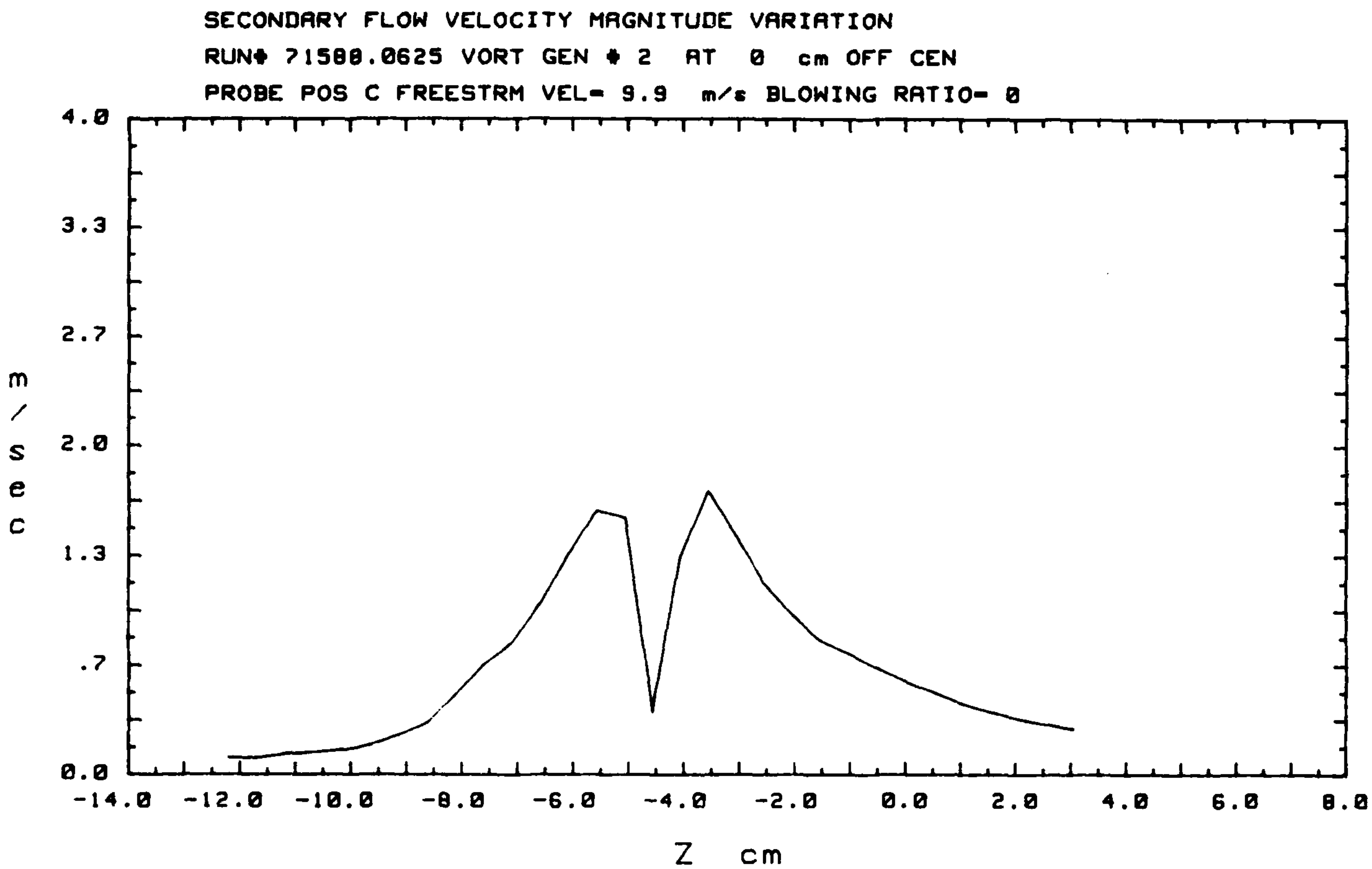

Figure 148. Secondary Flow Velocity (Radially)

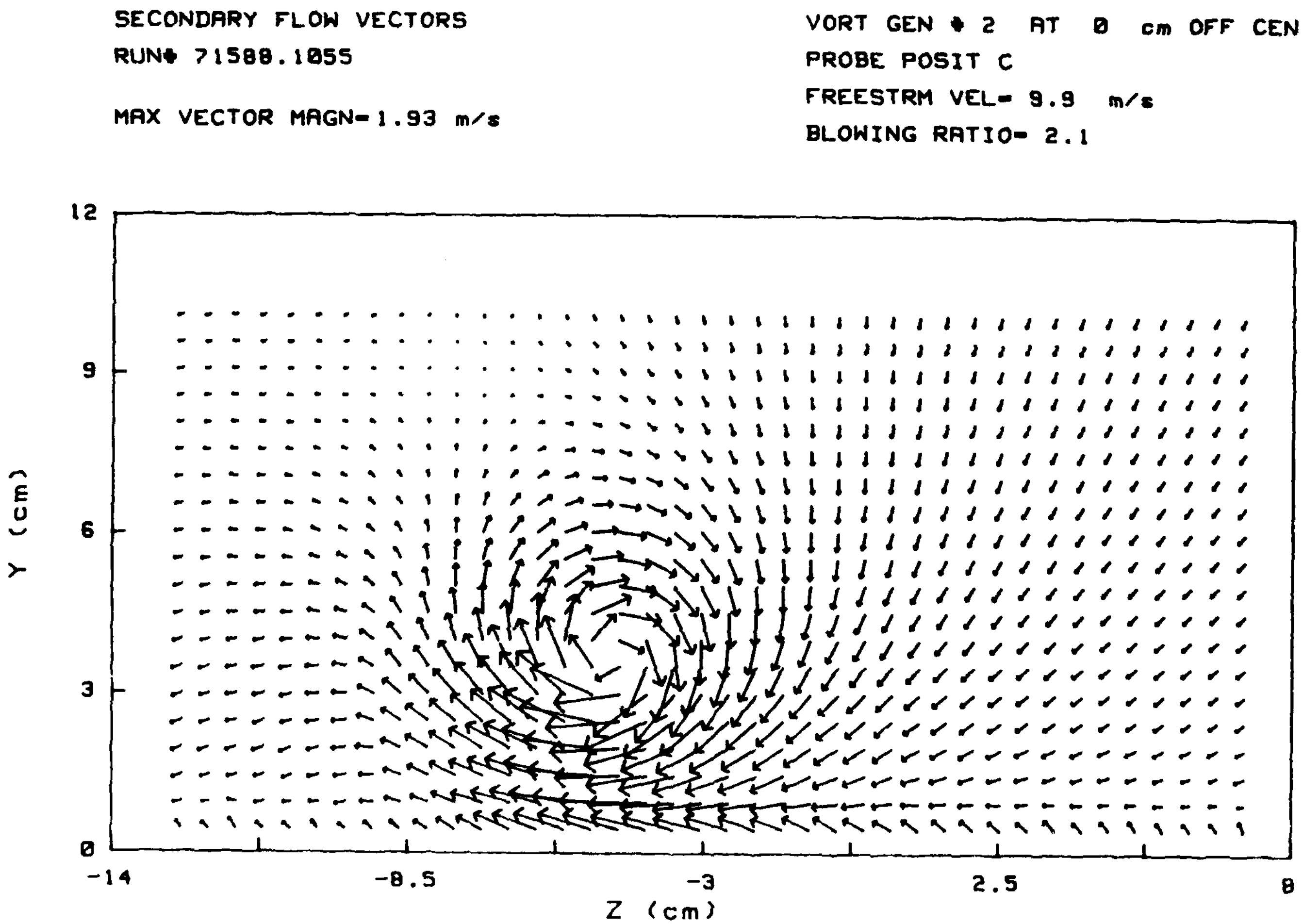

Figure 149. Secondary Flow Vectors

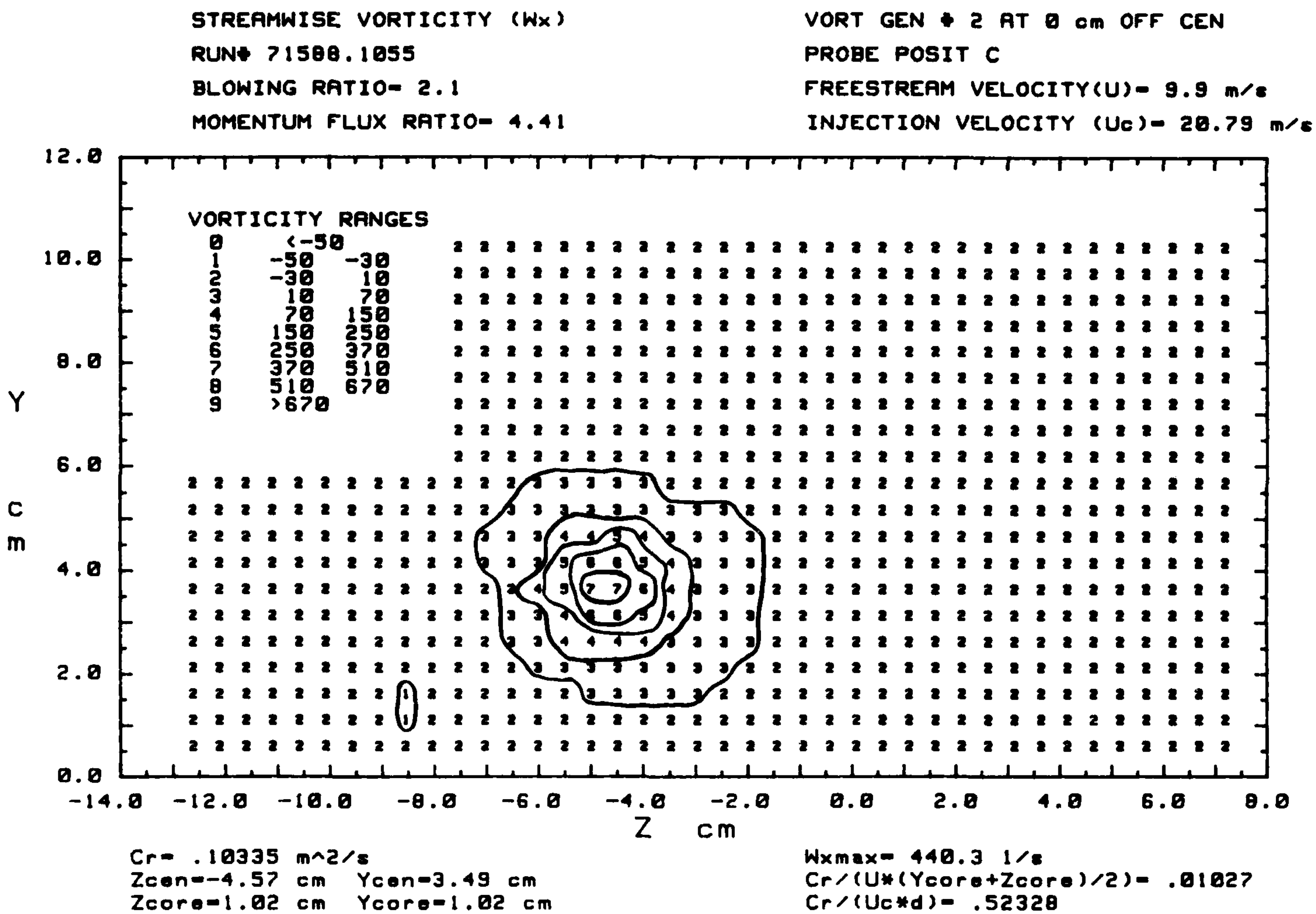

Figure 150. Streamwise Vorticity Contours

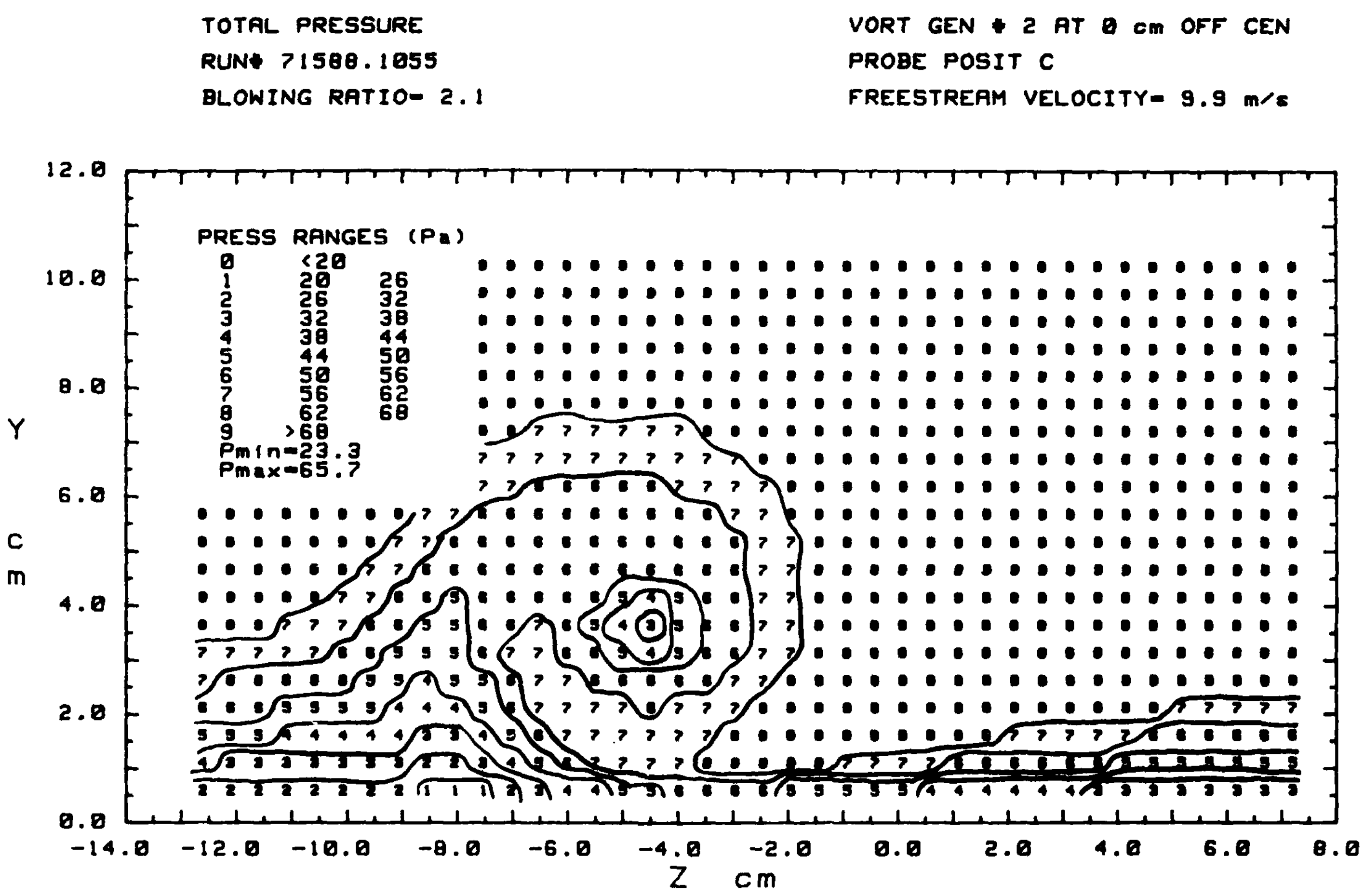

Figure 151. Total Pressure Contours

STREAMWISE VELOCITY COMPONENT
RUN# 71588.1055
BLOWING RATIO= 2.1

VORT GEN # 2 AT 0 cm OFF CEN
PROBE POSIT C
FREESTREAM VELOCITY= 9.9 m/s

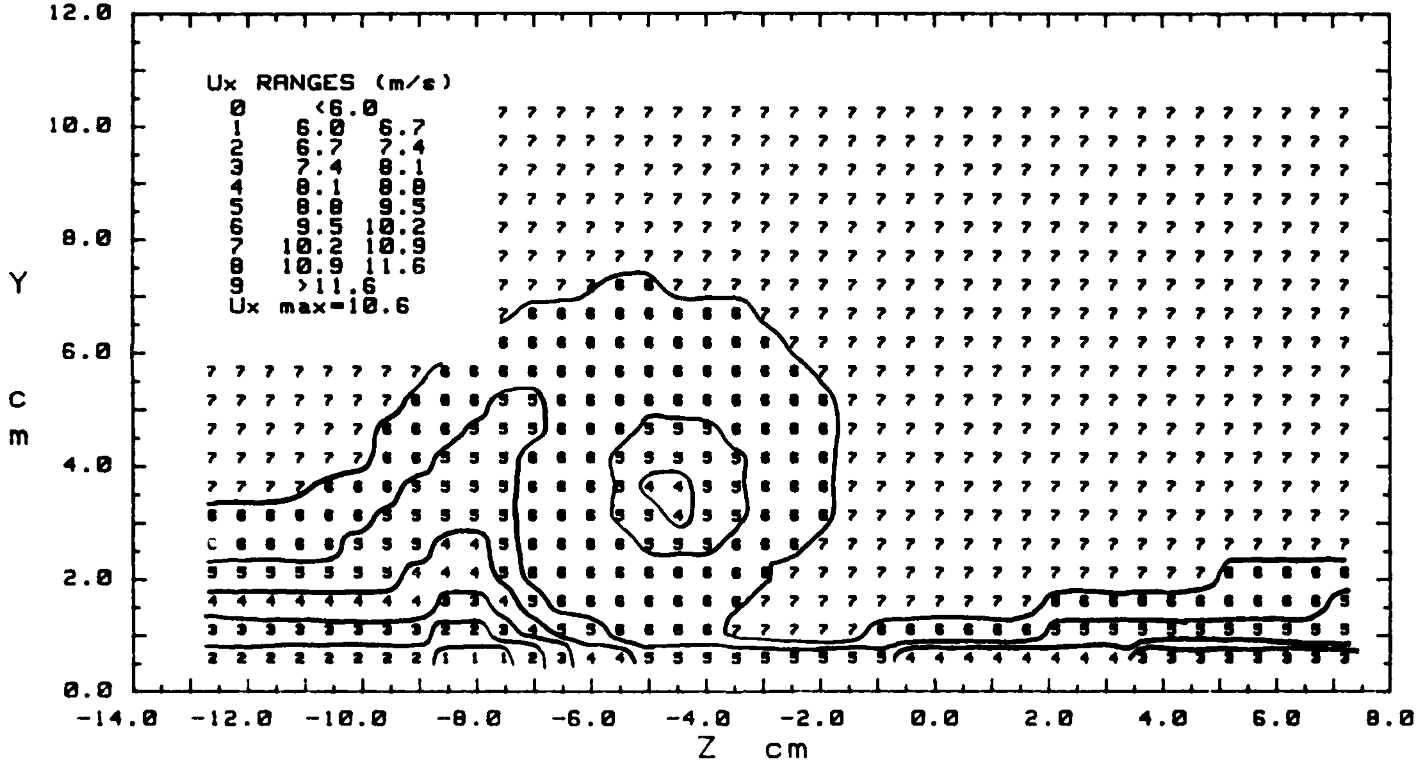

Figure 152. Streamwise Velocity Contours

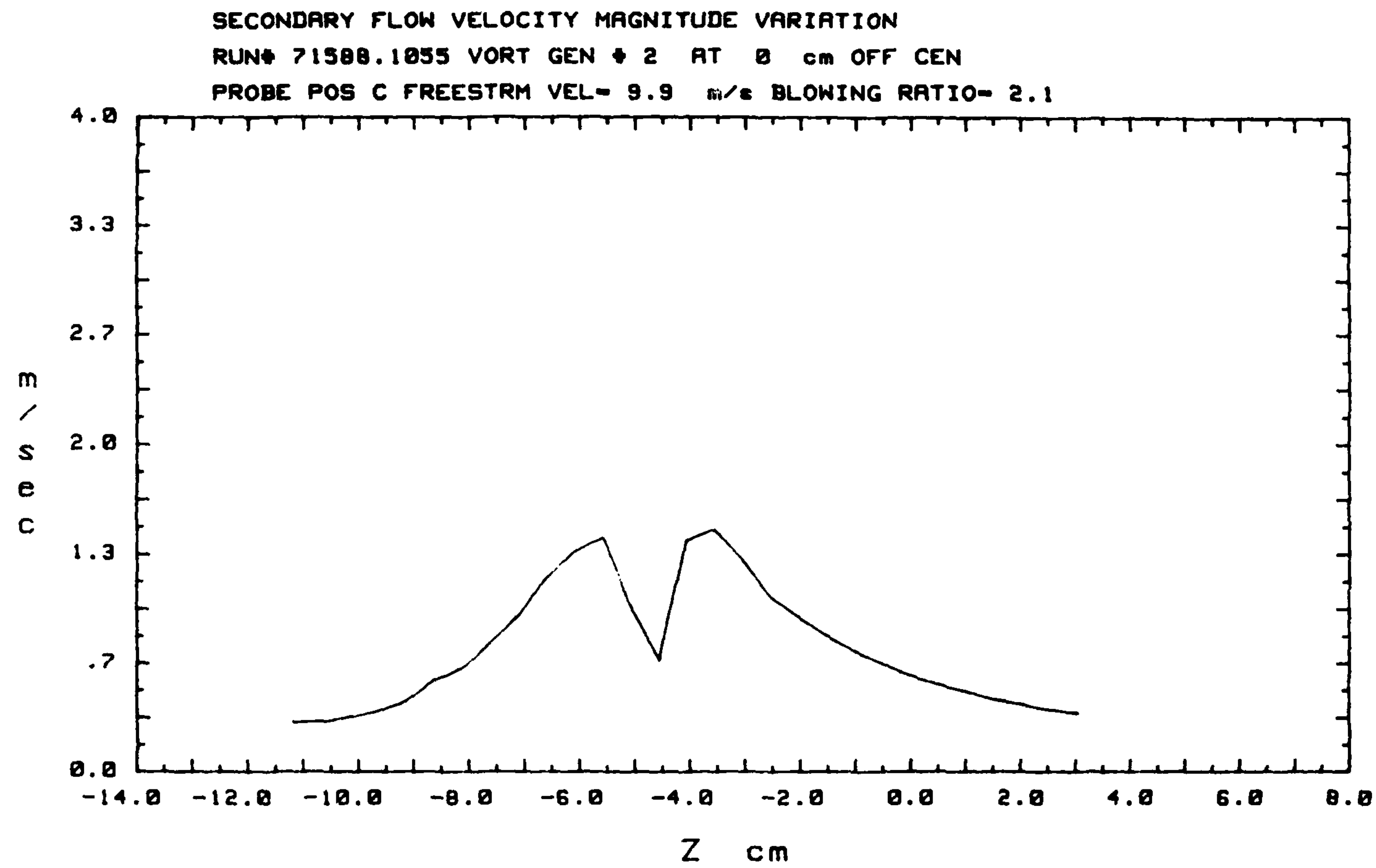

Figure 153. Secondary Flow Velocity (Radially)

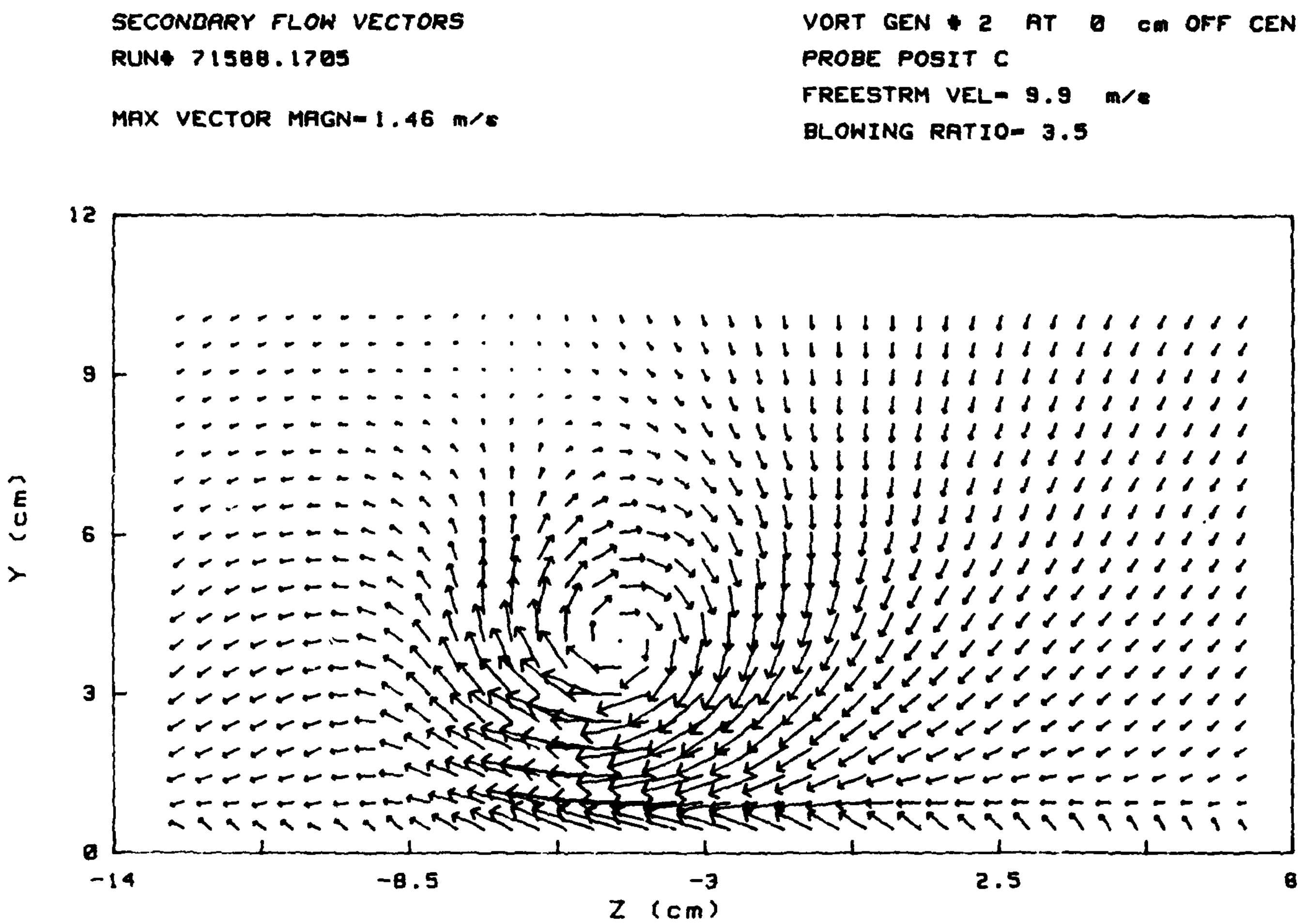

Figure 154. Secondary Flow Vectors

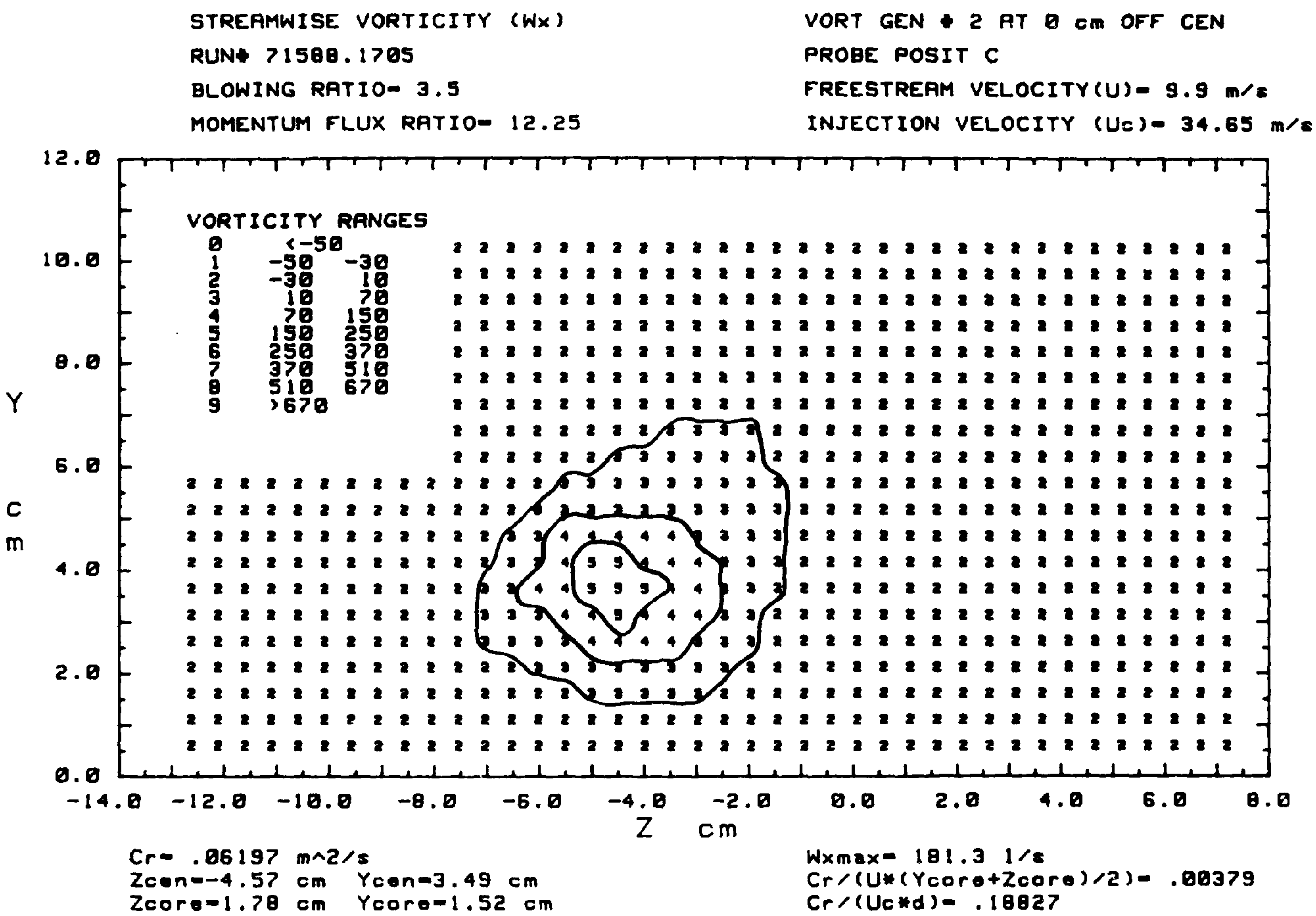

Figure 155. Streamwise Vorticity Contours

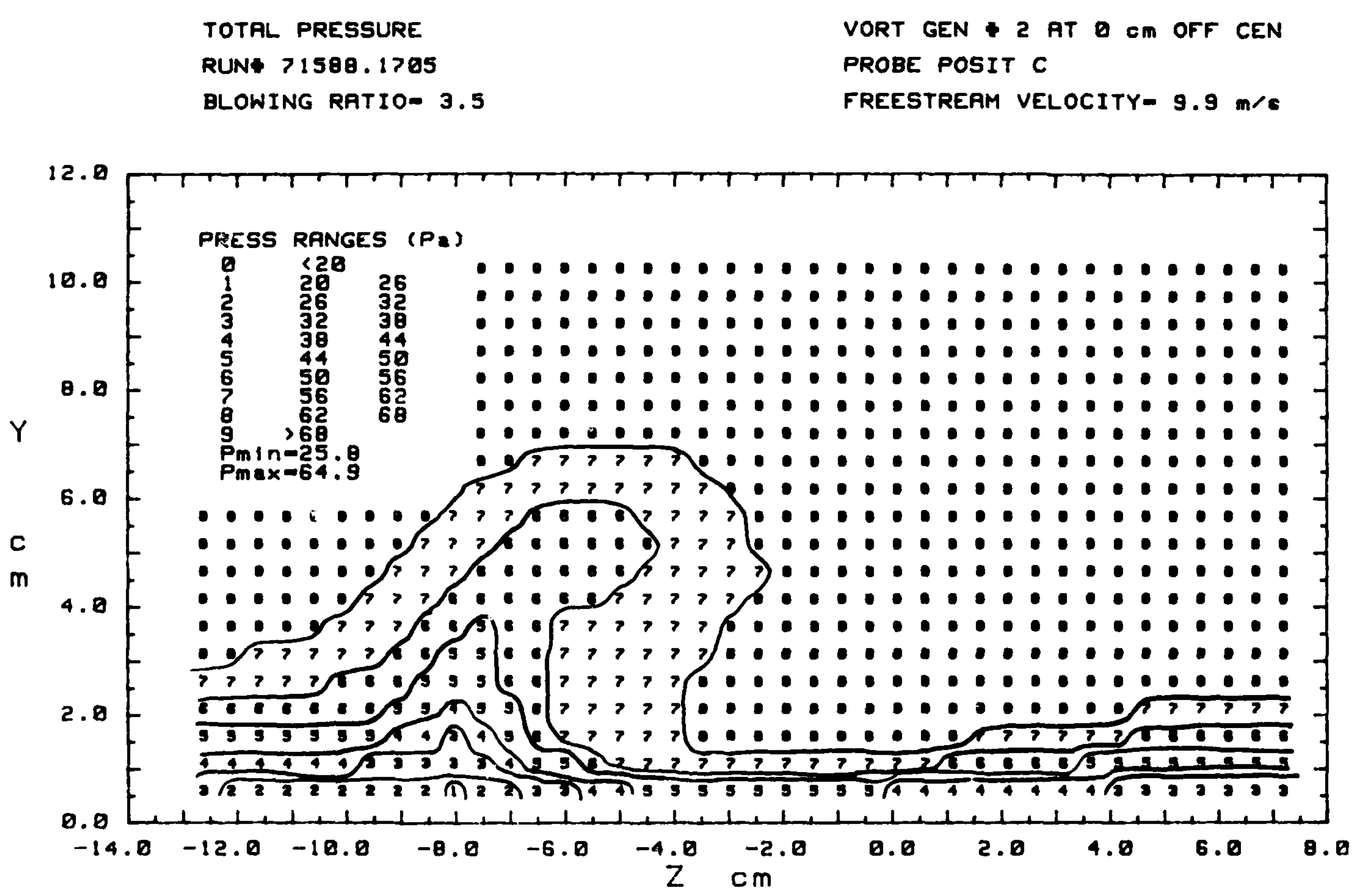

Figure 156. Total Pressure Contours

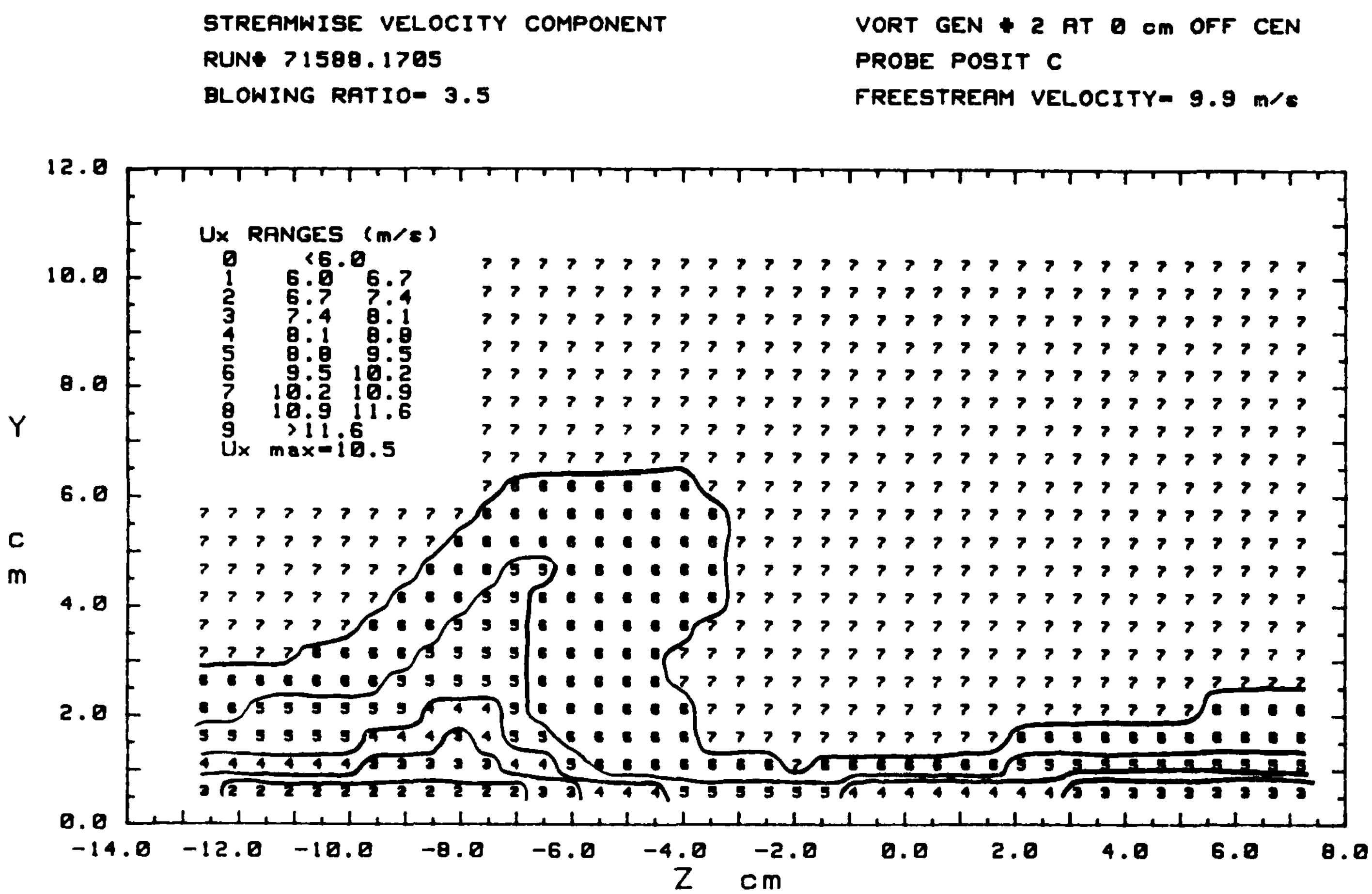

Figure 157. Streamwise Velocity Contours

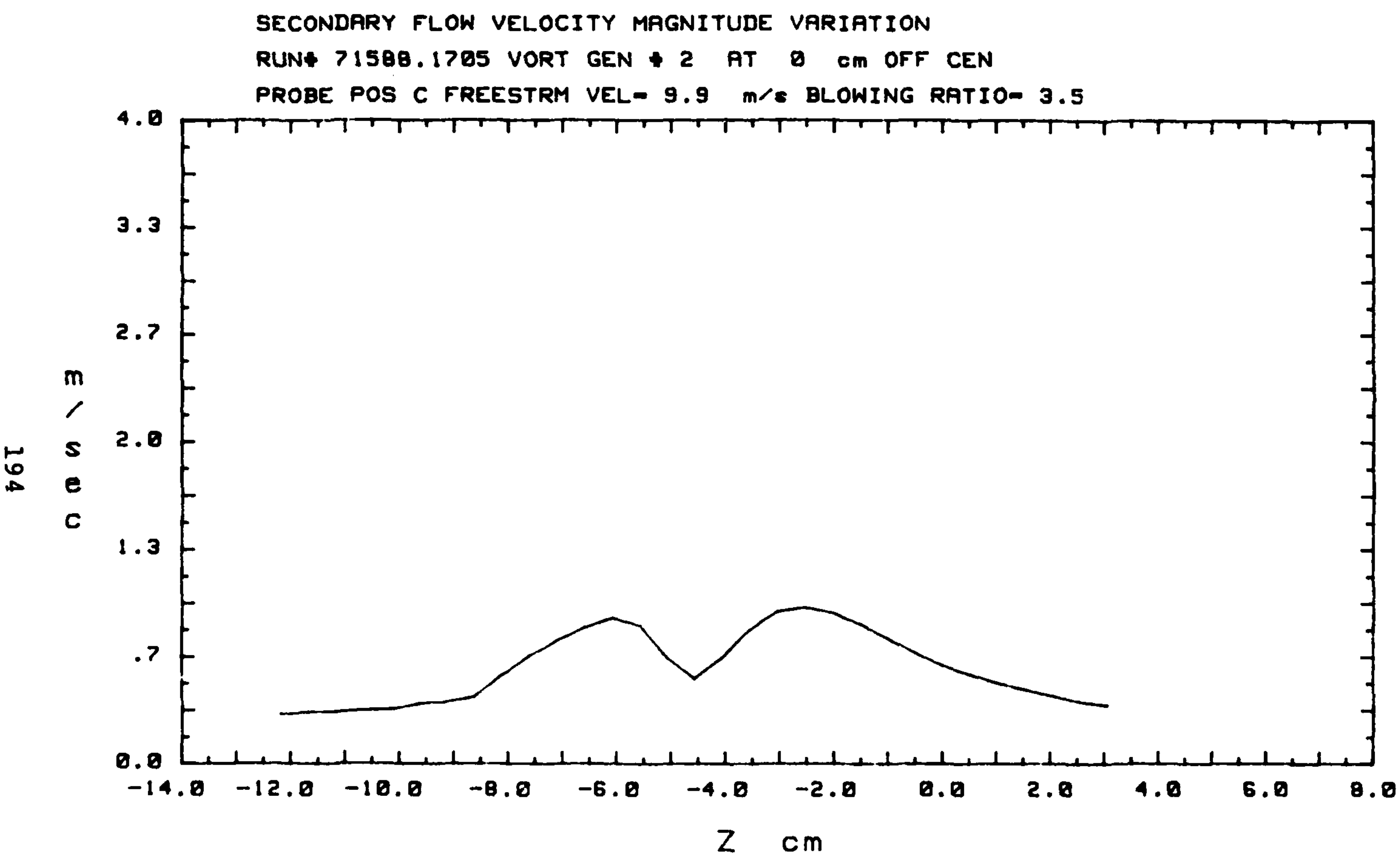

Figure 158. Secondary Flow Velocity (Radially)

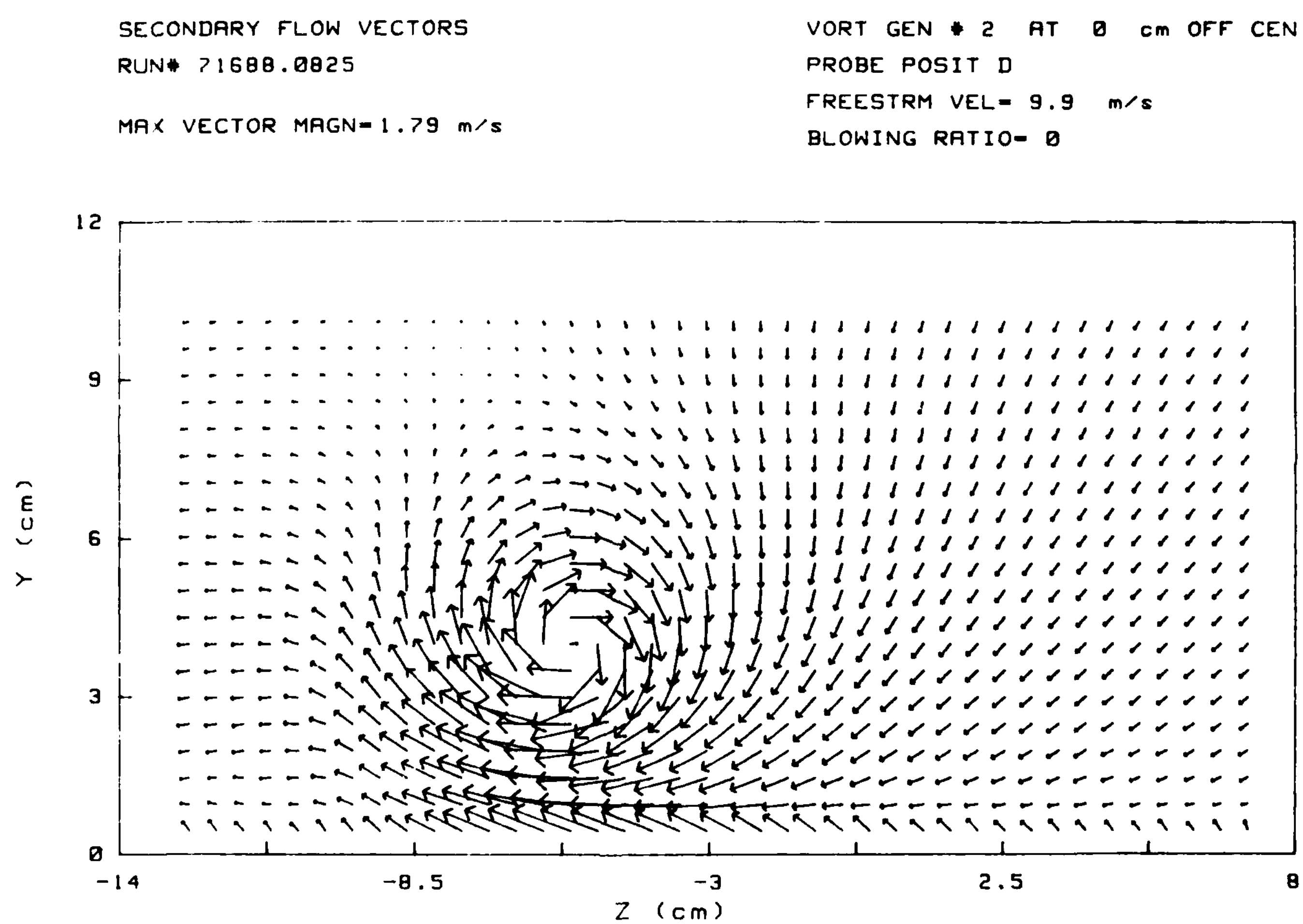

Figure 159. Secondary Flow Vectors

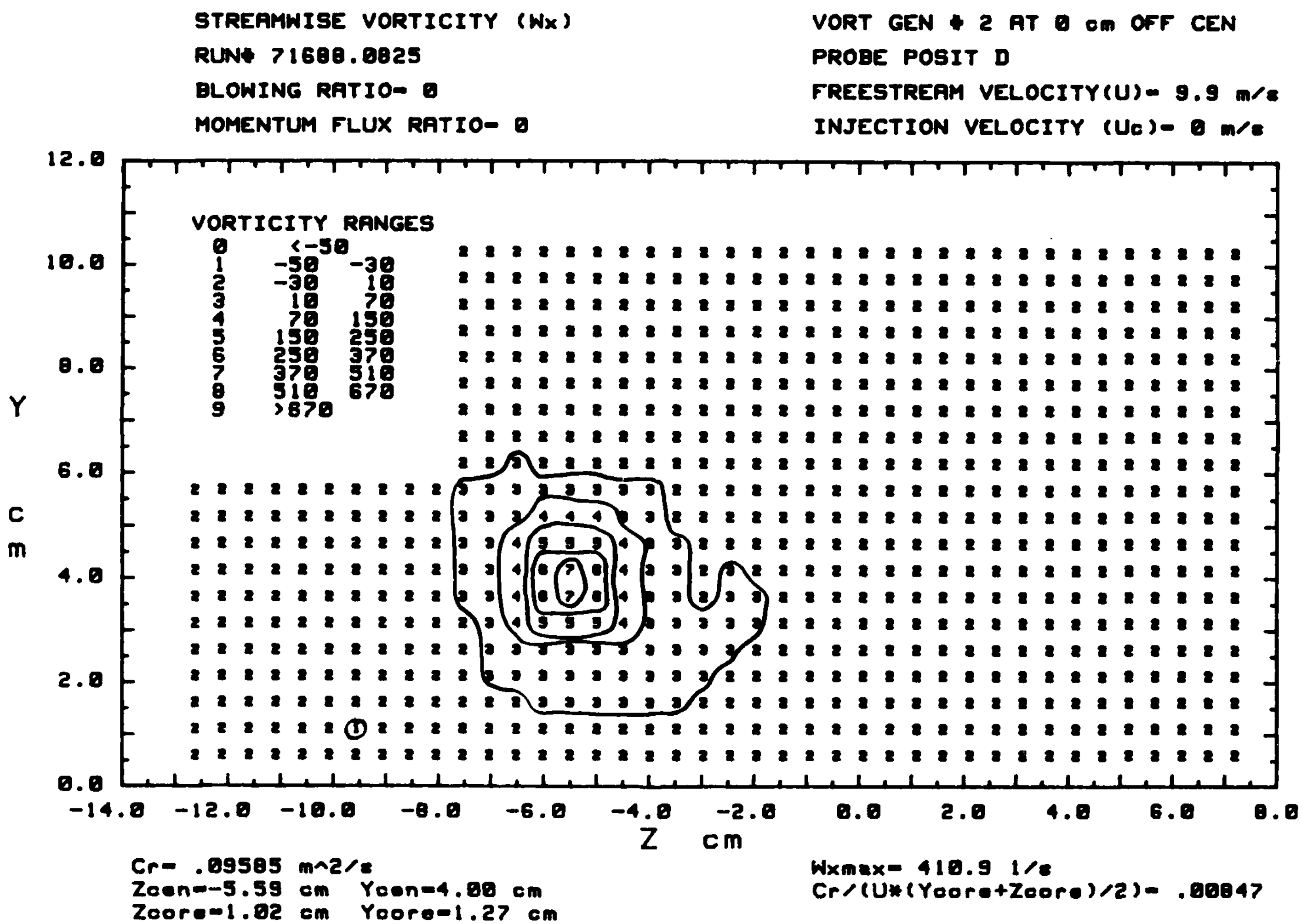

Figure 160. Streamwise Vorticity Contours

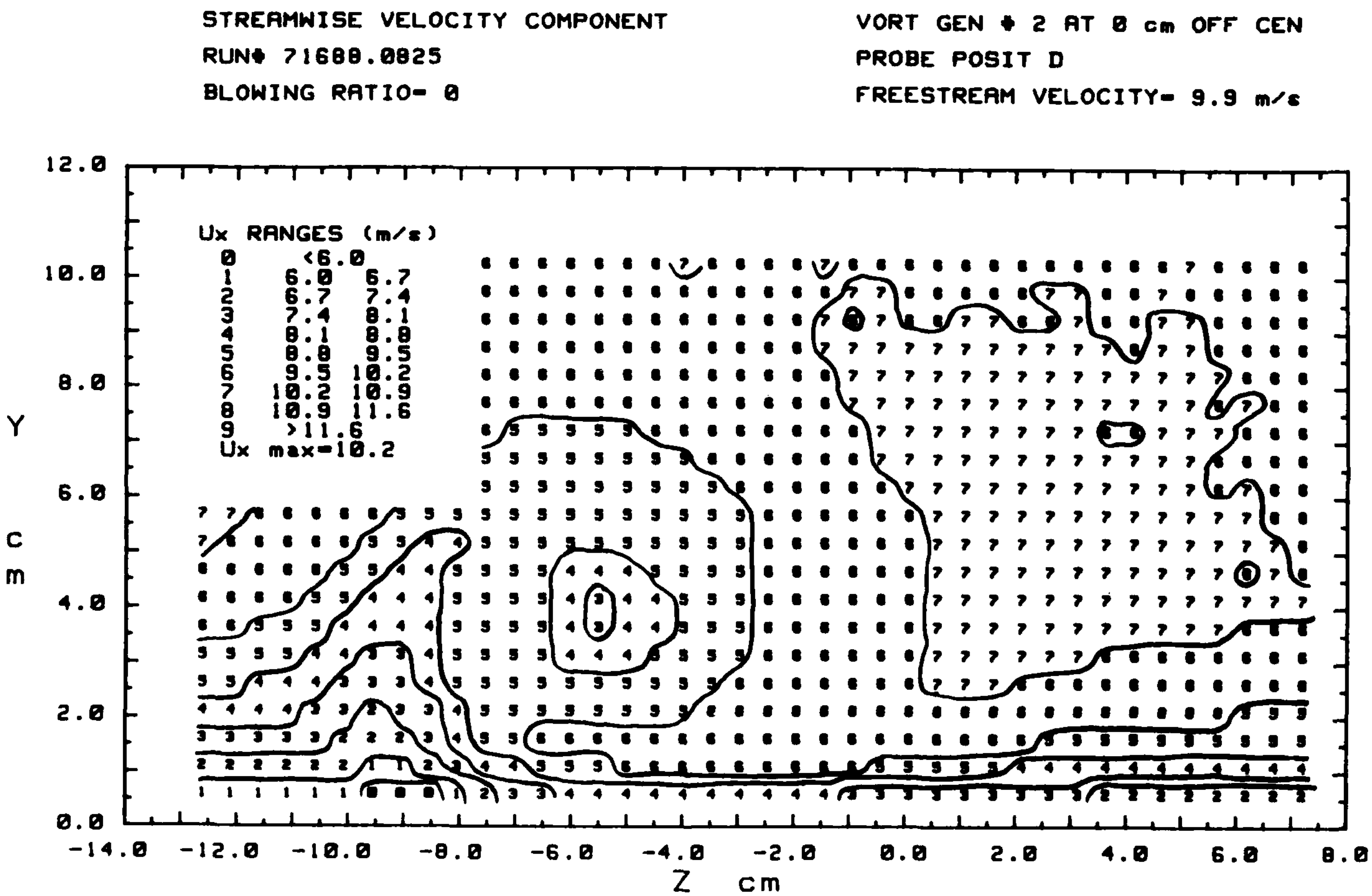

Figure 161. Total Pressure Contours

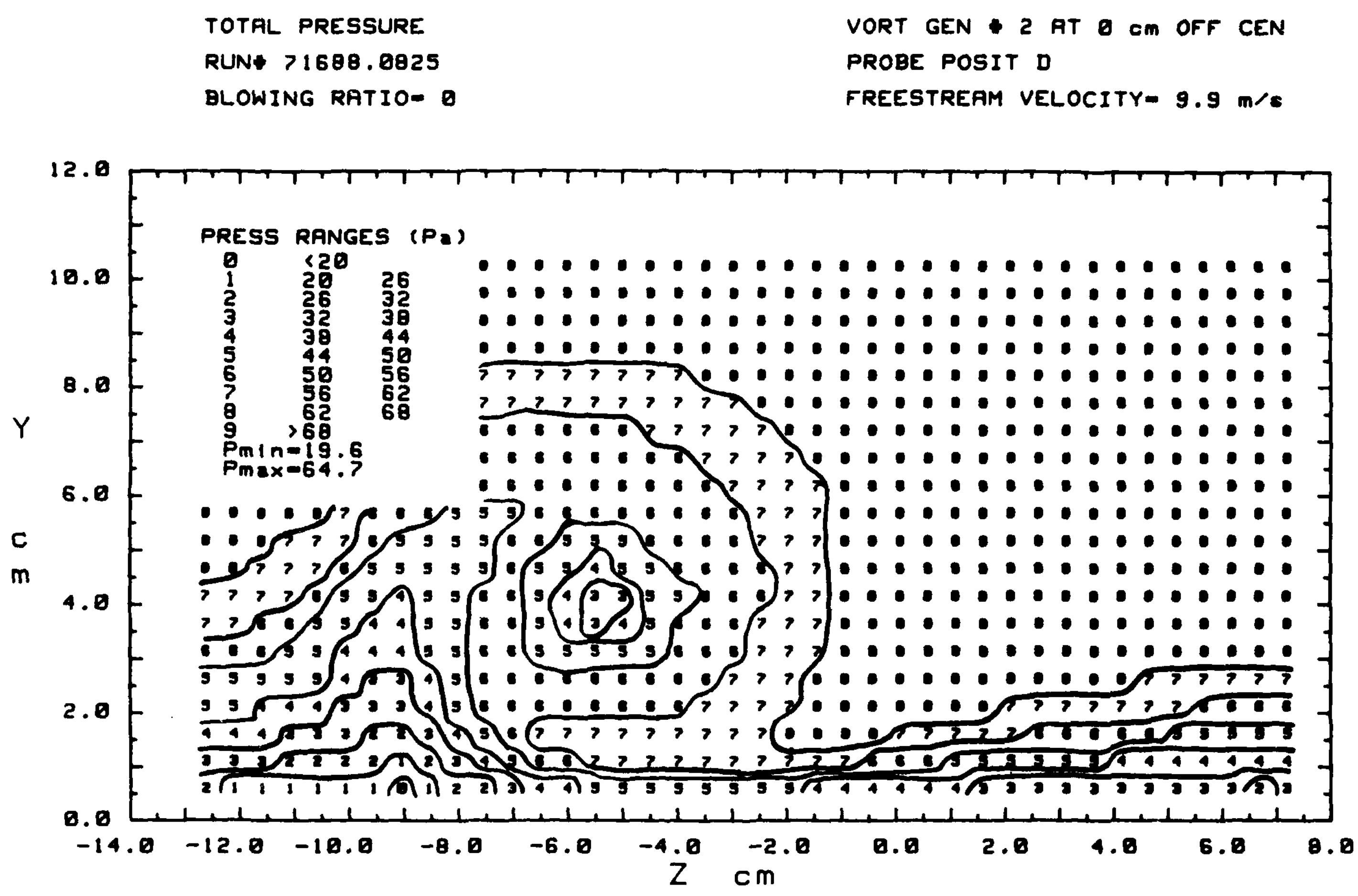

Figure 162. Streamwise Velocity Contours

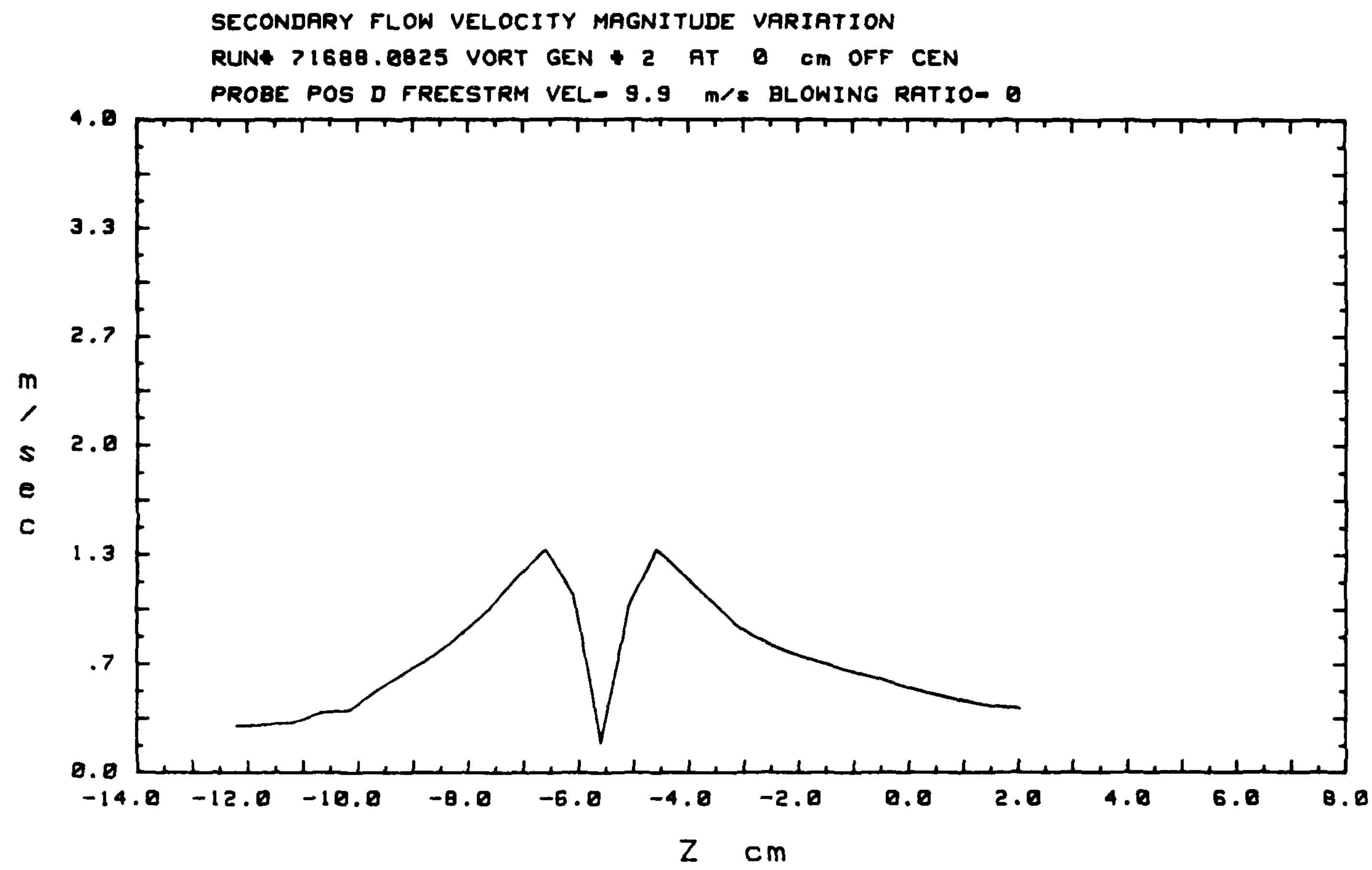

Figure 163. Secondary Flow Velocity (Radially)

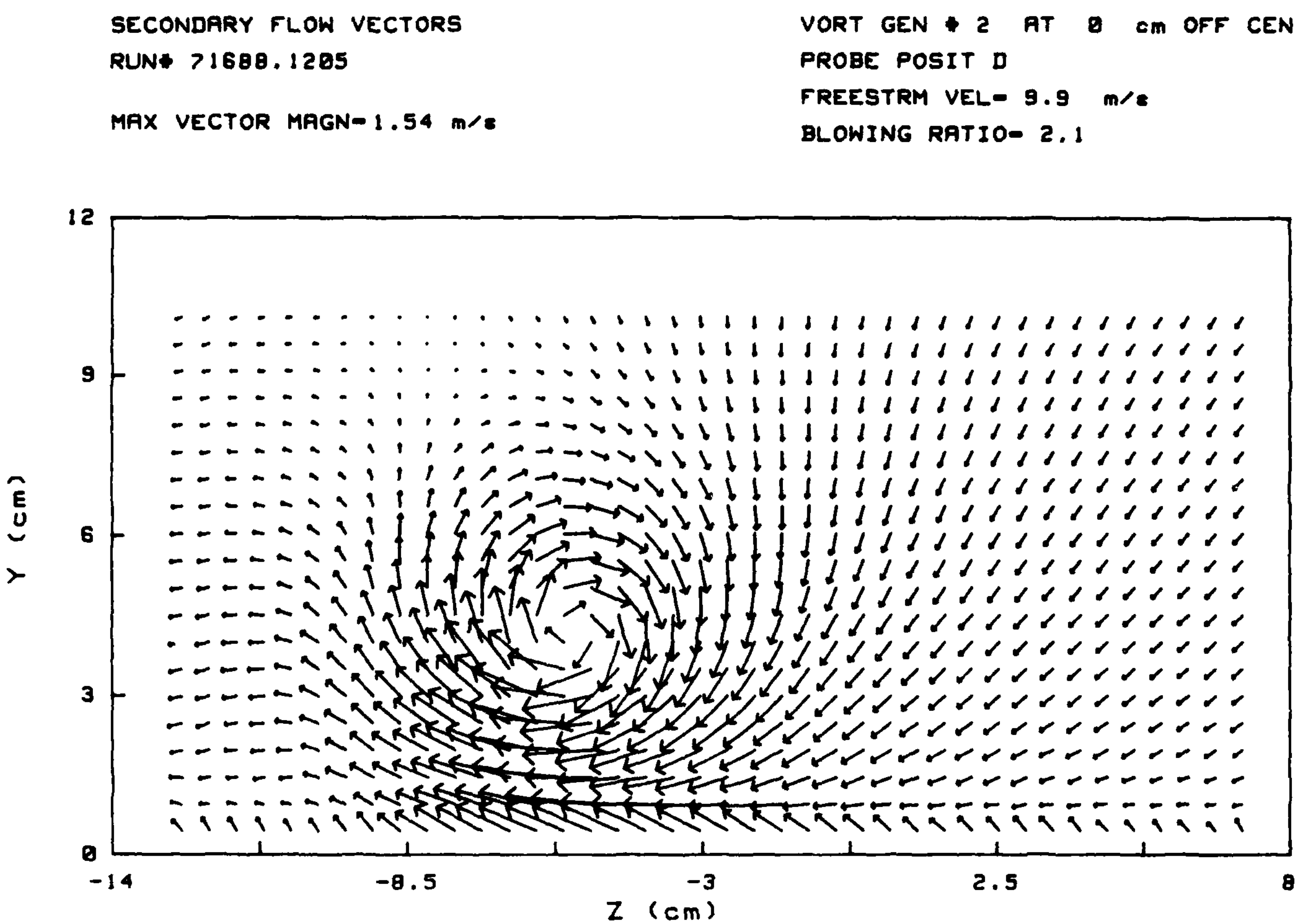

Figure 164. Secondary Flow Vectors

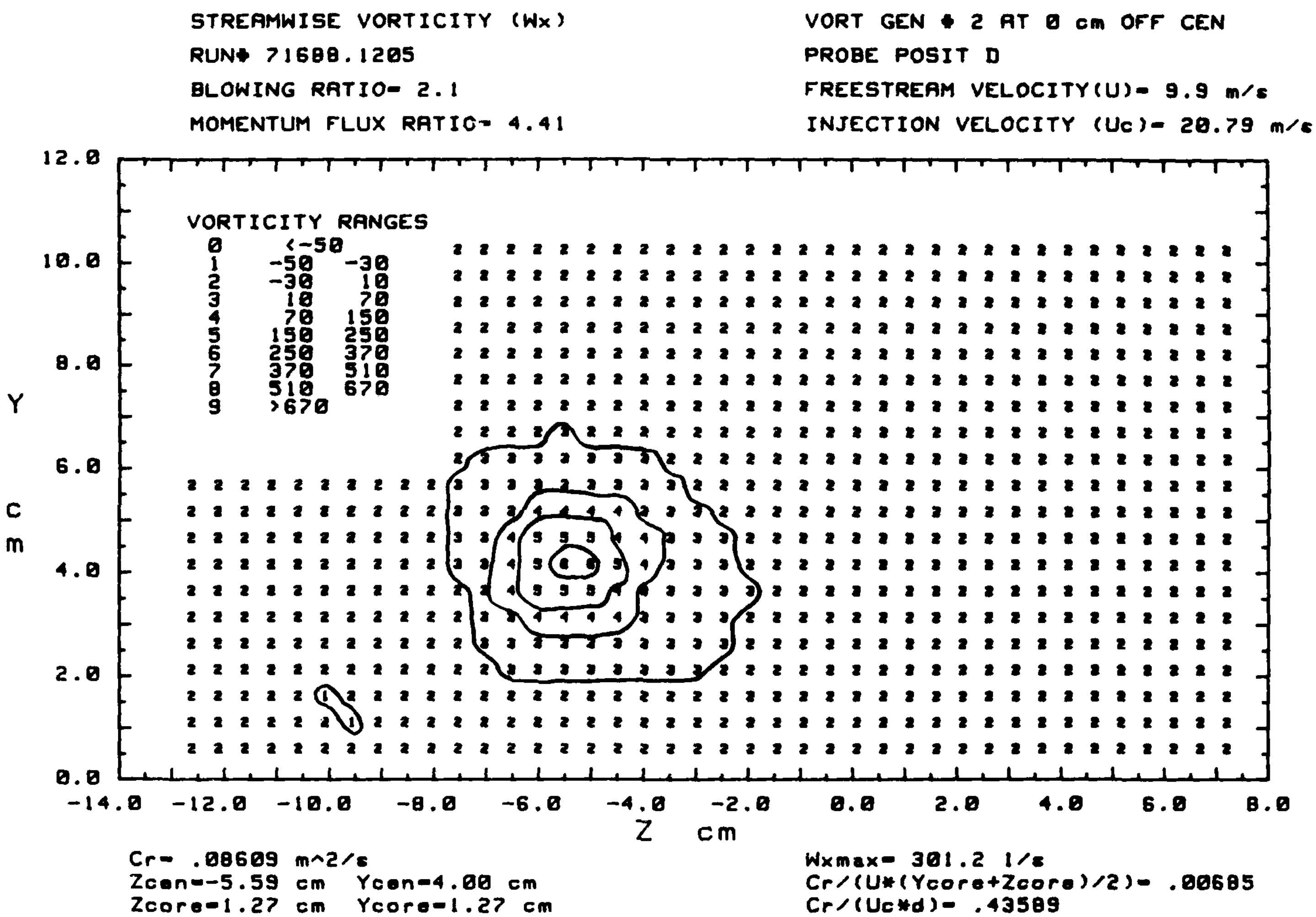

Figure 165. Streamwise Vorticity Contours

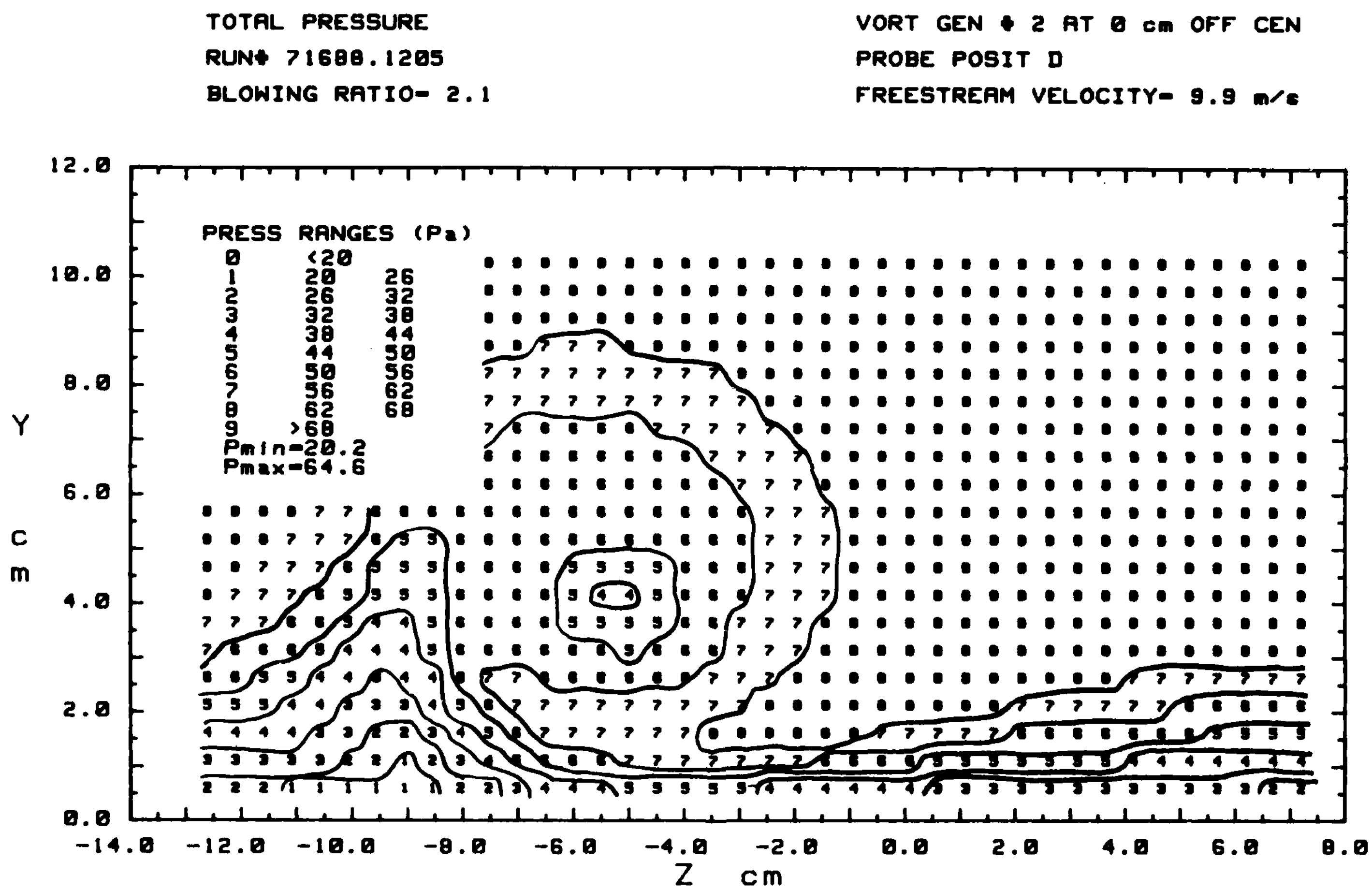

Figure 166. Total Pressure Contours

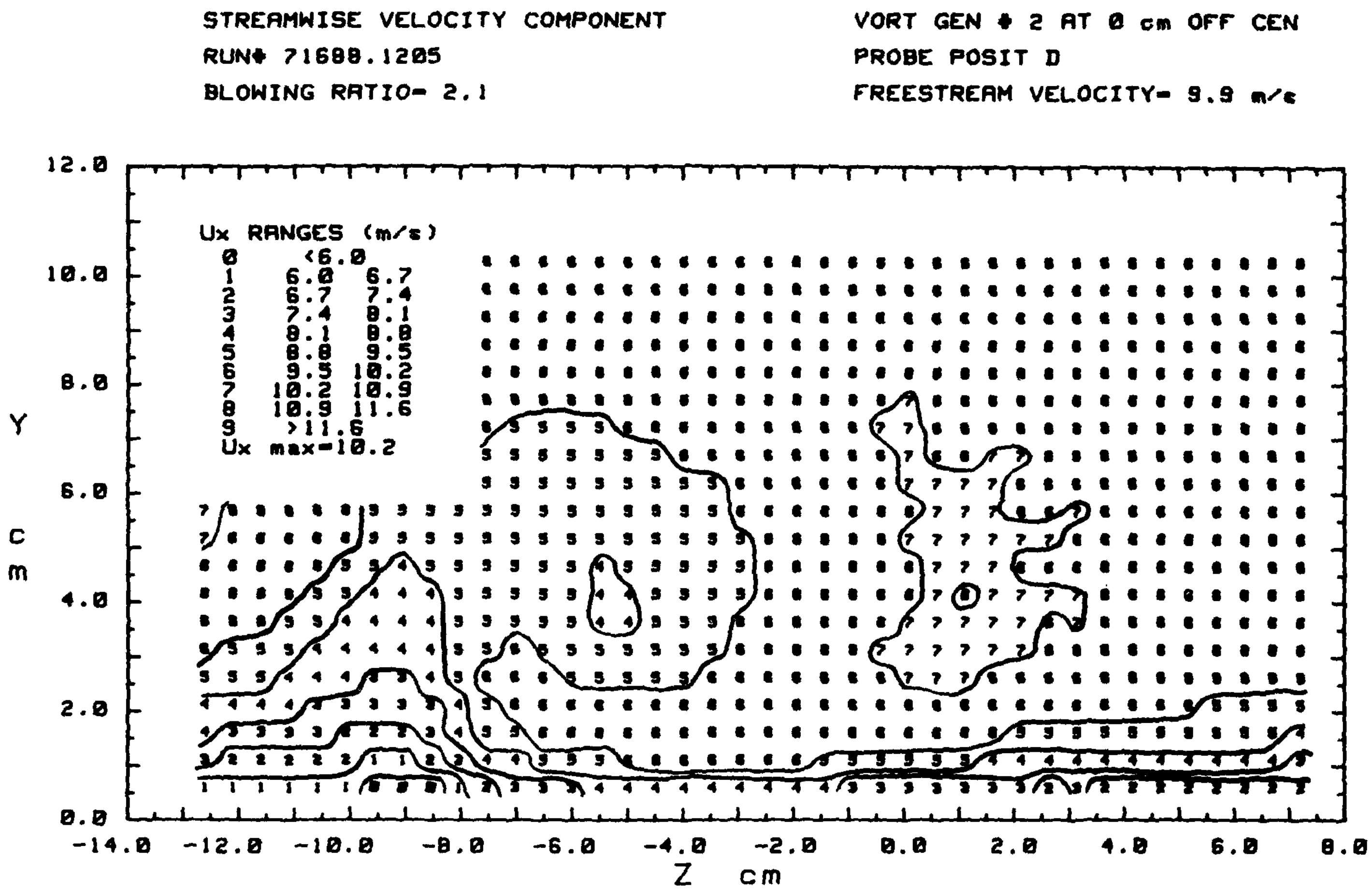

Figure 167. Streamwise Velocity Contours

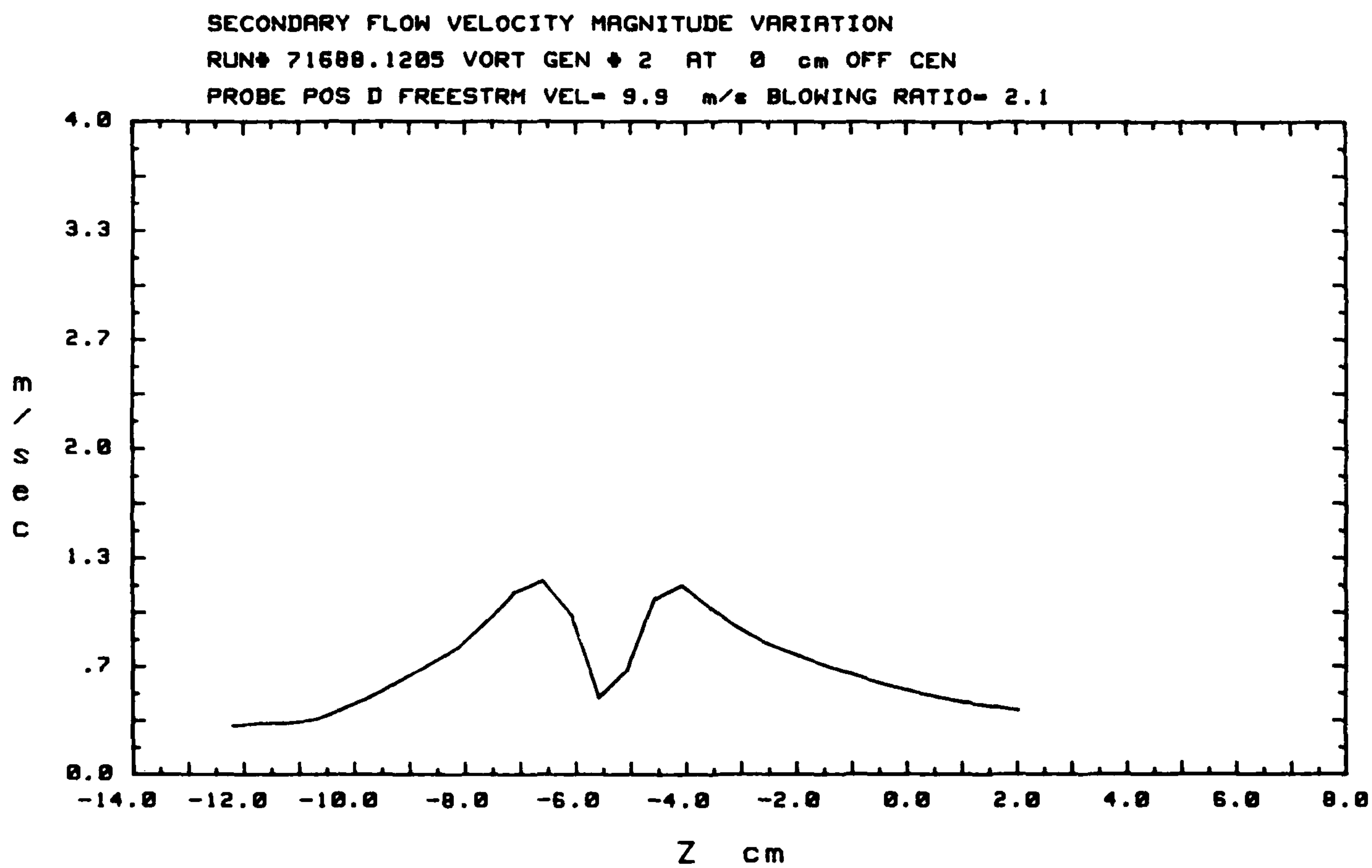

Figure 168. Secondary Flow Velocity (Radially)

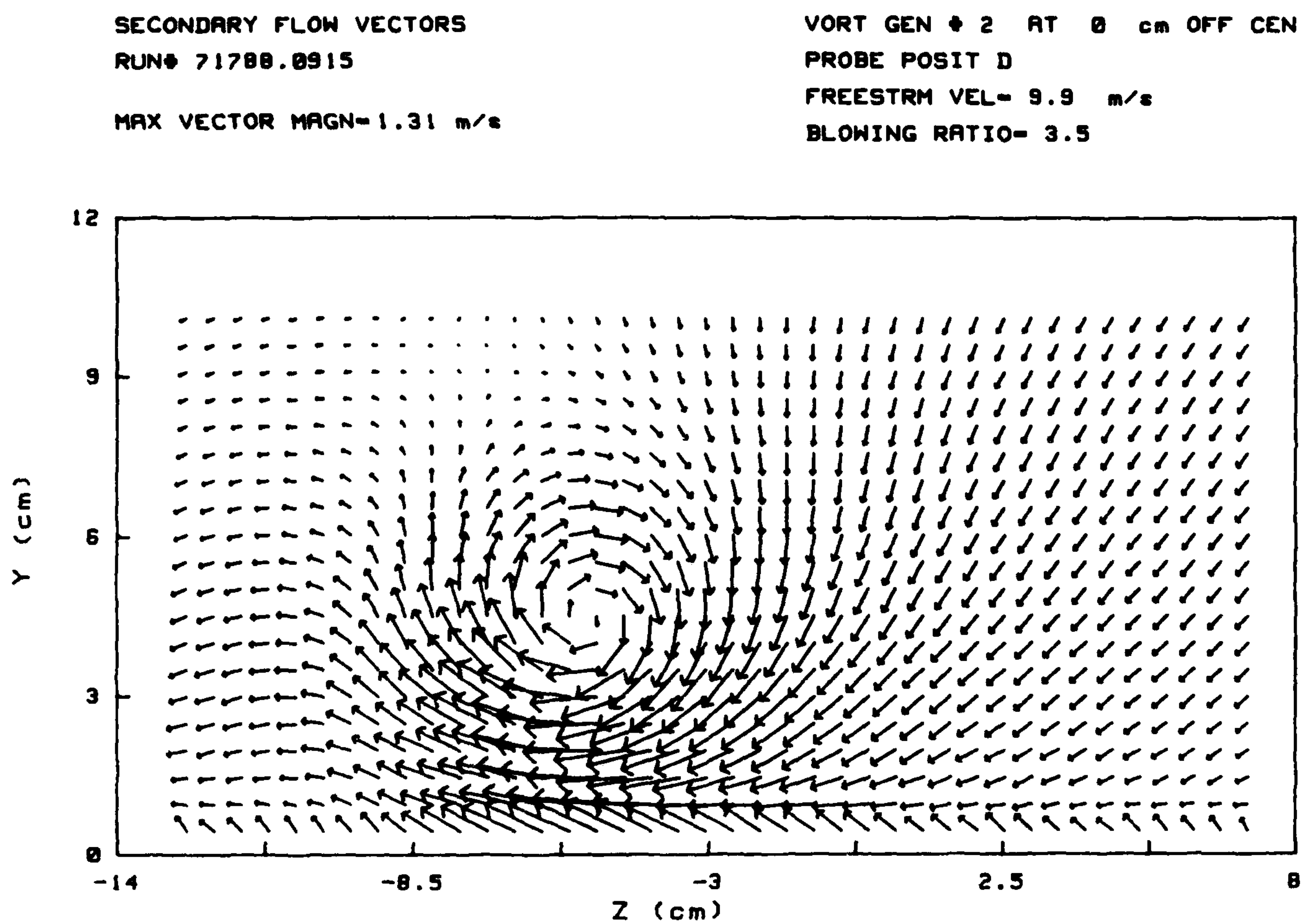

Figure 169. Secondary Flow Vectors

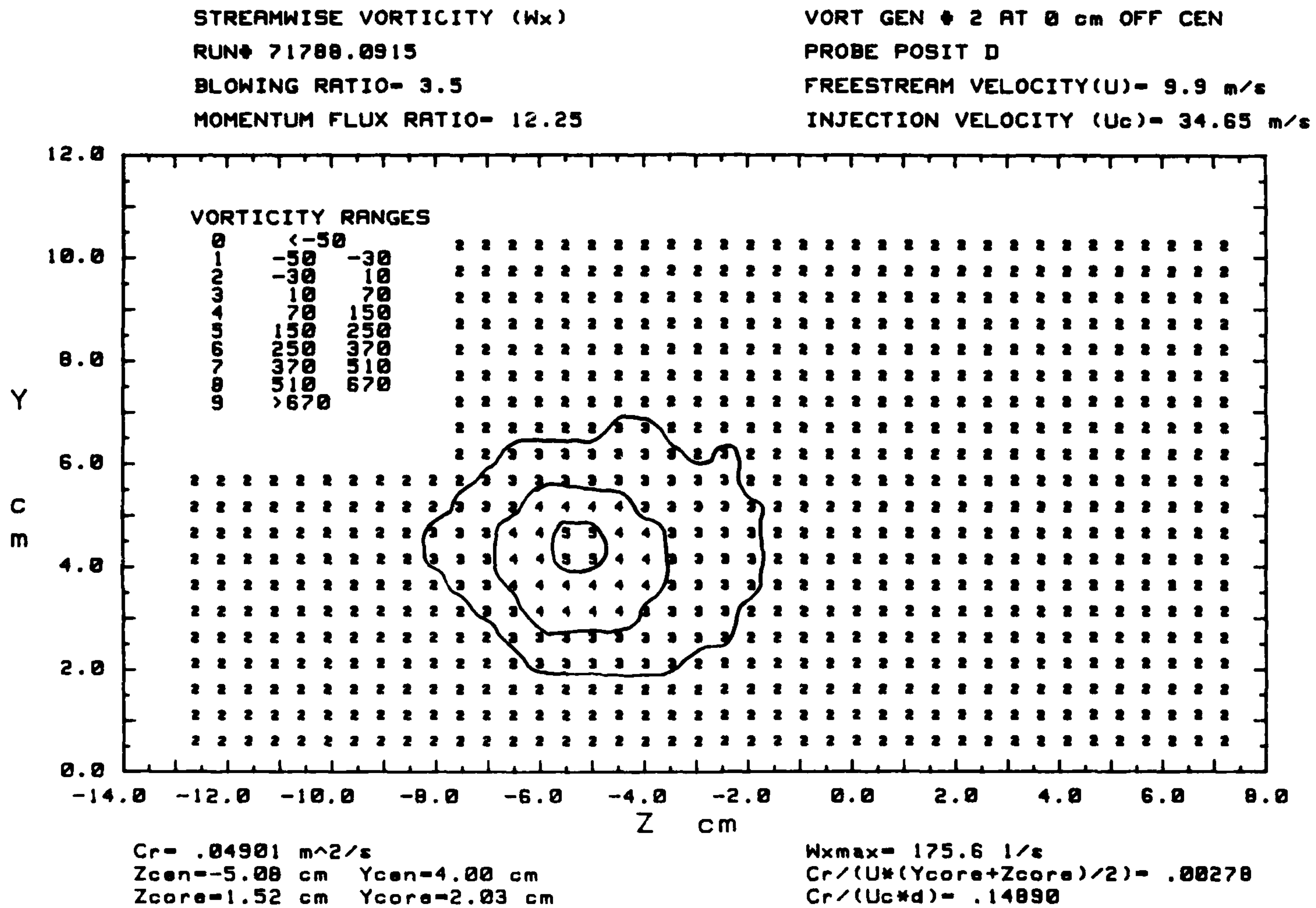

Figure 170. Streamwise Vorticity Contours

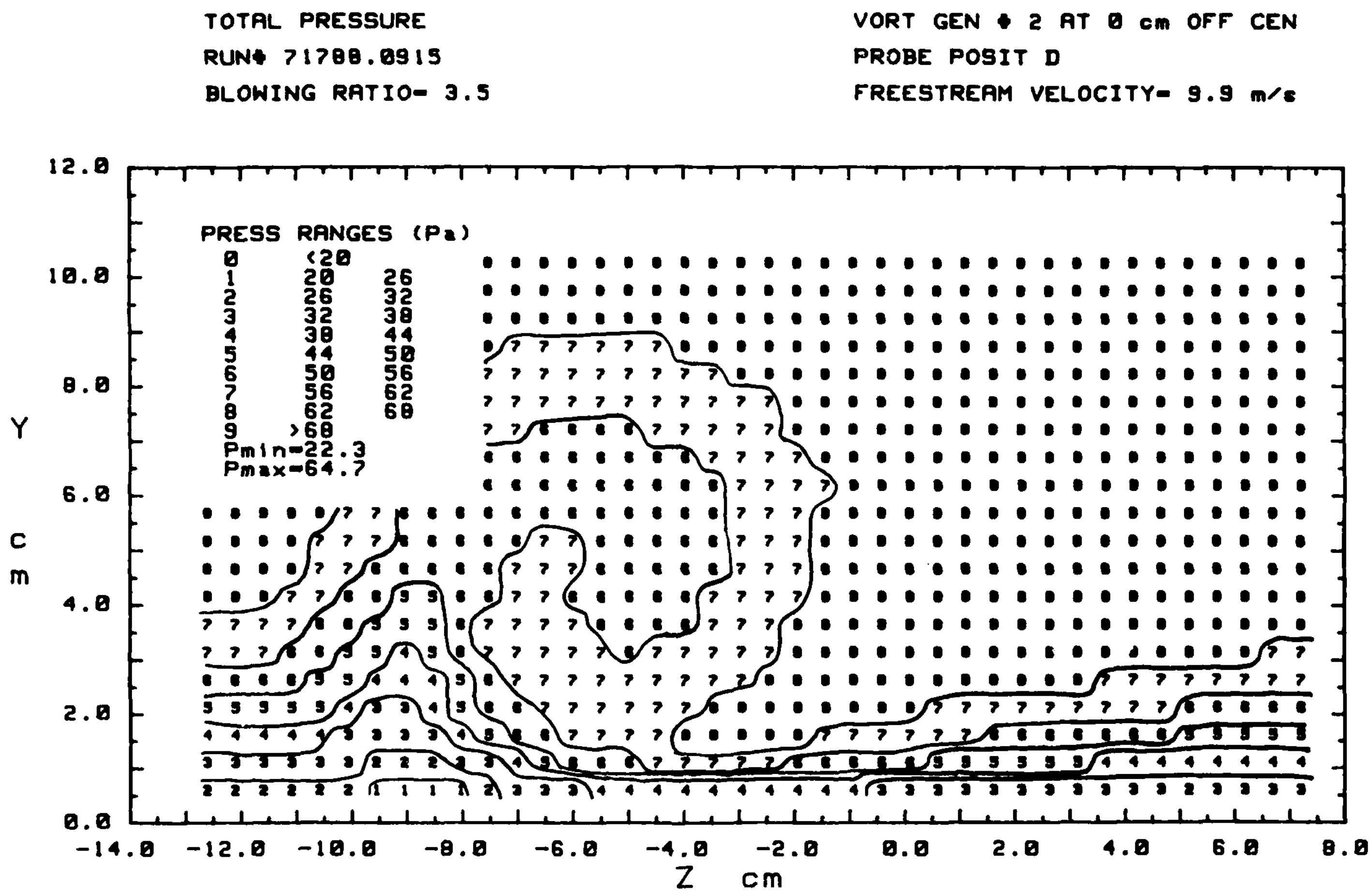

Figure 171. Total Pressure Contours

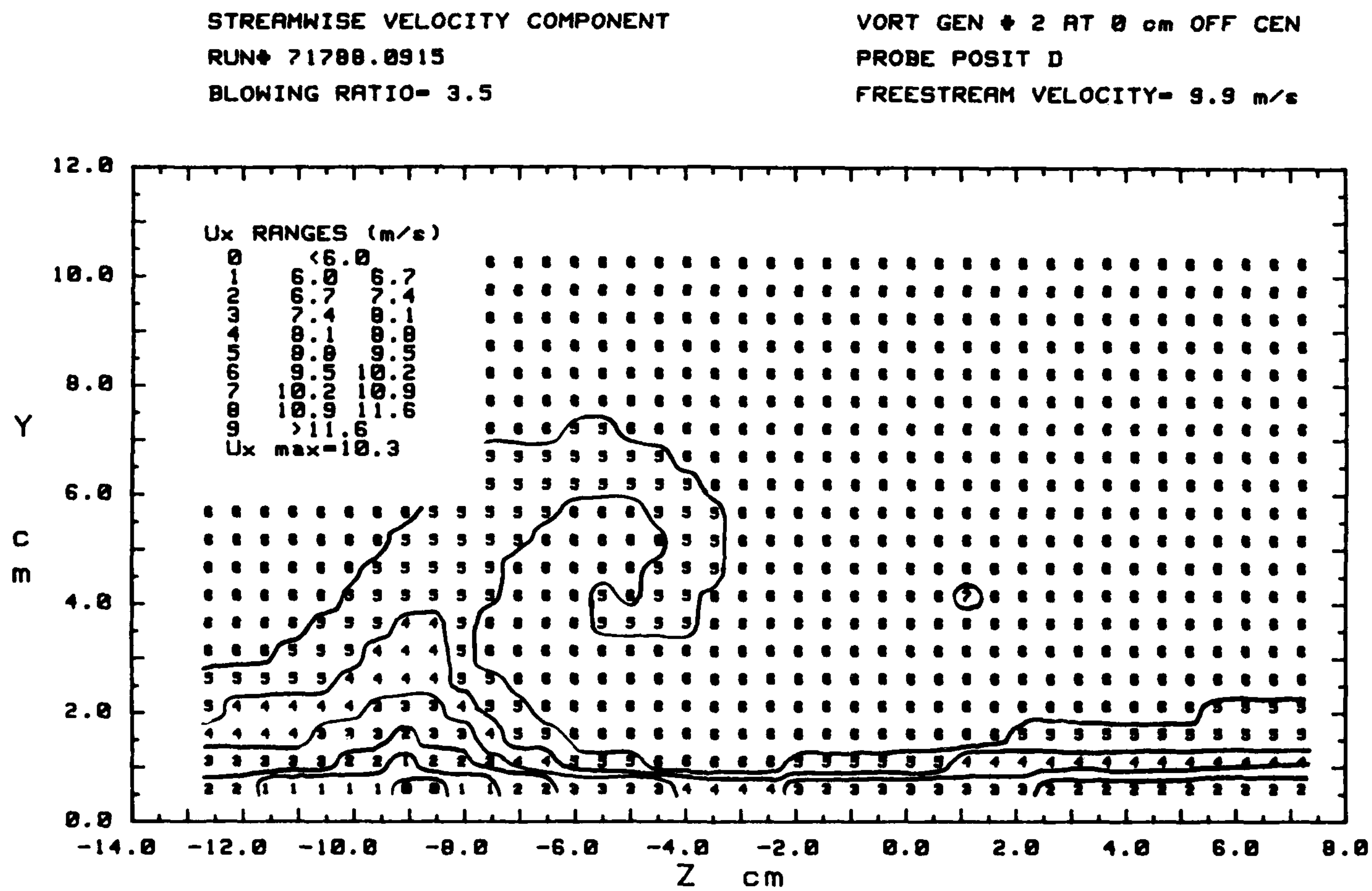

Figure 172. Streamwise Velocity Contours

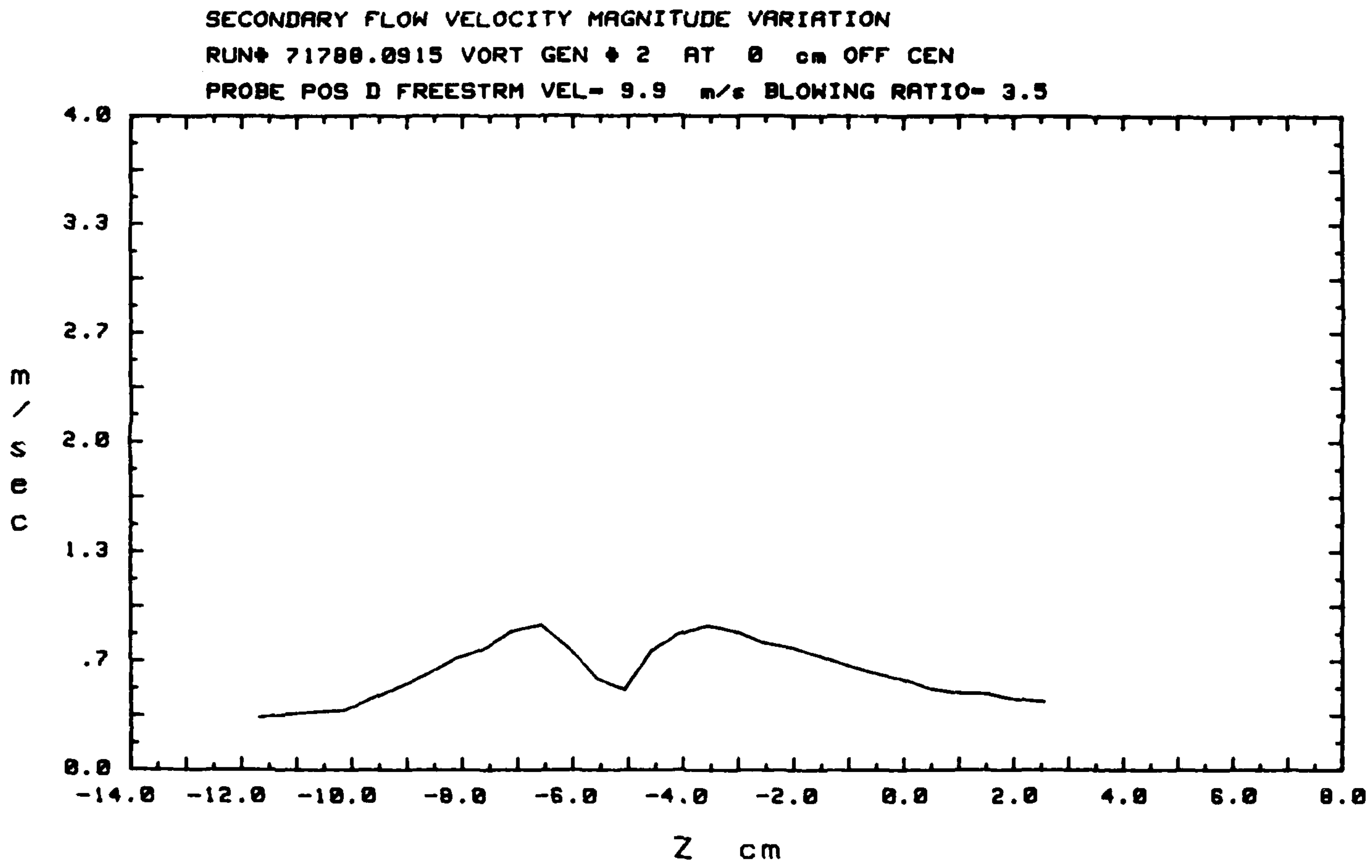

Figure 173. Secondary Flow Velocity (Radially)

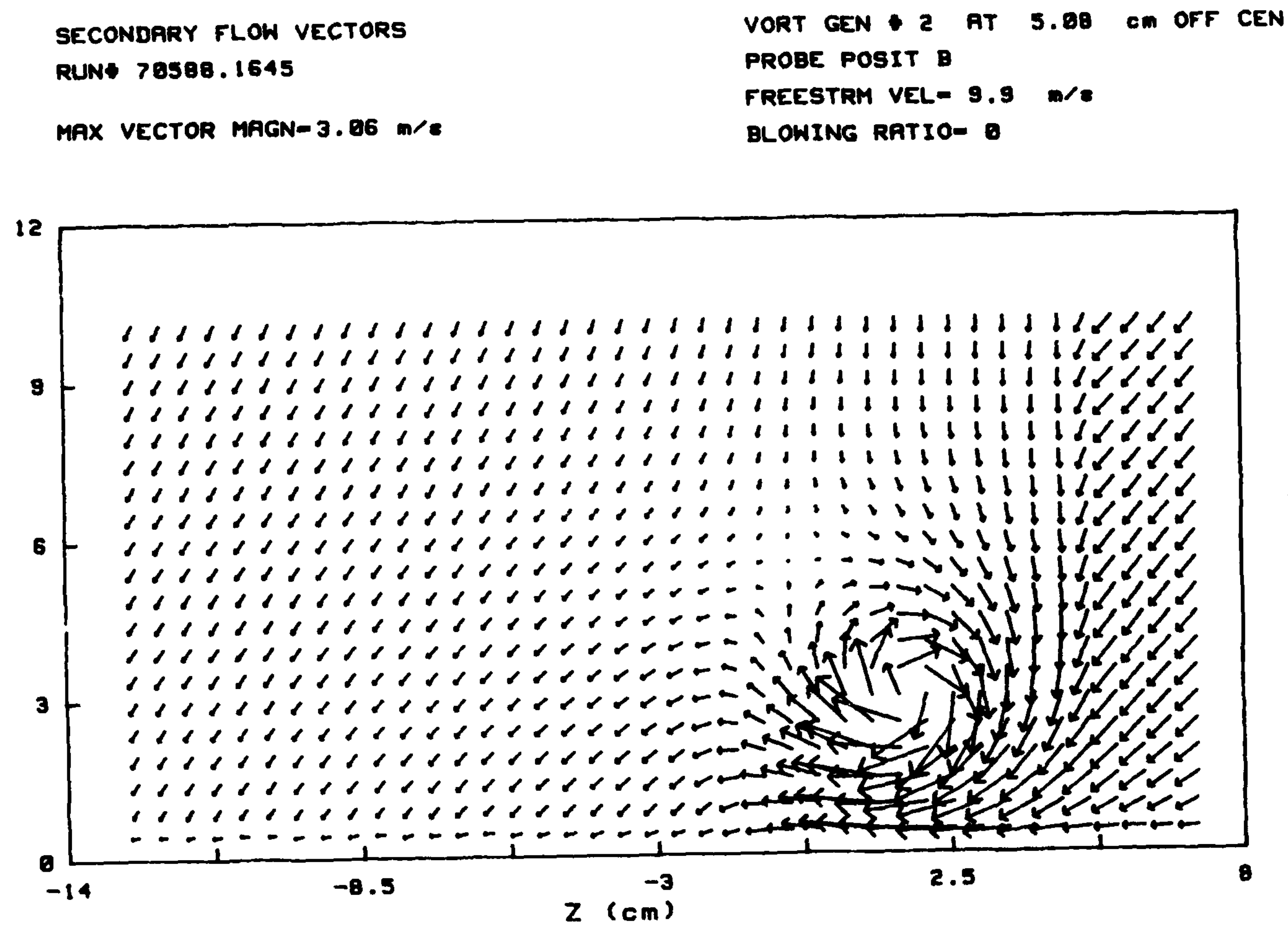

Figure 174. Secondary Flow Vectors

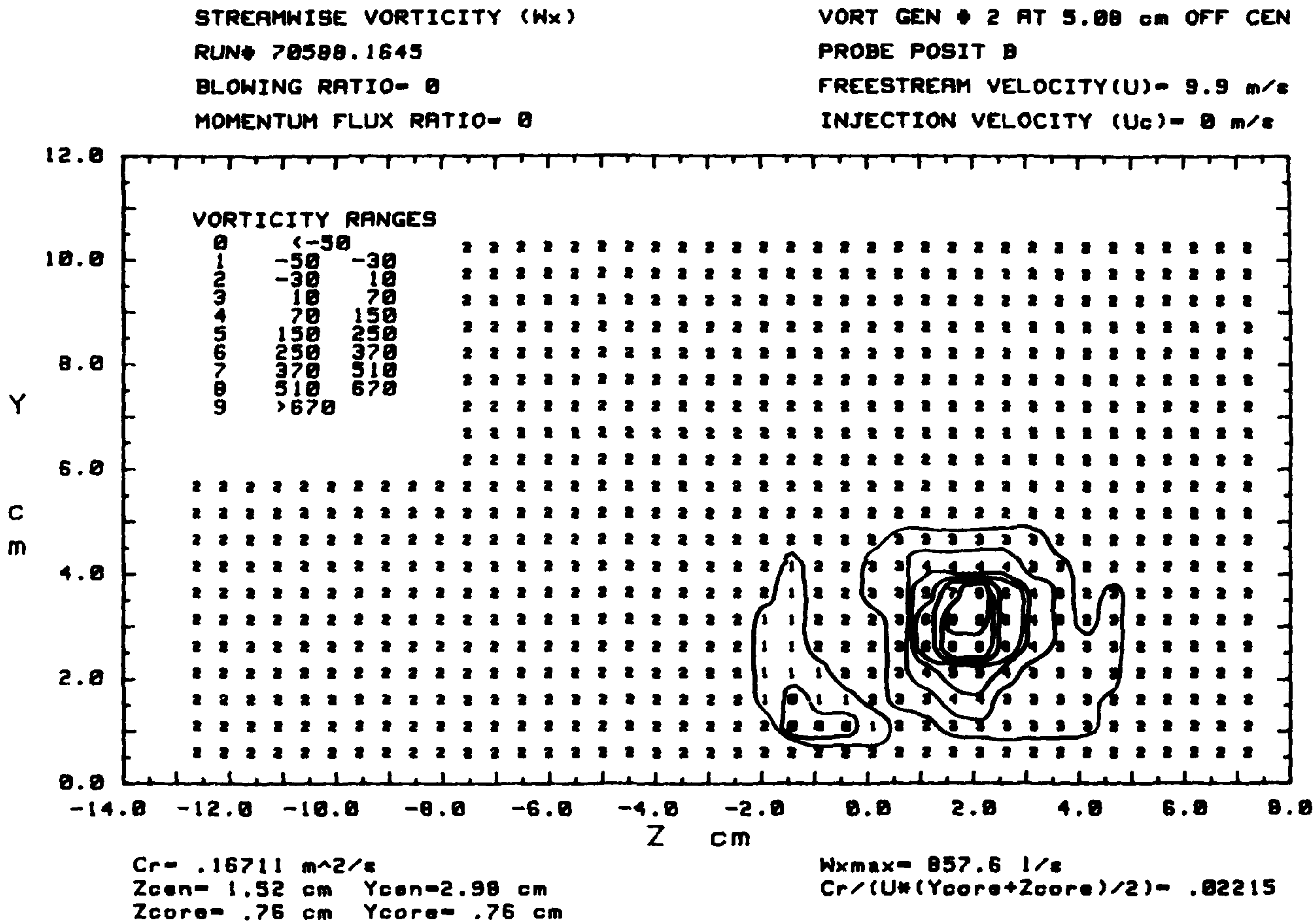

Figure 175. Streamwise Vorticity Contours

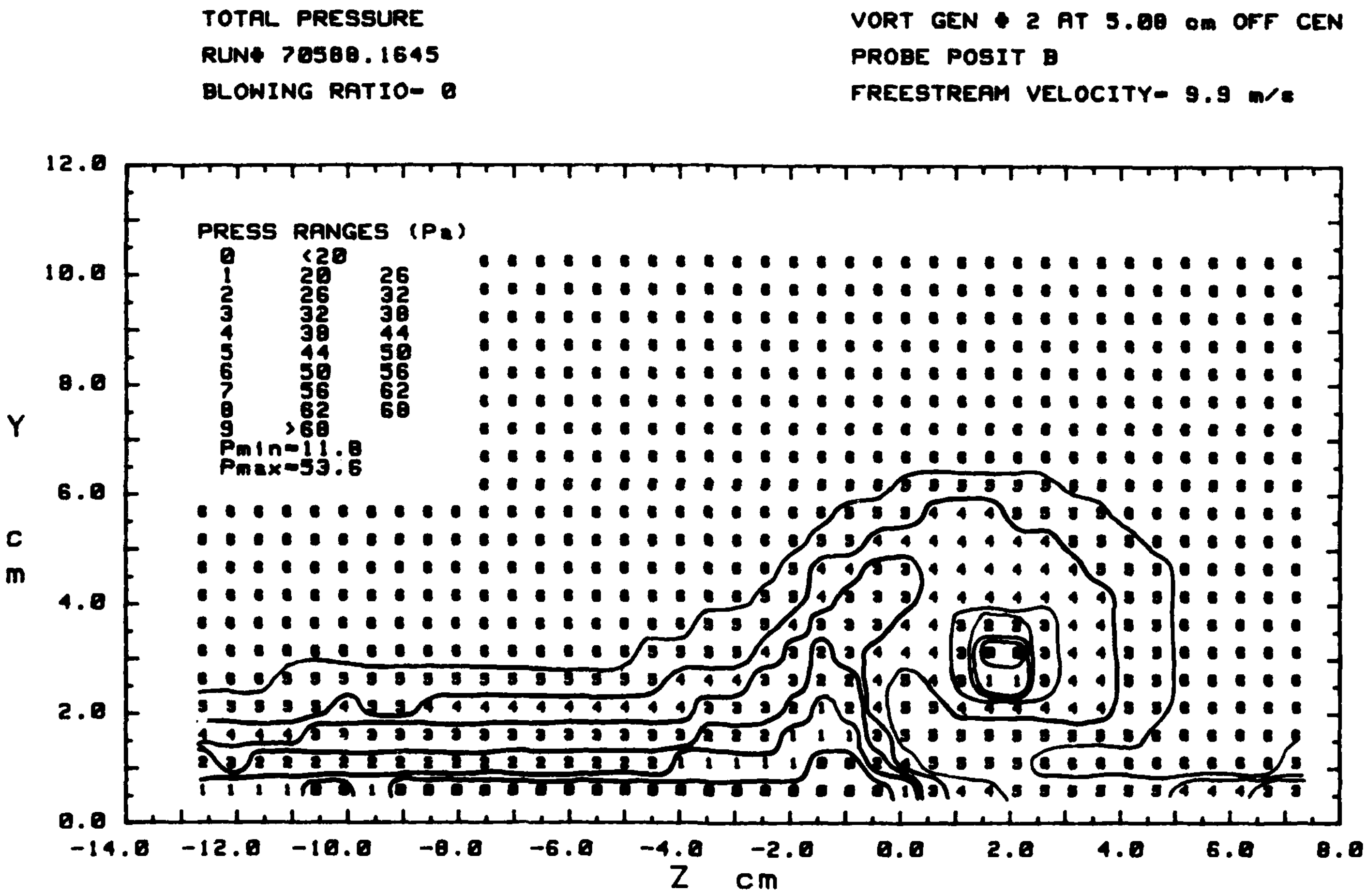

Figure 176. Total Pressure Contours

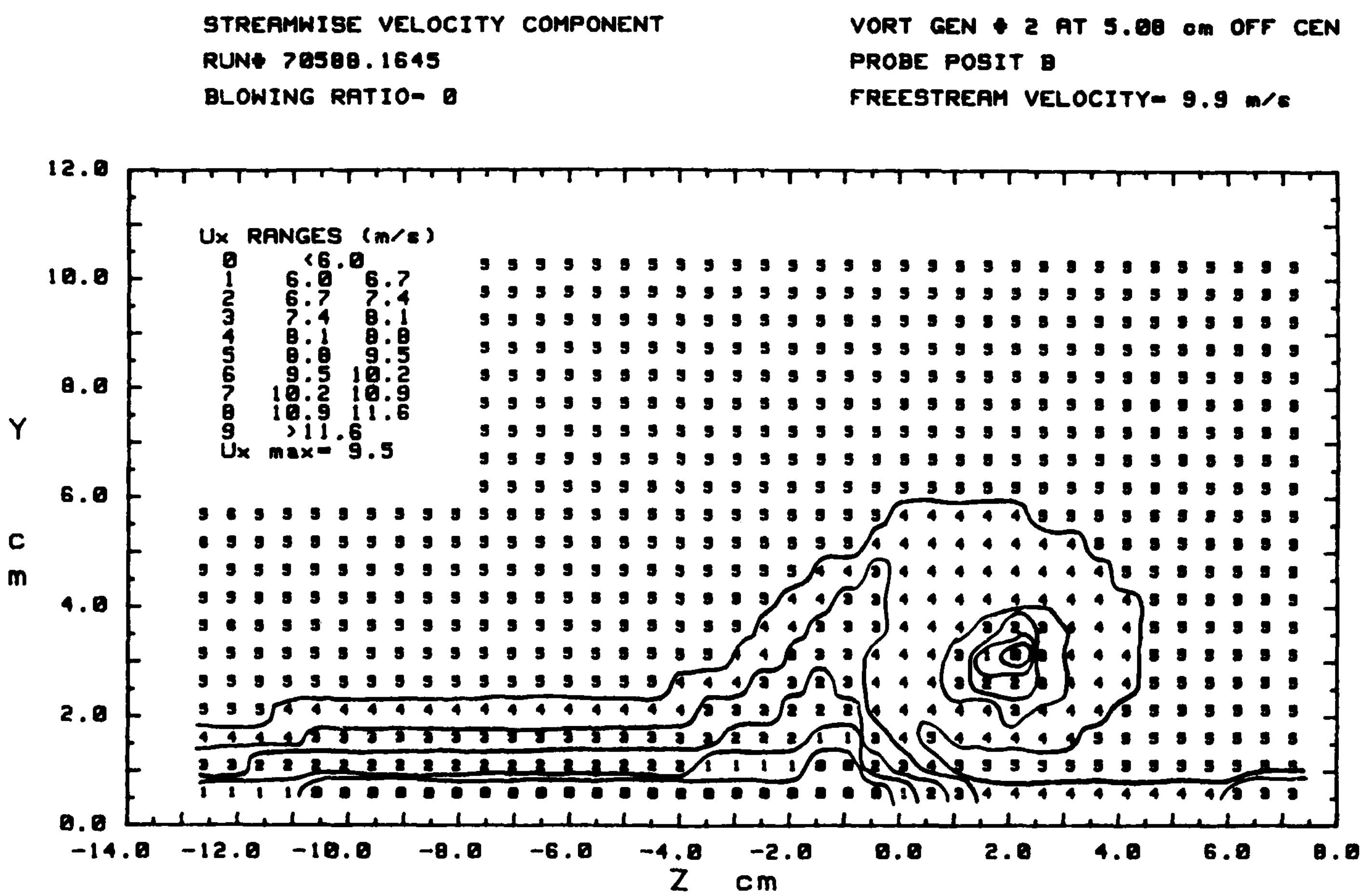

Figure 177. Streamwise Velocity Contours

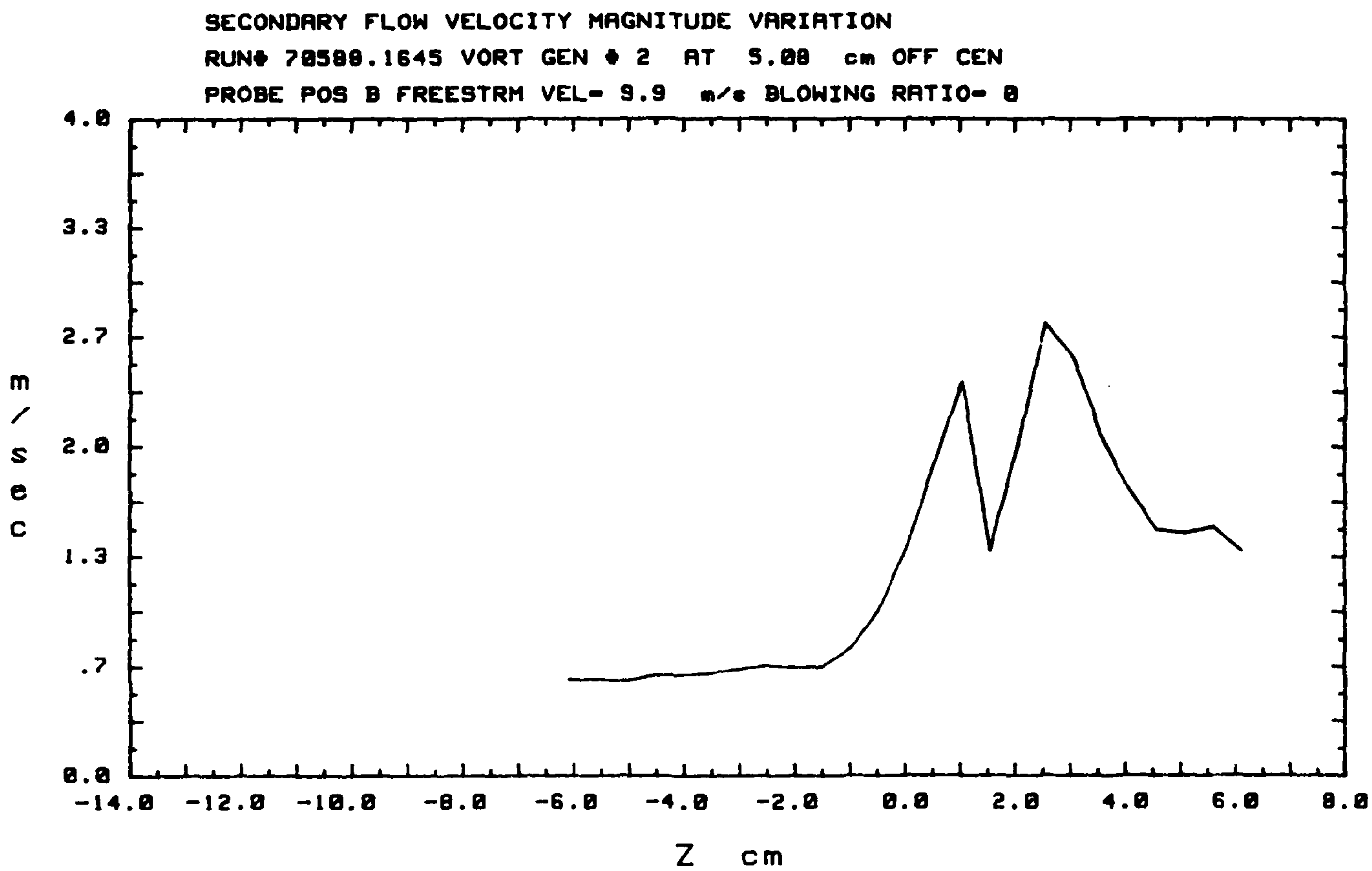

Figure 178. Secondary Flow Velocity (Radially)

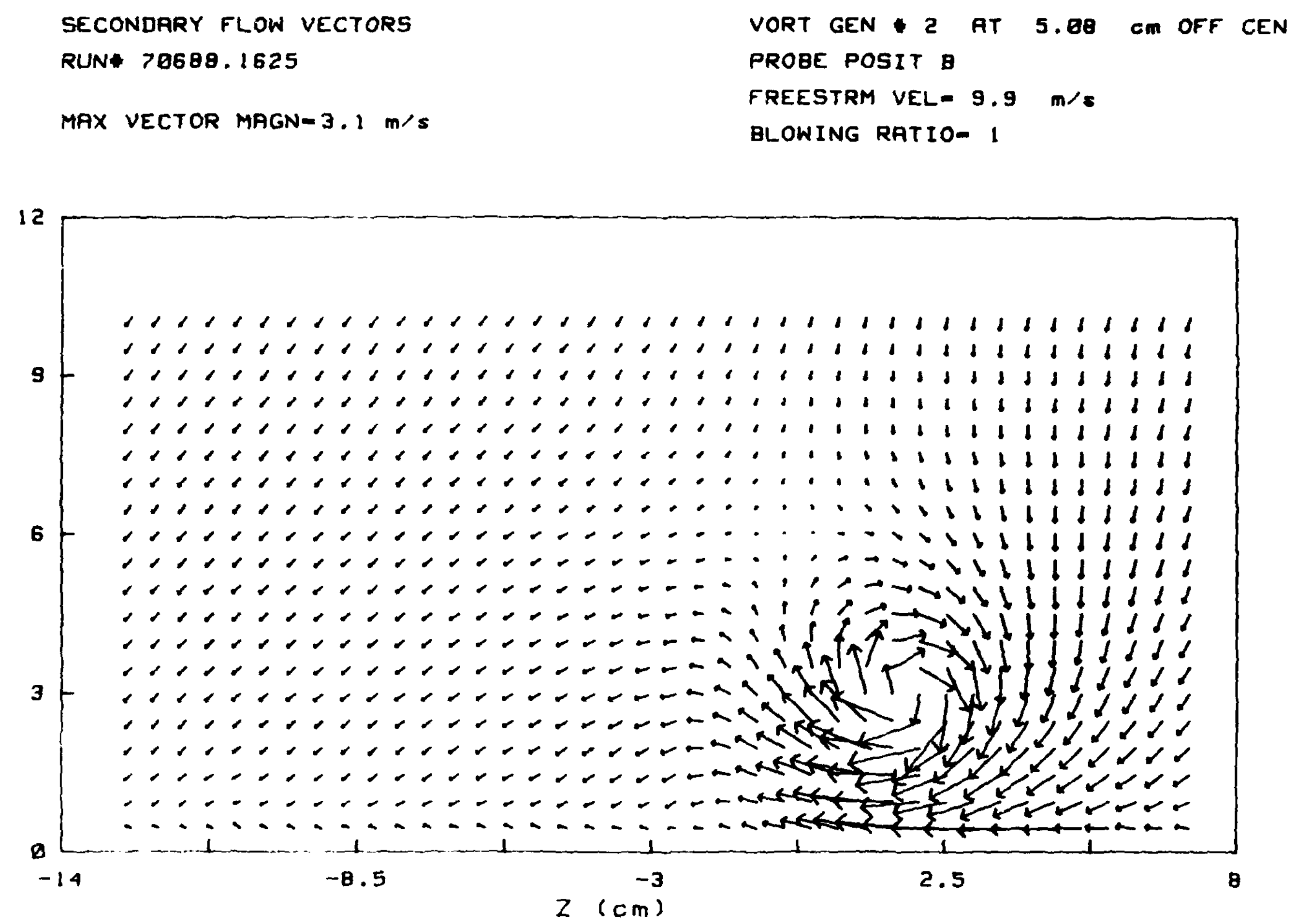

Figure 179. Secondary Flow Vectors

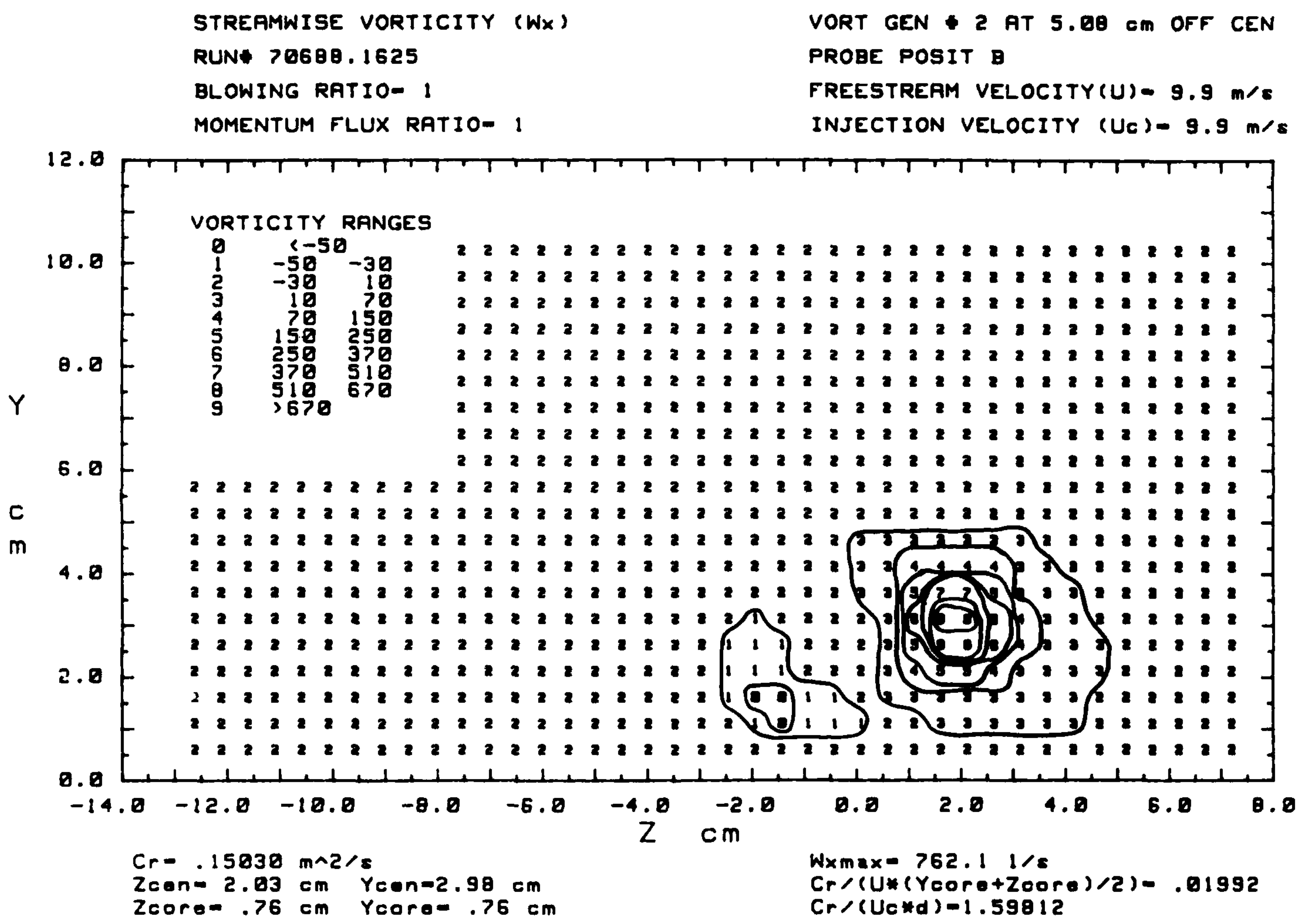

Figure 180. Streamwise Vorticity Contours

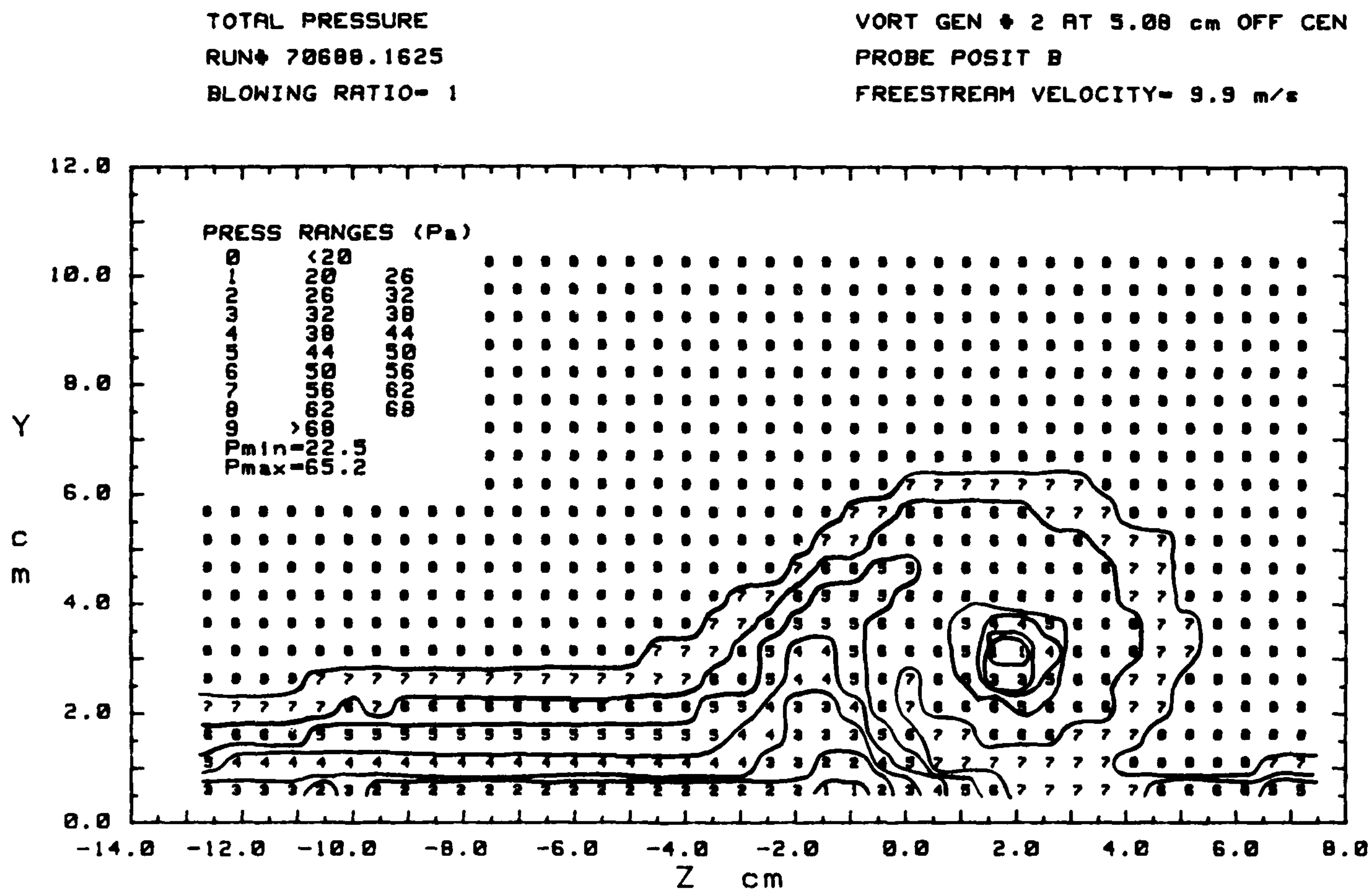

Figure 181. Total Pressure Contours

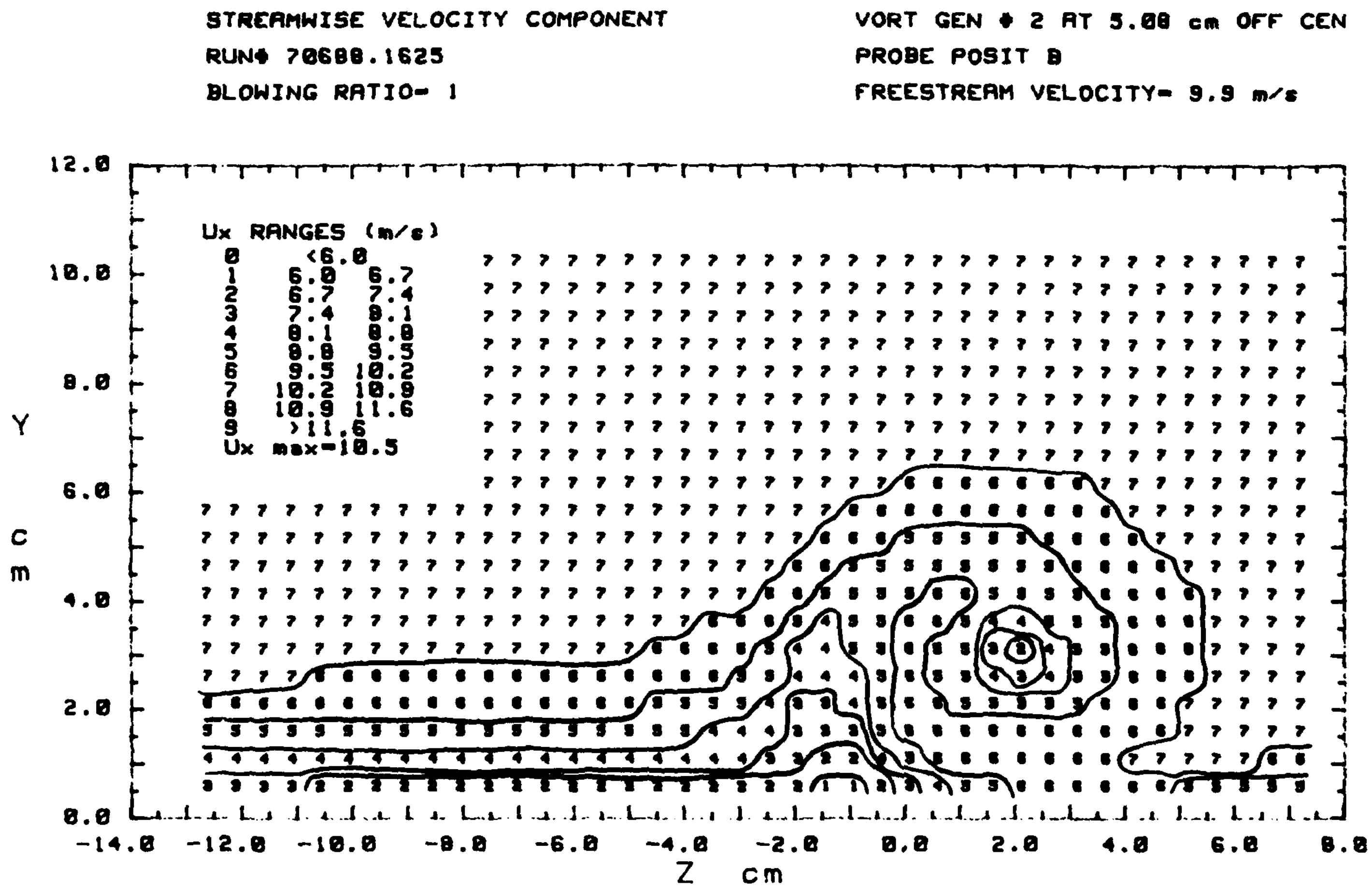

Figure 182. Streamwise Velocity Contours

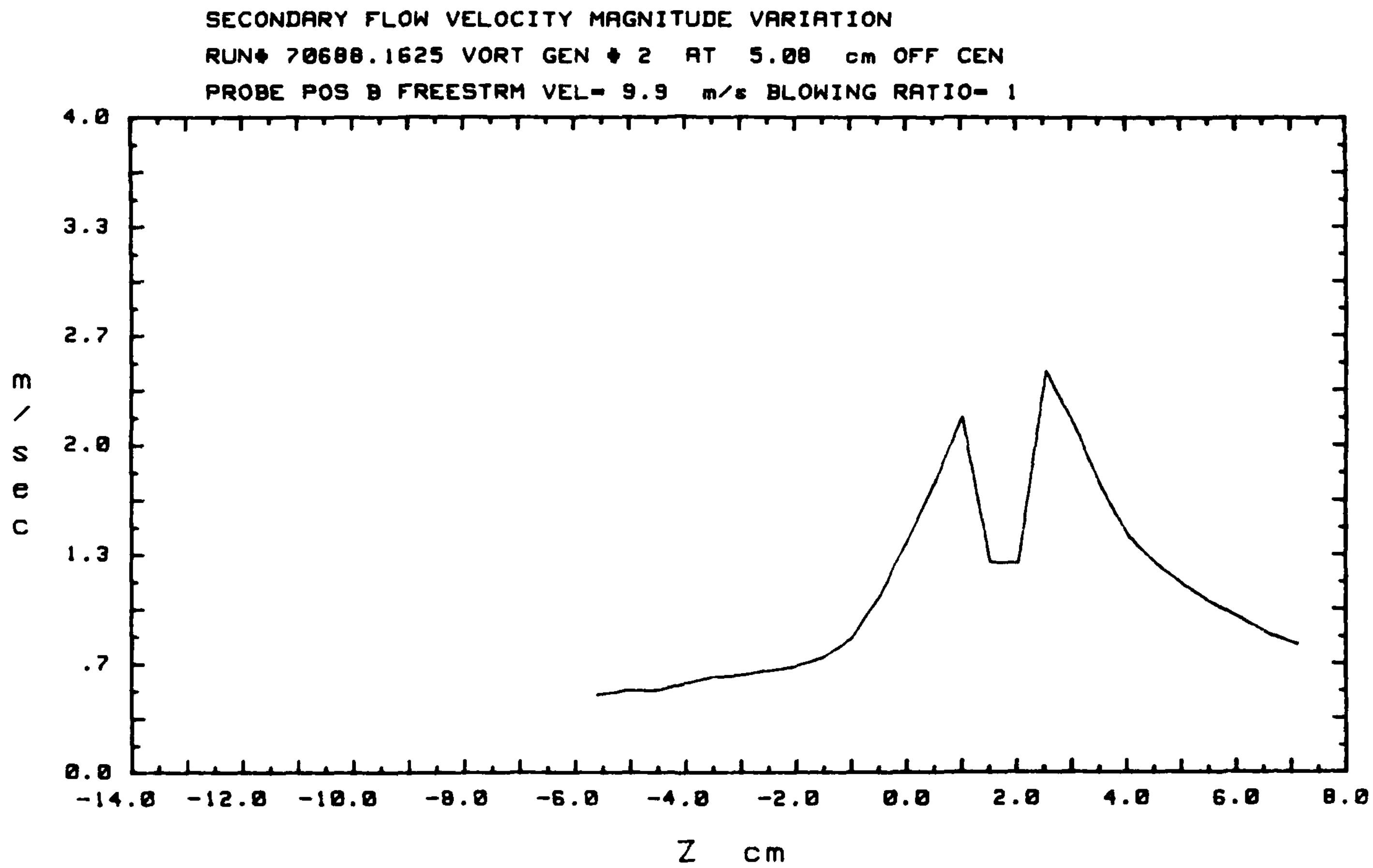

Figure 183. Secondary Flow Velocity (Radially)

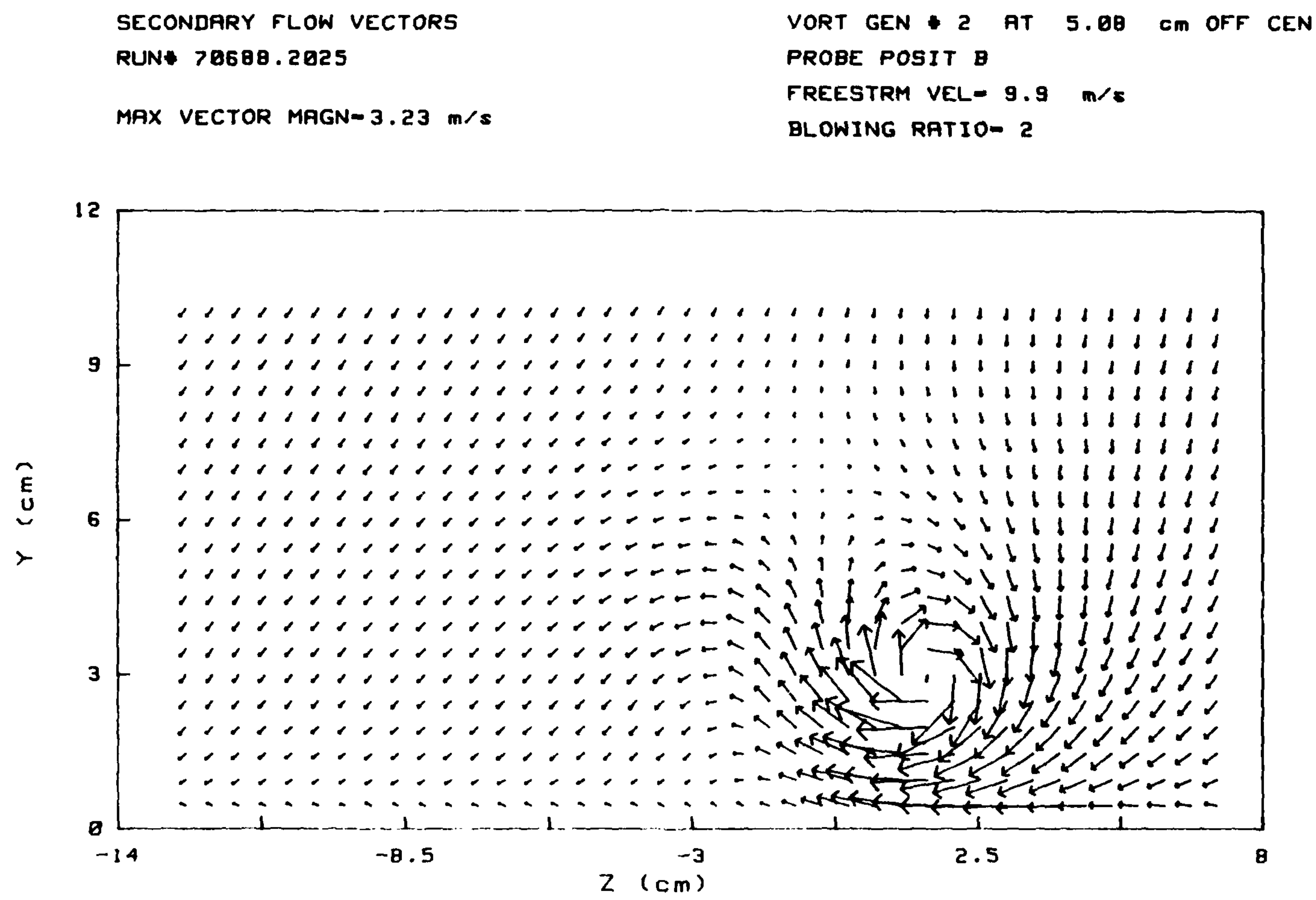

Figure 184. Secondary Flow Vectors

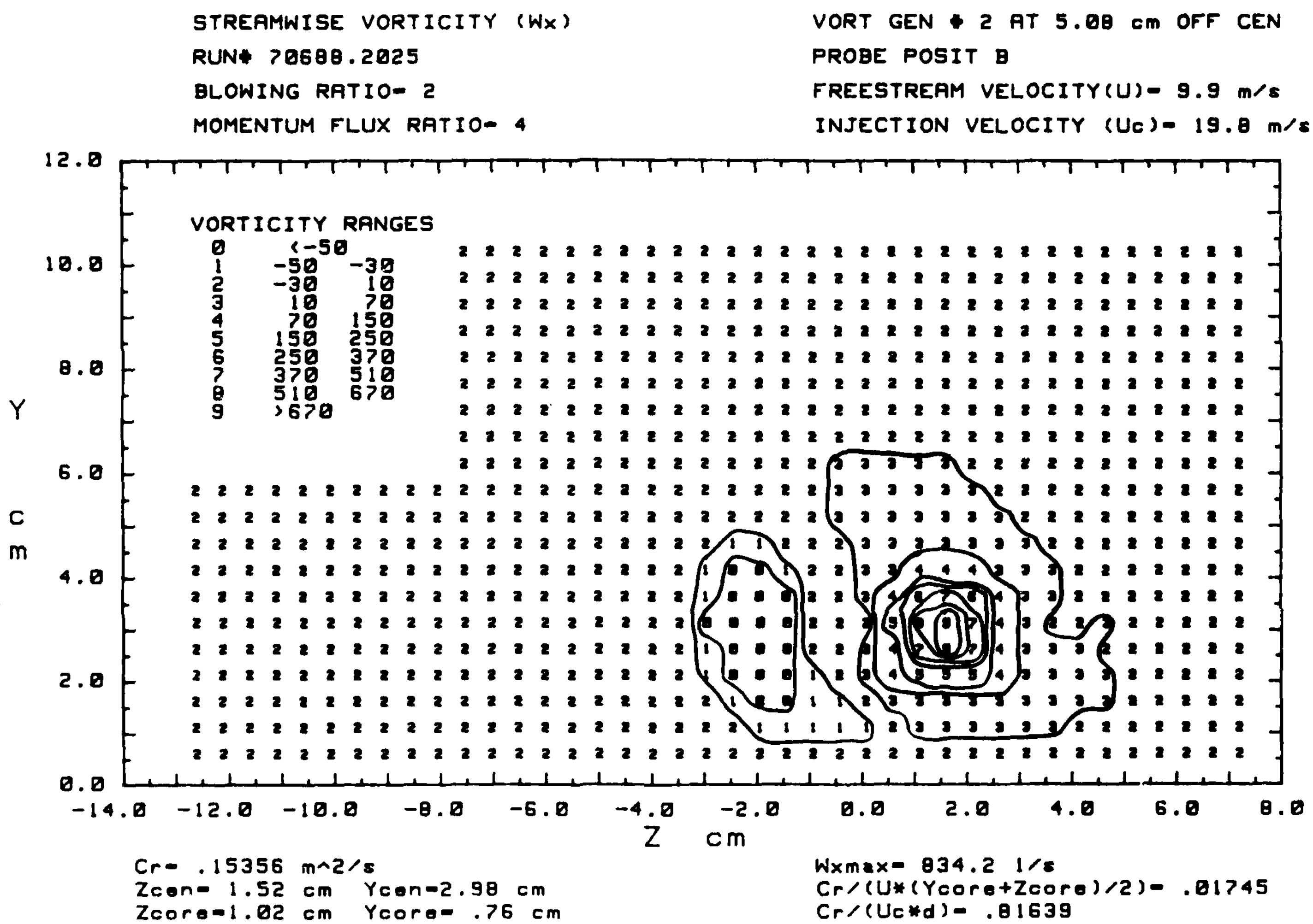

Figure 185. Streamwise Vorticity Contours

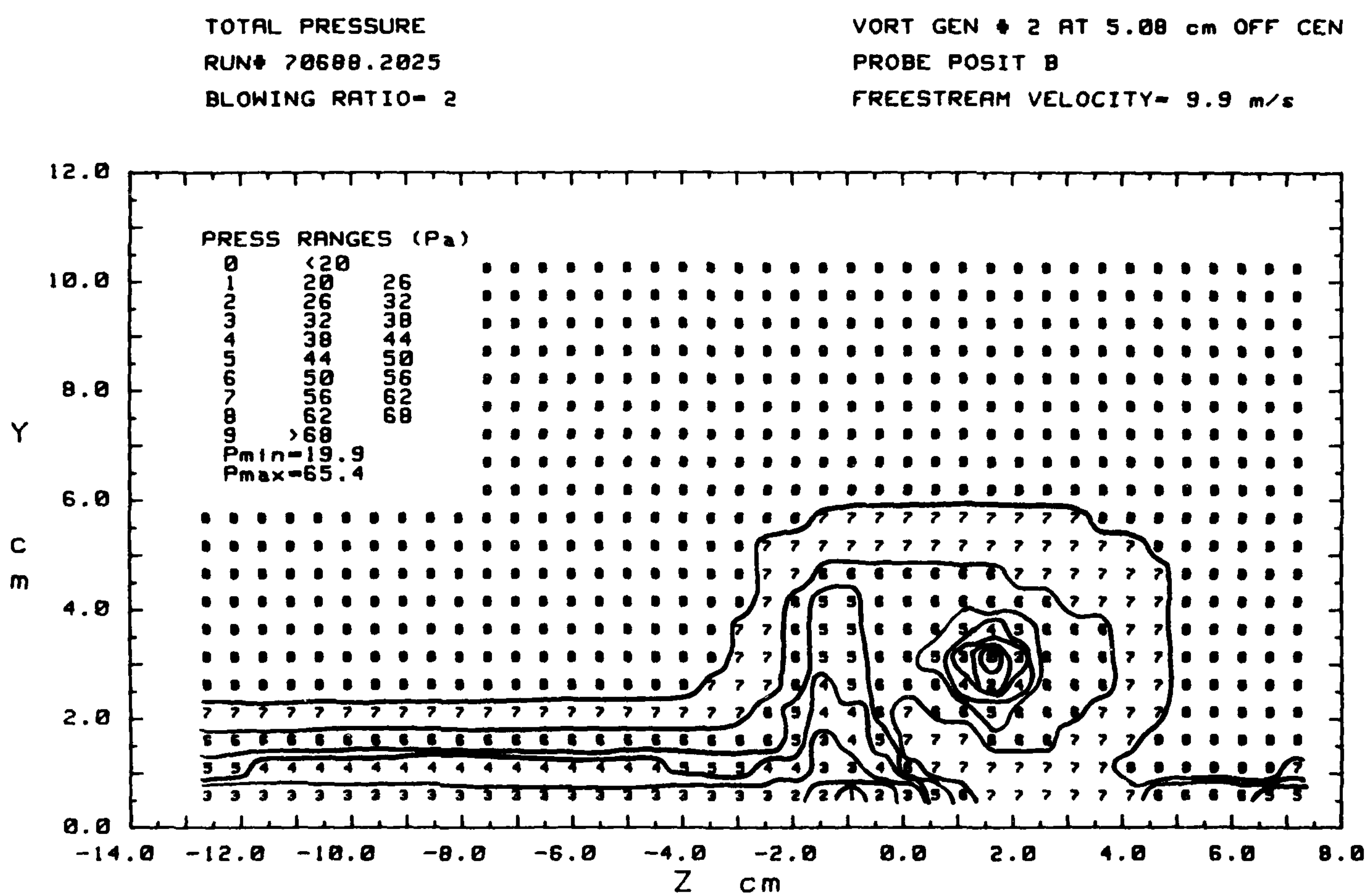

Figure 186. Total Pressure Contours

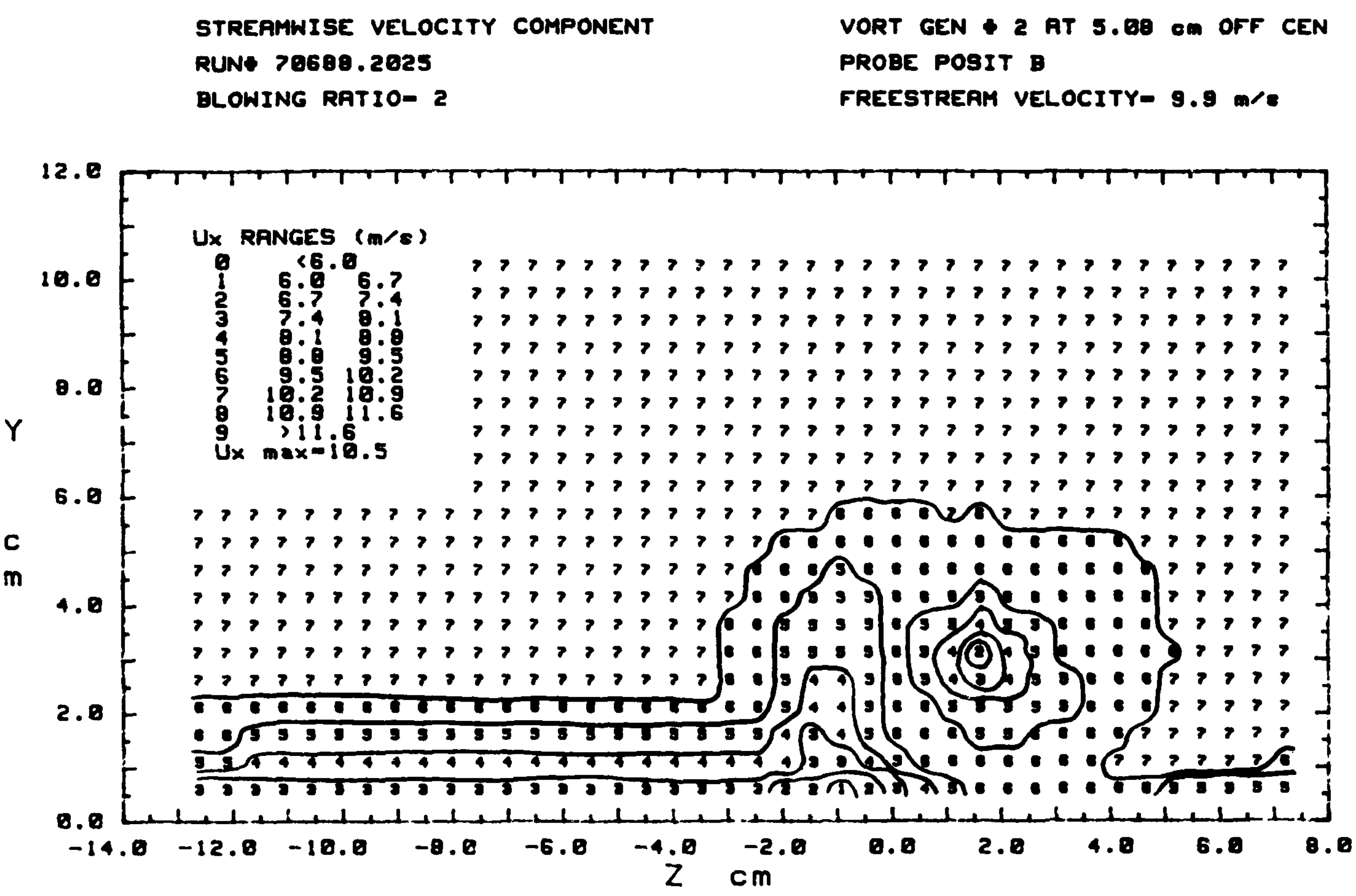

Figure 187. Streamwise Velocity Contours

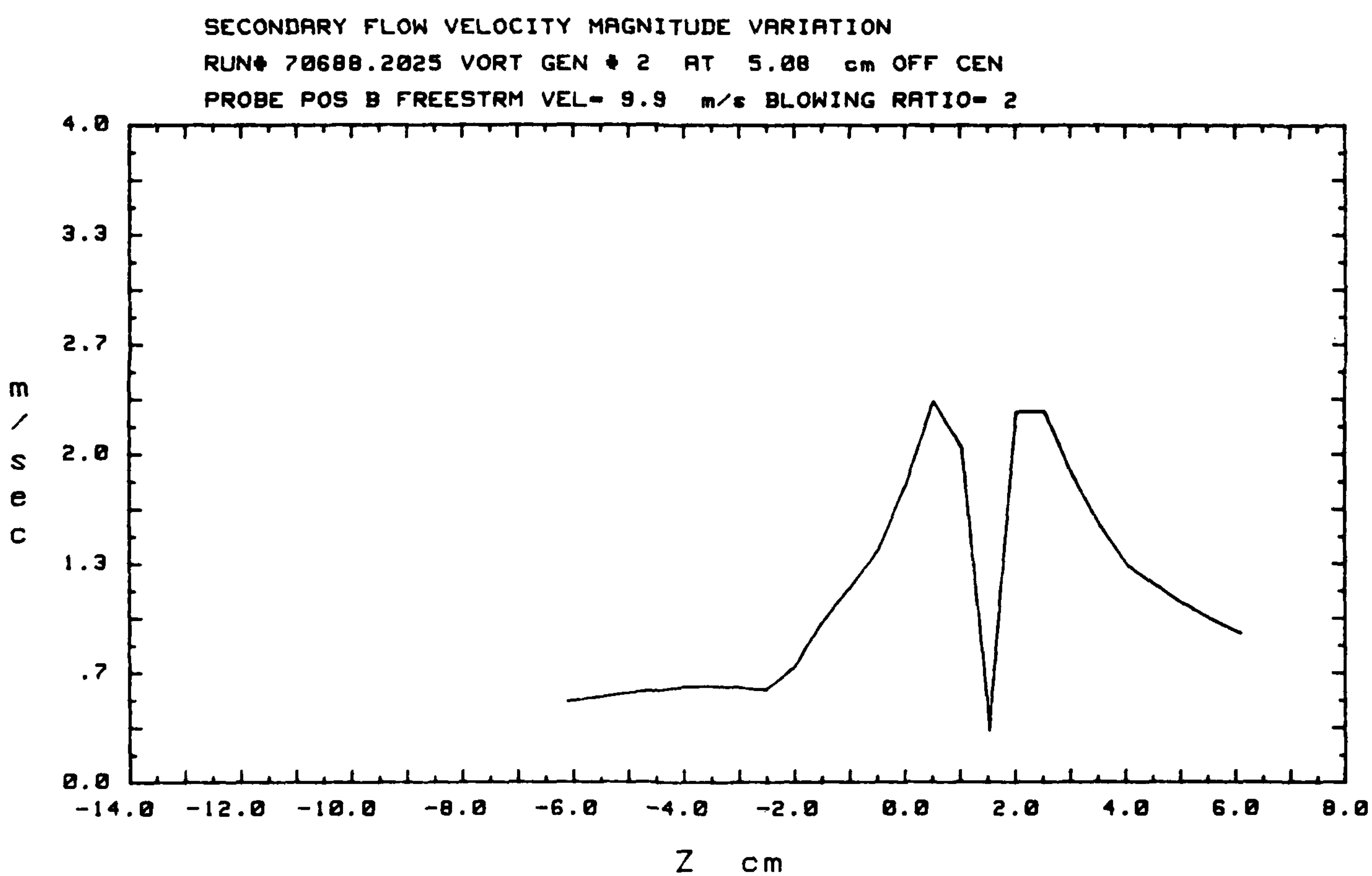

Figure 188. Secondary Flow Velocity (Radially)

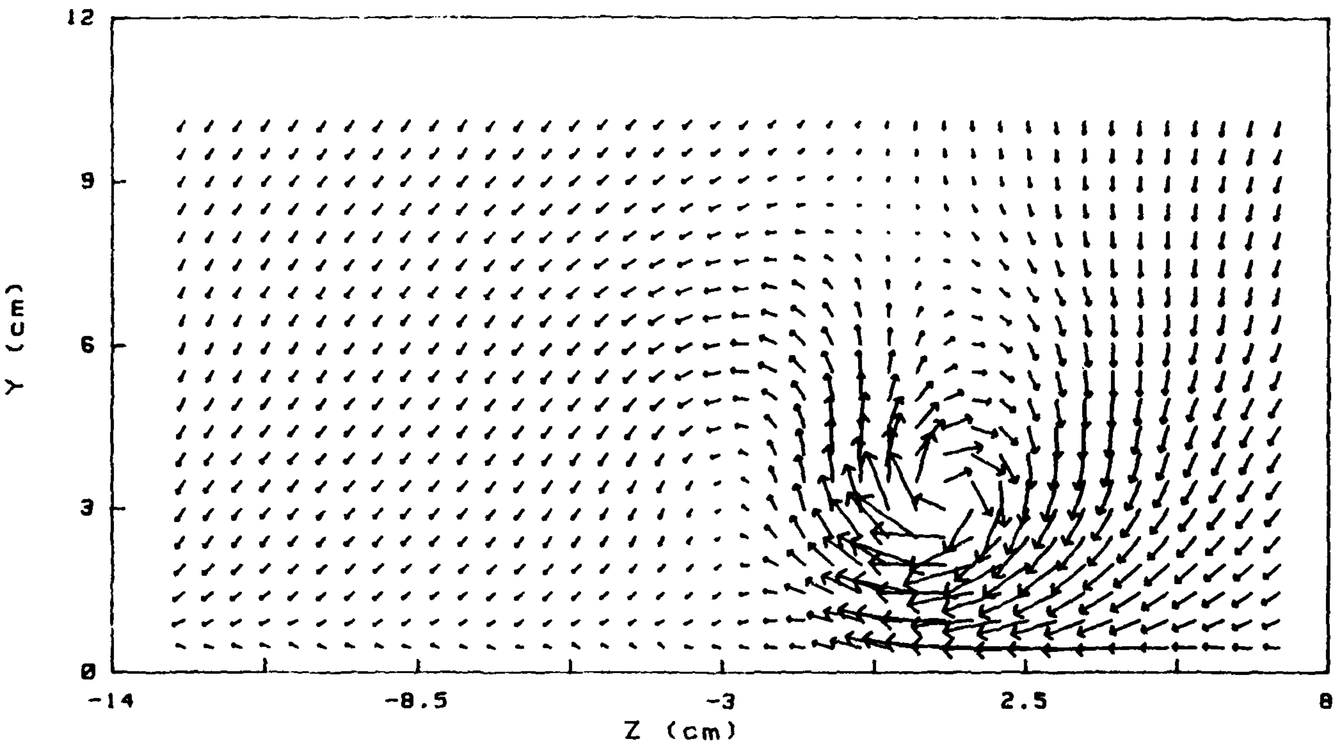

Figure 189. Secondary Flow Vectors

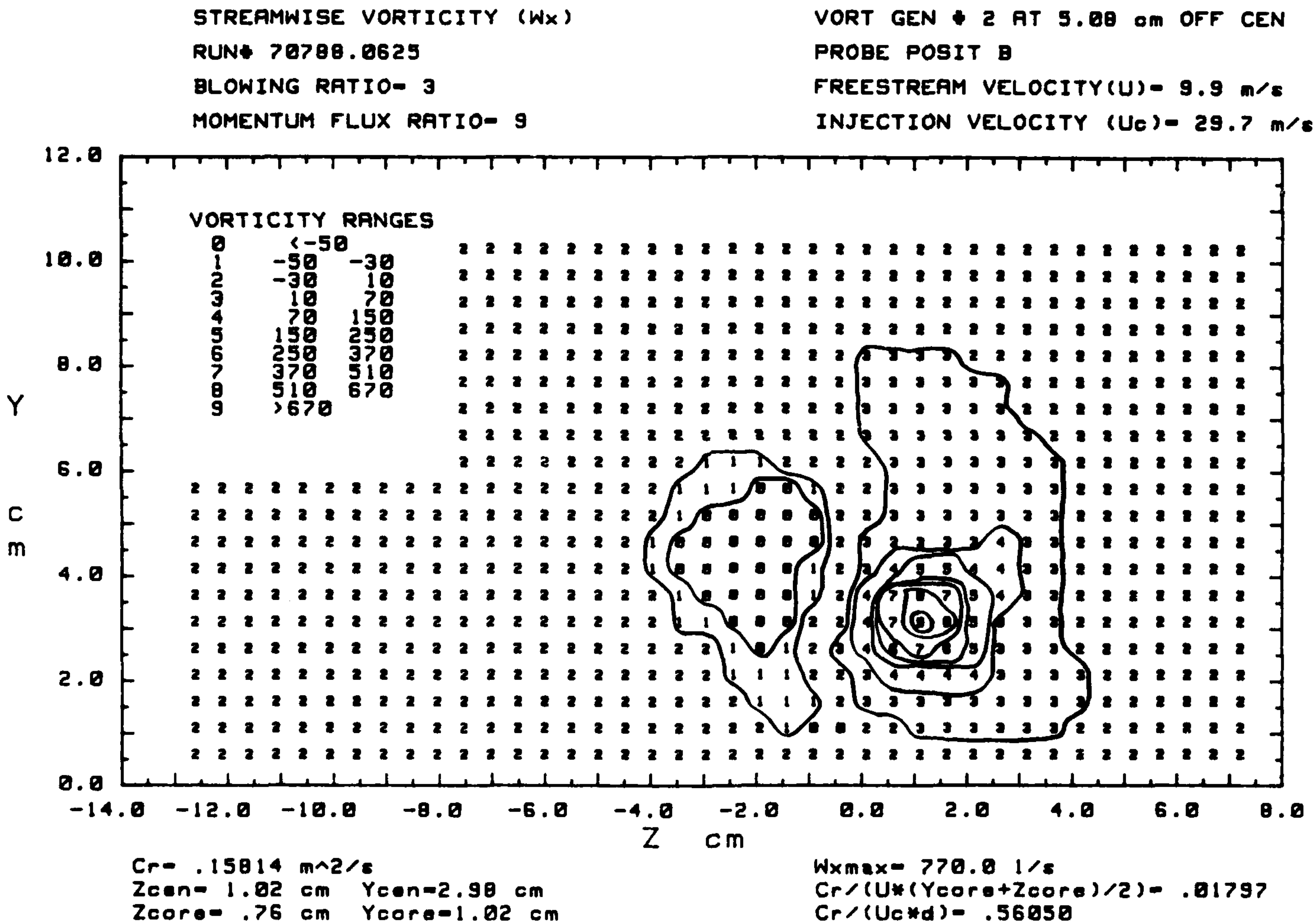

Figure 190. Streamwise Vorticity Contours

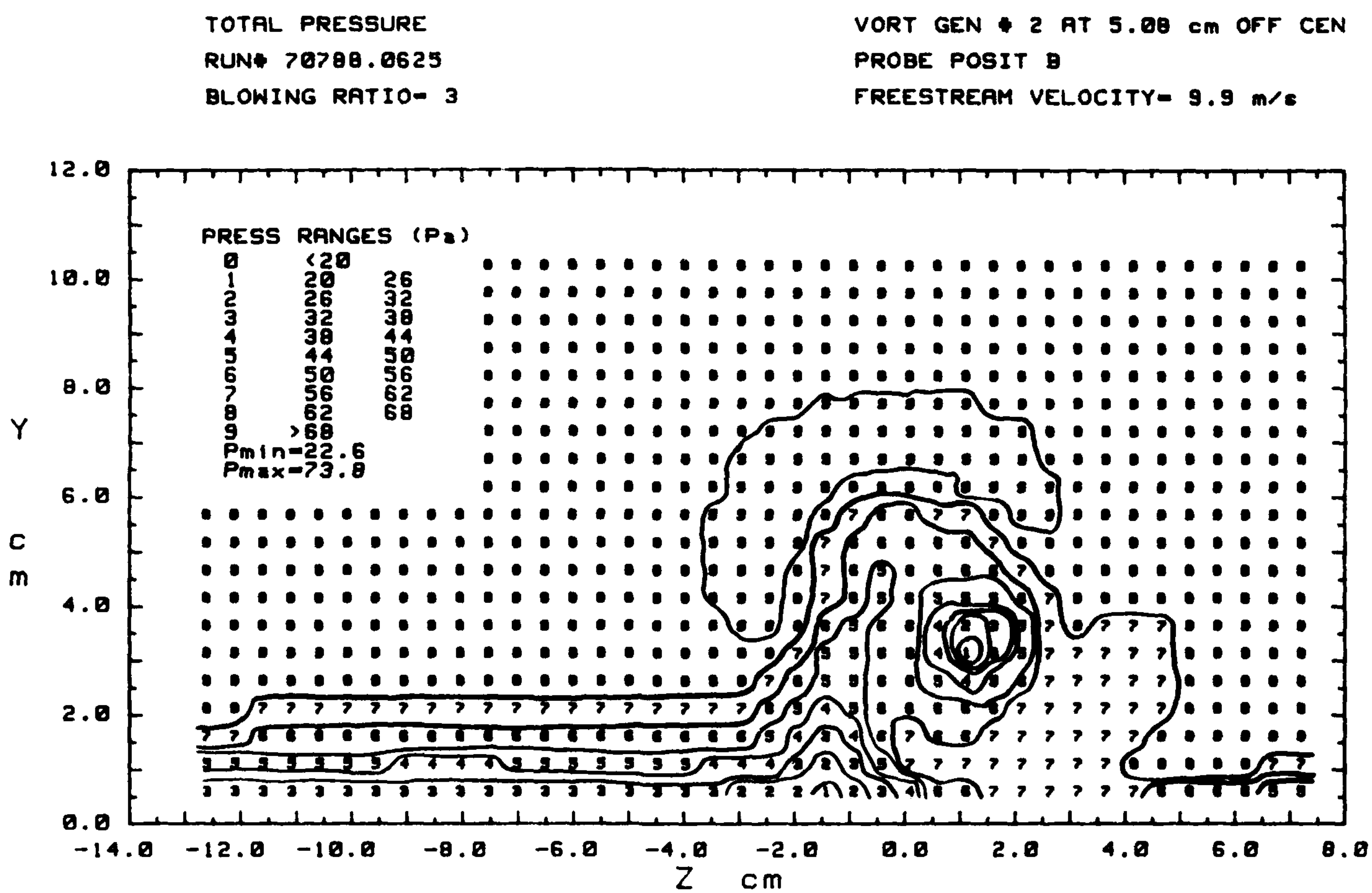

Figure 191. Total Pressure Contours

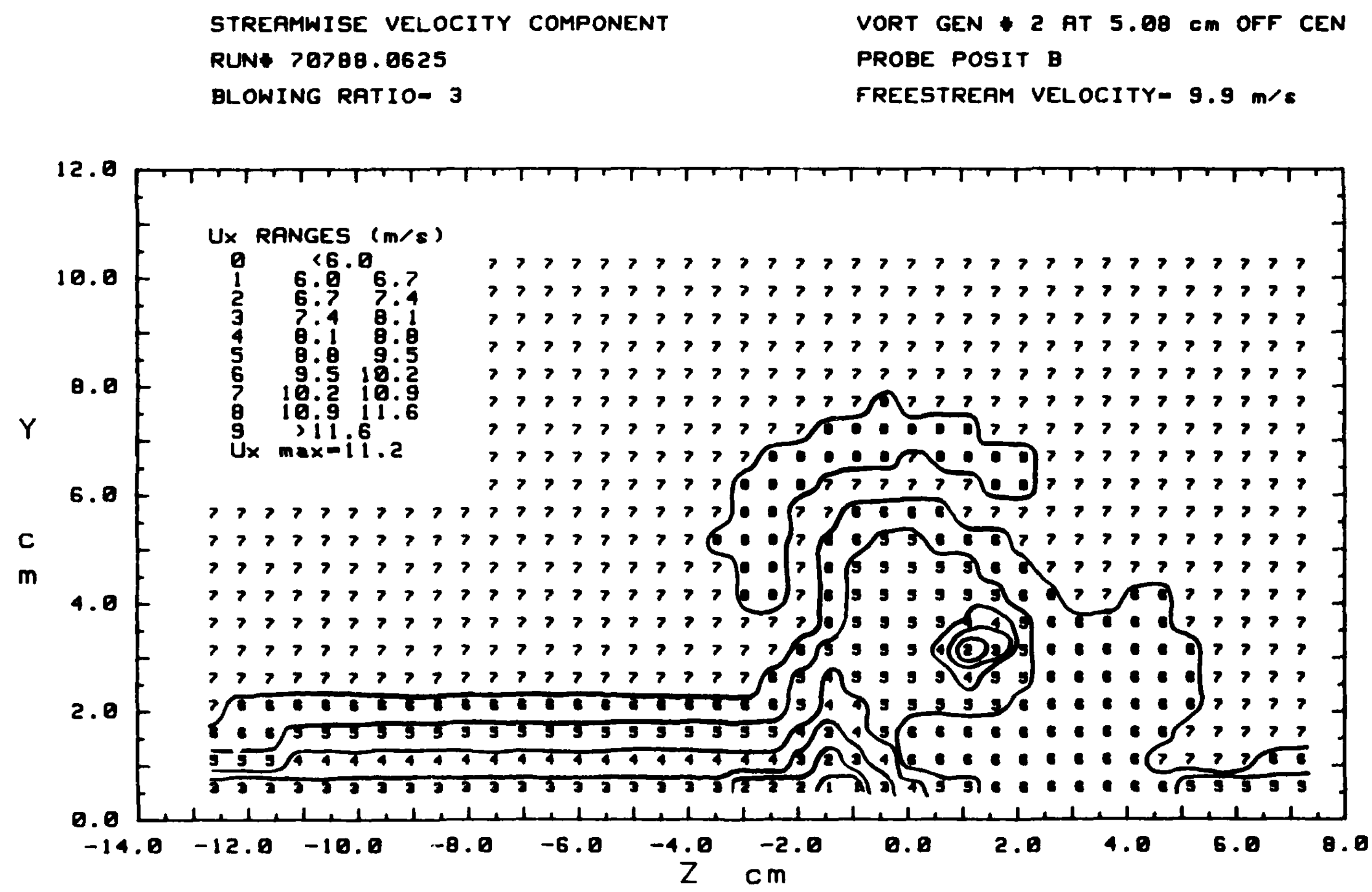

Figure 192. Streamwise Velocity Contours

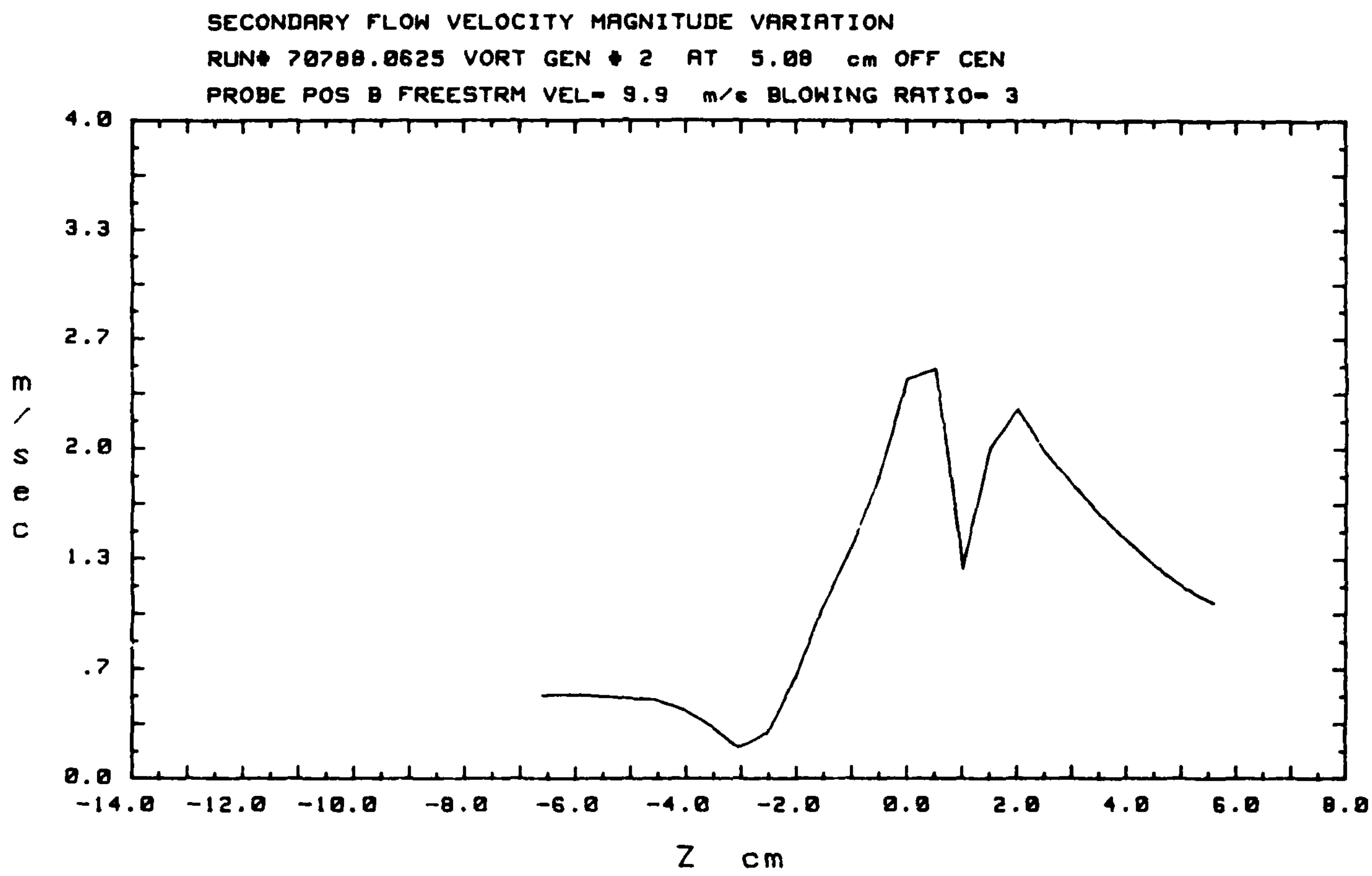

Figure 193. Secondary Flow Velocity (Radially)

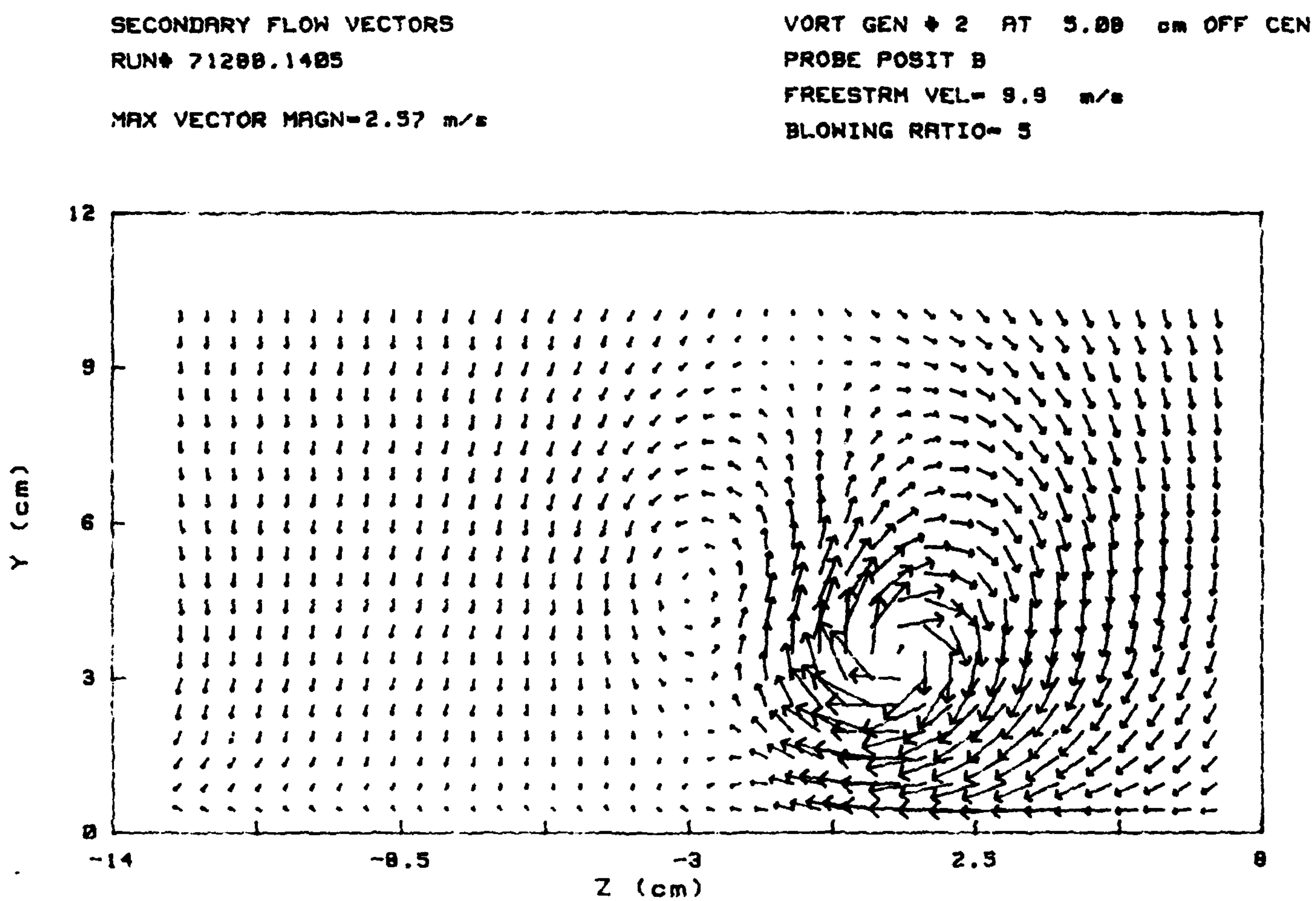

Figure 194. Secondary Flow Vectors

STREAMWISE VORTICITY (Wx)
RUN# 71288.1405
BLOWING RATIO= 5
MOMENTUM FLUX RATIO= 25

VORT GEN # 2 AT 5.08 cm OFF CEN
PROBE POSIT B
FREESTREAM VELOCITY(U)= 9.9 m/s
INJECTION VELOCITY (Uc)= 49.5 m/s

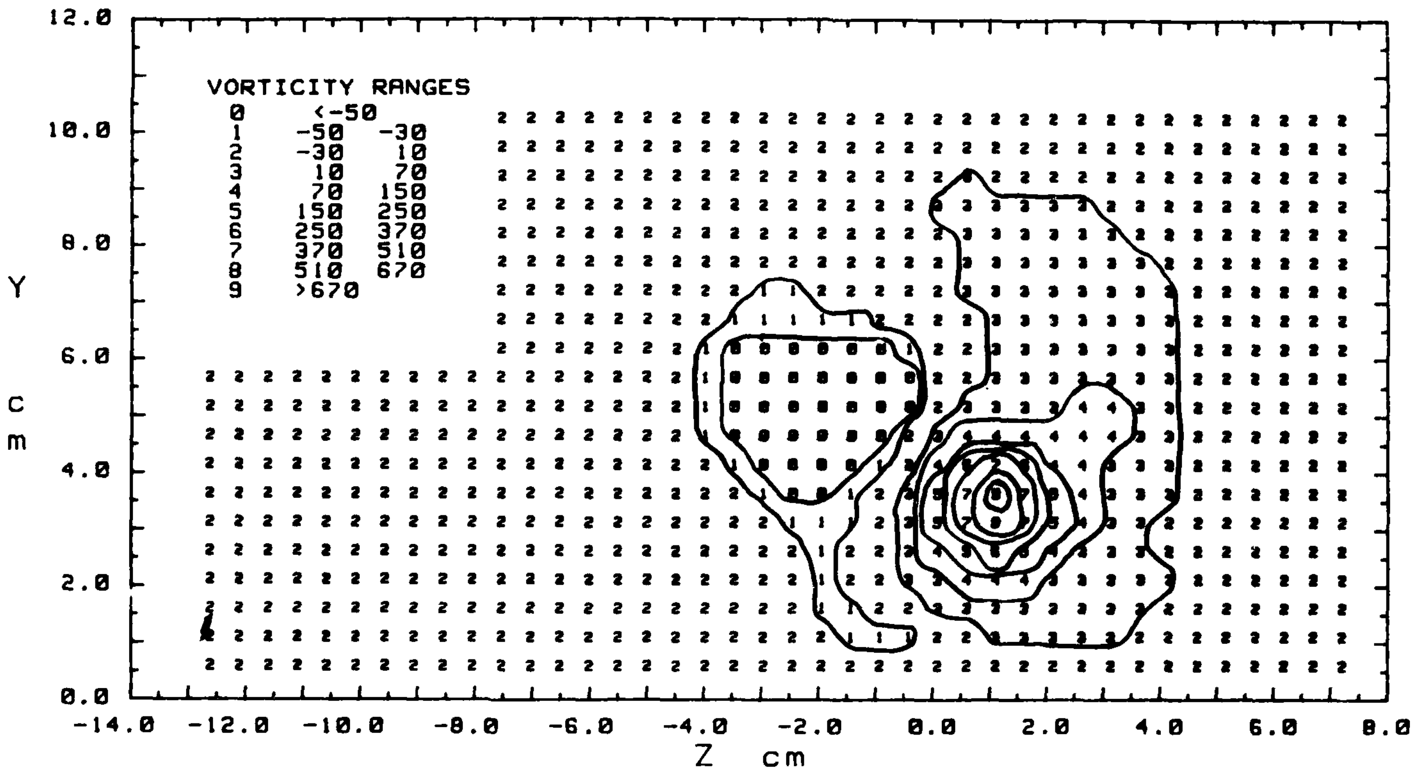

Cr= .15585 m^2/s
Zcen= 1.02 cm Ycen=3.49 cm
Zcore=1.02 cm Ycore= .76 cm

Wxmax= 677.0 1/s
Cr/(U*(Ycore+Zcore)/2)= .01771
Cr/(Uc*d)= .33141

Figure 195. Streamwise Vorticity Contours

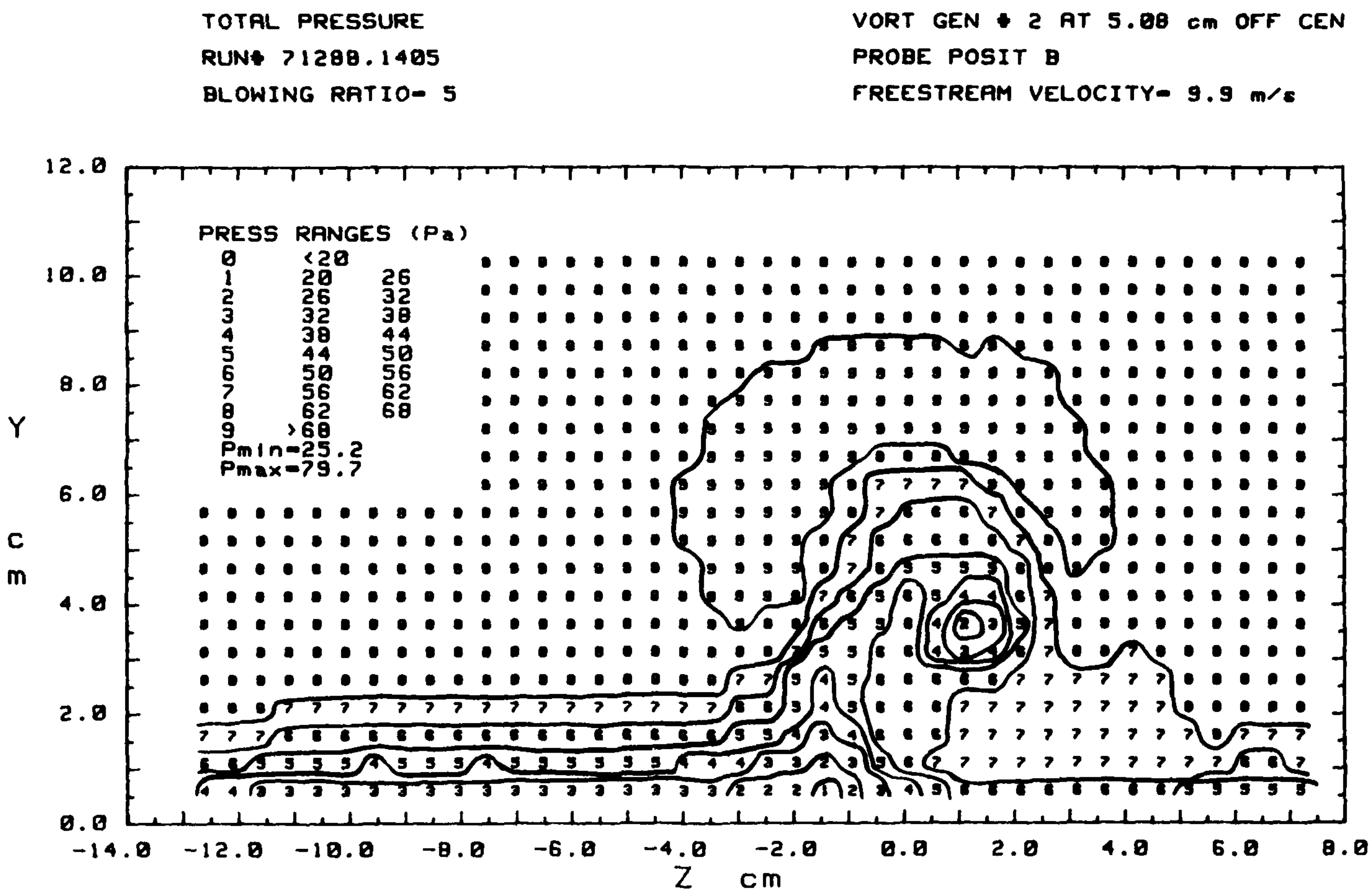

Figure 196. Total Pressure Contours

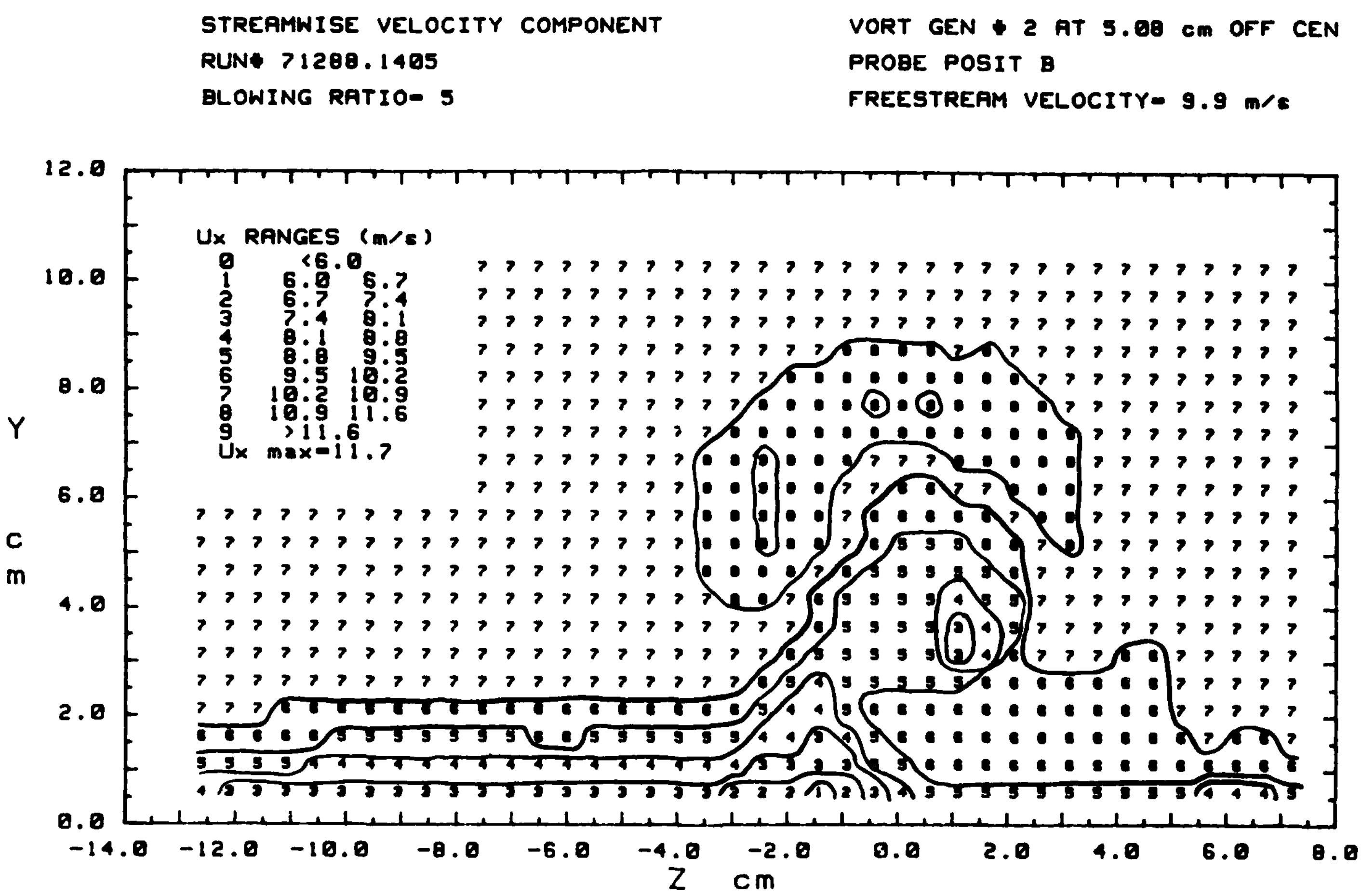

Figure 197. Streamwise Velocity Contours

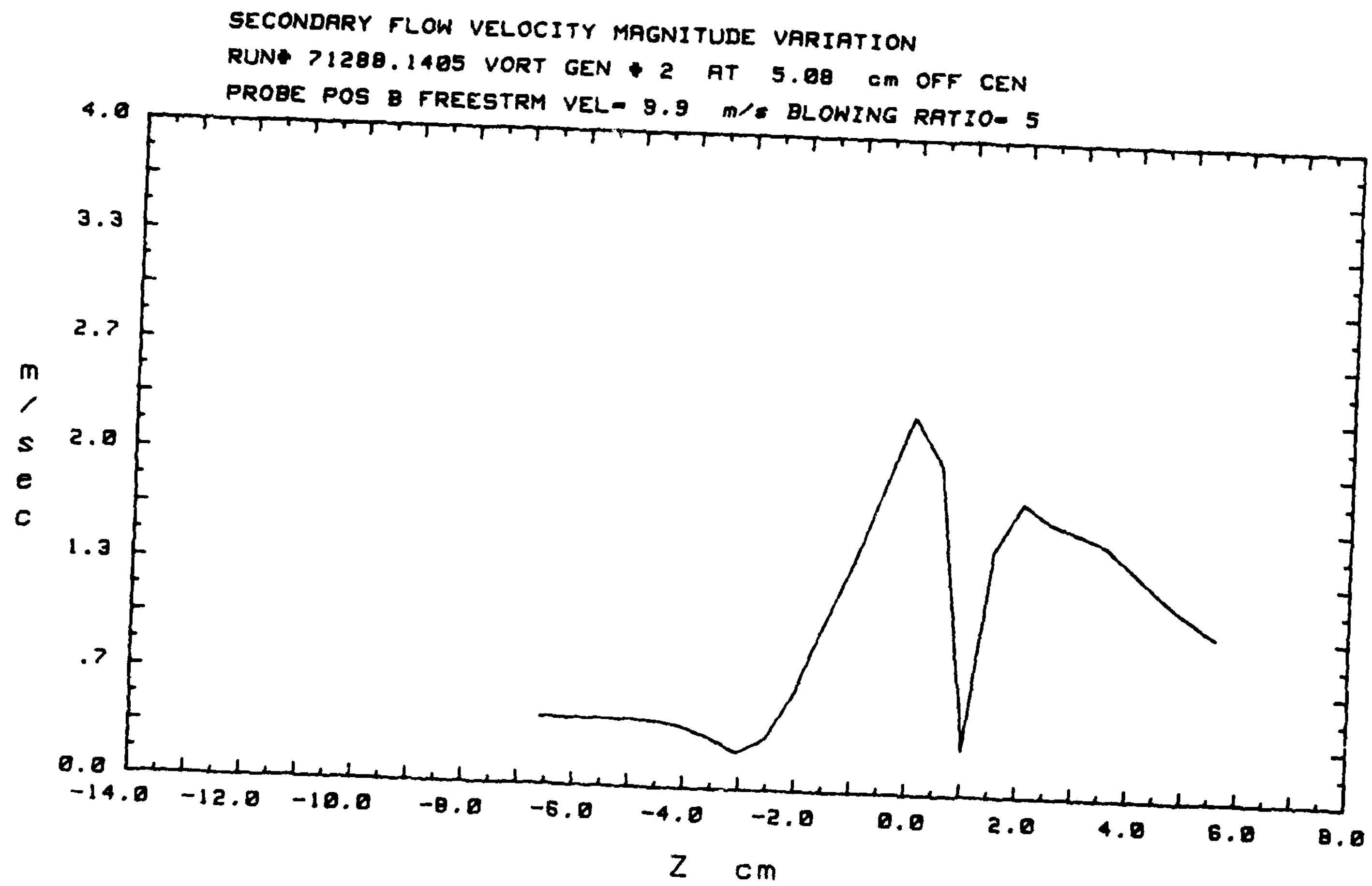

Figure 198. Secondary Flow Velocity (Radially)

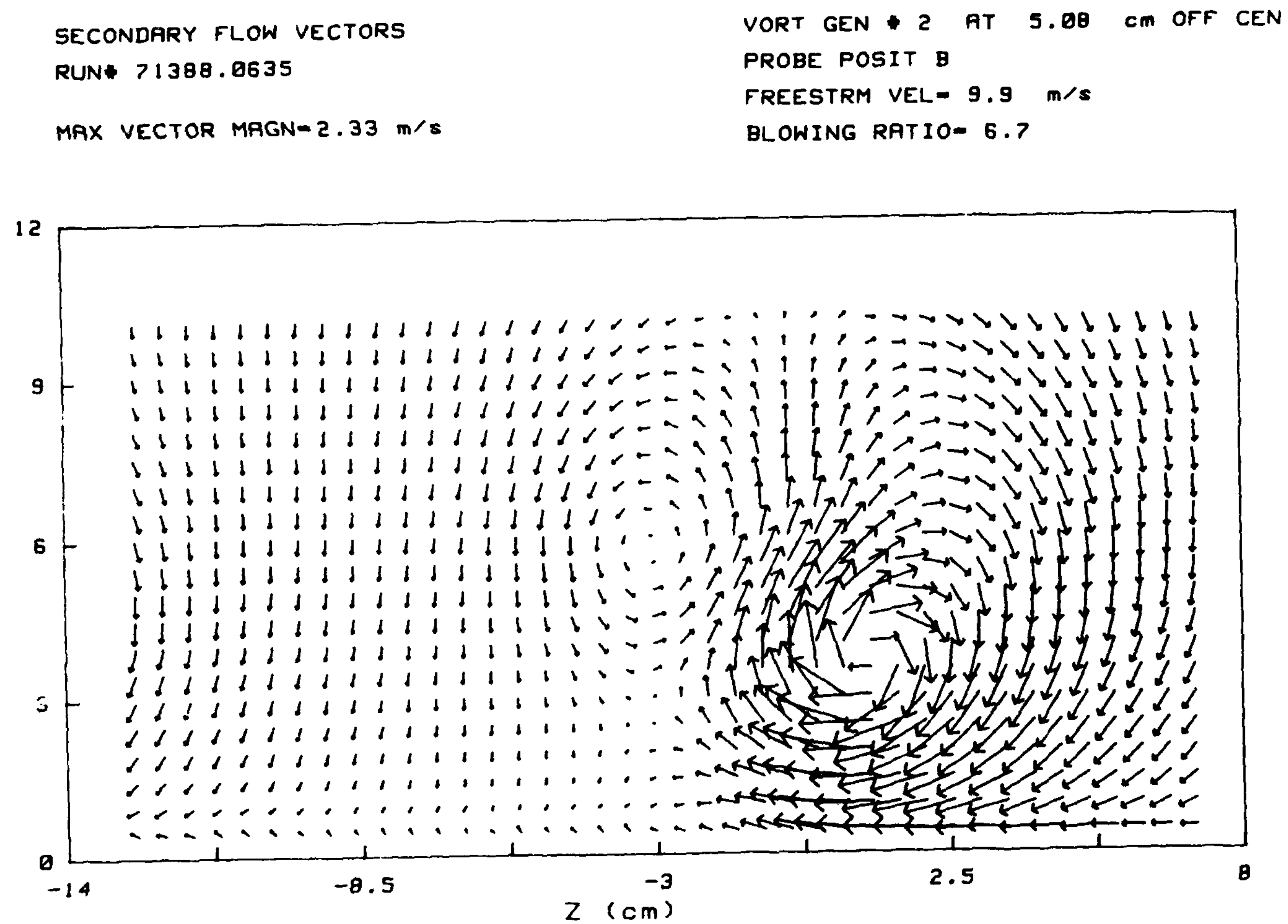

Figure 199. Secondary Flow Vectors

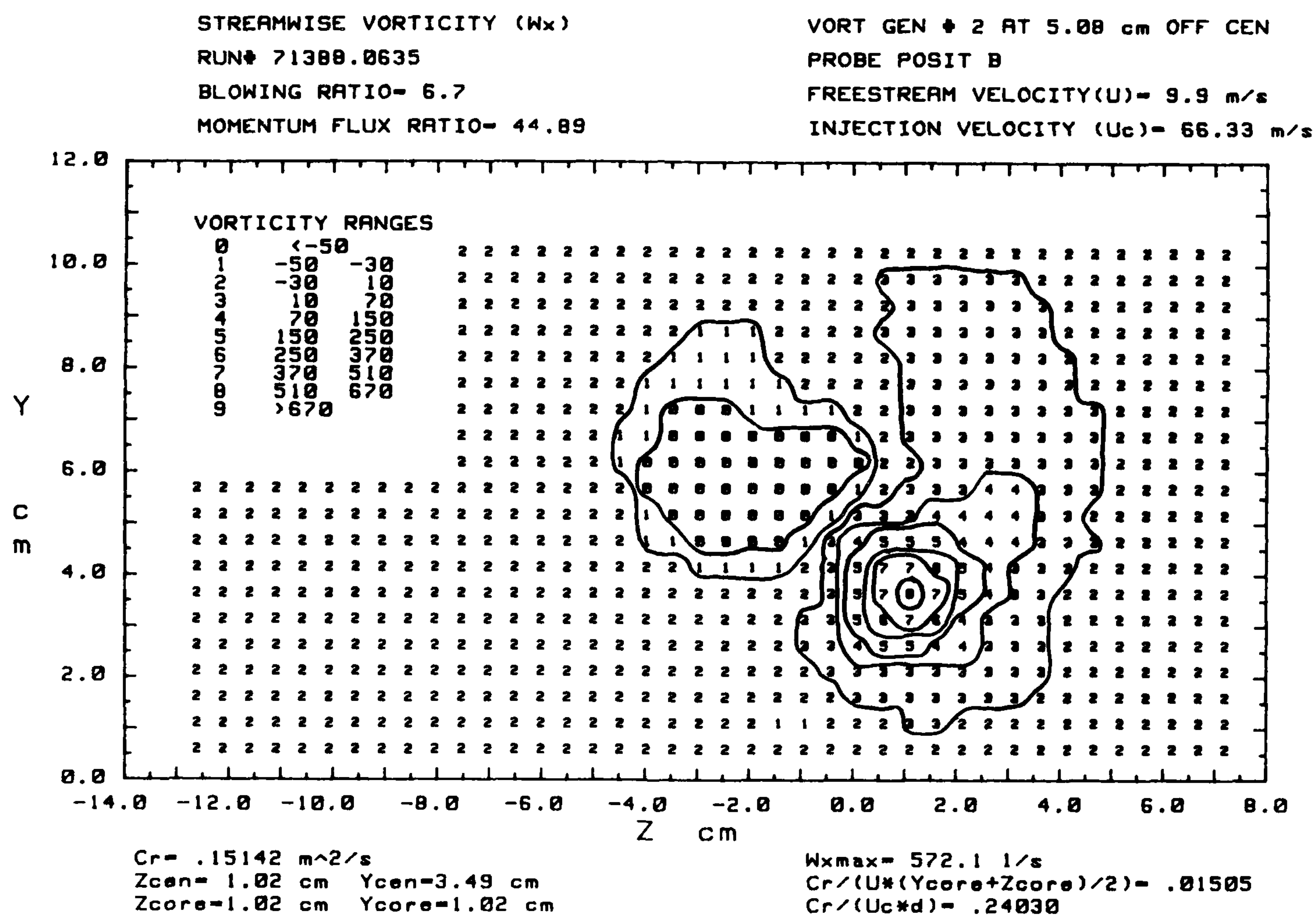

Figure 200. Streamwise Vorticity Contours

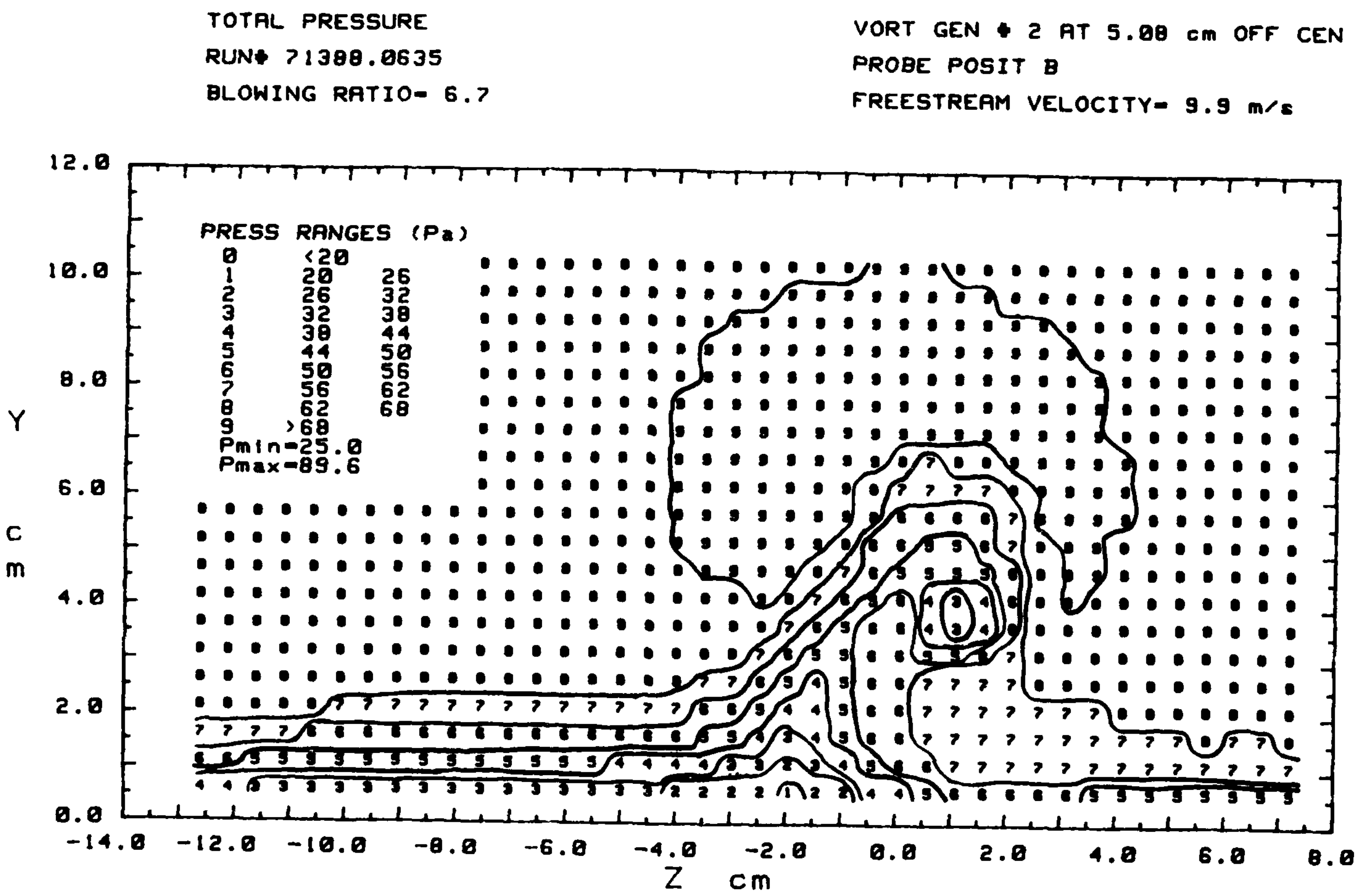

Figure 201. Total Pressure Contours

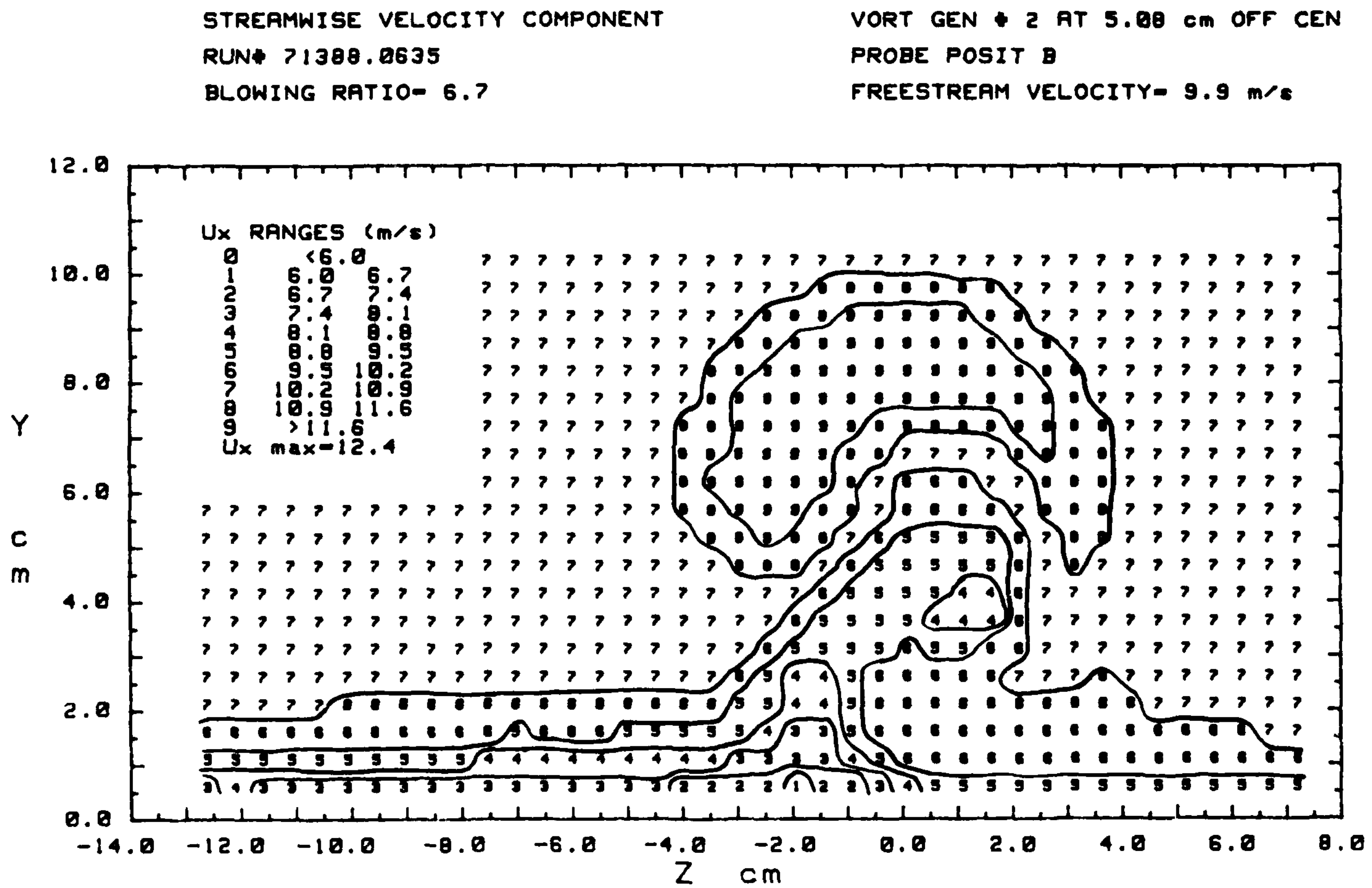

Figure 202. Streamwise Velocity Contours

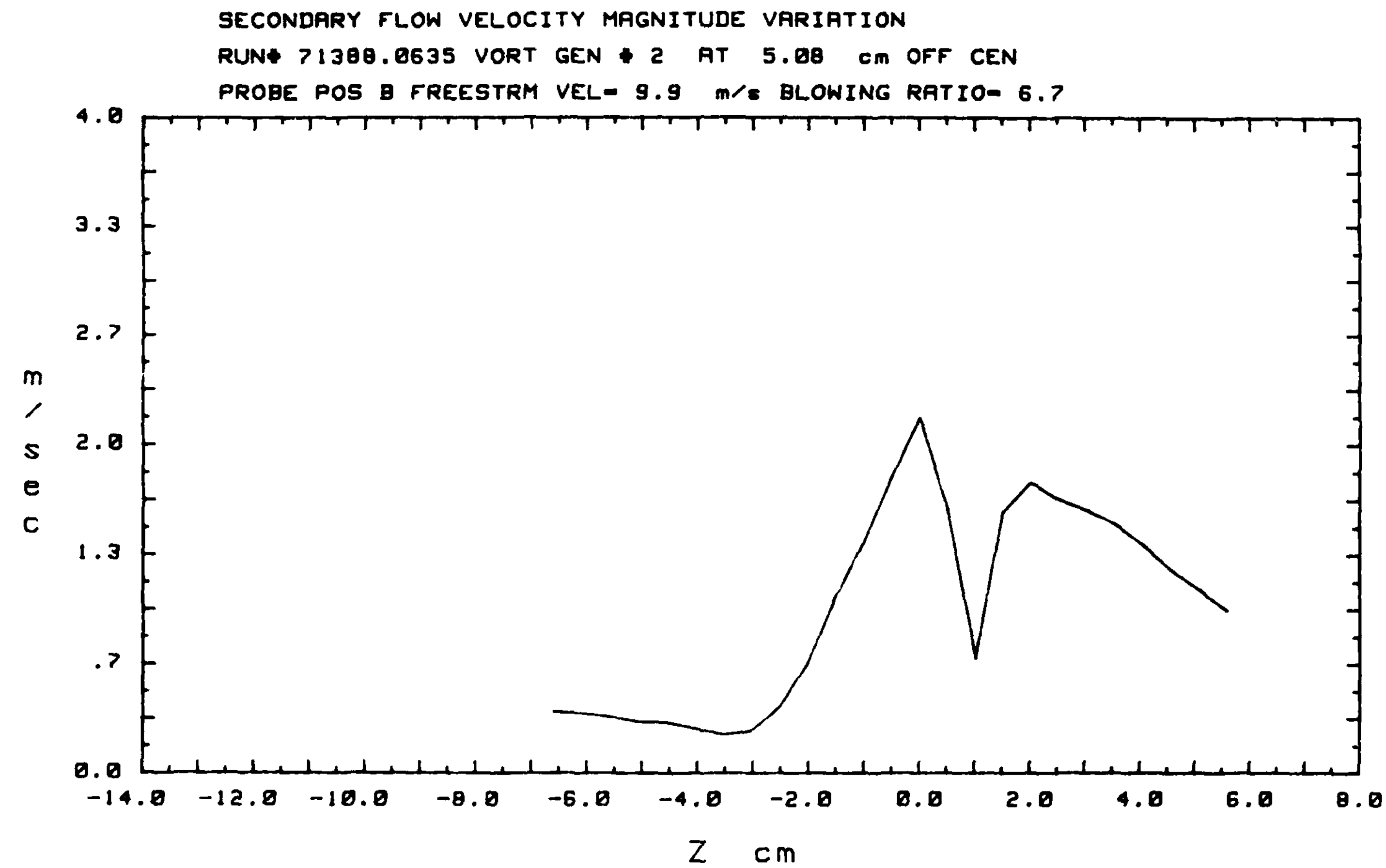

Figure 203. Secondary Flow Velocity (Radially)

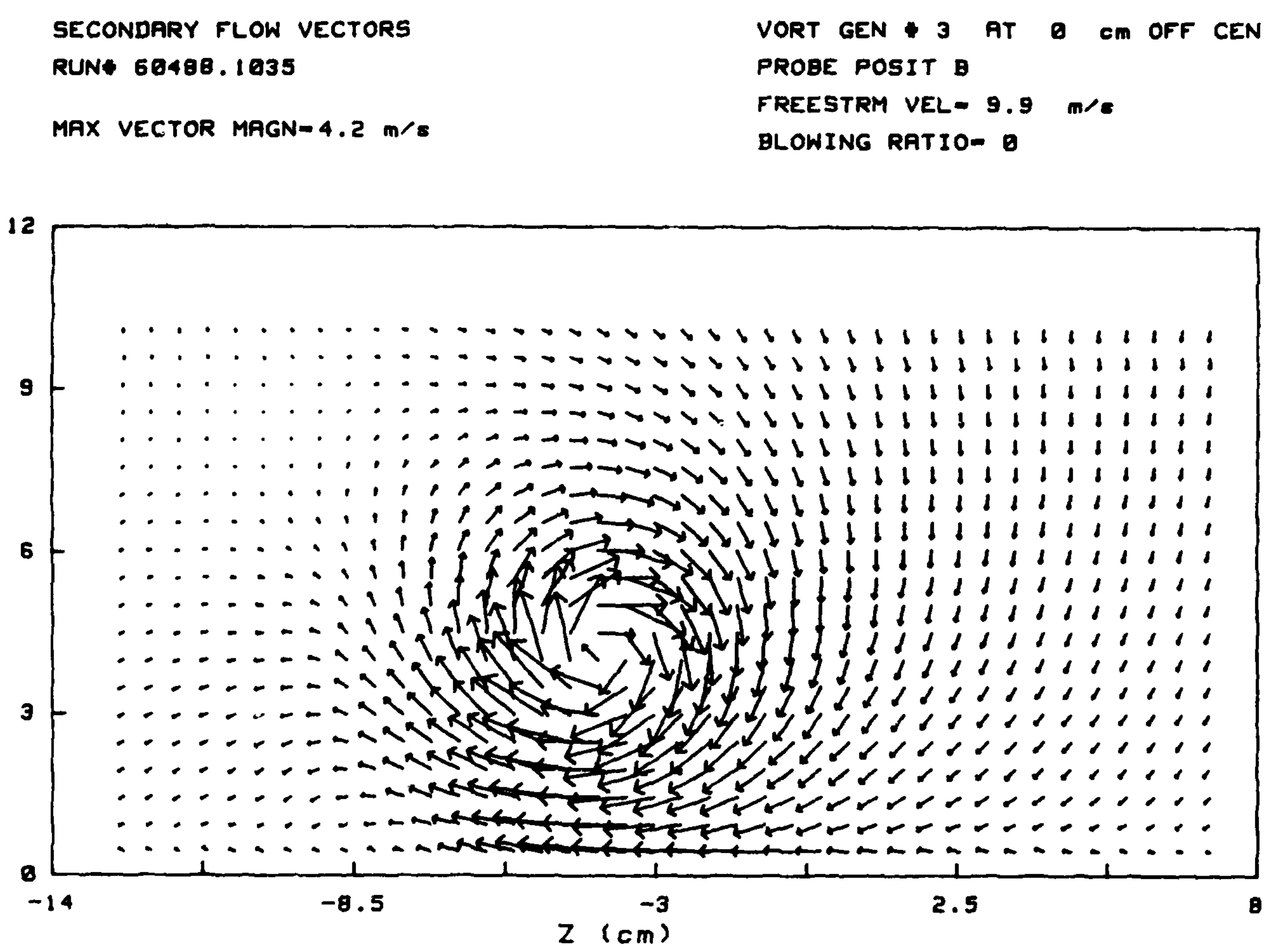

Figure 204. Secondary Flow Vectors

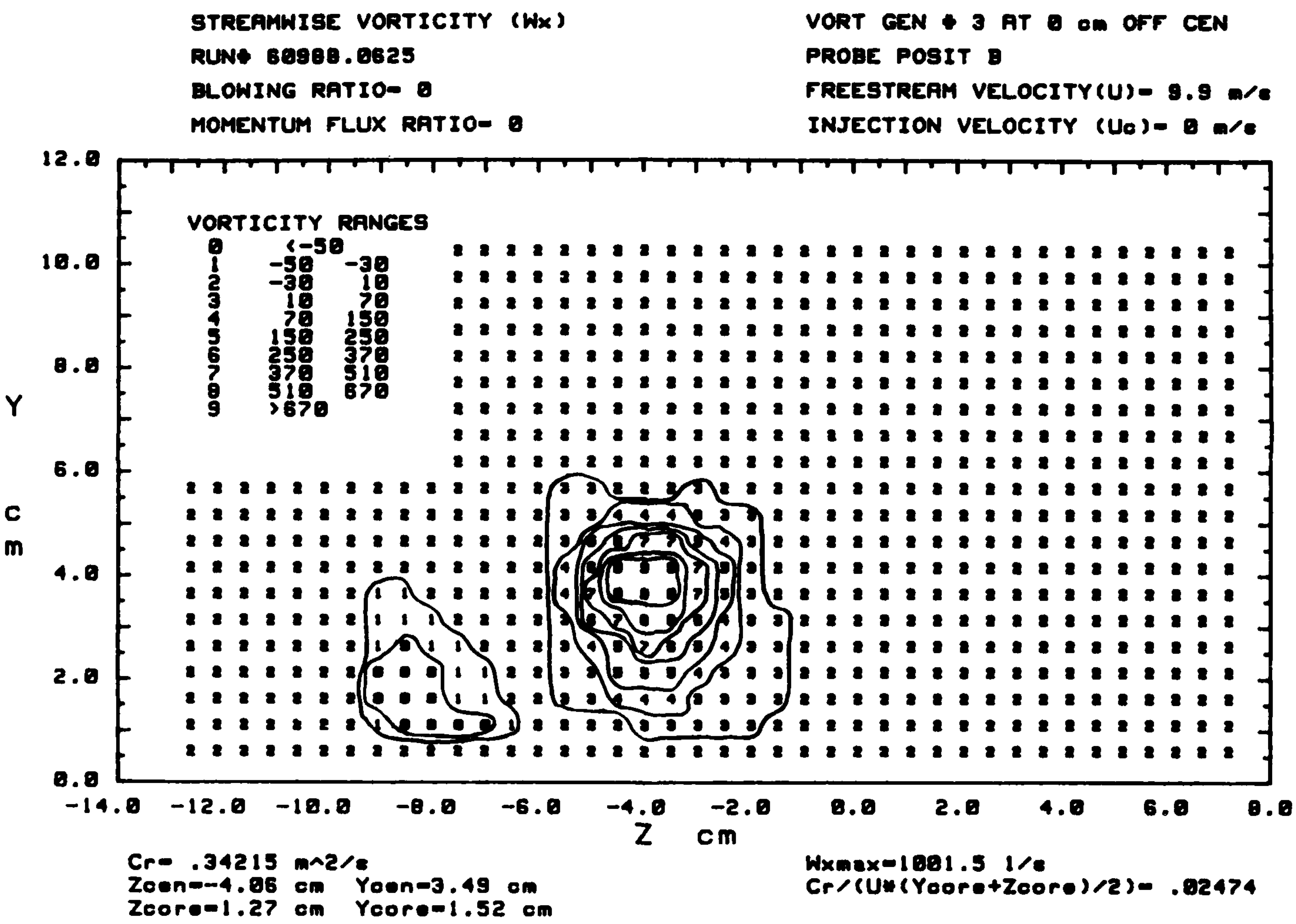

Figure 205. Streamwise Vorticity Contours

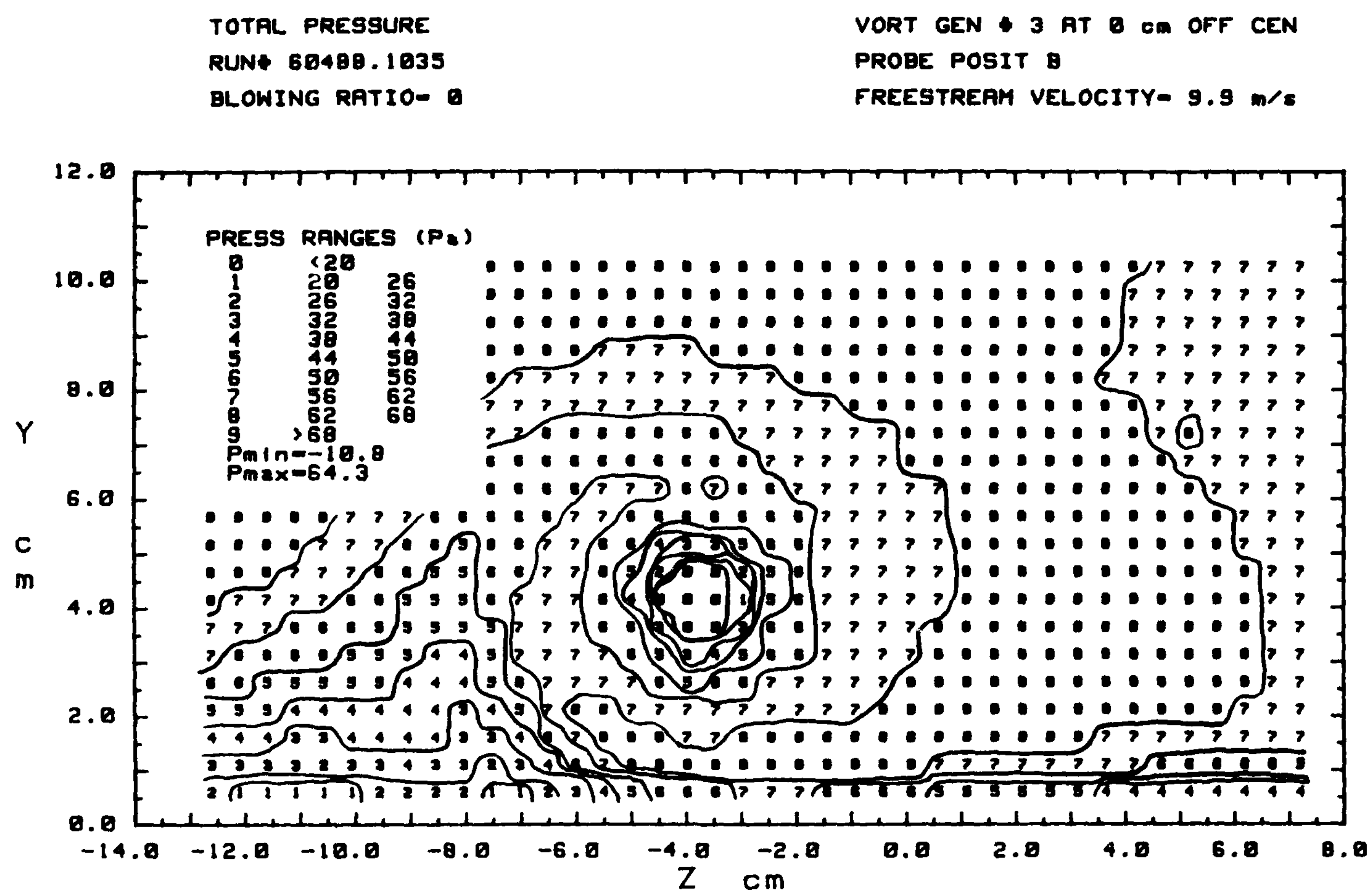

Figure 206. Total Pressure Contours

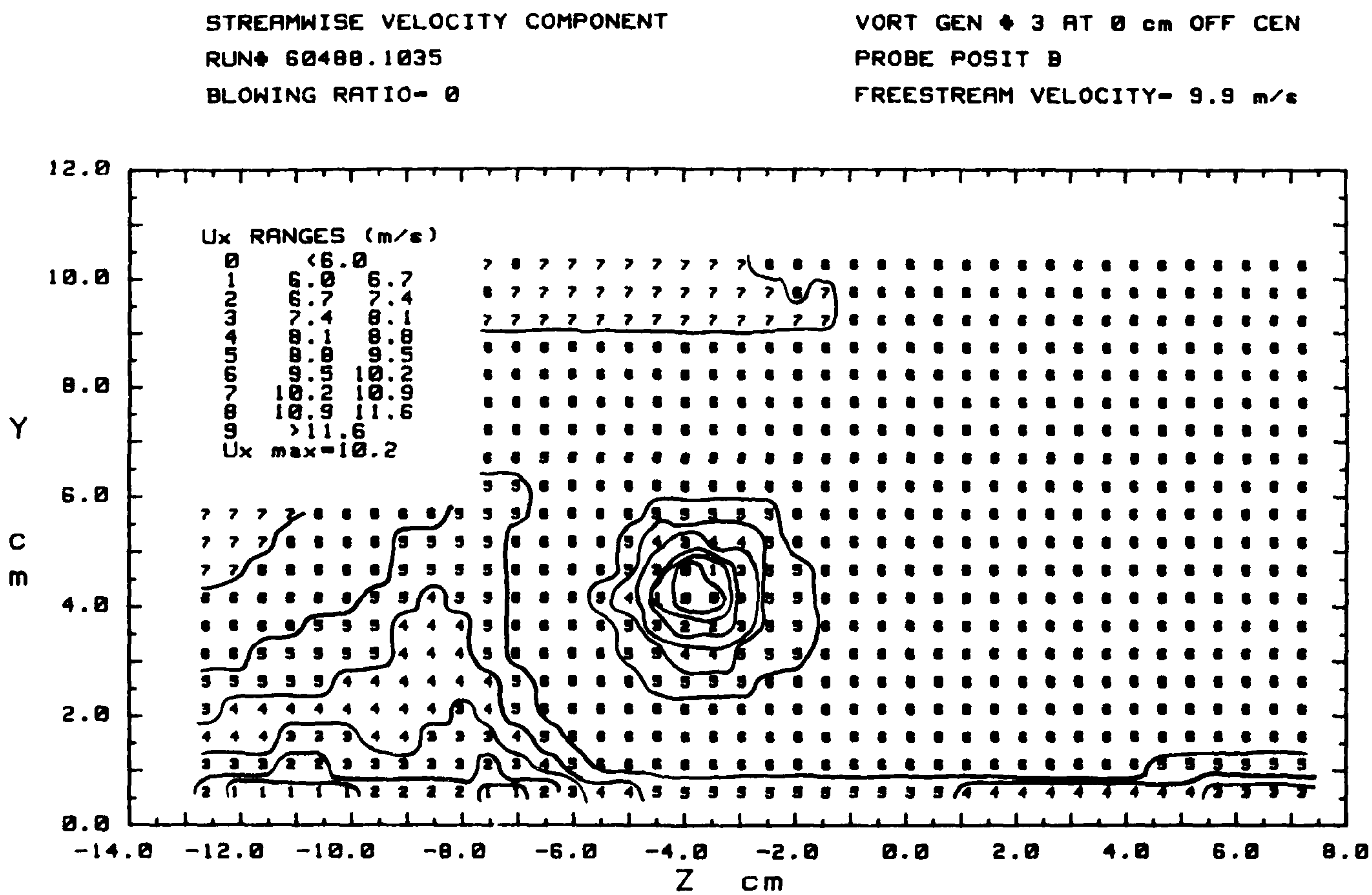

Figure 207. Streamwise Velocity Contours

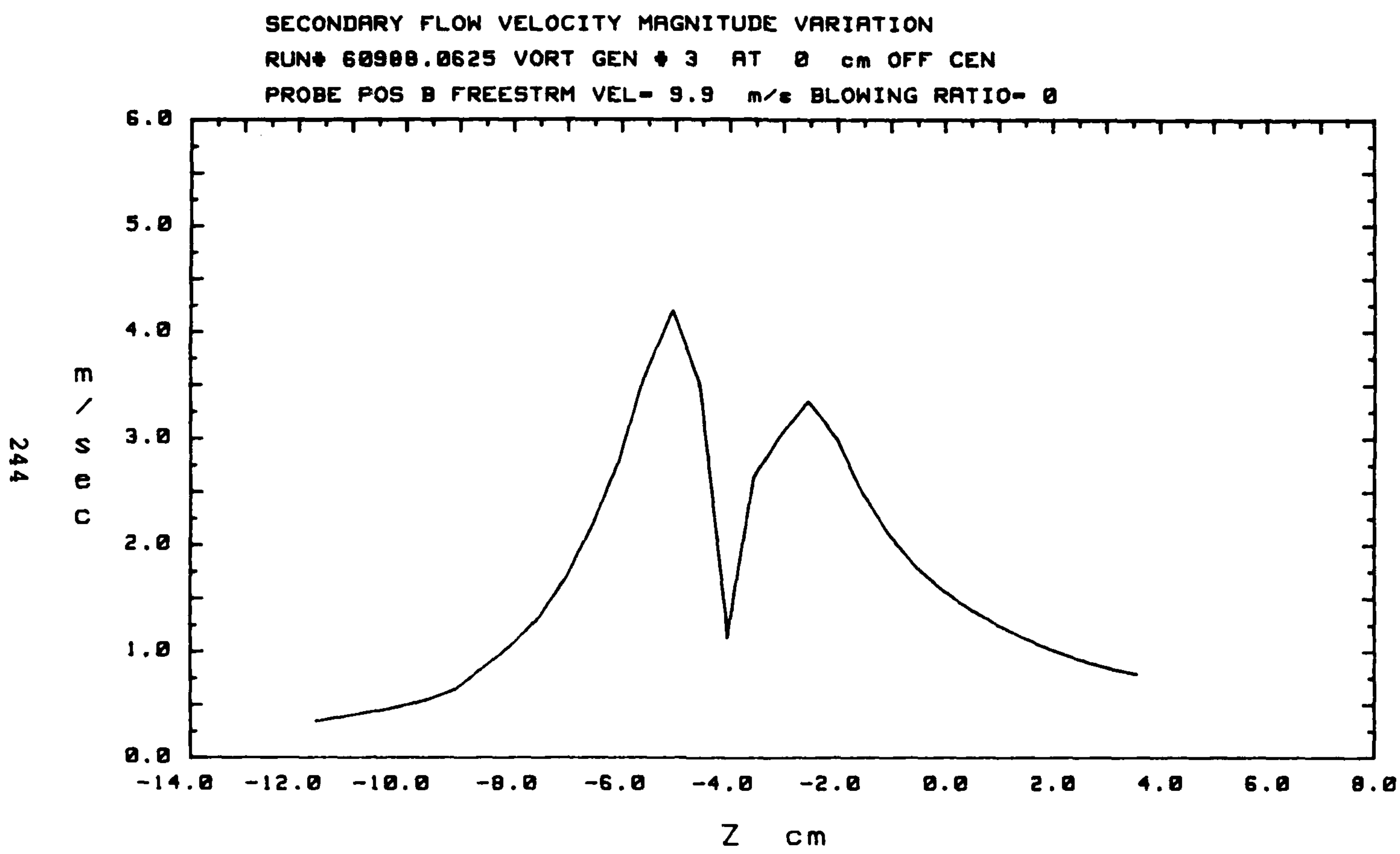

Figure 208. Secondary Flow Velocity (Radially)

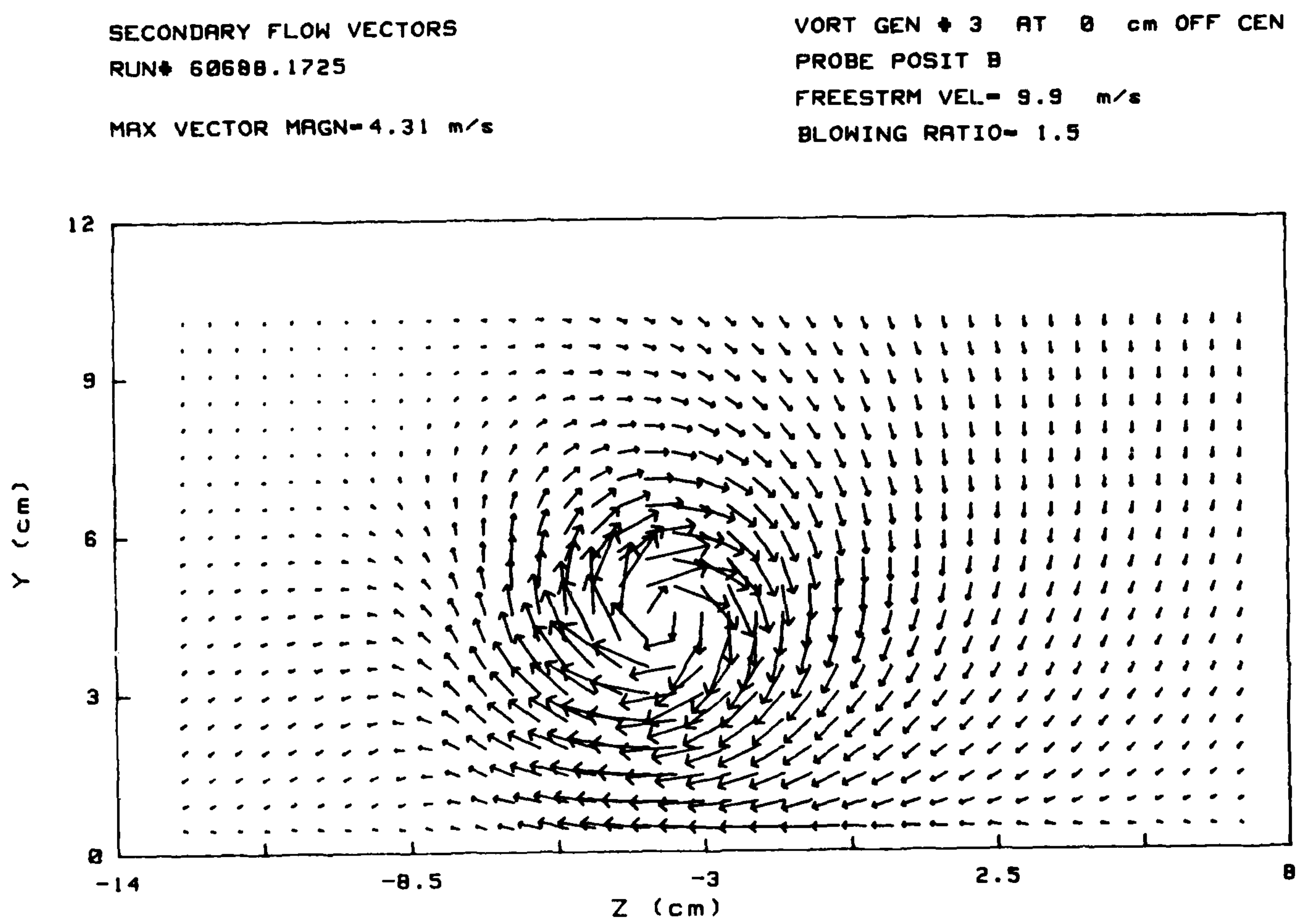

Figure 209. Secondary Flow Vectors

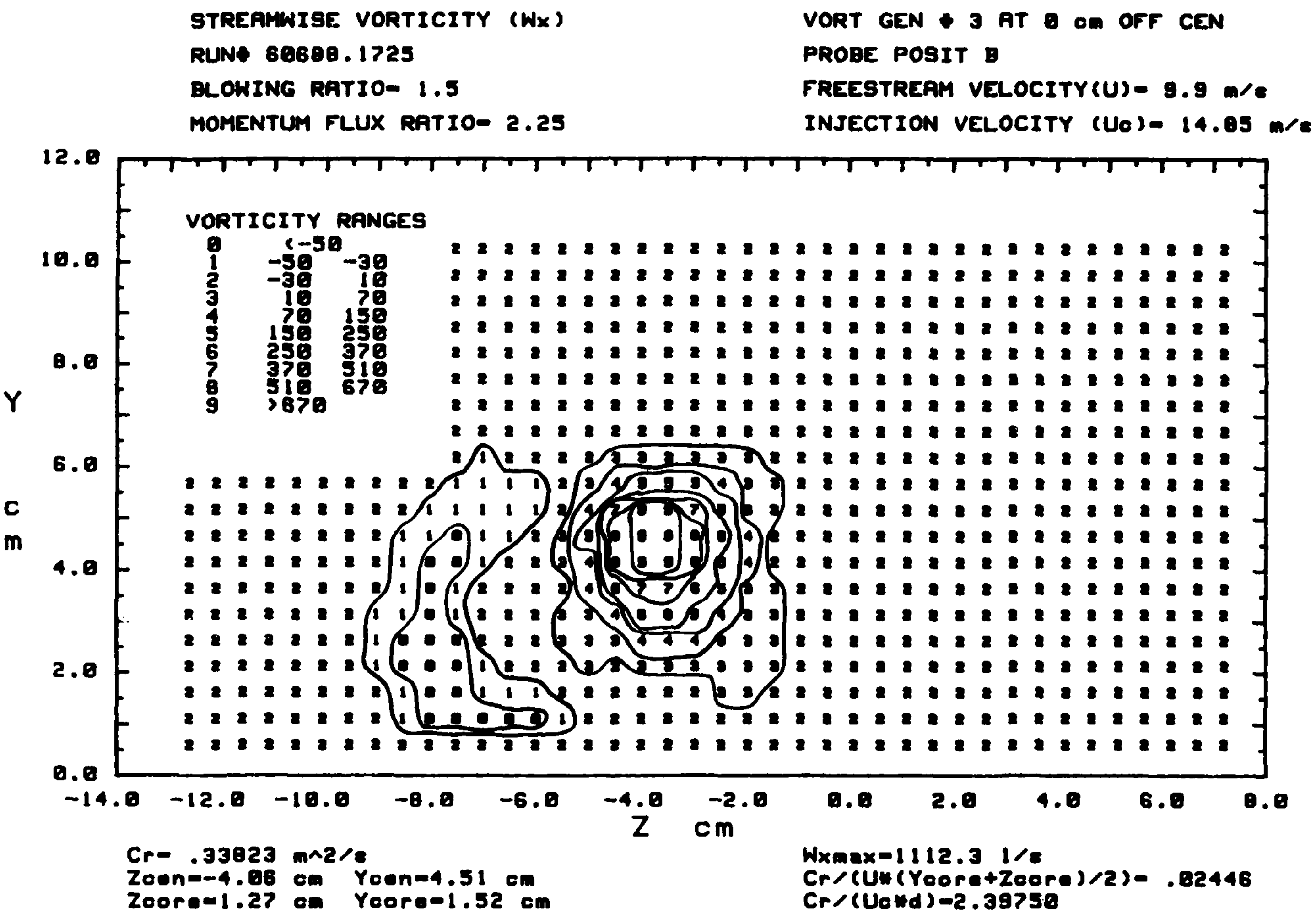

Figure 210. Streamwise Vorticity Contours

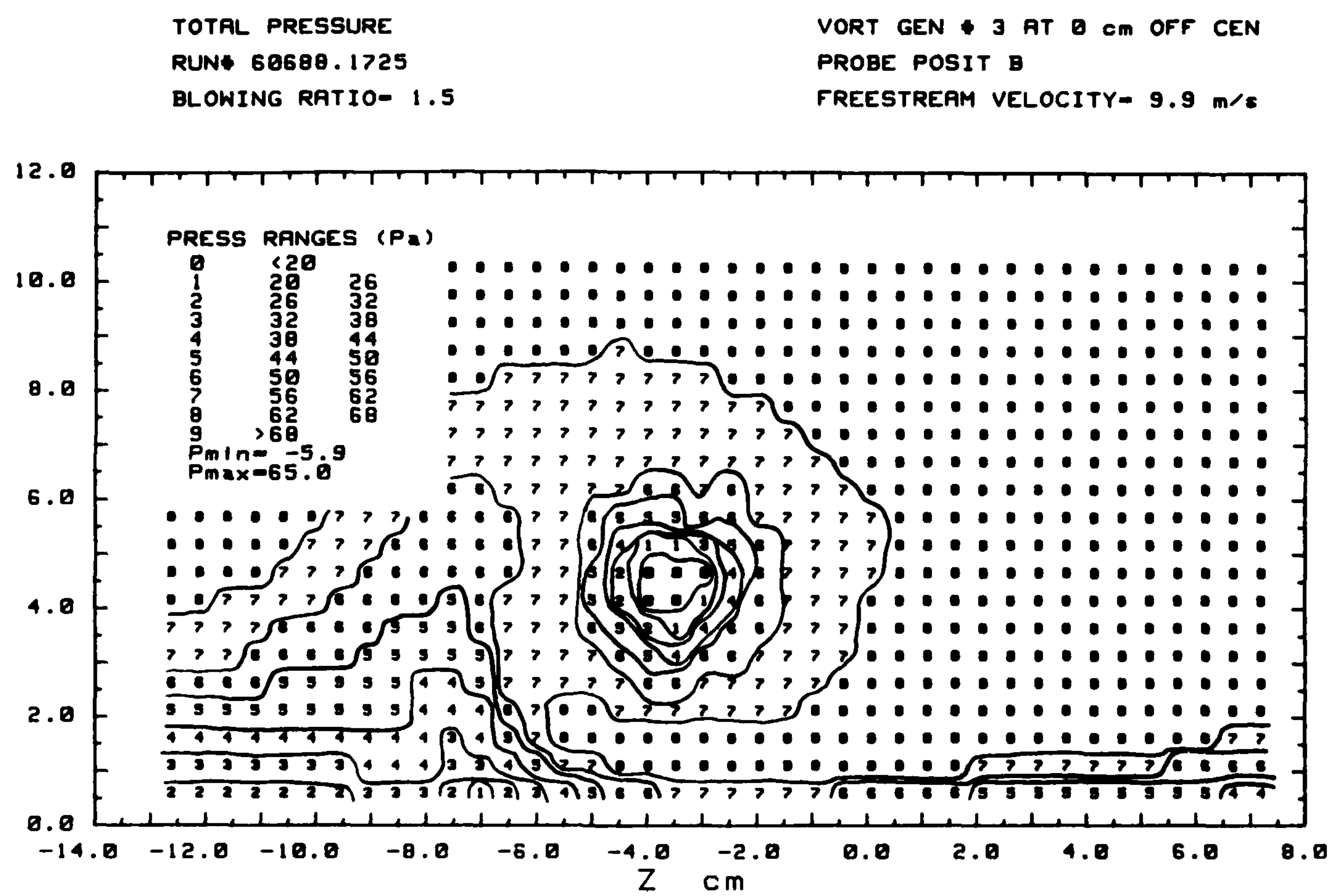

Figure 211. Total Pressure Contours

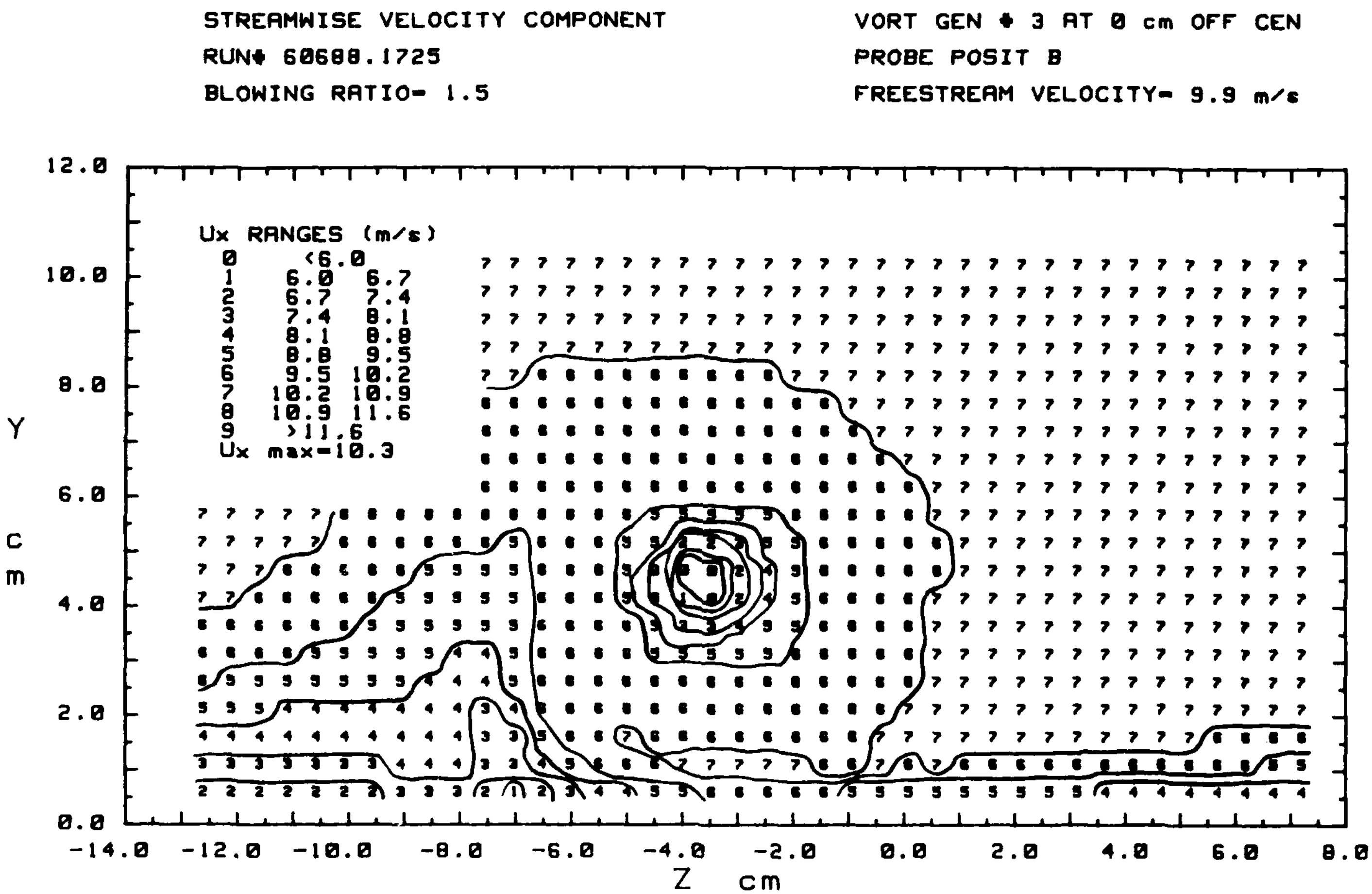

Figure 212. Streamwise Velocity Contours

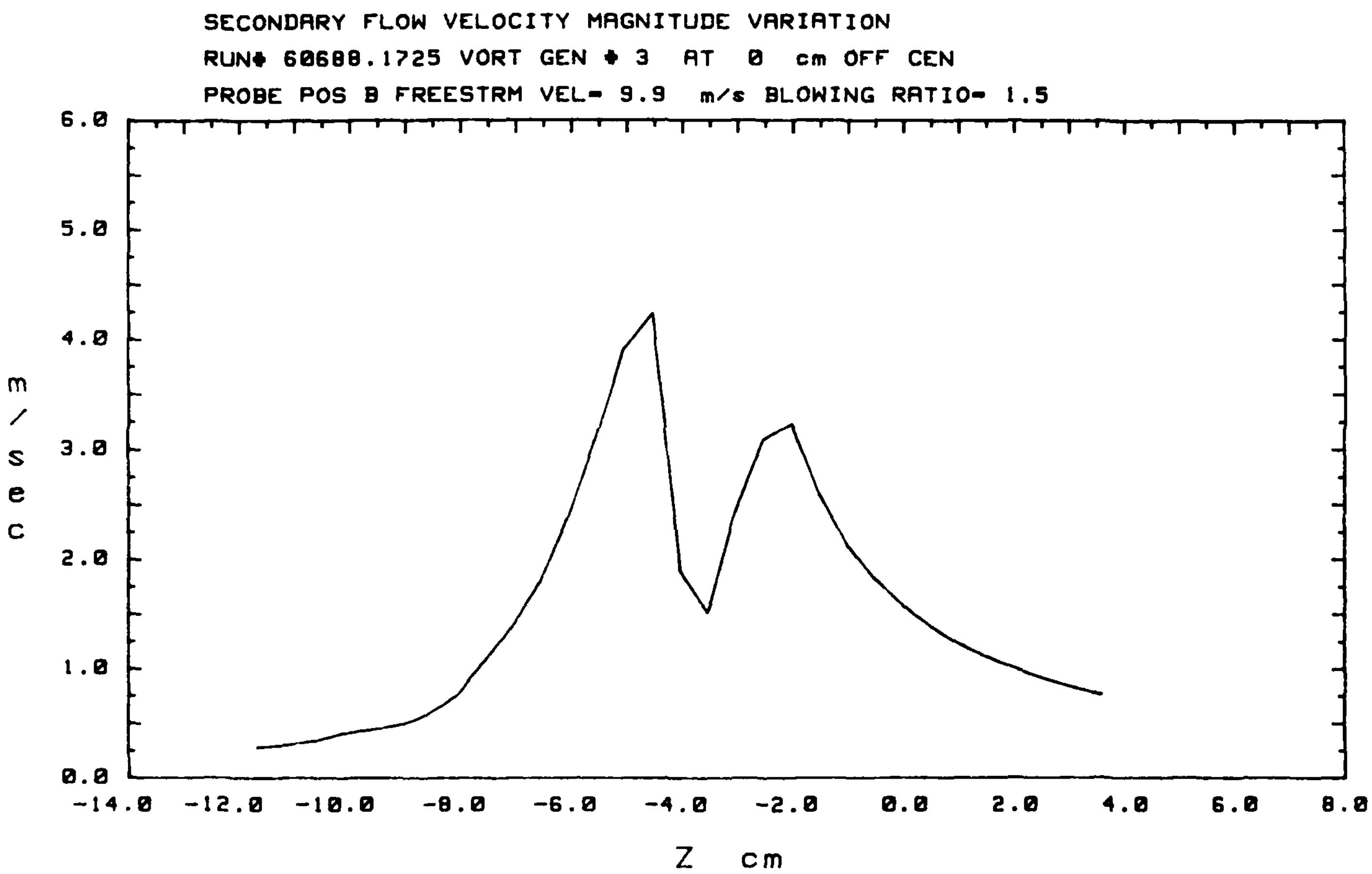

Figure 213. Secondary Flow Velocity (Radially)

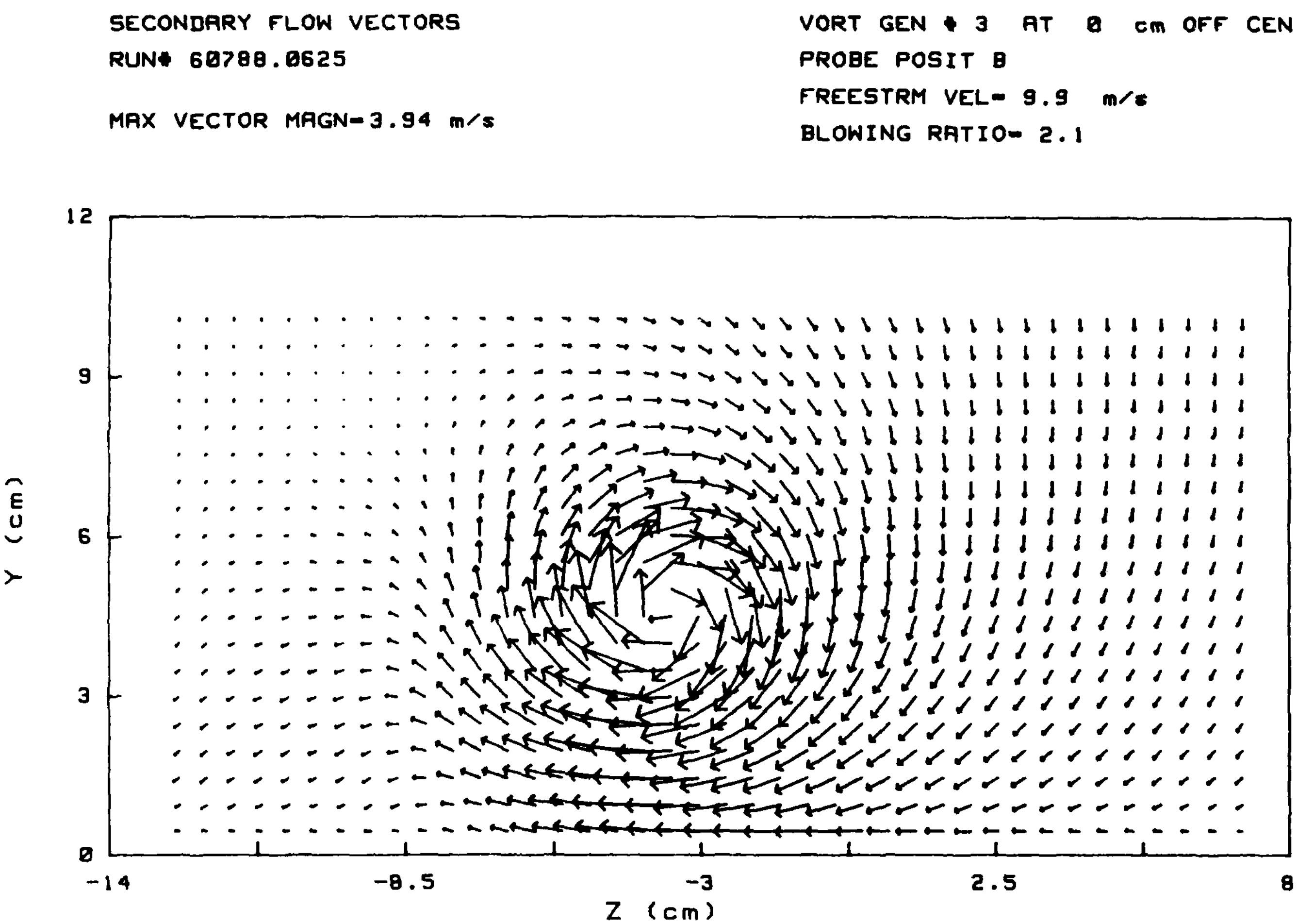

Figure 214. Secondary Flow Vectors

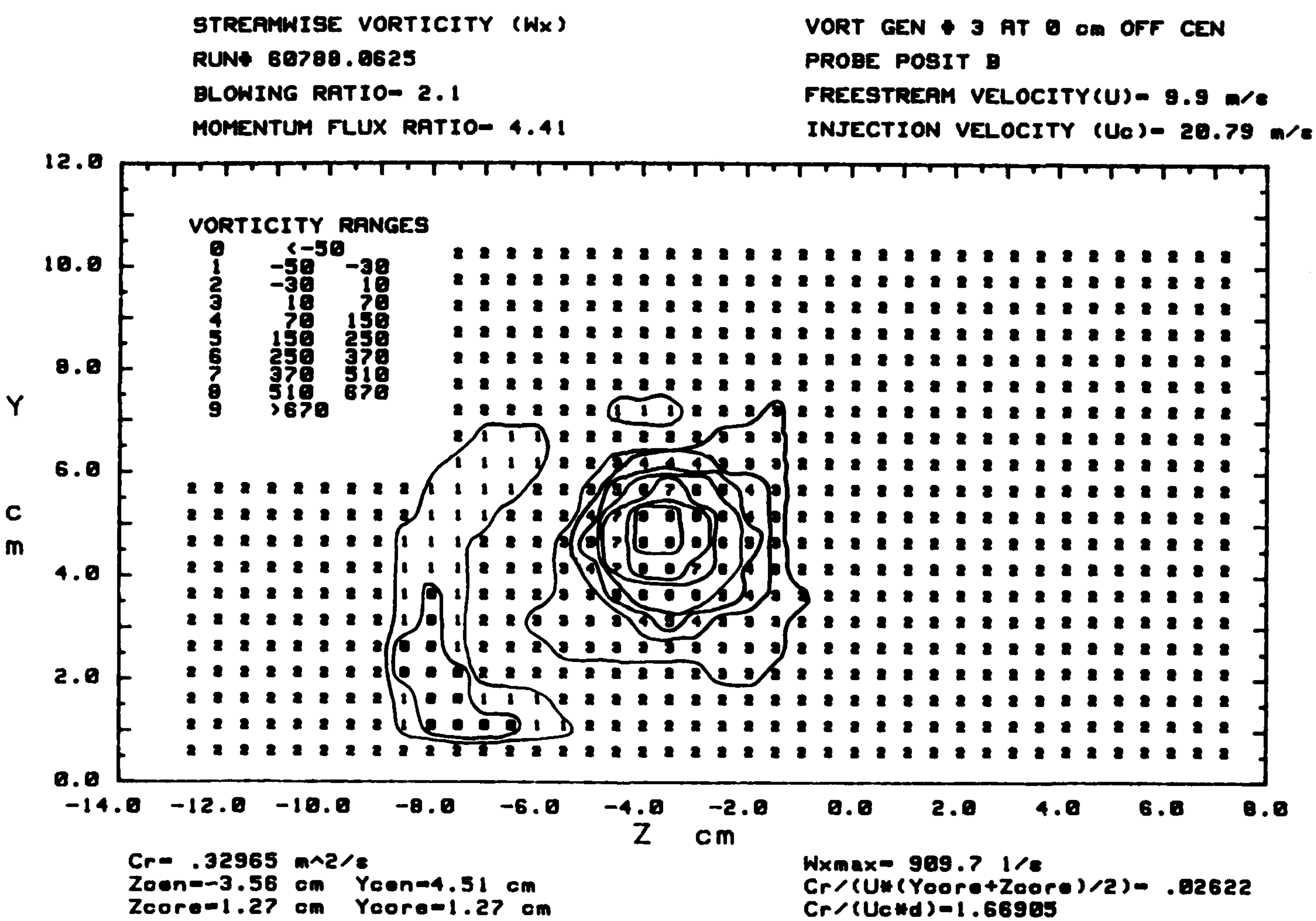

Figure 215. Streamwise Vorticity Contours

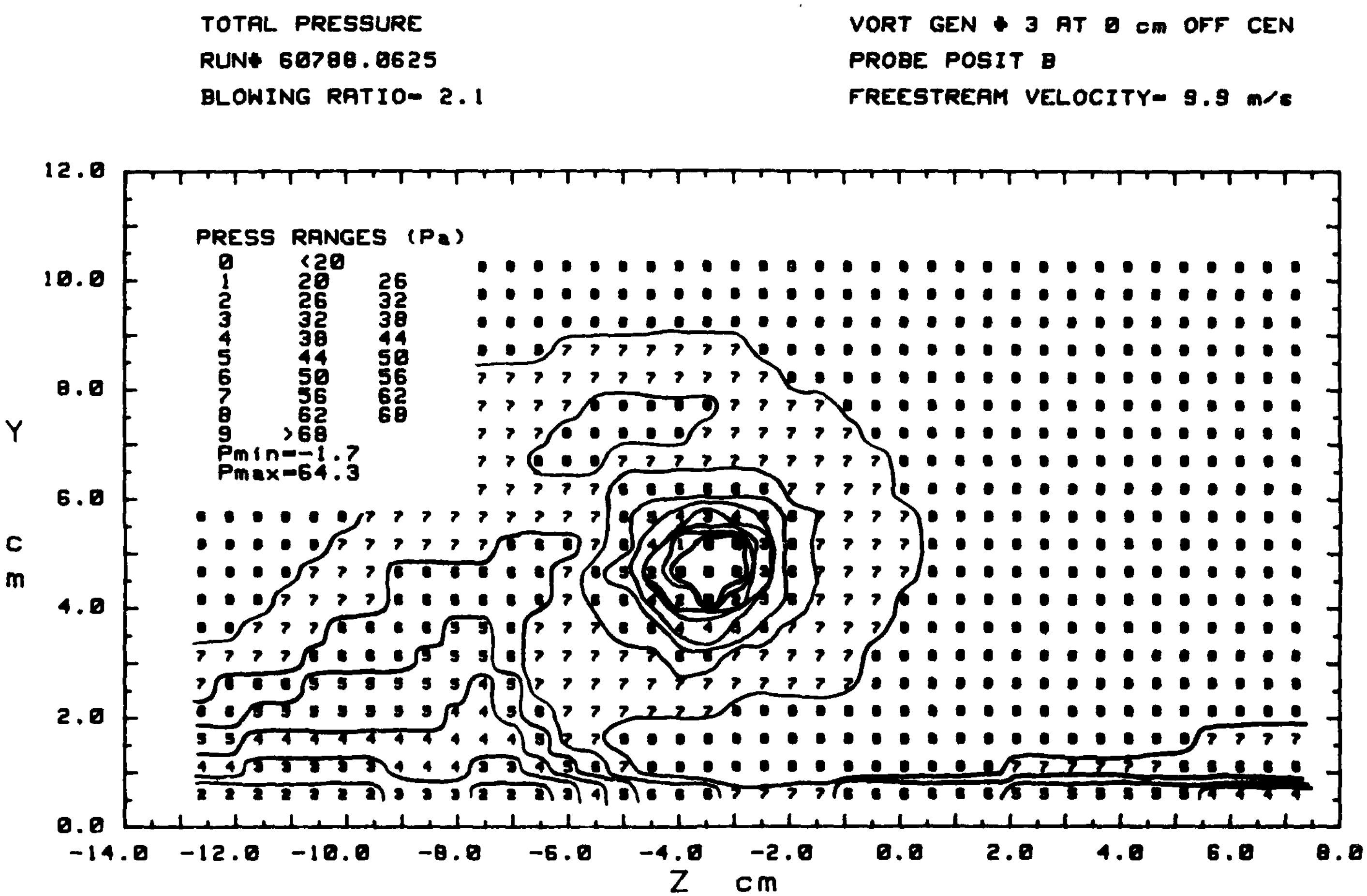

Figure 216. Total Pressure Contours

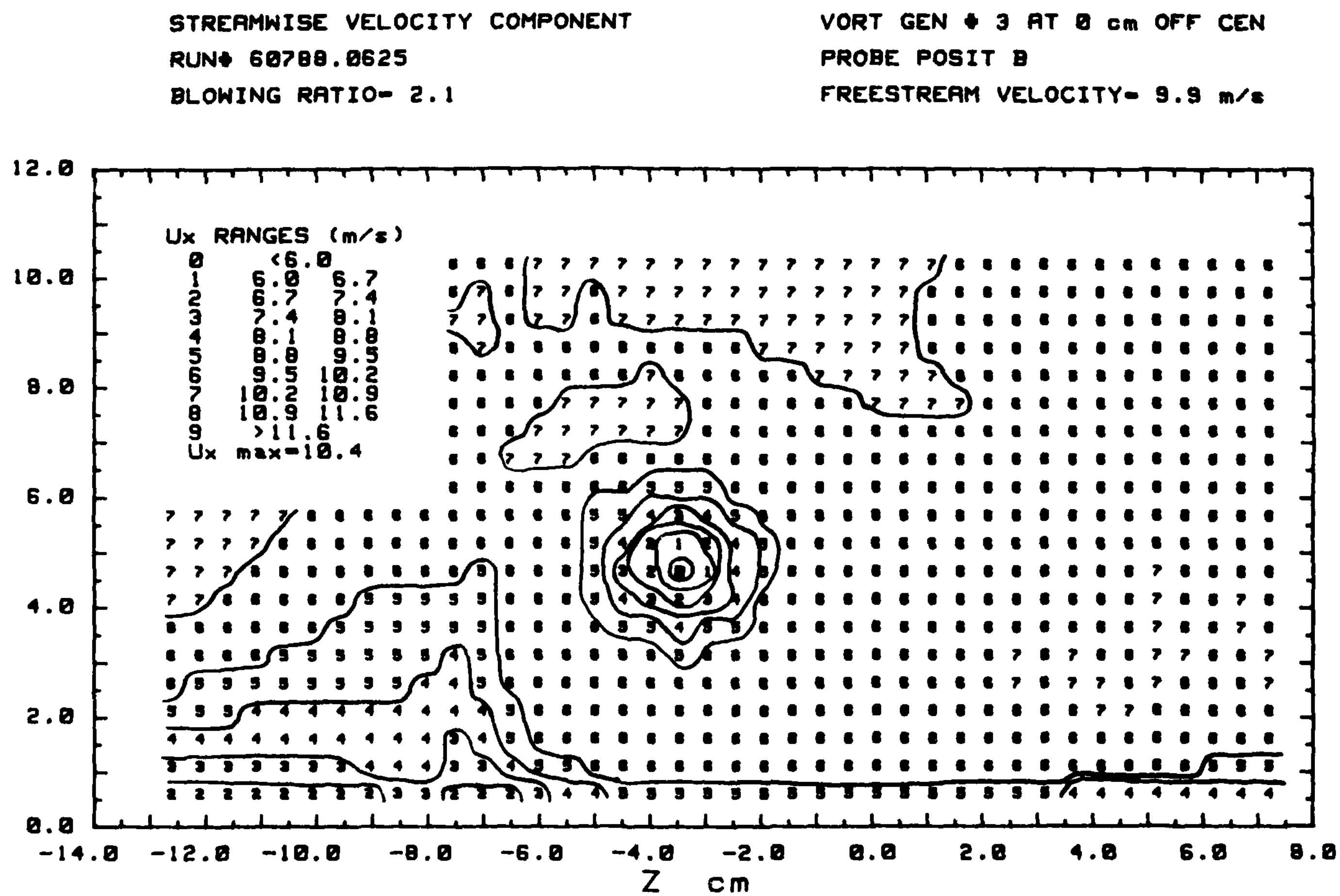

Figure 217. Streamwise Velocity Contours

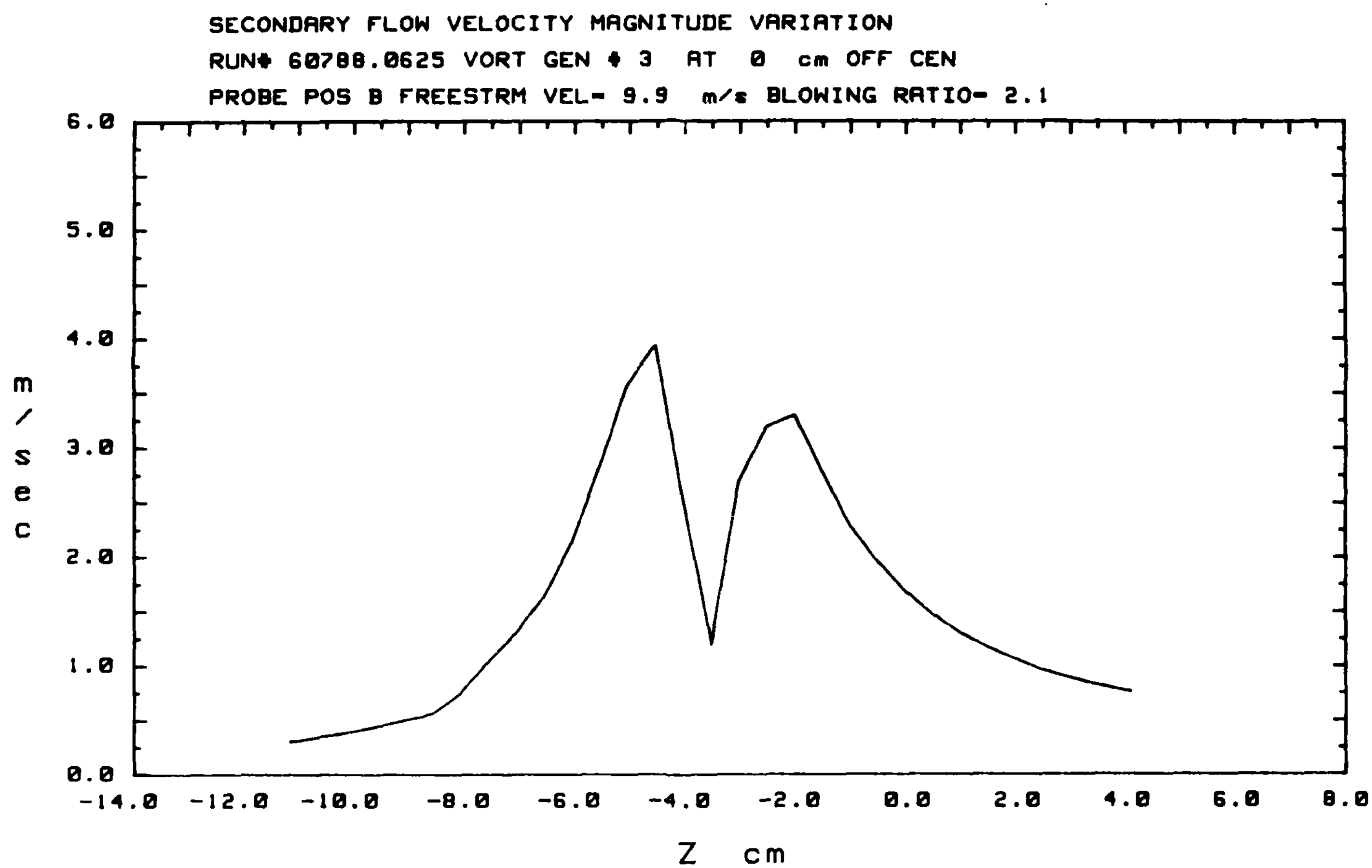

Figure 218. Secondary Flow Velocity (Radially)

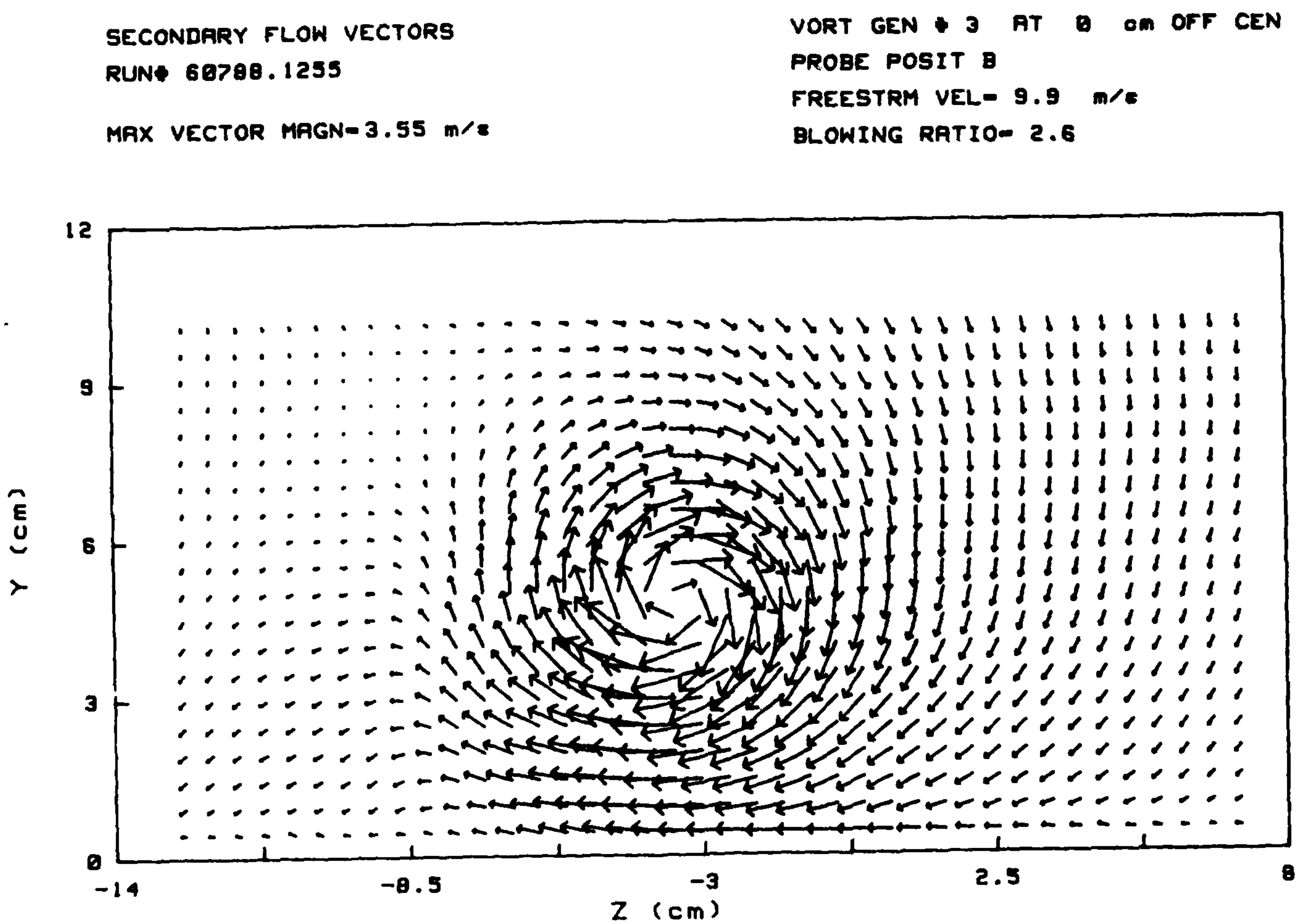

Figure 219. Secondary Flow Vectors

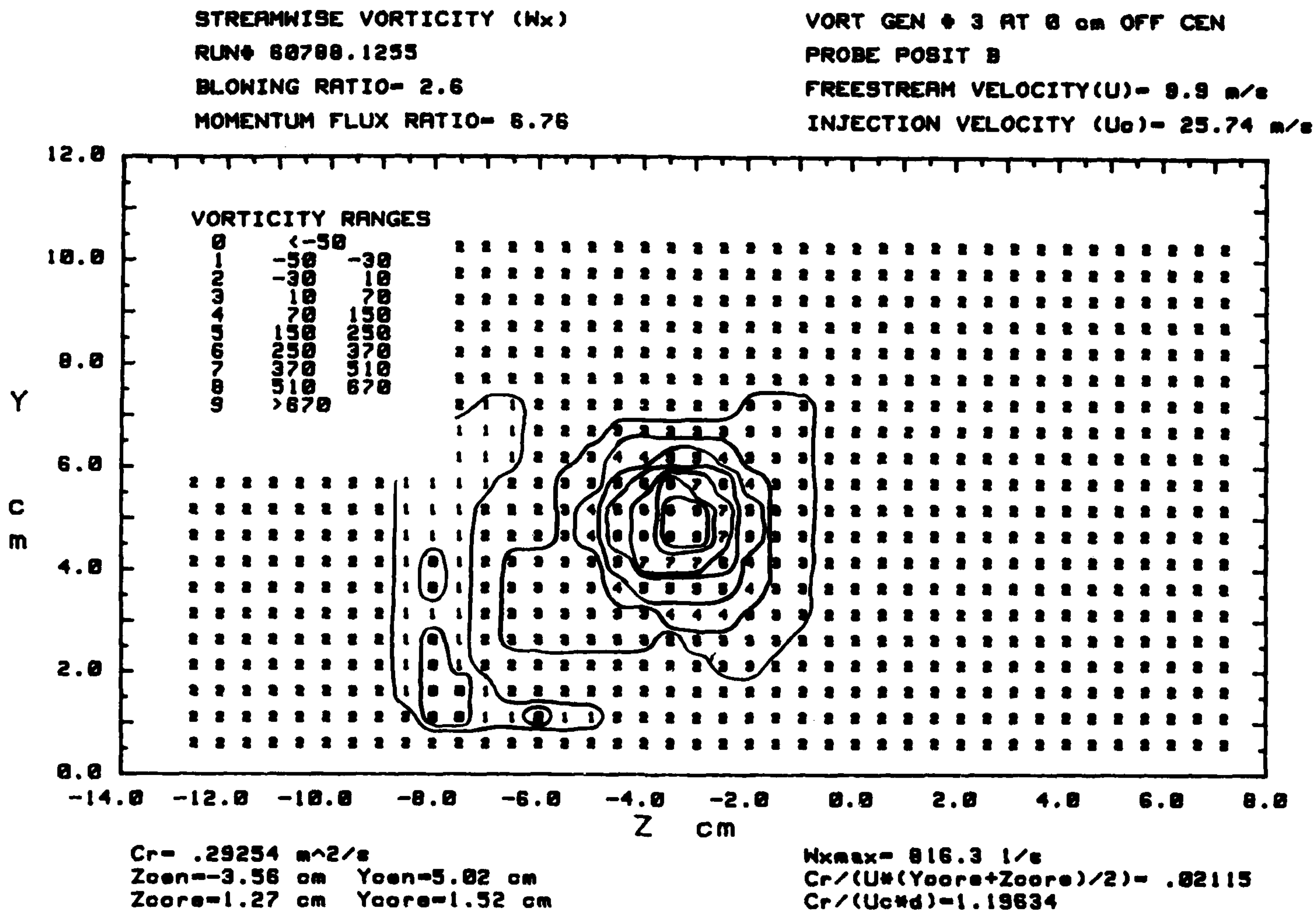

Figure 220. Streamwise Vorticity Contours

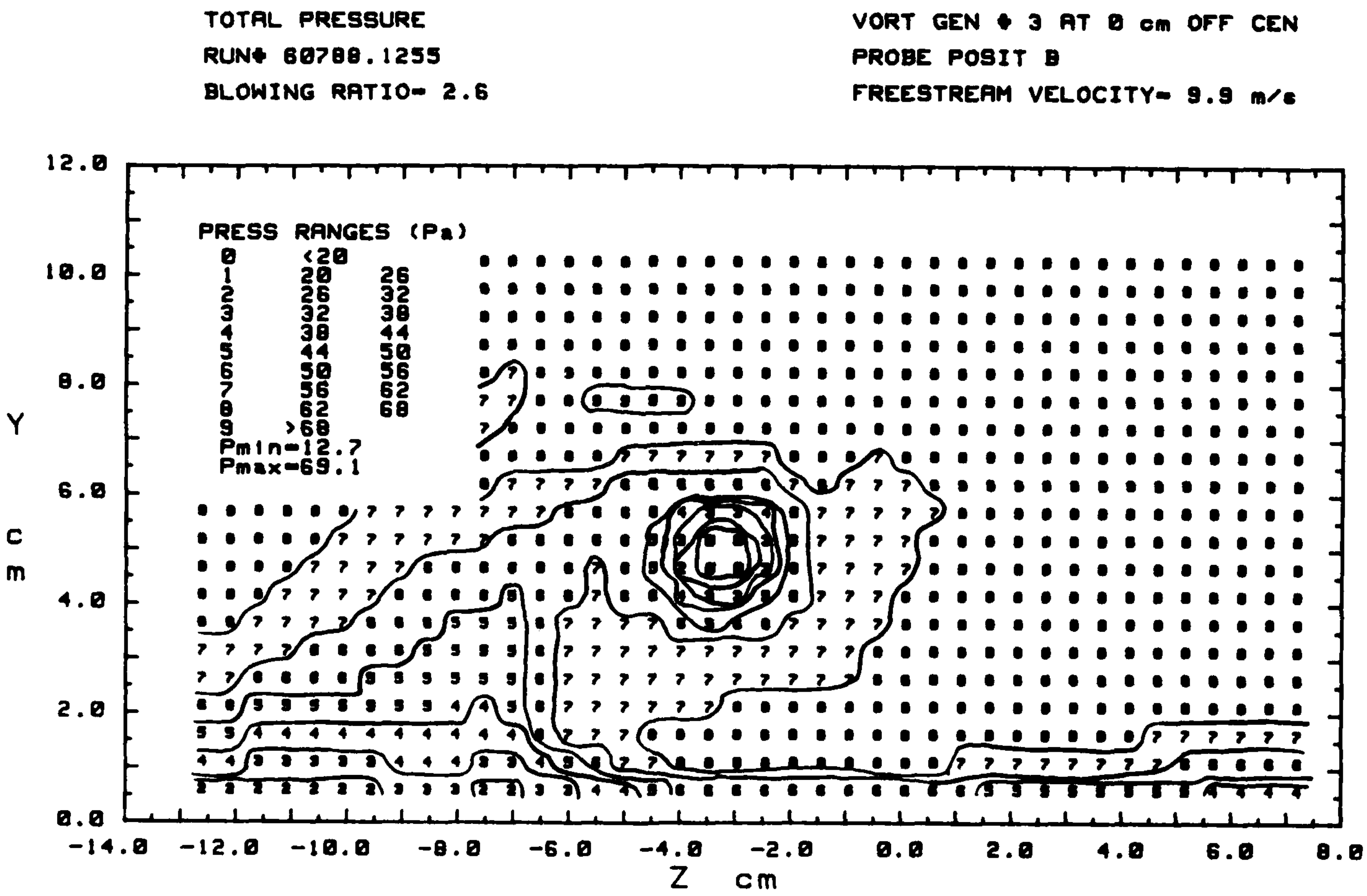

Figure 221. Total Pressure Contours

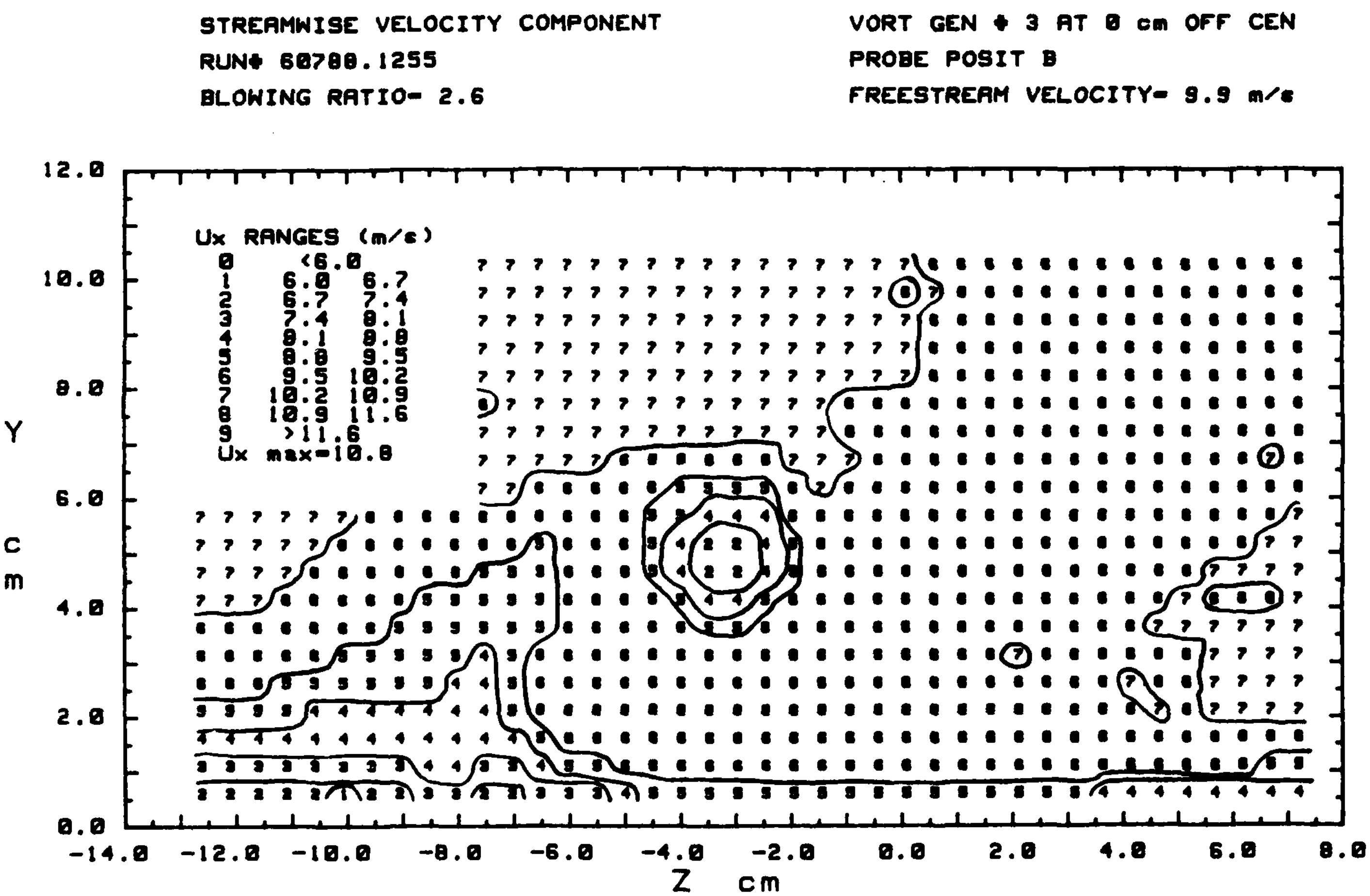

Figure 222. Streamwise Velocity Contours

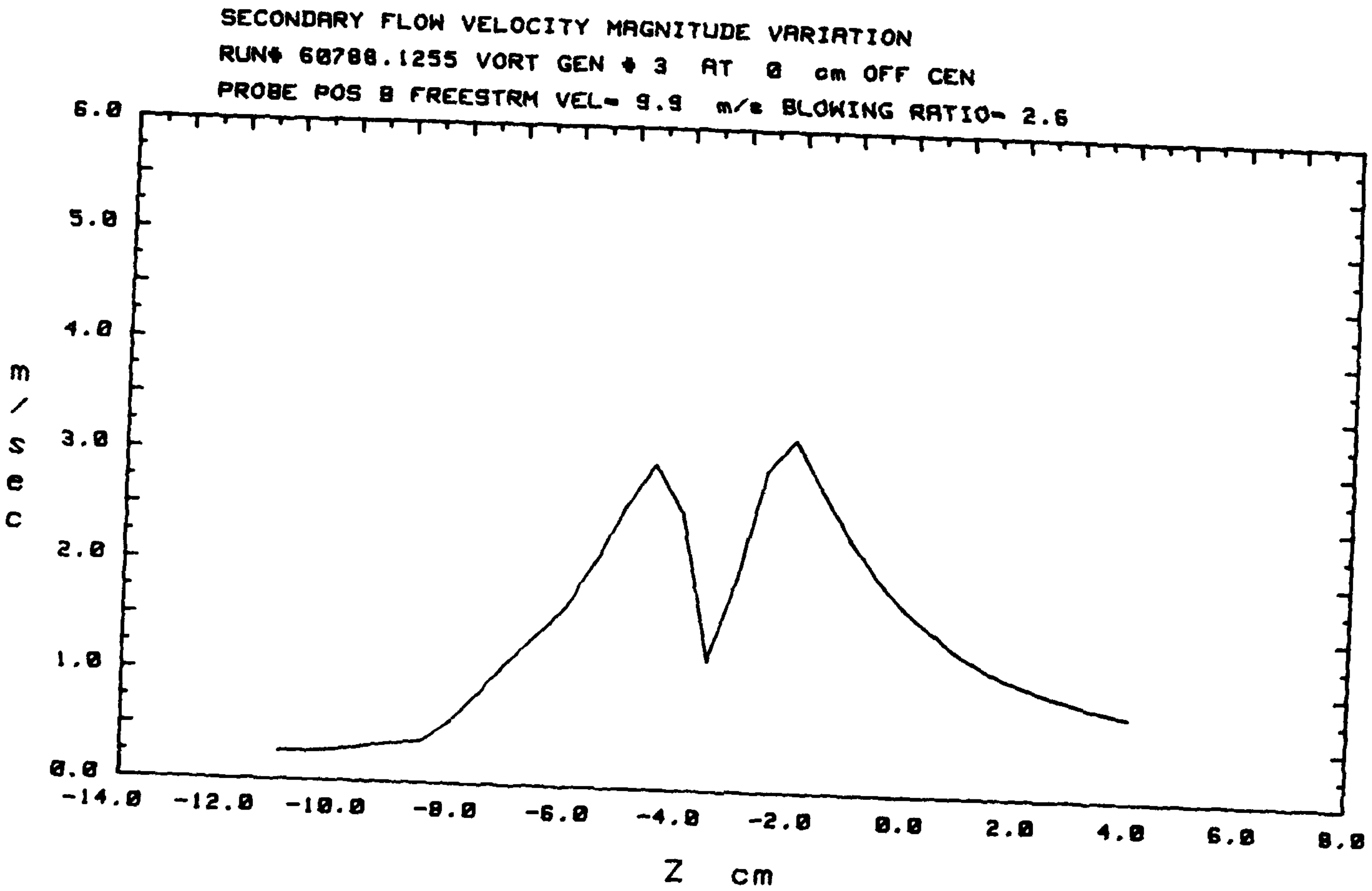

Figure 223. Secondary Flow Velocity (Radially)

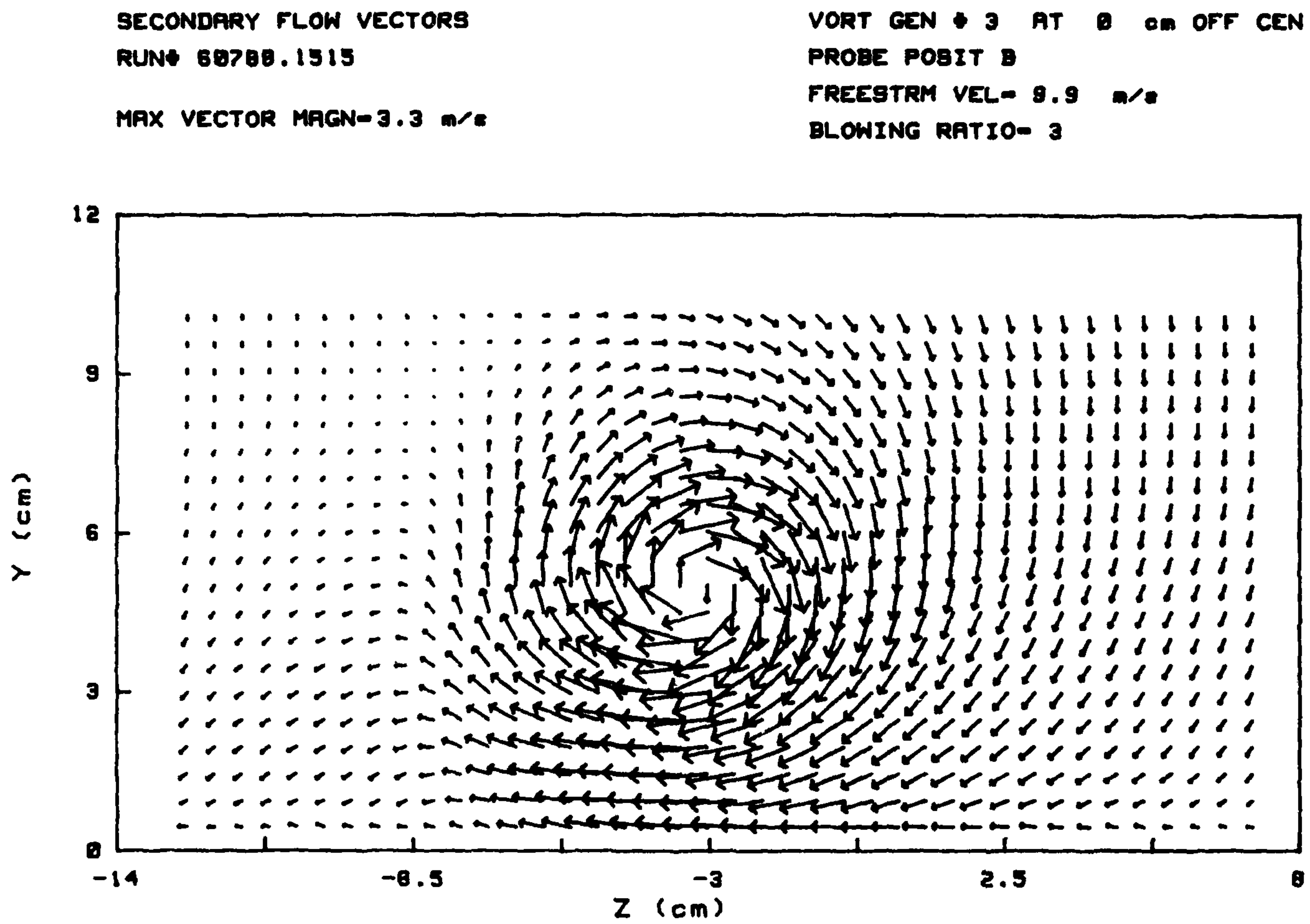

Figure 224. Secondary Flow Vectors

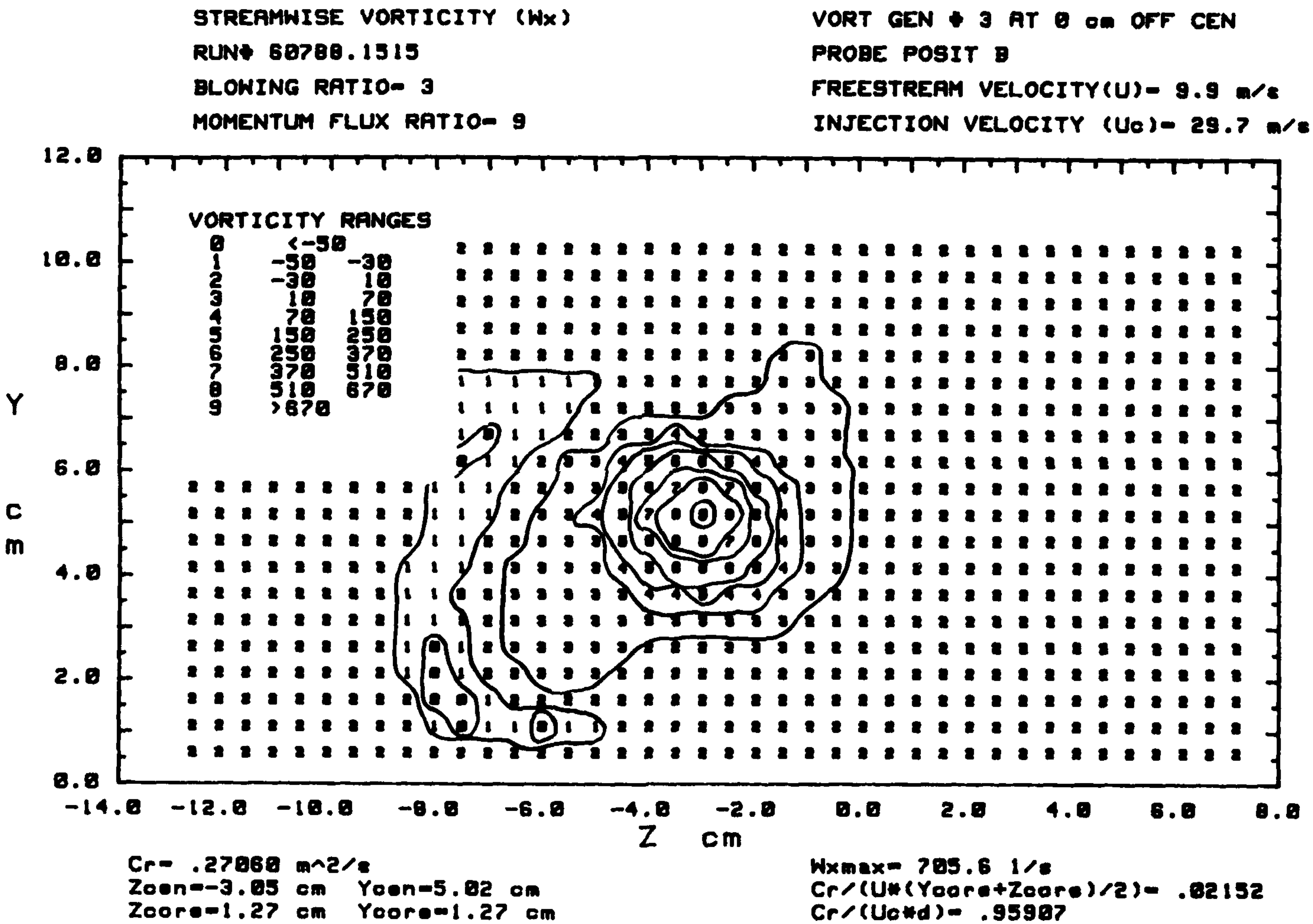

Figure 225. Streamwise Vorticity Contours

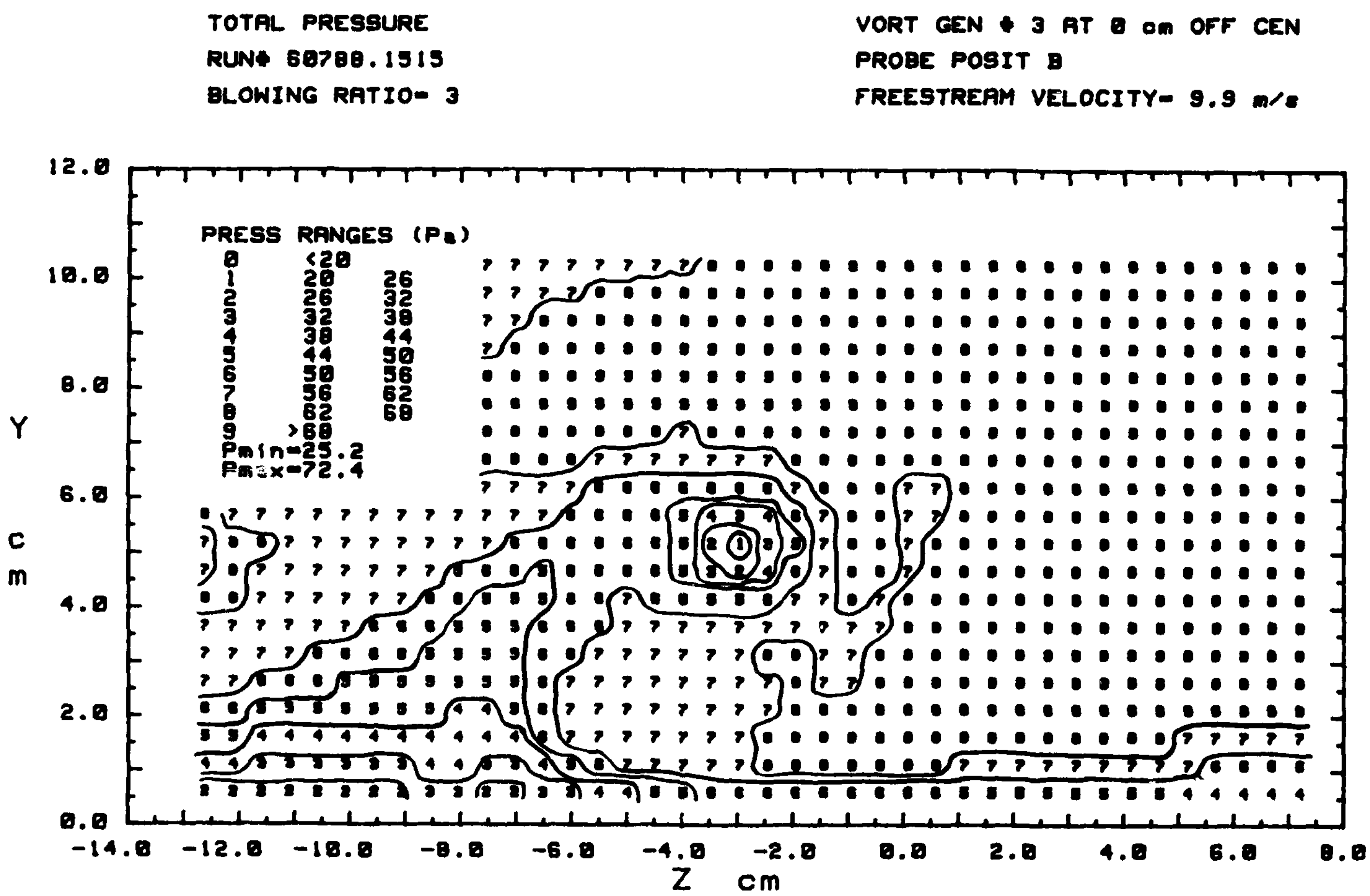

Figure 226. Total Pressure Contours

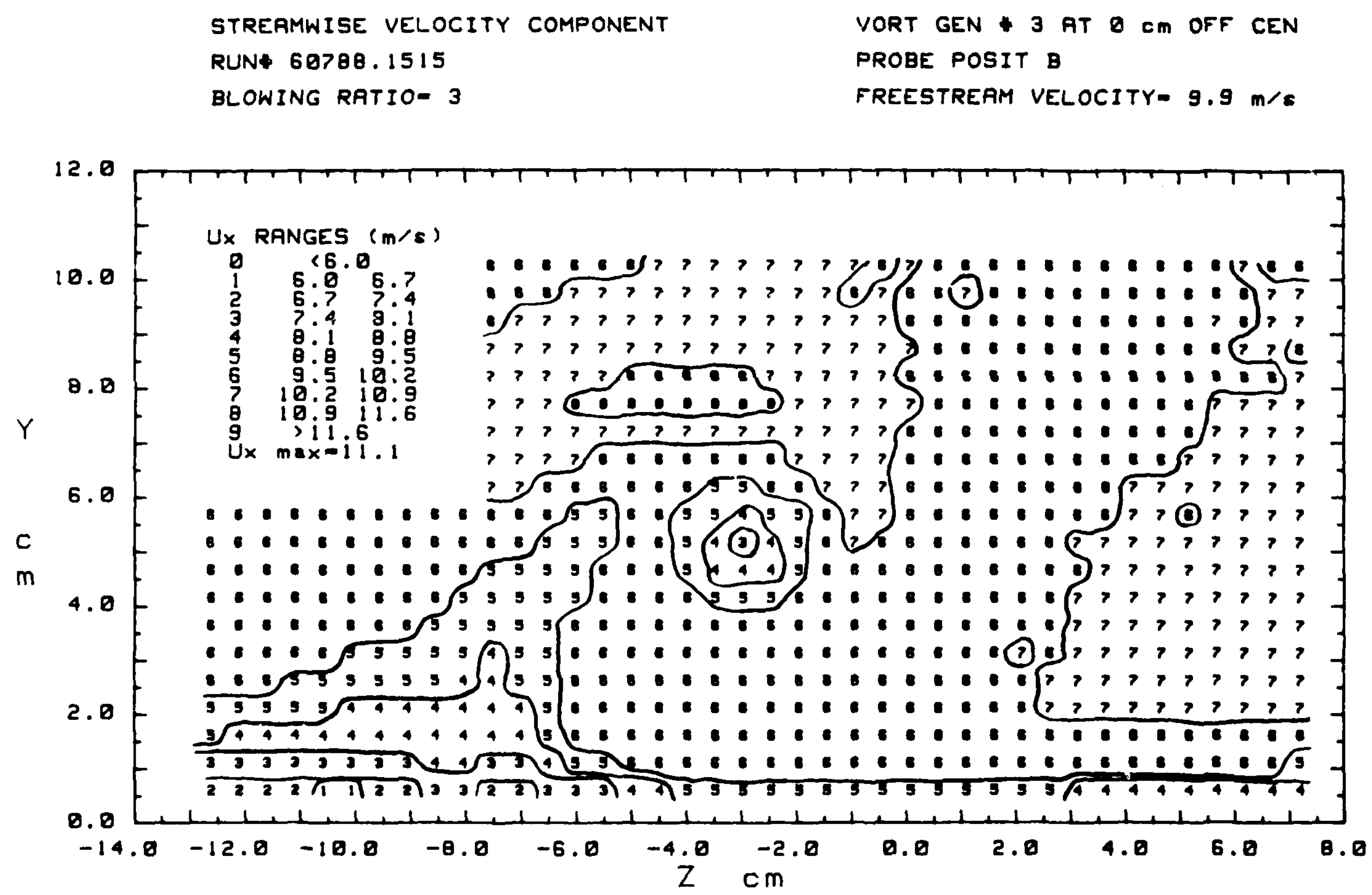

Figure 227. Streamwise Velocity Contours

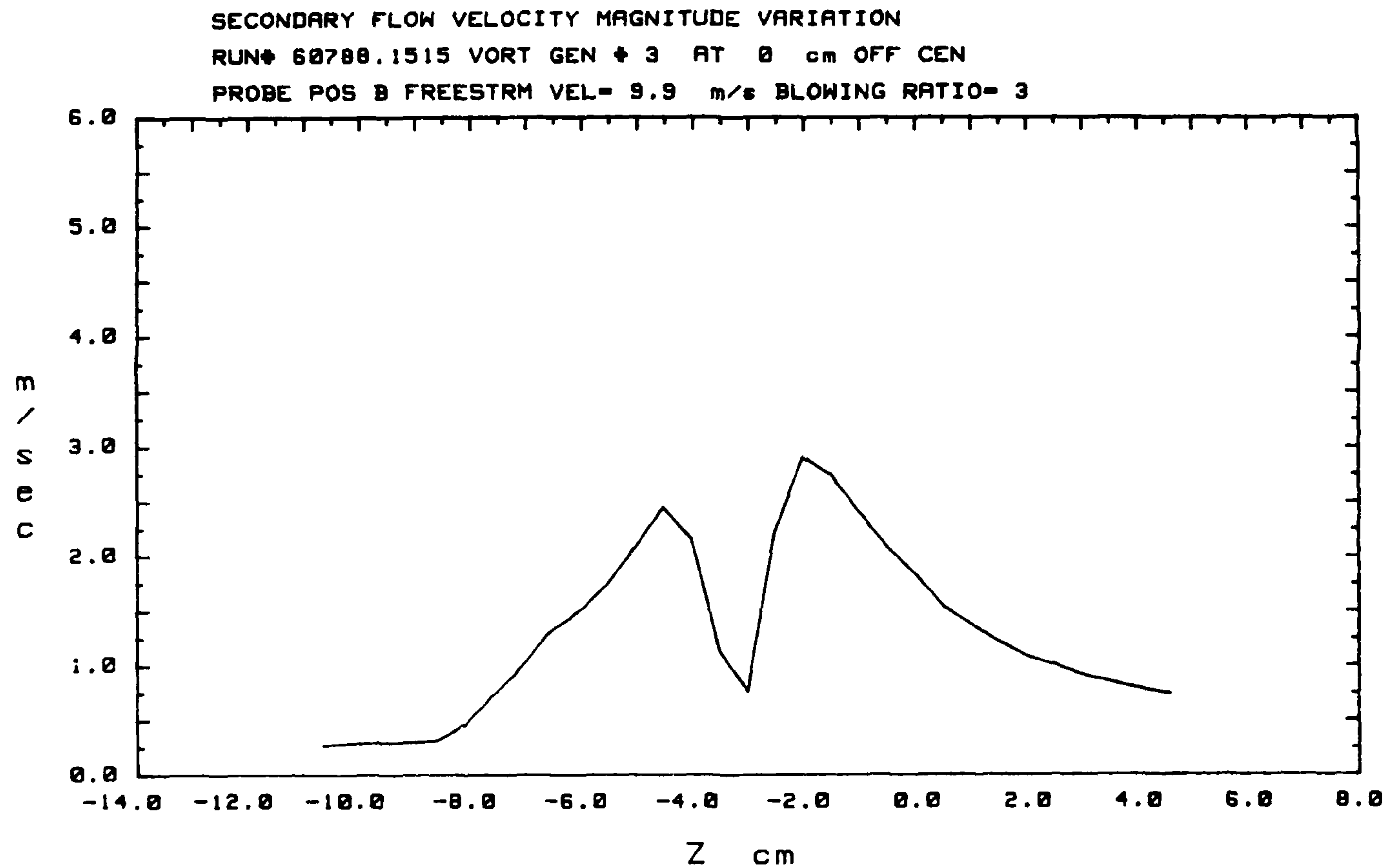

Figure 228. Secondary Flow Velocity (Radially)

APPENDIX B

SOFTWARE

Programs used in this study to acquire data and produce fluid mechanics and heat transfer plots were written in HP-BASIC and run on a Hewlett-Packard 9000-236 computer. Contributors to the software were the author, Professor P. Ligrani, Dr. B. Singer, S. Joseph, A. Ortiz, D. Evans, W. Williams, and L. Baun. Graphs of general parameter behavior were made by the author using program EASYPLOT and the Naval Postgraduate School IBM 3278-2 computer. HP-BASIC software descriptions follow (program name, description).

Program Name	Description
FIVEHOLE	Acquires raw data from five-hole pressure probe
PADJUST	Takes input data from FIVEHOLE, makes spatial resolution corrections
VELOCITY	Takes input data from PADJUST, computes velocity components and total pressures
VECTOR	Takes input data from VELOCITY, plots secondary flow vectors and computes maximum secondary flow vector magnitude
VORCIRC	Takes input data from VELOCITY, computes and plots streamwise vorticity contours by finite difference approximation. Also computes maximum streamwise vorticity, vortex core coordinates in yz plane, average vortex core radius, circulation based on threshold vorticity of 100 s^{-1}, momentum flux ratio, injection velocity, and dimensionless circulation parameters

PTOT	Takes input data from VELOCITY, plots total pressure contours, computes maximum and minimum total pressure
UX	Takes input data from VELOCITY, plots streamwise mean velocity contours, computes maximum mean streamwise velocity
RADVEL	Takes input data from VELOCITY, plots secondary flow velocity (vector magnitude) radially (z direction) from vortex center
STANFC1	Acquires multiple channel thermocouple data and outputs temperatures for calculation of Stanton numbers with and without injection
STANFC2	Takes output from STANFC1 and calculates heat transfer coefficients and Stanton numbers for spanwise thermocouple locations at various streamwise positions, with and without injection
STANR	Takes output from STANFC2 and calculates Stanton number ratios: with vortex and injection to no vortex or injection; with vortex and injection to vortex and no injection; with vortex and no injection to no vortex or injection
ORIENT	Used to orient five-hole pressure probe with respect to wind tunnel
SETCOND	Used to establish baseline conditions for wind tunnel runs, including free-stream velocity and blowing ratio

APPENDIX C

UNCERTAINTY ANALYSIS

For this study, uncertainty estimates for key variables were determined in a manner similar to that described in Reference 20. Individual uncertainties of input parameters were determined in the classic manner as set forth in Reference 21.

A. ORDERS OF UNCERTAINTY

For a given measured quantity x_i, the uncertainty δx_i, based on a 95% confidence interval, is determined by considering three orders of replication.

1. Zeroth Order

Zeroth order uncertainty in x_i, or δx_{io}, is due strictly to the level of accuracy achievable in the measurement (i.e., with instruments) of x_i. This is taken to be one-half the least measurement graduation (or one-half the least digit).

2. First Order

First order uncertainty in x_i, or δx_i, takes into consideration unsteadiness in the taking of a measurement, in addition to the zeroth order (accuracy) uncertainty. Thus, if δx_{iu} is uncertainty due to unsteadiness, then

$$\delta x_{i1} = (\delta x_{io}{}^2 + \delta x_{iu}{}^2)^{1/2}$$

3. Second Order

Second order uncertainty in x_i, or δx_{i2}, takes into consideration uncertainties due to calibration of measurement devices (δx_{ic}), and bias (δx_{ib}), in addition to first order uncertainty. Thus,

$$\delta x_{i2} = (\delta x_{ic}^2 + \delta x_{ib}^2 + \delta x_{i1}^2)^{1/2} .$$

δx_{i2} is the uncertainty value used in the final analysis.

B. RESULTS

Uncertainties are listed in Tables 10 and 11. The five-hole pressure probe used in this study was similar to Reference 22. The uncertainty determined therein for the probe pitch and yaw angles was used to determine uncertainty in velocity components listed in Table 10.

TABLE 10

MEAN VELOCITY UNCERTAINTY

Quantity (Units)	Typical Nominal Value	Experimental Uncertainty
K_y, K_p (units/^{o})	.09	.0086
C_{py}, C_{pp}	.7, .27	.02
α, β	10^o	1.2, 1.2
U_x	10 m/s	.25
U_y, U_z	1 m/s	.09

TABLE 11

STANTON NUMBER UNCERTAINTY

Quantity (Units)	Typical Nominal Value	Experimental Uncertainty
Tr_∞ (^{o}C)	18.0	.13
Tw (^{o}C)	40.0	.21
Pambient (mm Hg)	760.0	.71
P_∞ (mm Hg)	760.0	.71
($Po_\infty - P_\infty$) (mm water)	6.13	.047
P_∞ (kg/m^3)	1.23	.009
U_∞, U_C, U_X (m/s)	10.0	.06
C_p ($J/kg^{o}k$)	1006.0	1.0
q_wA (W)	270.0	10.5
St	0.00196	.000086
St/St_o	1.05	.058

APPENDIX D

VORTEX ARRAY IN A WIND TUNNEL

An additional experiment performed consisted of placing a spanwise array of vortices in the wind tunnel. Data were acquired with no injection and freestream velocity 9.9 m/s. Figure 229 shows construction of the generator array (thin stainless steel). Results of the experiment are summarized in Figures 230 and 231. The array creates counter-rotating vortex pairs, somewhat similar to the array of vortices from centrifugal instabilities near concave surfaces. Upwash and downwash regions and pairs of vortices are clearly evident in the figures.

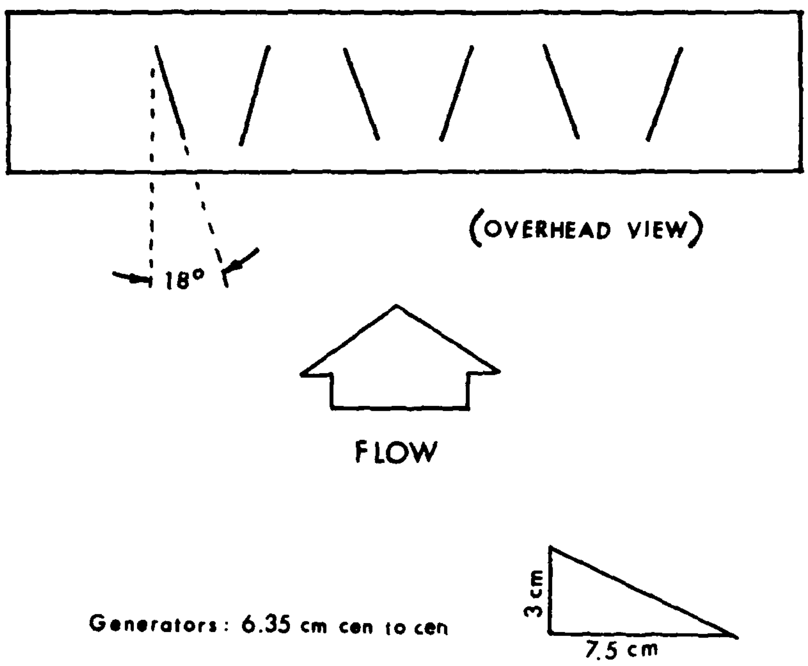

Figure 229. Vortex Generator Array

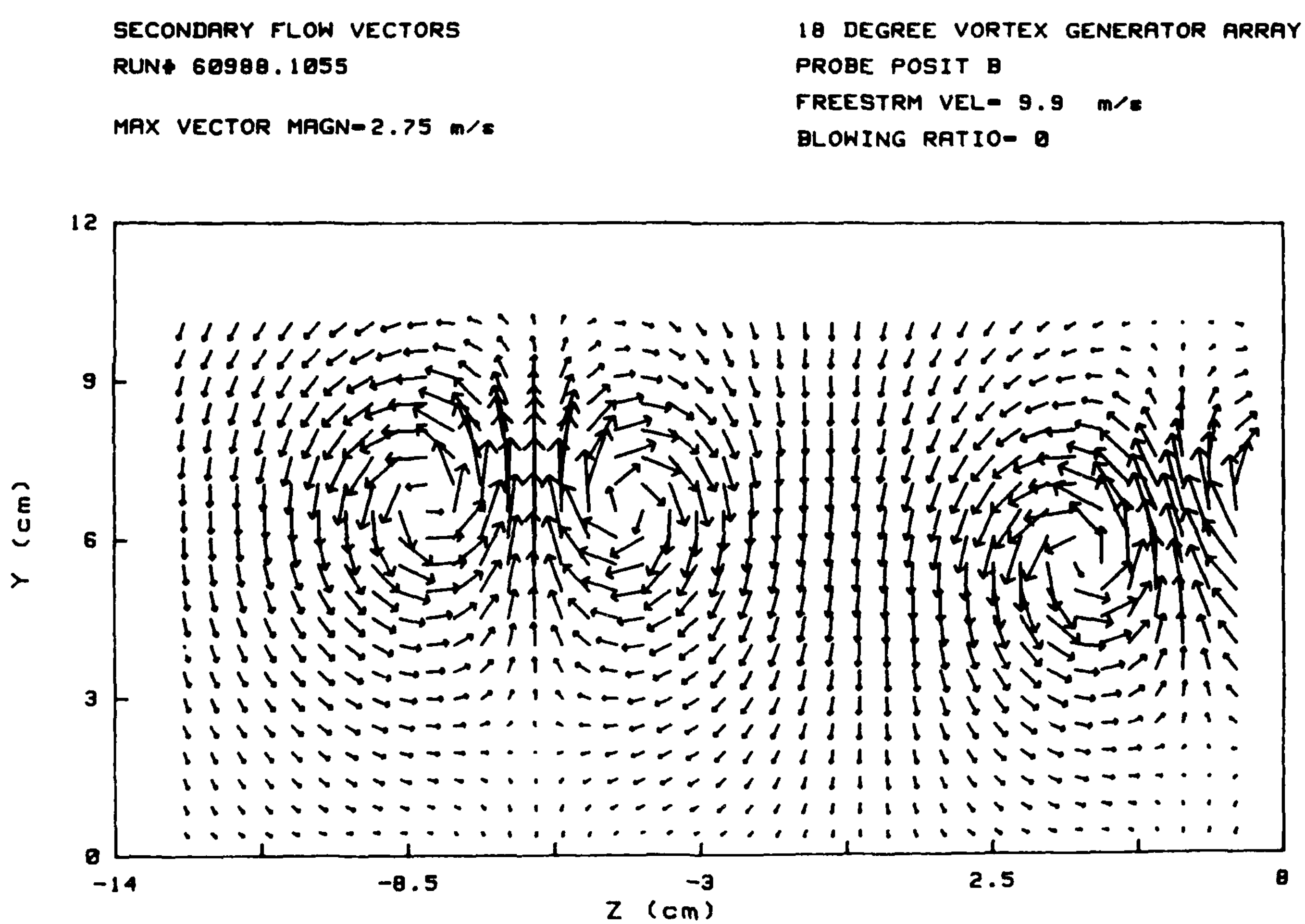

Figure 230. Secondary Flow Vectors. Vortex Generator Array, No Injection

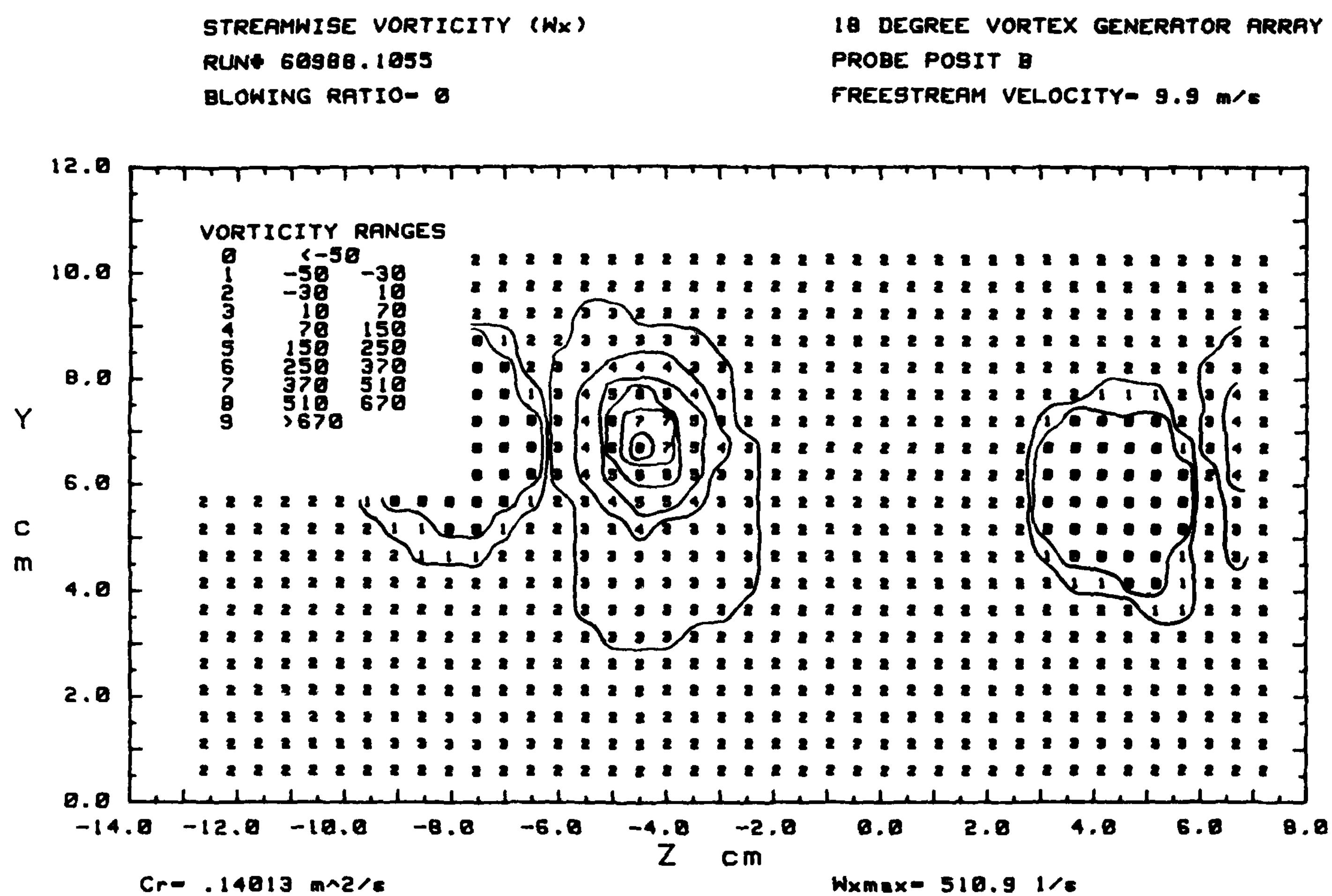

Figure 231. Streamwise Vorticity Contours. Vortex Generator Array, No Injection

APPENDIX E

CURVED CHANNEL HEAT TRANSFER SURFACE

Heat transfer surfaces for a 40 to 1 aspect ratio curved channel were also constructed. Upon completion and qualification, the channel will be used to measure wall heat transfer distributions. The channel will be similar to that used in Reference 22, but will allow heating of channel surfaces. The author's participation in this project consisted of devising a method of attachment (shown in Figure 232) and installing 200 copper-constantan thermocouples and four foil heaters to the channel walls (external to airstream). Several methods of attachment were attempted but found unsatisfactory prior to the final version shown in Figure 232. The final procedure consisted of the following steps:

(1) three layers of 2.5 mil 3M Company "Sticky Back" adhesive liner were carefully laid on the lexan channel wall, taking extreme care to ensure absence of air bubbles;

(2) narrow channels were cut in the liner and thermocouples were placed in the channels with the junction firmly in contact with the lexan;

(3) channels were filled with RTV epoxy and smoothed over;

(4) a fourth layer of liner was installed;

(5) the foil heater was installed over the last layer of liner.

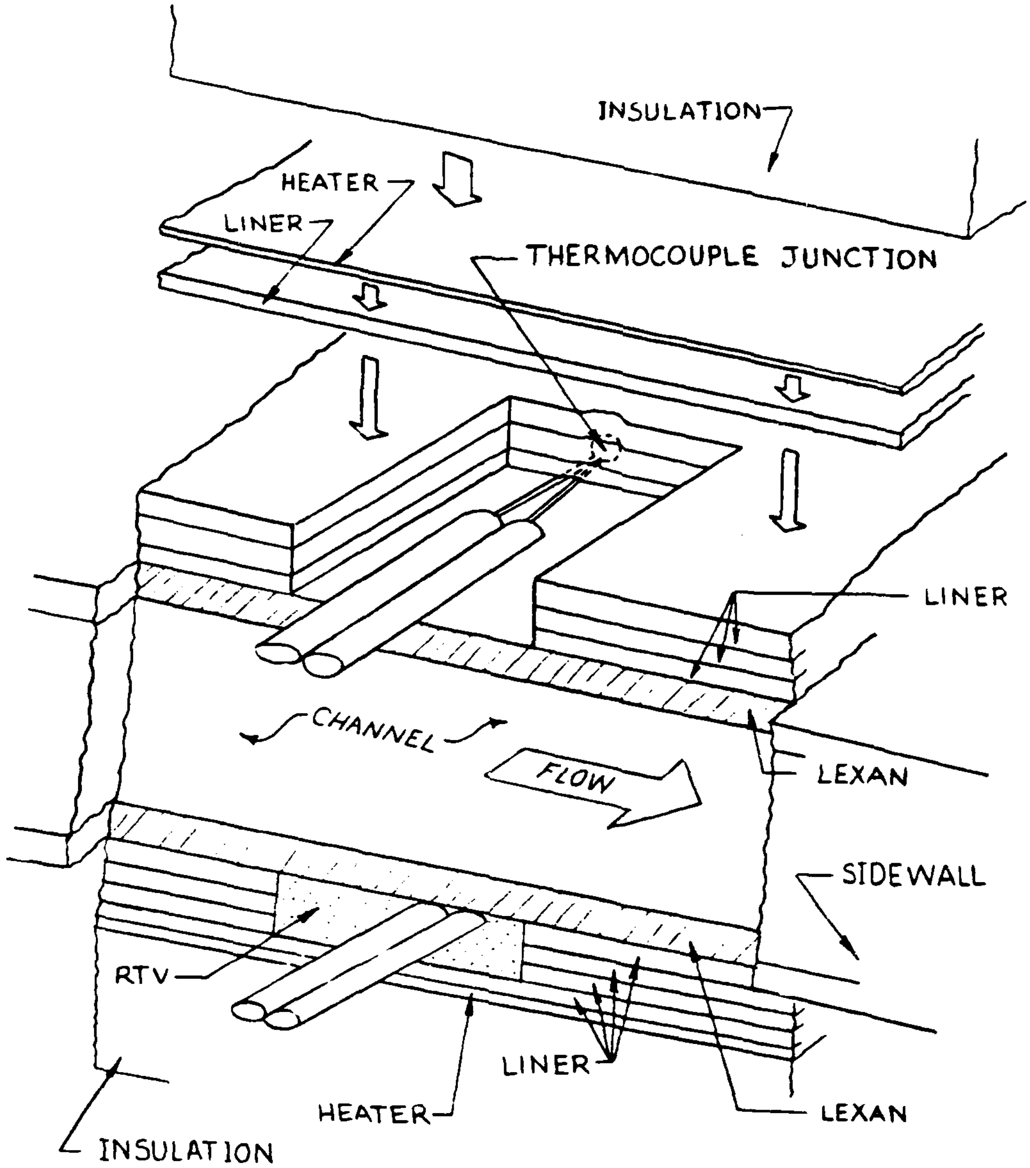

Figure 232. Thermocouple and Heater Installation for Curved Channel Heat Transfer Surface

LIST OF REFERENCES

1. Ongoren, A., "Heat Transfer on Endwalls of a Turbine Cascade With Film Cooling," Project report 1981-19, Von Karman Institute for Fluid Dynamics, Rhode Saint Genese, Belgium, June 1981.

2. Joseph, S.L., The Effects of an Embedded Vortex on a Film Cooled Turbulent Boundary Layer, M.E. Thesis, Naval Postgraduate School, Monterey, California, December 1986.

3. Evans, D.L., Study of Vortices Embedded in Boundary Layers With Film Cooling, M.S. Thesis, Naval Postgraduate School, Monterey, California, March 1987.

4. Ortiz, A., The Thermal Behavior of Film Cooled Turbulent Boundary Layers as Affected by Longitudinal Vortices, M.E. Thesis, Naval Postgraduate School, Monterey, California, September 1987.

5. Ligrani, P.M., et al., "Effects of Embedded Vortices on Film-Cooled Turbulent Boundary Layers," ASME-88-GT-170. Presented at the Gas Turbine and Aeroengine Congress and Exposition, June 1988.

6. Ligrani, P.M., et al., "Heat Transfer in Film-Cooled Turbulent Boundary Layers at Different Blowing RAtios as Affected by Longitudinal Vortices," To appear in Experimental Thermal and Fluid Science, Vol. 1, No. 4, 1988.

7. Eibeck, P.A., and Eaton, J.K., "Heat Transfer Effects of a Longitudinal Vortex Embedded in a Turbulent Boundary Layer," ASME Transactions--Journal of Heat Transfer, Vol. 104, pp. 355-362, 1987.

8. Blair, M.E., "An Experimental Study of Heat Transfer and Film Cooling on Large-Scale Turbine Endwalls," ASME Transactions--Journal of Heat Transfer, Vol. 96, pp. 524-529, 1974.

9. Goldstein, R.J., and Chen, H.P., "Film Cooling on a Gas Turbine Blade Near the End Wall," ASME Transactions--Journal of Engineering for Gas Turbines and Power, Vol. 107, pp. 117-122.

10. Goldstein, R.J., and Chen, H.P., "Film Cooling of a Turbine Blade With Injection Through Two Rows of Holes in the Near-Endwall Region," The ASME-87-GT-196, 1987.

11. Goldstein, R.J., and Yoshida, T., "The Influence of a Laminar Boundary Layer and Laminar Injection on Film Cooling Performance," ASME Transactions--Journal of Heat Transfer, Vol. 104, pp. 355-362, 1982.

12. Sieverding, C.H., "Recent Progress in the Understanding of Basic Aspects of Secondary Flows in Turbine Blade Passages," ASME Transactions--Journal of Engineering for Gas Turbines and Power, Vol. 107, pp. 248-257, 1985.

13. Westphal, R.V., Eaton, J.K., and Pauley, W.R., "Interaction Between a Vortex and a Turbulent Boundary Layer in a Streamwise Pressure Gradient." Fifth Symposium on Turbulent Shear Flows, Cornell University, Ithaca, New York, 1985.

14. Theisen, J.G., Scruggs, R.M., and Dixon, C.J., "Theoretical and Experimental Investigations of Vortex Lift Control by Spanwise Blowing." Report Contract No. N00014-72-C-0237, prepared by Lockheed-Georgia Company for the Office of Naval Research, 1973.

15. Heffernan, K.G., Trailing Vortex Attenuation Devices, M.S. Thesis, Naval Postgraduate School, Monterey, California, June 1985.

16. McGinley, C.G., and Beeler, G.B., "Large-Eddy Substitution via Vortex Cancellation for Wall Turbulence Control," AIAA-85-0549. Presented at the American Institute of Aeronautics and Astronautics Shear Flow Control Conference, Boulder, Colorado, March 1985.

17. Skow, A.M., and Penke, D.J., "Control of the Forebody Vortex Orientation by Asymmetric Air Injection." AGARD Special Course on Aerodynamic Characteristics and Controls, NASA--Ames Research Center, Moffett Field, California, 1982-1983.

18. Kobayashi, R., "Taylor-Gortler Instability of a Boundary Layer with Suction or Blowing," Rep. Inst. High Speed Mech., Vol. 32, No. 289, 1975.

19. Sabersky, R.H., Acosta, A.J., and Hauptmann, E.G., Fluid Flow--A First Course in Fluid Mechanics, 2nd ed., Macmillan Publishing Co., Inc., New York, 1971, 190 pp.

20. Moffat, R.J., "Contributions to the Theory of Single-Sample Uncertainty Analysis," ASME Transactions--Journal of Fluids Engineering, Vol. 104, pp. 250-260, 1982.

21. Kline, S.J., and McClintock, F.A., "Describing Uncertainties in Single-Sample Experiments," Mechanical Engineering, January 1953.

22. Baun, L.R., The Development and Structural Characteristics of Dean Vortices in a Curved Rectangular Channel with 40 to 1 Aspect Ratio, M.E. Thesis, Naval Postgraduate School, Monterey, California, September 1988.

INITIAL DISTRIBUTION LIST

		No. Copies
1.	Defense Technical Information Center Cameron Station Alexandria, Virginia 22304-6145	2
2.	Library, Code 0142 Naval Postgraduate School Monterey, California 93943-5002	2
3.	Department Chairman, Code 69 Department of Mechanical Engineering Naval Postgraduate School Monterey, California, 93943-5000	1
4.	Professor Phillip M. Ligrani, Code 69Li Department of Mechanical Engineering Naval Postgraduate School Monterey, California 93943-5000	10
5.	LCDR G.E. Schwartz, USN 1612 Emmerton Court Virginia Beach, Virginia 23456	2